# AN EXPERIMENTAL AND THEORETICAL STUDY OF THE EFFECT OF TEMPERATURE ON THE MECHANICAL BEHAVIOR OF NANOCLAY REINFORCED POLYMERS

**by**

**Selen Bayar**

A dissertation submitted to the Faculty and Engineering in partial fulfillment of the requirements for the degree of Doctor of Philosophy, The City University of New York

2012

This manuscript has been read and accepted for the

Graduate Faculty in Engineering in satisfaction of the

dissertation requirement for the degree of Doctor of Philosophy.

| | |
|---|---|
| 01/26/2012 | Prof. Feridun Delale |
| Date | Chair of Examining Committee |

| | |
|---|---|
| 01/26/2012 | Prof. Mumtaz Kassir |
| Date | Executive Offer |

Prof. Benjamin Liaw

Prof. Jackie Jie Li

Prof. Ali Sadegh

Dr. Jerry Chung

Supervisory Committee

THE CITY UNIVERSITY OF NEW YORK

## Abstract

**AN EXPERIMENTAL AND THEORETICAL STUDY OF THE EFFECT OF TEMPERATURE ON THE MECHANICAL BEHAVIOR OF NANOCLAY REINFORCED POLYMERS**

by

**Selen Bayar**

Adviser: Professor Feridun Delale

The goals of this study are to investigate the tensile loading and low velocity impact response of nanoclay reinforced polymers at various temperatures. Three types of polypropylene (PP 3371, Borealis and TP 3868) and epoxy with various nanoclay reinforcement percentages were considered. Tensile tests were conducted on ASTM Type I specimens instrumented with strain gauges using an MTS testing machine equipped with an environmental chamber. Low velocity impact tests were also performed using an Instron-Dynatup 8250 impact test machine equipped with an environmental chamber. Tensile test results were used to determine the effect of nanoclay reinforcement and different resins on the mechanical properties at various temperatures.

The tensile tests results indicate that the Young's modulus of the nanocomposite increases with increasing nanoclay reinforcement percentage. The temperature has even a more significant

effect. It was observed that as the temperature decreases the material becomes brittle, has higher stiffness and fails at lower strains. High temperatures have the opposite effect, in that, as the temperature increases the material loses stiffness and becomes more ductile. Temperature and nanoclay reinforcement affect the Poisson's ratio also, but this effect is less significant. In general, as the temperature increases the Poisson's ratio also increases. However, an increase in nanoclay reinforcement generally reduces the Poisson's ratio.

The mechanical properties of polymer/clay nanocomposites were also calculated using the Mori-Tanaka formulation and the finite element method. Furthermore, the Mori-Tanaka model was modified to include the effect of temperature and voids. In the Mori-Tanaka formulation three types of nanoclay particle distribution was assumed: oriented nanoclay particles parallel to the direction of tensile loading, 2-D randomly distributed particles and 3-D randomly distributed particles. The finite element calculations were performed on a representative volume element having the same reinforcement percentage as the test specimens, with the nanoclay particles placed in a plane parallel to the loading direction.

The comparison of theoretical and experimental results shows that both the Mori-Tanaka formulation and the finite element method provide effective tools to predict the mechanical properties of nanoclay reinforced composites. Furthermore, including the effect of temperature and voids provided a better match with experimental results.

**ACKNOWLEGMENT**

I would like to thank and express my sincere gratitude to my adviser, Professor Feridun Delale. His valuable advice, guidance, understanding and encouragement had a significant impact in the completion of this thesis. His support and encouragement helped me to overcome many difficulties I encountered through the course of my research.

I would like also to acknowledge the support and advice of my Ph.D. examining committee: Professors Benjamin Liaw, Jackie Jie Li, Ali Sadegh and Dr. Jerry Chung.

This research was supported by TARDEC was supported by US Army-TARDEC under contract #W56HZV-09-C-0569.

I would like also to offer special thanks to my professors and friends at City College for all the support and help they provided during my Ph.D. study.

Most importantly, I would like to thank my family, my father Aytun Bayar, my mother Fatma Bayar and my brother Mertcan for their unlimited support, understanding and help during my studies.

Finally, I would like to thank my true love, Erol, for his love, patience and understanding.

**Table of Contents**

**ABSTRACT** iv

**ACKNOWLEGMENT** vi

**1. INTRODUCTION** 1

1.1 Objectives of This Study 2

1.2 Contribution of This Study 3

**2. LITERATURE REVIEW** 4

2.1 Studies on the Characterization of Polymer/Clay Nanocomposites 5

2.2 Studies on the Mechanical Properties of Polymer/Clay Nanocomposites 8

2.2.1 Experimental Studies 8

2.2.2 Theoretical Studies 11

2.3 Studies on the Low Velocity Impact Response of Polymer/Clay Nanocomposites 12

2.4 Studies on Thermal Response of Polymer/Clay Nanocomposites 13

2.5 Studies on Fire Retardation and Toxicity Response of Polymer/Clay Nanocomposites 15

**3. EXPERIMENTAL STUDY ON POLYMER/CLAY NANOCOMPOSITES** 17

3.1 The Specimens and Materials 17

3.2 Tensile Testing 19

3.2.1 Effect of Nanoclay Reinforcement 19

3.2.2 Effect of Temperature 26

3.2.2-a Tensile test of PP 3371 at 160ºF (71ºC) 26

3.2.2-b Tensile test of PP 3371 at 120ºF (49ºC) 31

| | | | |
|---|---|---|---|
| | 3.2.2-c | Tensile test of PP 3371 at -4ºF (-20ºC) | 35 |
| | 3.2.2-d | Tensile test of PP 3371 at -65ºF (-54ºC) | 40 |
| | 3.2.2-e | Comparison of stress-strain curves of PP 3371specimens with 0%, 0.2%, 1%, 3%, 6% and 10% nanoclay reinforcement at -65°F (-54°C), -4°F (-20°C), room temperature, 120°F (49°C) and 160°F (71°C) | 44 |
| | 3.2.2-f | Variation of Young's Modulus & Poisson's Ratio with Temperature | 49 |
| | 3.2.2-g | Variation of Young's Modulus & Poisson's Ratio with Nanoclay Reinforcement Percentage | 52 |
| | 3.2.3 | Effect of Different Resins | 54 |
| | 3.2.3-a | Testing of Borealis specimens with 3% nanoclay reinforcement at –65ºF (-54ºC), -4ºF (-20ºC), room temperature, 120°F (49ºC) and 160°F (71ºC) | 54 |
| | 3.2.3-b | Testing of Total Petrochemical 3868 specimens with 3% nanoclay reinforcement at -65°F (-54°C),-4°F (-20°C), room temperature, 120°F (49°C) and 160°F (71°C) | 58 |
| | 3.2.3-c | Testing of EPON 828 Epoxy specimens with 0%, 1%, 3%, 6% and 10% nanoclay reinforcement at room temperature | 61 |
| | 3.2.4 | Comparison of Various Resins at Room Temperature | 67 |
| 3.3 | Low Velocity Impact | | 69 |
| | 3.3.1 | Low Velocity Drop Weight Test Results at Various Temperatures | 73 |
| | 3.3.2 | Comparison of Low Velocity Drop Weight Test Results at a Given Temperature | 88 |
| 3.4 | Electron Microscopy | | 98 |
| **4.** | **MODELING AND SIMULATION** | | 106 |
| 4.1 | Micromechanics Modeling | | 106 |
| | 4.1.1 | Application of Mori-Tanaka formulation for tensile testing | 106 |

4.1.1-a Oriented Nanoclay Particles 107

4.1.1-b Results of Parametric Study for Oriented Nanoclay Particles 112

4.1.1-c 2-D Randomly Distributed Nanoclay Partciles 122

4.1.1-d Results of Parametric Study for 2-D Randomly Distributed Particles 124

4.1.1-e 3-D Randomly Ditributed Nanoclay Particles 134

4.1.1-f Results of Parametric Study for 3-D Randomly Distributed Particles 135

4.1.2 Results Obtained From Various Mori-Tanaka Calculation 144

4.1.2-a Comparison of Experimental Results with Mori-Tanaka Calculations 145

4.1.2-b Comparison of Experimental Results with Mori-Tanaka Calculations for Epoxy Based Nanocomposites 156

4.1.3 Mori-Tanaka Calculation with Effect of Voids 157

4.1.3-a Oriented Nanoclay Particles with Effect of Voids 159

4.1.3-b 2-D Randomly Distributed Nanoclay Particles with Effect of Voids 165

4.1.3-c 3-D Randomly Distributed Nanoclay Particles with Effect of Voids 170

4.1.4 Modification of Mori-Tanaka Model with the Inclusion of Temperature Effects 176

4.2 3-D Finite Element Modeling for Tensile Testing 181

**5. DISCUSSION AND CONCLUSION** 197

**6. FUTURE WORK** 201

**7. REFERENCES** 202

**List of Tables**


| | | |
|---|---|---|
| Table 3.1 | Average values of material properties of PP 3371 specimens with 0%, 0.2%, 1%, 3%, 6% and 10% nanoclay reinforcement at room temperature | 24 |
| Table 3.2 | Average values of material properties of PP 3371 specimens with 0%, 0.2%, 1%, 3%, 6% and 10% nanoclay reinforcement at 160ºF (71ºC) | 30 |
| Table 3.3 | Average values of material properties of PP 3371 specimens with 0%, 0.2%, 1%, 3%, 6% and 10% nanoclay reinforcement at 120ºF (49ºC) | 35 |
| Table 3.4 | Average values of material properties of PP 3371 specimens with 0%, 0.2%, 1%, 3%, 6% and 10% nanoclay reinforcement at -4ºF (-20ºC) | 39 |
| Table 3.5 | Average values of material properties of PP 3371 specimens with 0%, 0.2%, 1%, 3%, 6% and 10% nanoclay reinforcement at -65ºF (-49ºC) | 43 |
| Table 3.6 | Material properties of PP 3371 specimens with 0%, 0.2%, 1%, 3%, 6% and 10% nanoclay reinforcement at -65°F (-54°C), -4°F (- 20°C),room temperature, 120°F (49°C) and 160°F (71°C) | 48 |
| Table 3.7 | Average Young's Moduli | 51 |
| Table 3.8 | Average Poisson's Ratio | 52 |
| Table 3.9 | Average material properties of Borealis specimens with 3% nanoclay reinforcement at -65ºF (-54ºC),-4ºF (-20ºC), room temperature, 120°F (49ºC) and 160°F (71ºC) | 57 |
| Table 3.10 | Average material properties of TP 3868 specimens with 3% nanoclay reinforcement at -65°F (-54°C),-4°F (-20ºC), room temperature, 120°F (49°C) and 160°F (71°C) | 61 |
| Table 3.11 | Material properties of EPON 828 specimens with 0%, 1%, 3%, 6% and 10% nanoclay reinforcement at room temperature | 66 |
| Table 3.12 | Average material properties of EPON 828 specimens with 0%, 1%, 3%, 6% and 10% nanoclay reinforcement at room temperature | 67 |
| Table 3.13 | Drop weight tests results at -65ºF (-54ºC),-4ºF (-20ºC), roomtemperature, 120°F (49ºC) and 160°F (71ºC) | 71 |

| | | |
|---|---|---|
| Table 4.1 | Conversion of weight fractions of nanoclay to volume fractions | 112 |
| Table 4.2 | Comparison of Mori-Tanaka calculations and experimental results of PP 3371/clay nanocomposites for oriented particles at 160ºF | 114 |
| Table 4.3 | Comparison of Mori-Tanaka calculations and experimental results of PP 3371/clay nanocomposites for oriented particles at 120ºF | 115 |
| Table 4.4 | Comparison of Mori-Tanaka calculations and experimental results of PP 3371/clay nanocomposites for oriented particles at room temperature | 117 |
| Table 4.5 | Comparison of Mori-Tanaka calculations and experimental results of PP 3371/clay nanocomposites for oriented particles at -4ºF | 118 |
| Table 4.6 | Comparison of Mori-Tanaka calculations and experimental results of PP 3371/clay nanocomposites for oriented particles at -65ºF | 120 |
| Table 4.7 | Comparison of Mori-Tanaka calculations and experimental results of EPON 828/clay nanocomposites for oriented particles at room temperature | 121 |
| Table 4.8 | Comparison of Mori-Tanaka calculations and experimental results of PP 3371/clay nanocomposites for 2-D randomly distributed particles at 160ºF | 126 |
| Table 4.9 | Comparison of Mori-Tanaka calculations and experimental results of PP 3371/clay nanocomposites for 2-D randomly distributed particles at 120ºF | 127 |
| Table 4.10 | Comparison of Mori-Tanaka calculations and experimental results of PP 3371/clay nanocomposites for 2-D randomly distributed particles at room temperature | 129 |
| Table 4.11 | Comparison of Mori-Tanaka calculations and experimental results of PP 3371/clay nanocomposites for 2-D randomly distributed particles at -4ºF | 130 |
| Table 4.12 | Comparison of Mori-Tanaka calculations and experimental results of PP 3371/clay nanocomposites for 2-D randomly distributed particles at -65ºF | 132 |
| Table 4.13 | Comparison of Mori-Tanaka calculations and experimental results of EPON 828/clay nanocomposites for 2-D randomly distributed particles at room temperature | 133 |

| | | |
|---|---|---|
| Table 4.14 | Comparison of Mori-Tanaka calculations and experimental results of PP 3371/clay nanocomposites for3-D randomly distributed particles at 160ºF | 136 |
| Table 4.15 | Comparison of Mori-Tanaka calculations and experimental results of PP 3371/clay nanocomposites for3-D randomly distributed particles at 120ºF | 137 |
| Table 4.16 | Comparison of Mori-Tanaka calculations and experimental results of PP 3371/clay nanocomposites for 3-D randomly distributed particles at room temperature | 139 |
| Table 4.17 | Comparison of Mori-Tanaka calculations and experimental results of PP 3371/clay nanocomposites for 3-D randomly distributed particles at -4ºF | 140 |
| Table 4.18 | Comparison of Mori-Tanaka calculations and experimental results of PP 3371/clay nanocomposites for 3-D randomly distributed particles at -65ºF | 142 |
| Table 4.19 | Comparison of Mori-Tanaka calculations and experimental results of EPON 828/clay nanocomposites for 3-D randomly distributed particles at room temperature | 143 |
| Table 4.20 | Nanoclay flakes number composition for each percentage | 144 |
| Table 4.21 | Young's modulus values based on tangent and secant calculation at 120ºF | 179 |
| Table 4.22 | Young's modulus values based on tangent and secant calculation at 160ºF | 180 |
| Table 4.23 | The particle parameters used in the finite element calculation for each reinforcement percentage | 184 |
| Table 4.24 | Comparison of $E/E_m$ values obtained from experiments and the Mori-Tanaka calculations at various temperatures | 191 |
| Table 4.25 | Comparison of $v_{12}/v_m$ values obtained from experiments and the Mori-Tanaka calculations at various temperatures | 192 |

**List of Figures**


| | | |
|---|---|---|
| Figure 3.1 | Type I dog-bone shaped tensile specimens a) PP3371, b) EPON 828, c) Borealis and d) TP 3868 | 17 |
| Figure 3.2 | PP 3371 specimen with attached strain gages | 18 |
| Figure 3.3 | Low velocity impact test specimen with attached strain gages (PP 3371) | 29 |
| Figure 3.4 | Stress-strain curves of pure PP 331 specimens | 20 |
| Figure 3.5 | Stress-strain curves of PP 331 specimens with 0.2% nanoclay reinforcement | 20 |
| Figure 3.6 | Stress-strain curves of PP 331 specimens with 1% nanoclay reinforcement | 21 |
| Figure 3.7 | Stress-strain curves of PP 331 specimens with 3% nanoclay reinforcement | 21 |
| Figure 3.8 | Stress-strain curves of PP 331 specimens with 6% nanoclay reinforcement | 22 |
| Figure 3.9 | Stress-strain curves of PP 331 specimens with 10% nanoclay reinforcement | 22 |
| Figure 3.10 | Comparison of stress-strain curves of PP 331 specimens with various nanoclay reinforcement percentages | 23 |
| Figure 3.11 | A ruler and a marked specimen under tensile load | 25 |
| Figure 3.12 | Comparison of crosshead and optical stress-strain curves for neat PP 3371 specimens | 25 |
| Figure 3.13 | Comparison of crosshead and optical stress-strain curves for PP 3371 specimens reinforced with 10% nanoclay | 26 |
| Figure 3.14 | Stress-strain curve of neat PP 3371 specimens at 160ºF (71ºC) | 27 |
| Figure 3.15 | Stress-strain curve of PP 3371 specimens with 0.2% nanoclay reinforcement at 160ºF (71ºC) | 27 |
| Figure 3.16 | Stress-strain curve of PP 3371 specimens with 1% nanoclay reinforcement at 160ºF (71ºC) | 28 |

| | | |
|---|---|---|
| Figure 3.17 | Stress-strain curve of PP 3371 specimens with 3% nanoclay reinforcement at 160ºF (71ºC) | 28 |
| Figure 3.18 | Stress-strain curve of PP 3371 specimens with 6% nanoclay reinforcement at 160ºF (71ºC) | 29 |
| Figure 3.19 | Stress-strain curve of PP 3371 specimens with 10% nanoclay reinforcement at 160ºF (71ºC) | 29 |
| Figure 3.20 | Comparison of stress-strain curve of PP 3371 specimens with 0%, 0.2%, 1%, 3%, 6% and 10% nanoclay reinforcement at 160ºF(71ºC) | 30 |
| Figure 3.21 | Stress-strain curve of neat PP 3371 specimens at 120ºF (49ºC) | 31 |
| Figure 3.22 | Stress-strain curve of PP 3371 specimens with 0.2% nanoclay reinforcement at 120ºF (49ºC) | 32 |
| Figure 3.23 | Stress-strain curve of PP 3371 specimens with 1% nanoclay reinforcement at 120ºF (49ºC) | 32 |
| Figure 3.24 | Stress-strain curve of PP 3371 specimens with 3% nanoclay reinforcement at 120ºF (49ºC) | 33 |
| Figure 3.25 | Stress-strain curve of PP 3371 specimens with 6% nanoclay reinforcement at 120ºF (49ºC) | 33 |
| Figure 3.26 | Stress-strain curve of PP 3371 specimens with 10% nanoclay reinforcement at 120ºF (49ºC) | 34 |
| Figure 3.27 | Comparison of stress-strain curve of PP 3371 specimens with 0%, 0.2%, 1%, 3%, 6% and 10% nanoclay reinforcement at 120ºF(49ºC) | 34 |
| Figure 3.28 | Stress-strain curve of PP 3371 specimens with 0% nanoclay reinforcement at -4ºF (-20ºC) | 36 |
| Figure 3.29 | Stress-strain curve of PP 3371 specimens with 0.2% nanoclay reinforcement at -4ºF (-20ºC) | 36 |
| Figure 3.30 | Stress-strain curve of PP 3371 specimens with 1% nanoclay reinforcement at -4ºF (-20ºC) | 37 |
| Figure 3.31 | Stress-strain curve of PP 3371 specimens with 3% nanoclay reinforcement at -4ºF (-20ºC) | 37 |

| | | |
|---|---|---|
| Figure 3.32 | Stress-strain curve of PP 3371 specimens with 6% nanoclay reinforcement at -4ºF (-20ºC) | 38 |
| Figure 3.33 | Stress-strain curve of PP 3371 specimens with 10% nanoclay reinforcement at -4ºF (-20ºC) | 38 |
| Figure 3.34 | Comparison of stress-strain curve of PP 3371 specimens with 0%, 0.2%, 1%, 3%, 6% and 10% nanoclay reinforcement at -4ºF (-20ºC) | 39 |
| Figure 3.35 | Stress-strain curves of neat PP 331 specimens at -65ºF(-54ºC) | 40 |
| Figure 3.36 | Stress-strain curve of PP 3371 specimens with 0.2% nanoclay reinforcement at -65ºF (-54ºC) | 40 |
| Figure 3.37 | Stress-strain curve of PP 3371 specimens with 1% nanoclay reinforcement at -65ºF (-54ºC) | 41 |
| Figure 3.38 | Stress-strain curve of PP 3371 specimens with 3% nanoclay reinforcement at -65ºF (-54ºC) | 41 |
| Figure 3.39 | Stress-strain curve of PP 3371 specimens with 6% nanoclay reinforcement at -65ºF (-54ºC) | 39 |
| Figure 3.40 | Stress-strain curve of PP 3371 specimens with 10% nanoclay reinforcement at -65ºF (-54ºC) | 39 |
| Figure 3.41 | Comparison of stress-strain curve of PP 3371 specimens with 0%, 0.2%, 1%, 3%, 6% and 10% nanoclay reinforcement at -65ºF (-54ºC) | 43 |
| Figure 3.42 | Comparison of stress - strain curves of neat PP 3371 specimens at -65°F (-54°C), -4°F (-20°C), RT, 120°F (49°C) | 44 |
| Figure 3.43 | Comparison of stress - strain curves of PP 3371 specimens with 0.2% nanoclay reinforcement at -65°F (-54°C), -4°F (-20°C), RT, 120°F (49°C) | 45 |
| Figure 3.44 | Comparison of stress - strain curves of PP 3371 specimens with 1% nanoclay reinforcement at -65°F (-54°C), -4°F (-20°C), RT, 120°F (49°C) | 45 |
| Figure 3.45 | Comparison of stress - strain curves of PP 3371 specimens with 3% nanoclay reinforcement at -65°F (-54°C), -4°F(-20°C), RT, 120°F (49°C) | 46 |

| | | |
|---|---|---|
| Figure 3.46 | Comparison of stress - strain curves of PP 3371 specimens with 6% nanoclay reinforcement at -65°F (-54°C), -4°F (-20°C), RT, 120°F (49°C) | 46 |
| Figure 3.47 | Comparison of stress - strain curves of PP 3371 specimens with 10% nanoclay reinforcement at -65°F (-54°C), -4°F (-20°C), RT, 120°F (49°C) | 47 |
| Figure 3.48 | Variation of Young's modulus with temperature | 49 |
| Figure 3.49 | Variation of Poisson's ratio with temperature | 50 |
| Figure 3.50 | Range of Young's modulus for PP 3371 with 3% nanoclay reinforcement | 50 |
| Figure 3.51 | Variation of Young's modulus with nanoclay reinforcement percentage at various test temperatures | 52 |
| Figure 3.52 | Variation of Poisson's ratio with nanoclay reinforcement percentage at various test temperatures | 53 |
| Figure 3.53 | Range of Young's modulus test results vs. reinforcement at room temperature | 53 |
| Figure 3.54 | Stress - strain curves of Borealis resin specimens with 3% nanoclay reinforcement at -65ºF (-54ºC) | 55 |
| Figure 3.55 | Stress - strain curves of Borealis resin specimens with 3% nanoclay reinforcement at –4ºF (–20ºC) | 55 |
| Figure 3.56 | Stress - strain curves of Borealis resin specimens with 3% nanoclay reinforcement at room temperature | 56 |
| Figure 3.57 | Stress - strain curves of Borealis resin specimens with 3% nanoclay reinforcement at 120ºF (49ºC) | 56 |
| Figure 3.58 | Stress - strain curves of Borealis resin specimens with 3% nanoclay reinforcement at 160ºF (71ºC) | 57 |
| Figure 3.59 | Stress - strain curves of TP 3868 specimens with 3% nanoclay reinforcement at -65ºF (-54ºC) | 58 |
| Figure 3.60 | Stress - strain curves of TP 3868 specimens with 3% nanoclay reinforcement at -4ºF (-20ºC) | 59 |

| | | |
|---|---|---|
| Figure 3.61 | Stress - strain curves of TP 3868 specimens with 3% nanoclay reinforcement at room temperature | 59 |
| Figure 3.62 | Stress - strain curves of TP 3868 specimens with 3% nanoclay reinforcement at 120ºF (49ºC) | 60 |
| Figure 3.63 | Stress - strain curves of TP 3868 specimens with 3% nanoclay reinforcement at 160ºF (71ºC) | 60 |
| Figure 3.64 | Stress - strain curves of neat EPON 828 specimens at room temperature | 62 |
| Figure 3.65 | Stress - strain curves of EPON 828 specimens with 1% nanoclay reinforcement | 62 |
| Figure 3.66 | Stress - strain curves of EPON 828 specimens with 3% nanoclay reinforcement | 63 |
| Figure 3.67 | Stress - strain curves of EPON 828 specimens with 6% nanoclay reinforcement | 63 |
| Figure 3.68 | Stress - strain curves of EPON 828 specimens with 10% nanoclay reinforcement | 64 |
| Figure 3.69 | Comparison of stress-strain curves of EPON 828 specimens with various nanoclay reinforcement | 65 |
| Figure 3.70 | Comparison of stress-strain curves of PP 3371, Borealis, TP 3868 and EPON 828 specimens with 3% nanoclay reinforcement at room temperature | 67 |
| Figure 3.71 | Comparison of stress-strain curves of Borealis specimens with 3% nanoclay reinforcement at various temperatures | 68 |
| Figure 3.72 | Comparison of stress-strain curves of TP 3868 specimens with 3% nanoclay reinforcement at various temperatures | 69 |
| Figure 3.73 | Force vs. displacement curves for neat PP specimens at -4°F, -65°F, room temperature, 120°F and 160°F | 73 |
| Figure 3.74 | Displacement vs. time curves for neat PP specimens at -4°F, -65°F, room temperature, 120°F and 160°F | 74 |
| Figure 3.75 | Energy vs. time curves for neat PP specimens at -4°F, -65°F, room temperature, 120°F and 160°F | 74 |

| | | |
|---|---|---|
| Figure 3.76 | Force vs. time curves for neat PP specimens at -4°F, -65°F, room temperature, 120°F and 160°F | 75 |
| Figure 3.77 | Force vs. displacement curves for PP with 0.2% nanoclay reinforced specimens at -4°F, -65°F, room temperature, 120°F and 160°F | 76 |
| Figure 3.78 | Displacement vs. time curves for PP with 0.2% nanoclay reinforced specimens at -4°F, -65°F, room temperature, 120°F and 160°F | 76 |
| Figure 3.79 | Energy vs. time curves for PP with 0.2% nanoclay reinforced specimens at -4°F, -65°F, room temperature, 120°F and 160°F | 77 |
| Figure 3.80 | Force vs. time curves for PP with 0.2% nanoclay reinforced specimens at -4°F, -65°F, room temperature, 120°F and 160°F | 77 |
| Figure 3.81 | Force vs. displacement curves for PP with 1% nanoclay reinforced specimens at -4°F, -65°F, room temperature, 120°F and 160°F | 78 |
| Figure 3.82 | Displacement vs. time curves for PP with 1% nanoclay reinforced specimens at -4°F, -65°F, room temperature, 120°F and 160°F | 79 |
| Figure 3.83 | Energy vs. time curves for PP with 1% nanoclay reinforced specimens at -4°F, -65°F, room temperature, 120°F and 160°F | 79 |
| Figure 3.84 | Force vs. time curves for PP with 1% nanoclay reinforced specimens at -4°F, -65°F, room temperature, 120°F and 160°F | 80 |
| Figure 3.85 | Force vs. displacement curves for PP with 3% nanoclay reinforced specimens at RT, 120°F and 160°F | 81 |
| Figure 3.86 | Displacement vs. time curves for PP with 3% nanoclay reinforced specimens at RT, 120°F and 160°F | 81 |
| Figure 3.87 | Energy vs. time curves for PP with 3% nanoclay reinforced specimens at RT, 120°F and 160°F | 82 |
| Figure 3.88 | Force vs. time curves for PP with 3% nanoclay reinforced specimens at RT, 120°F and 160°F | 82 |
| Figure 3.89 | Force vs. displacement curves for PP with 6% nanoclay reinforced specimens at RT, 120°F and 160°F | 83 |
| Figure 3.90 | Displacement vs. time curves for PP with 6% nanoclay reinforced specimens at RT, 120°F and 160°F | 84 |

| | | |
|---|---|---|
| Figure 3.91 | Energy vs. time curves for PP with 6% nanoclay reinforced specimens at RT, 120F and 160F | 84 |
| Figure 3.92 | Force vs. time curves for PP with 6% nanoclay reinforced specimens at RT, 120F and 160F | 85 |
| Figure 3.93 | Force vs. displacement curves for PP with 10% nanoclay reinforced specimens at 120°F and 160°F | 86 |
| Figure 3.94 | Displacement vs. time curves for PP with 10% nanoclay reinforced specimens at 120°F and 160°F | 86 |
| Figure 3.95 | Energy vs. time curves for PP with 10% nanoclay reinforced specimens at 120°F and 160°F | 87 |
| Figure 3.96 | Force vs. time curves for PP with 10% nanoclay reinforced specimens at 120°F and 160°F | 87 |
| Figure 3.97 | Force vs. displacement curves for PP specimens reinforced with different nanoclay percentages at 160°F | 88 |
| Figure 3.98 | Displacement vs. time curves for PP specimens reinforced with different nanoclay percentages at 160°F | 89 |
| Figure 3.99 | Energy vs. time curves for PP specimens reinforced with different nanoclay percentages at 160°F | 89 |
| Figure 3.100 | Force vs. time curves for PP specimens reinforced with different nanoclay percentages at 160°F | 90 |
| Figure 3.101 | Force vs. displacement curves for PP specimens reinforced with different nanoclay percentages at 120°F | 90 |
| Figure 3.102 | Displacement vs. time curves for PP specimens reinforced with different nanoclay percentages at 120°F | 91 |
| Figure 3.103 | Energy vs. time curves for PP specimens reinforced with different nanoclay percentages at 120°F | 91 |
| Figure 3.104 | Force vs. time curves for PP specimens reinforced with different nanoclay percentages at 120°F | 92 |
| Figure 3.105 | Force vs. displacement curves for PP specimens reinforced with different nanoclay percentages at RT | 92 |

| | | |
|---|---|---|
| Figure 3.106 | Displacement vs. time curves for PP specimens reinforced with different nanoclay percentages at RT | 93 |
| Figure 3.107 | Energy vs. time curves for PP specimens reinforced with different nanoclay percentages at RT | 93 |
| Figure 3.108 | Force vs. time curves for PP specimens reinforced with different nanoclay percentages at RT | 94 |
| Figure 3.109 | Force vs. displacement curves for PP specimens reinforced with different nanoclay percentages at -4°F | 94 |
| Figure 3.110 | Displacement vs. time curves for PP specimens reinforced with different nanoclay percentages at -4°F | 95 |
| Figure 3.111 | Energy vs. time curves for PP specimens reinforced with different nanoclay percentages at -4°F | 95 |
| Figure 3.112 | Force vs. time curves for PP specimens reinforced with different nanoclay percentages at -4°F | 96 |
| Figure 3.113 | Force vs. displacement curves for PP specimens reinforced with different nanoclay percentages at -65°F | 96 |
| Figure 3.114 | Displacement vs. time curves for PP specimens reinforced with different nanoclay percentages at -65°F | 97 |
| Figure 3.115 | Energy vs. time curves for PP specimens reinforced with different nanoclay percentages at -65°F | 97 |
| Figure 3.116 | Force vs. time curves for PP specimens reinforced with different nanoclay percentages at -65°F | 98 |
| Figure 3.117 | Dispersion of nanoclay particles in 10% nanoclay reinforced PP specimen | 99 |
| Figure 3.118 | Dispersion of nanoclay particles in 10% nanoclay reinforced PP specimen | 100 |
| Figure 3.119 | Dispersion of nanoclay particles in 10% nanoclay reinforced PP specimen | 100 |
| Figure3.120 | Nanoclay particle showing agglomeration of nanoclay flakes | 101 |
| Figure 3.121 | Dispersion of nanoclay particles in 10% nanoclay reinforced PP | 102 |

| | | |
|---|---|---|
| | specimen | |
| Figure 3.122 | Dispersion of nanoclay particles in 10% nanoclay reinforced PP specimen | 102 |
| Figure 3.123 | Dispersion of nanoclay particles in 10% nanoclay reinforced PP specimen | 103 |
| Figure 3.124 | Dispersion of nanoclay particles in 10% nanoclay reinforced PP specimen | 103 |
| Figure 3.125 | Dispersion of nanoclay particles in 1% nanoclay reinforced PP specimen | 104 |
| Figure 3.126 | Dispersion of nanoclay particles in 1% nanoclay reinforced PP specimen | 104 |
| Figure 3.127 | Dispersion of nanoclay particles in 1% nanoclay reinforced PP specimen | 105 |
| Figure 4.1 | Model of nanoclay particle [181] | 111 |
| Figure 4.2 | Comparison of Young's modulus obtained from Mori-Tanaka and experimental results for 0.2% nanoclay reinforced PP 3371 specimens at various temperatures | 145 |
| Figure 4.3 | Comparison of Poisson's ratio obtained from Mori-Tanaka and experimental results for 0.2% nanoclay reinforced PP 3371 specimens at various temperatures | 146 |
| Figure 4.4 | Comparison of Young's modulus obtained from Mori-Tanaka and experimental results for 1% nanoclay reinforced PP 3371 specimens at various temperatures | 146 |
| Figure 4.5 | Comparison of Poisson's ratio obtained from Mori-Tanaka and experimental results for 1% nanoclay reinforced PP 3371 specimens at various temperatures | 147 |
| Figure 4.6 | Comparison of Young's modulus obtained from Mori-Tanaka and experimental results for 3% nanoclay reinforced PP 3371 specimens at various temperatures | 147 |
| Figure 4.7 | Comparison of Poisson's ratio obtained from Mori-Tanaka and experimental results for 3% nanoclay reinforced PP 3371 specimens at various temperatures | 148 |
| Figure 4.8 | Comparison of Young's modulus obtained from Mori-Tanaka and | 148 |

| | | |
|---|---|---|
| | experimental results for 6% nanoclay reinforced PP 3371 specimens at various temperatures | |
| Figure 4.9 | Comparison of Poisson's ratio obtained from Mori-Tanaka and experimental results for 6% nanoclay reinforced PP 3371 specimens at various temperatures | 149 |
| Figure 4.10 | Comparison of Young's modulus obtained from Mori-Tanaka and experimental results for 10% nanoclay reinforced PP 3371 specimens at various temperatures | 149 |
| Figure 4.11 | Comparison of Poisson's ratio obtained from Mori-Tanaka and experimental results for 10% nanoclay reinforced PP 3371 specimens at various temperatures | 150 |
| Figure 4.12 | Comparison of Young's modulus obtained from experiments and oriented, 2-D and 3-D random Mori - Tanaka calculations at 160°F | 150 |
| Figure 4.13 | Comparison of Poisson's ratio obtained from experiments and oriented, 2-D and 3-D random Mori - Tanaka calculations at 160°F | 151 |
| Figure 4.14 | Comparison of Young's modulus obtained from experiments and oriented, 2-D and 3-D random Mori - Tanaka calculations at 120°F | 151 |
| Figure 4.15 | Comparison of Poisson's ratio obtained from experiments and oriented, 2-D and 3-D random Mori - Tanaka calculations at 120°F | 152 |
| Figure 4.16 | Comparison of Young's modulus obtained from experiments and oriented, 2-D and 3-D random Mori - Tanaka calculations at RT | 152 |
| Figure 4.17 | Comparison of Poisson's ratio obtained from experiments and oriented, 2-D and 3-D random Mori - Tanaka calculations at RT | 153 |
| Figure 4.18 | Comparison of Young's modulus obtained from experiments and oriented, 2-D and 3-D random Mori - Tanaka calculations at -4°F | 153 |
| Figure 4.19 | Comparison of Poisson's ratio obtained from experiments and oriented, 2-D and 3-D random Mori - Tanaka calculations at -4°F | 154 |
| Figure 4.20 | Comparison of Young's modulus obtained from experiments and | 154 |

| | | |
|---|---|---|
| | oriented, 2-D and 3-D random Mori - Tanaka calculations at -65°F | |
| Figure 4.21 | Comparison of Poisson's ratio obtained from experiments and oriented, 2-D and 3-D random Mori - Tanaka calculations at -65°F | 155 |
| Figure 4.22 | Comparison of Young's modulus obtained from experiments and oriented, 2-D and 3-D random Mori - Tanaka calculations at room temperature | 156 |
| Figure 4.23 | Comparison of Poisson's ratio obtained from experiments and oriented, 2-D and 3-D random Mori - Tanaka calculations at room temperature | 157 |
| Figure 4.24 | Comparison of Young's modulus obtained from experiments and oriented Mori - Tanaka calculations with and without voids at 160°F | 160 |
| Figure 4.25 | Comparison of Poisson's ratio obtained from experiments and oriented Mori - Tanaka calculations with and without voids at 160°F | 160 |
| Figure 4.26 | Comparison of Young's modulus obtained from experiments and oriented Mori - Tanaka calculations with and without voids at 120°F | 161 |
| Figure 4.27 | Comparison of Poisson's ratio obtained from experiments and oriented Mori - Tanaka calculations with and without voids at 120°F | 161 |
| Figure 4.28 | Comparison of Young's modulus obtained from experiments and oriented Mori - Tanaka calculations with and without voids at RT | 162 |
| Figure 4.29 | Comparison of Poisson's ratio obtained from experiments and oriented Mori - Tanaka calculations with and without voids at RT | 162 |
| Figure 4.30 | Comparison of Young's modulus obtained from experiments and oriented Mori - Tanaka calculations with and without voids at -4°F | 163 |
| Figure 4.31 | Comparison of Poisson's ratio obtained from experiments and oriented Mori - Tanaka calculations with and without voids at -4°F | 163 |
| Figure 4.32 | Comparison of Young's modulus obtained from experiments and | 164 |

| | | |
|---|---|---|
| | oriented Mori - Tanaka calculations with and without voids at -65°F | |
| Figure 4.33 | Comparison of Poisson's ratio obtained from experiments and oriented Mori - Tanaka calculations with and without voids at -65°F | 164 |
| Figure 4.34 | Comparison of Young's modulus obtained from experiments and 2-D random Mori - Tanaka calculations with and without voids at 160°F | 165 |
| Figure 4.35 | Comparison of Poisson's ratio obtained from experiments and 2-D random Mori - Tanaka calculations with and without voids at 160°F | 166 |
| Figure 4.36 | Comparison of Young's modulus obtained from experiments and 2-D random Mori - Tanaka calculations with and without voids at 120°F | 166 |
| Figure 4.37 | Comparison of Poisson's ratio obtained from experiments and 2-D random Mori - Tanaka calculations with and without voids at 120°F | 167 |
| Figure 4.38 | Comparison of Young's modulus obtained from experiments and 2-D random Mori - Tanaka calculations with and without voids at RT | 167 |
| Figure 4.39 | Comparison of Poisson's ratio obtained from experiments and 2-D random Mori - Tanaka calculations with and without voids at RT | 168 |
| Figure 4.40 | Comparison of Young's modulus obtained from experiments and 2-D random Mori - Tanaka calculations with and without voids at -4°F | 168 |
| Figure 4.41 | Comparison of Poisson's ratio obtained from experiments and 2-D random Mori - Tanaka calculations with and without voids at -4°F | 169 |
| Figure 4.42 | Comparison of Young's modulus obtained from experiments and 2-D random Mori - Tanaka calculations with and without voids at -65°F | 169 |
| Figure 4.43 | Comparison of Poisson's ratio obtained from experiments and | 170 |

| | | |
|---|---|---|
| | 2-D random Mori - Tanaka calculations with and without voids at -65°F | |
| Figure 4.44 | Comparison of Young's modulus obtained from experiments and 3-D random Mori - Tanaka calculations with and without voids at 160°F | 171 |
| Figure 4.45 | Comparison of Poisson's ratio obtained from experiments and 3-D random Mori - Tanaka calculations with and without voids at 160°F | 171 |
| Figure 4.46 | Comparison of Young's modulus obtained from experiments and 3-D random Mori - Tanaka calculations with and without voids at 120°F | 172 |
| Figure 4.47 | Comparison of Poisson's ratio obtained from experiments and 3-D random Mori - Tanaka calculations with and without voids at 120°F | 172 |
| Figure 4.48 | Comparison of Young's modulus obtained from experiments and 3-D random Mori - Tanaka calculations with and without voids at RT | 173 |
| Figure 4.49 | Comparison of Poisson's ratio obtained from experiments and 3-D random Mori - Tanaka calculations with and without voids at RT | 173 |
| Figure 4.50 | Comparison of Young's modulus obtained from experiments and 3-D random Mori - Tanaka calculations with and without voids at -4°F | 174 |
| Figure 4.51 | Comparison of Poisson's ratio obtained from experiments and 3-D random Mori - Tanaka calculations with and without voids at -4°F | 174 |
| Figure 4.52 | Comparison of Young's modulus obtained from experiments and 3-D random Mori - Tanaka calculations with and without voids at-65°F | 175 |
| Figure 4.53 | Comparison of Poisson's ratio obtained from experiments and 3-D random Mori - Tanaka calculations with and without voids at -65°F | 175 |
| Figure 4.54 | Stress vs. strain curves for linear and non- linear materials | 176 |

| | | |
|---|---|---|
| Figure 4.55 | Stress vs. strain curves for viscoelastic behavior and lost energy | 177 |
| Figure 4.56 | Calculation of secant Young's modulus from nonlinear material curve at 120°F and 160°F | 177 |
| Figure 4.57 | Comparison of experimental and calculated Young's Modulus values at 120°F | 179 |
| Figure 4.58 | Comparison of experimental and calculated Young's Modulus values for at 160°F | 179 |
| Figure 4.59 | Representative Volume Element | 181 |
| Figure 4.60 | The boundary conditions and displacement loading for the 0.2% specimens | 185 |
| Figure 4.61 | The mesh structure of the finite element model | 186 |
| Figure 4.62 | Distribution of stresses in y- direction ($\sigma_{yy}$) at the particle plane | 187 |
| Figure 4.63 | Distribution of y-component of displacement ($U_{yy}$) | 188 |
| Figure 4.64 | Total force values in y-direction at the nodal points of the top surface ($TF_{yy}$) | 189 |
| Figure 4.65 | Total force values ($TF_{yy}$) at elements of the top surface | 190 |
| Figure 4.66 | Comparison of $E/E_m$ values obtained from the experimentally, Mori-Tanaka calculation and the finite element model at -65°F | 193 |
| Figure 4.67 | Comparison of $E/E_m$ values obtained from the experimentally, Mori-Tanaka calculation and the finite element model at -4°F | 193 |
| Figure 4.68 | Comparison of $E/E_m$ values obtained from the experimentally, Mori-Tanaka calculation and the finite element model at room temperature | 194 |
| Figure 4.69 | Comparison of $\nu_{12}/\nu_m$ values obtained from the experimentally, | 194 |

Mori-Tanaka calculation and the finite element model at -65°F

Figure 4.70 Comparison of $\nu_{12}/\nu_m$ values obtained from the experimentally, Mori-Tanaka calculation and the finite element model at -4°F 195

Figure 4.71 Comparison of $\nu_{12}/\nu_m$ values obtained from the experimentally, Mori-Tanaka calculation and the finite element model at room temperature 195

## 1. INTRODUCTION

Since the 1960's composites have been studied extensively due to their high strength to weight and stiffness to weight ratios and tailorability. Conventional composites consist of a matrix (in many cases a polymeric resin) reinforced with fibers or fabrics. Composites have enjoyed a spectacular success as evidenced by their widespread use in military and commercial aircraft, the automotive industry, sporting goods and even health care products. However, the new trend in structural material design is to make the material multifunctional, i.e. to impart to it thermal, electrical, optical properties in addition to the conventional properties of strength, stiffness and impact and fatigue resistance. One way of making the material multifunctional is with nanoadditives. With the recent advances in nanotechnology resin systems have been developed with carbon nanotubes (CNTs), nanoclay particles or flakes, carbon black, etc. to achieve new properties for multifunctionality. In this research, we propose to study the properties of nanoclay reinforced polymers through an experimental and analytical/numerical program.

The polymer/nanoclay composites will not be strong enough by themselves to be used as structure materials. Thus, they need to be reinforced with fibers or fabrics. It is believed that the reinforcement of polymers with nanoclay may improve the strength, stiffness and high temperature resistance of the polymer which in turn may help to reduce its flammability and also toxicity. Thus the main application of using nanoclay additives in polymeric composite systems is to improve their fire retardancy properties, and also reduce toxicity which may ensure as a consequence of fire.

Research in reinforced polymeric nanocomposites has been increasing at a fast pace due to their potential for improved mechanical and chemical properties compared to conventionally filled

composites [1-5]. These improvements may include increased strength [6], higher modulus [7-12], thermal stability [13-15] and decreased flammability [16-20]. After reinforced with fibers or fabrics a structural material able to resist static and dynamic loads can be obtained.

The polymer/nanoclay composite specimens used in this research were manufactured by injection molding Novus Technologies Corporation as ASTM standard Type I dog-bone shaped specimens with varying weight fractions of nanoclay (0%, 0.2%, 1%, 3%, 6% and 10%). Three different polypropylenes (PP) and one type of epoxy namely, EPON 828 were also used as resin. For most specimens PP 3371 was used as the resin. However, to study the effect of different types of PP, a limited number of specimens were manufactured with Borealis and Total Petrochemical 3868 polymers. Also 4"x4"x(1/8) " nanoclay reinforced PP specimens were subjected to low velocity drop weight tests.

Since the main objective of this thesis is to study the effect of temperature on nanoclay reinforced polymers, the specimens were subjected to tensile and low velocity impact loads at temperatures varying from -65ºF to 160ºF. To predict the experimentally determined nanocomposite properties a numerical/analytical model was developed.

## 1.1 OBJECTIVES OF THIS STUDY

The main objective of this thesis is to study the effect of temperature on nanoclay reinforced polymers. The research plan calls for subjecting the specimens to tensile and low velocity impact loads at temperatures varying from -65ºF to 160ºF. Also specimens with various nanoclay reinforcement percentage are used to ascertain the effect of nanoclay reinforcement on the properties of the nanocomposite. By using different polypropylene resins and epoxy, the effect of different resins is also studied. To predict the experimentally determined nanocomposite

properties, micromechanics based models supplemented with 3-D finite element calculations are developed.

## 1.2 CONTRIBUTIONS OF THIS STUDY

The most important contributions of this thesis are: a) determining the effect of nanoclay reinforcement on the mechanical properties of various resins b) determining the effect of temperature on the mechanical properties of the nanocomposites c) using different resins to ascertain the effect of resin on the nanocomposites and d) developing analytical/numerical methods which include the effect of temperature to predict the observed properties of the nanocomposite without conducting expensive and time consuming experiments.

## 2. LITERATURE REVIEW

The literature on composite material systems under mechanical and hygrothermal loadings is extensive. Accordingly, we will restrict our literature review to nanoclay reinforced polymers and related topics.

Since the 1980's, research in polymer based nanocomposites has increased dramatically with the production of nylon-clay nanocomposites by Toyota [1,21] and their actual or potential applications in diverse areas, such as aerospace components, automotive structures, military equipment, etc.

As stated in [22] "two main types of polymer-clay morphology can be obtained depending on the interaction between the clay and the polymer matrix: namely, intercalated and exfoliated. Usually exfoliated nanocomposites are preferred because of showing the best property improvements [23]". The improvement of the material properties in nylon/clay nanocomposites was demonstrated by the Toyota research group [24]. Also many researchers investigated numerous other polymers. Some of the polymers include polypropylene [25-70], polyethylene[71-80], polystryrene [81-87], poly(ethylene oxide) [88-92], polycaprolactone [93,94], polyimides [95-112], polycarbonate [113,114], and epoxy resin [115-119].

The usage of nanoscale fillers in polymers has provided an opportunity to design new materials with significantly improved performance and multifunctionality.

Ongoing research and studies have shown that, in general, polymer based nanocomposites exhibit great improvement in mechanical properties such as strength and stiffness compared to pure polymers with the addition of minimal amount of nanosize clay particles [120-128].

The nanoclay related studies found in the literature are grouped around a common characteristic. The review is given below.

## 2.1. STUDIES ON THE CHARACTERIZATION OF POLYMER/CLAY NANOCOMPOSITES

Recent research shows that processing variables have a significant effect on the mechanical properties of polymer/ clay nanocomposites (PCNs). There are several studies on the effects of processing variables and characterization of nanocomposites.

The basic physical and chemical properties of (PCNs) are crucial in engineering studies. Characterization tools also are extremely important in obtaining these properties. Several techniques have been used to characterize the nanocomposites [129]. Wide-angle X-ray diffraction (WAXD), small-angle X-ray scattering (SAXS), scanning electron microscopy (SEM) and transmission electron microscopy (TEM) are the commonly used techniques in characterization of nanocomposite [130, 131]. TEM allows a qualitative understanding of the internal structure, spatial distribution of the various phases and views of the defect structure through direct visualization [132].

Nam [133] focused on advanced preparation methods for PCNs by following previous research which dealt with the complete exfoliation of silicate layers in the polymer matrix [134, 135] and succeeded in preparing well-ordered intercalated polypropylene (PP)/clay nanocomposites (PPCNs) with melt extrusion process [136]. Identification of the hierarchical structure was conducted by using wide-angle X-ray diffraction (XRD), small-angle X-ray scattering, transmission electron microscopy (TEM), polarizing optical microscopy and light scattering to discuss the structure-property relationships of PPCNs having various clay particles [136]. The

limitation of the exfoliation toward the individual silicate layers is observed as an effect of the increment of intercalation.

Wu [137] prepared nanoparticles filled polypropylene nanocomposites with pre-grafted nanoparticles by some polymers using irradiation. Transmission electron microscopy (TEM) was used to observe the appearance of the irradiation grafted nanocomposites. Sharma [138] studied polypropylene/surface modified clay nanocomposites and followed a different preparation method. Transmission electron microscopy (TEM), X-ray diffraction and scanning electron microscopy (SEM) were used to understand exfoliation structure and morphology, respectively.

Rohlman [139] studied the preparation of polypropylene (PP) based nanocomposites by melt mixing using modified polypropylene and various organophilic montmorillonites. Scanning electron microscopy (SEM) was used for examination of the morphology and X-ray diffraction (XRD) was used to analyze the structure of the material. It was found that organophilic montmorillonites have strong effect on the morphology of the nanocomposite for given processing and composition conditions.

Epoxy is another polymer used with nanoclay and there are many ongoing studies on epoxy-clay nanocomposites. Wang [140] prepared epoxy-clay nanocomposites using two organoclays which were cured with various chemicals at different temperatures. TEM and X-ray diffraction (XRD) were used to understand the interlayer distance of the clay layers. In this study Wang showed that the relative curing speeds of extralayer and interlayer played a big role in determining clay exfoliation. It was also shown that the curing speed of inter and extralayer intercalated epoxy/clay is the key factor of exfoliation. Jiankun [141] focused on the exfoliation behavior of organoclays in epoxy resin. X-ray diffraction was used to obtaine exfoliation and intercalation

properties of organoclyas. Also the nature of the clays and the curing agent used to determine the exfoliating ability of the organoclays was also investigated. Xu [142] also studied the intercalation and exfoliation behavior of epoxy resin in the presence of organophilic montmorillonite. It was observed that exfoliation and intercalation properties are not affected by curing condition. Kornmann [143] explored a different processing method to obtain epoxy-clay nanocomposites. The nanocomposites were obtained using different caution-exchange capacities (CEC) and two montmorillonite clays (MMT). X-Ray diffraction (XRD), TEM and SEM were used to investigate the dispersion of clay. The most important conclusion of this study is that the caution-exchange capacity of the clays affects the intercalation between the layers. SEM observations showed that a better dispersion of the clay particles in the nanocomposite compared to conventional nanocolay based composites. Sarathi [144] studied on the exfoliation characteristics in epoxy nanaocomposites with wide-angle X-Ray diffraction (WAXD); Saber-Samandari [145] used TEM to investigate the effect of different types of clay with various processing conditions on intercalation/exfoliation of clay/epoxy nanocomposites; and Yasmin [146] determined the exfoliation and intercalation characteristic of epoxy based nanocomposites with different type of clays using TEM. As a result a classification was obtained as to which modified clay and which processing method produced better intercalation/exfoliation.

In some of these studies mechanical properties were discussed in light of better intercalation/exfoliation of nanoclay.

Several other studies have been reported on the property and structure of inorganic particle-polymer combinations which exhibited superior modulus and yield strength in association with high toughness [147-170].

## 2.2 STUDIES ON THE MECHANICAL PROPERTIES OF POLYMER/CLAY NANOCOMPOSITES

### 2.2.1 Experimental Studies

There is a large number of studies dealing with the mechanical properties of polymer/clay nanocomposites. Here we present the studies more related to our research.

Wu [137] performed tensile testing on low nanoparticles loaded polymer composites at five different cross-head speeds at room temperature. The effect of nanoparticles on stiffness, strength and toughness was determined. Simultaneous improvement in Young's modulus strength and elongation was observed. Sharma [138] measured mechanical properties such as tensile strength, tensile modulus and elongation at break in addition to studying the effects of organically modified clay on the physical, thermal and morphological properties of nanocomposites. Differential scanning calorimetry (DSC), thermo gravimetric analysis (TGA) and melt flow index (MFI) methods were used to determine the properties of polymer nanocomposites prepared with polypropylene/modified clays. Thermal and mechanical test results showed that the interaction of polymer and clay in nanocomposites have high effect on mechanical and thermal properties because of the favorable interface of nanoclay and matrix. Different manufacturing machinery, clay modifiers and conditions can significantly affect the resulting polymer nanocomposites [22]. In Dolgovskij [171], the effect of different mixer types on the exfoliation of polypropylene(PP) nanocomposites was explicitly demonstrated. In the same vein, the importance of extruder types on the delimitation and dispersion of layered silicate nanocomposites was shown by Dennis et al [172]. Another tried dispersion methods is the usage of supercritical carbon dioxide as a processing aid by Quang T. Nquen [173]. Galgali [174]

worked on the effect of clay orientation on the tensile modulus of polypropylene nanoclay composites and the relationship between clay orientation and shear rate. The test results indicate that for compatibilized nanocomposites the orientation of the clay increased with extrusion shear rate and for uncompatibilized nanocomposites the clay orientation was independent of the shear rate. Bureau [175] and Drozdov [176] performed similar studies on tensile testing of polypropylene-clay nanocomposites. Bureau used a polypropylene matrix with organo-modified clays. The nanocomposites showed significant improvement in Young's modulus and yield stress. Drozdov performed also tensile tests with different strain rates, creep tests with different stresses and relaxation tests at different strains at room temperature. Test results showed the effect of nanoclay reinforcement on mechanical properties and creep resistance. Clay types can have critical effect on the physical properties of the nanocomposites. To understand the effect of different clays, polypropylenes and preparation methods, Dong [177] performed tensile tests with PP/organoclay nanocomposites which were prepared by using three types of organomodified montmorillonite clay, three grades of PP and a twice direct compounding manufacturing method. The results showed that the PP grade plays the most significant role in the overall mechanical properties and clay content is the second most important factor. Santos [178] optimized the mechanical properties of polypropylene-clay nanocomposites with combination of two different modified clays. Tensile test results showed that the combination of two different clays caused an increase in flexural modulus and higher impact strength.

Beside studies on polypropylene/clay nanocomposites, there are also several studies on epoxy/clay nanocomposites. Yasmin [146] studied the mechanical and thermal behavior of epoxy/clay nanocomposites. Epoxy/clay nanocomposites were prepared by shear mixing using different types and concentrations of clay particles and the mechanical and viscoelastic

properties of the nanocomposites were obtained. Furthermore, the thermal expansion coefficient (CTE) was measured using a thermomechanical analyzer. Test results showed that the elastic modulus and storage modulus were improved and the thermal expansion coefficient was reduced by the addition of clay particles. Sarathi [144] studied the thermal, mechanical and electrical properties of epoxy/clay nanocomposites. Nanoclay reinforcement was increased to up to 5% wt to ascertain the effect of clay reinforcement. Short time breakdown voltage test, accelerated aging test, tracking test were used to analyze the electrical insulation characteristics of the nanocomposite. The thermal properties were obtained by thermogravimetric-differential thermal analysis (TG-DTA). The storage modulus of nanocomposites was obtained by dynamic mechanical analysis (DMA). All the test results showed that the breakdown strength, mechanical properties and the tracking time of epoxy nanocomposites were higher than those for the epoxy resin.

Saber-Samandari [145] manufactured clay/epoxy nanocomposites and performed several experiments including different types of clay with various processing methods such as different centrifuge rotor speeds and curing temperatures. The elastic modulus of epoxy-clay nanocomposites increased with the amount of clay up to a maximum of 6%. The tensile strength and energy to failure increased with clay percentage of up to 10%. Slower rotor speed gave the best results for the properties. On the other hand lower curing temperature led to better results while higher curing temperature caused specimen brittleness and deterioration of properties. Zhao [179] focused on the toughening mechanism of epoxy resin mixed with micro/nano particles and studied the effects of particle size on the maximum stress. The critical particle size for the material system was determined to be 0.95μm. Thus it was deduced that particle size should not be more than 0.95μm to reduce stress concentrations in the material.

### 2.2.2 Theoretical Studies

Compared to experimental studies, the number of publications on polymer/clay nanocomposites is relatively small. Fornes [180] applied the Halpin-Tsai and Mori-Tanaka re-enforcement theories to predict the modulus of nylon based nanocomposites. The modulus obtained using Mori-Tanaka calculation increased with nanoclay reinforcement as predicted. The Halpin-Tsai gave higher values for the modulus but still could be used to predict the value of modulus. Sheng [181] preformed a more detailed study on theoretical analysis of nanocomposites. A micromechanical model was developed to account for the morphology of the nanocomposite, particle volume fraction, particle aspect ratio, mechanical properties of matrix, exfoliated clay layer thickness and layer spacing. For each case the Halpin-Tsai and Mori-Tanaka models were applied to calculate the variation of the normalized Young's modulus of the nanocomposite with volume fraction, particle aspect ratio, layer thickness and layer spacing. In addition some calculated results were compared with tensile test data. Comparing the Halphin-Tsai and Mori-Tanaka results it was observed that the Mori-Tanaka calculations give closer results to the tensile test data.

Drozdov [176] studied the viscoelasticity and viscoplasticity of polypropylene/clay nanocomposites. New constitutive equations were developed taking into account the viscoelasticity and viscoplasticity of the nanocomposite and these equations were used to analysis of the time-dependent response in long-term creep tests. The results show the time to failure of nanocomposites exceeds that of polypropylene for all stresses.

Sheng also presented in [181] a FEM model to estimate the Young's modulus of polymer/clay nanocomposites with the representative volume element constructed using TEM results. The

plane strain FEM simulation results for the normalized Young's modulus of the nanocomposite were compared with those obtained from the Mori-Tanaka model. The main reason for comparing the FE results with the Mori-Tanaka model solution is that it gives the most accurate estimates among analytical models [182]. Sheng [181] also compared the experimental data with Halpin-Tsai, Mori-Tanaka and FEM results. The comparison shows that the Mori-Tanaka model and FE simulation are in good agreement with experimental data, while there is more deviation with the Halpin-Tsai calculations.

## 2.3. STUDIES ON THE LOW VELOCITY IMPACT RESPONSE OF POLYMER/CLAY NANOCOMPOSITES

There are not many studies on the impact response of polymer nanocomposites. Generally impact tests are performed on fiber (nano)composites which include polymer/clay mixture as a matrix and fibers for reinforcement. Because of their brittleness under impact polymer/clay nanocomposites are more prone to damage than conventional fiber or fabric reinforced composites. There are few studies on low velocity impact test of polymer/clay nanocomposites and many on fiber reinforced polymer/clay nanocomposites.

Yuan [183] studied and analyzed the micromechanism of deformation during impact loading of polypropylene-clay nanocomposites. The temperature range was 0ºC to +70ºC during impact loading and in this range the addition of clay to polypropylene increased the impact strength for low nanoclay percentage. Furthermore, Yuan used differential scanning calorimetry (DSC), dynamic mechanical analysis (DMA), transmission electron microscopy (TEM), wide-angle X-ray diffraction (WAXD) and scanning electron microscopy (SEM) techniques to understand the behavior of polypropylene/clay nanocomposites. The crystal structure and dispersion of nanoclay

particles affected the toughness of nanoclay reinforced PP composites. Lin [184], performed low velocity impact tests on polymer and two different nanocparticle reinforced composites. The impact strength of the nanocomposites was improved somewhat by the filler content. The impact energy and the corresponding initial velocity for the two nanocomposites were determined and showed to have a linear relationship with the impact results. Also it was noted that the impact strength of nanocomposites is extensively affected by the temperature, geometry, type of filler content, volume and dispersion of the nanoparticles. Iqbal [185] investigated the impact damage resistance of carbon fiber nanaoclay filled epoxy composites. Up to 3 % wt inclusion of nanoclay in the matrix helped to lower the impact damage size, and improve the damage tolerance. Ye [186] used epoxy-based nanocomposites with natural nanotubes which were manufactured with a process similar to solution intercalation of layered silicate into polymers [187, 188]. The test results showed that blending epoxy with 2.3 wt % nanotubes caused to obtain higher impact strength.

## 2.4. STUDIES ON THERMAL RESPONSE OF POLYMER/CLAY NANOCOMPOSITES

The main objective of this thesis is to ascertain the temperature effect on polymer/clay nanocomposites. Literature search showed that there are not many studies on the temperature effect.

Most of the temperature studies are related to curing temperature, temperature of resin and hardener during processing, thermal stability of nanocomposites etc. Studies do not include the temperature effect on material properties, except for [146] which deals with epoxy based nanocomposites.

Yasmin [146] studied the temperature effect on the elastic modulus of epoxy based nanocomposites. Epoxy/ clay nanacomposites with 1%-10% clay reinforcement were considered. The elastic modulus of the nanocomposites was measured at various temperatures. The nanocomposites exhibited higher elastic modulus with higher clay reinforcement percentage but lower stiffnes at higher temperatures. Yasmin [146] also studied on the thermal expansion coefficients and showed that the thermal expansion coefficient was reduced with incorporation of clay particles.

Other studies focus on the thermal stability of nanocomposites because it is expected that the inclusion of clay flakes increase thermal stability while promoting flame retardancy. Blumstein [189] studied the thermal stability of polymethyl methacrylate (PMMA). He showed that the thermal stability of PMMA with montmorillonite clay was higher than pure PMMA. Guo [190] worked on the thermal behavior of nanocomposites made of polypropylene and organically modified clays. Thermal gravimetric method was used to obtain thermal behavior of the nanocomposites. The results showed that thermal stability increased with the addition of nanoclay into the pure polypropylene matrix. Kashiwagi [191] studied the thermal stability of polyamide 6/clay nanocomposites and samples were tested from 30ºC to 800ºC. The results showed that the inclusion of clay flakes caused a reduction in the peak heat release rate. Qin [192] also studied the thermal stability of polypropylene/montmorillonite nanocomposites. The results showed that the addition of clay particles increased the decomposition temperature of PP resin. Also the peak heat release rate of combustion reduced with addition of clay particles. Modesti [193] used the thermogravimetric analysis with a heating rate from room temperature to 900ºC to predict the thermal stability of polypropylene nanocomposites. It was claimed that the composition of the nanocomposites plays an important role in determining thermal stability. The

results of thermogravimetric analyses showed that the inclusion of clay increased thermal stability.

## 2.5. STUDIES ON FIRE RETARDATION AND TOXICITY RESPONSE OF POLYMER/CLAY NANOCOMPOSITES

Polymer/clay nanocomposites may be used in structural composites for vehicles. Beyond structural integrity, fire retardation or flame retardancy and toxicity are considered as critical issues. Gilman [194] reviewed the flame retardation properties of nanocomposites. Heat release rate, peak of heat release rate, heat of combustion, etc. are important parameters measured by cone calorimetry in the flame retardant behavior of nanocomposites. The main process to test fire retardation is to expose the sample to a heat flux and record the heat release rate as a function of time. In clay reinforced nanocomposites a significant reduction in the peak of heat release rate is observed. Gilman [195] showed that the effect of the exfoliated and/or intercalated structures on the flame retardancy. Guo [190] studied the flame retardancy behavior of neat polypropylene and polypropylene/clay nanocomposites. Neat polypropylene burned easily, yielded a sharp heat release rate and produced a large amount of smoke, while polypropylene/clay nanocomposites had reduced values of heat release rate. Furthermore, the dispersion of clays in the matrix affect the flame retardancy, such that if the clay flakes are well dispersed in the polypropylene nanocomposite, then high rate of flame retardancy is observed. Kashiwagi [191] performed a study on flammability properties of polyamide 6/clay nanocomposites with 2% and 5% weight fraction of clay. The results showed that, increasing the weight fraction of clay had the effect of increasing the ignition delay time and reducing the peak heat release rate. An important result obtained from this study is that the level of clay in the nanocomposite does not significantly affect the reduction in total heat release. Qin [192] investigated the flammability properties of

polypropylene/montmorillonite (PP/MMT) nanocomposites and observed reduction of flammability of the nanocomposites. To study the flammability properties of polypropylene (PP) nanocomposites, Modesti [193] used the glow wire test and concluded that the dispersion of nanoclays in PP resin with compatibilizer leads to an enhancement of fire resistance.

All the studies show that adding nanoclay to the polymeric resin greatly improves the fire behavior of nanocomposites.

# 3. EXPERIMENTAL STUDY ON POLYMER/CLAY NANOCOMPOSITES

## 3.1 THE SPECIMENS AND MATERIALS

Novus Technologies Corporation, manufactured nanoclay reinforced Polypropylene (PP) and epoxy Type I dog-bone shaped specimens for tensile testing, following ASTM D638-08: Standard Test Method for Tensile Properties of Plastics using injection molding. The main resins used were PP 3371 and epoxy with 0%, 0.2%, 1%, 3%, 6% and 10% nanoclay reinforcement by weight. Also additional specimens using two different resins, namely Borealis and Total Petrochemical 3868, were manufactured with 3% nanoclay reinforcement to ascertain the effect of resin on mechanical properties. Figure 3.1 shows the specimens for a) neat PP 3371, b) EPON 828 epoxy with 3% nanoclay reinforcement, c) Borealis and d) Total Petrochemical (TP) 3868 with 3% nanolcay reinforcement. Figure 3.2 shows the specimens which were instrumented with strain gages.

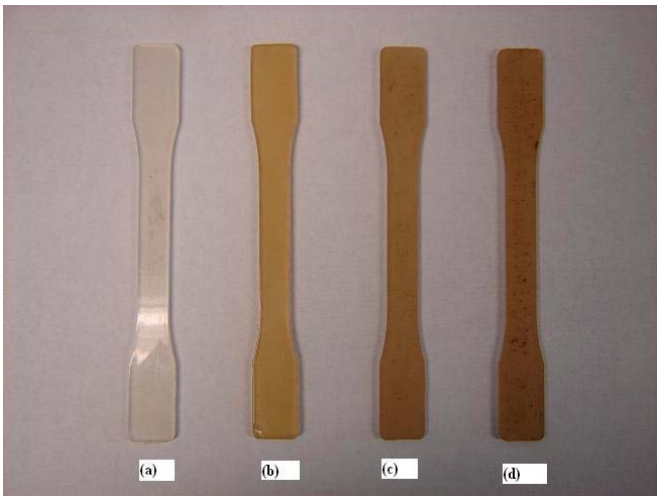


**Figure 3.1** Type I dog-bone shaped tensile specimens a) PP 3371, b) EPON 828, c) Borealis and d) TP 3868

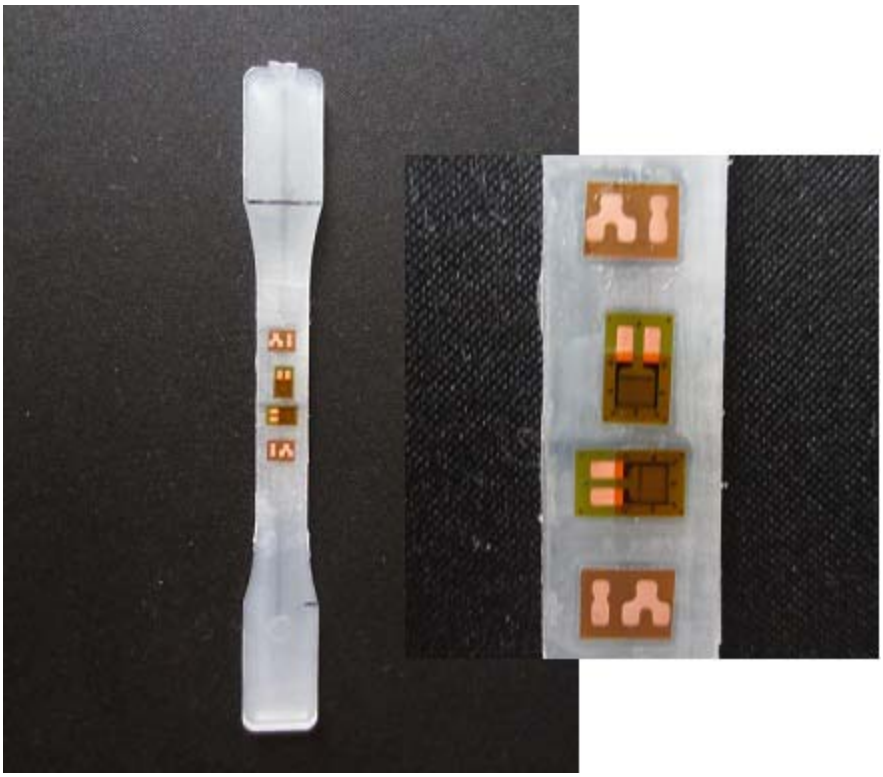

**Figure 3.2** PP 3371 specimen with attached strain gages

After tensile testing all the specimens at low, room and high temperatures, low impact drop-weight tests were performed at various temperatures on nanoclay reinforced Polypropylene (PP) 4"x4"x(1/8)" square specimens which were also manufactured by Novus Technologies Corporation. The main resin used was PP 3371 with 0%, 0.2%, 1%, 3%, 6% and 10% nanoclay reinforcement by weight. In Figure 3.3, the low velocity impact test specimen instrumented with strain gages is shown.

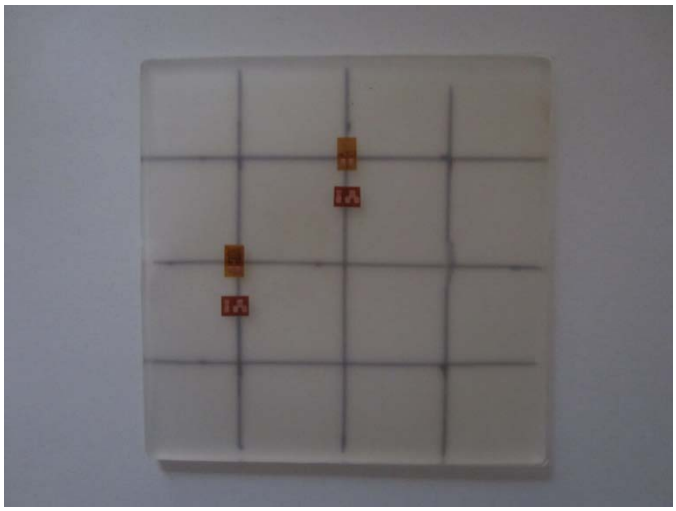

**Figure 3.3** Low velocity impact test specimen (PP 3371)

## 3.2 TENSILE TESTING

### 3.2.1 Effect of Nanoclay Reinforcement

The PP 3371 specimens were first subjected to room-temperature tensile loading at a crosshead speed of 5 mm/min in an MTS machine. Both loading and elongation histories were recorded through a National Instruments (NI)-DAQ based Lab View data acquisition system. The room-temperature stress-strain curves of PP 3371 specimens with various nanoclay reinforcements were then obtained using time-history readings from load-cell and crosshead motion. Stress - strain curves were plotted for each PP 3371 specimen with different nanoclay reinforcement with the strains calculated from the crosshead displacements. For each case 5 to 10 specimens were used and the stress - strain curves obtained are shown in Figures 3.4 - 3.9. One should note that the specimens did not fail and testing was stopped at a strain level of approximately 95%.

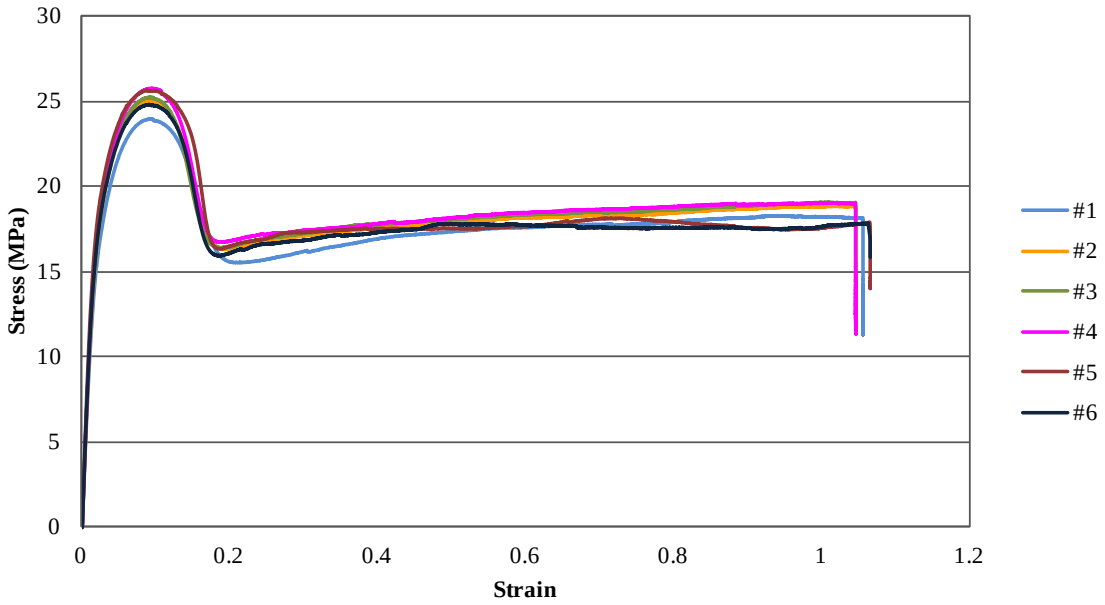


**Figure 3.4** Stress-strain curves of neat PP 3371 specimens

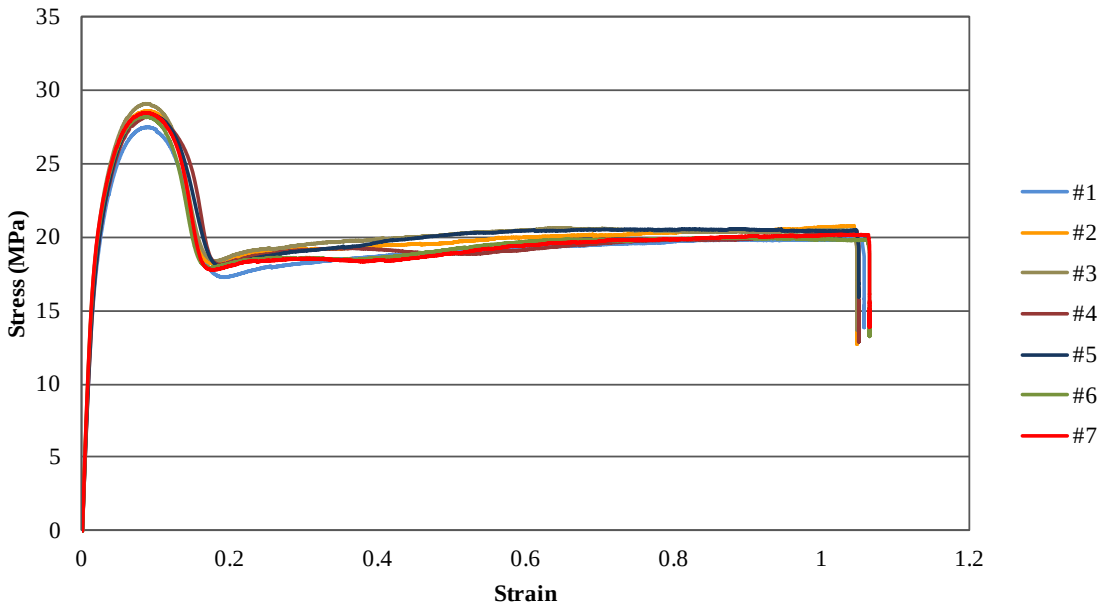


**Figure 3.5** Stress - strain curves of PP 3371 specimens with 0.2% nanoclay reinforcement

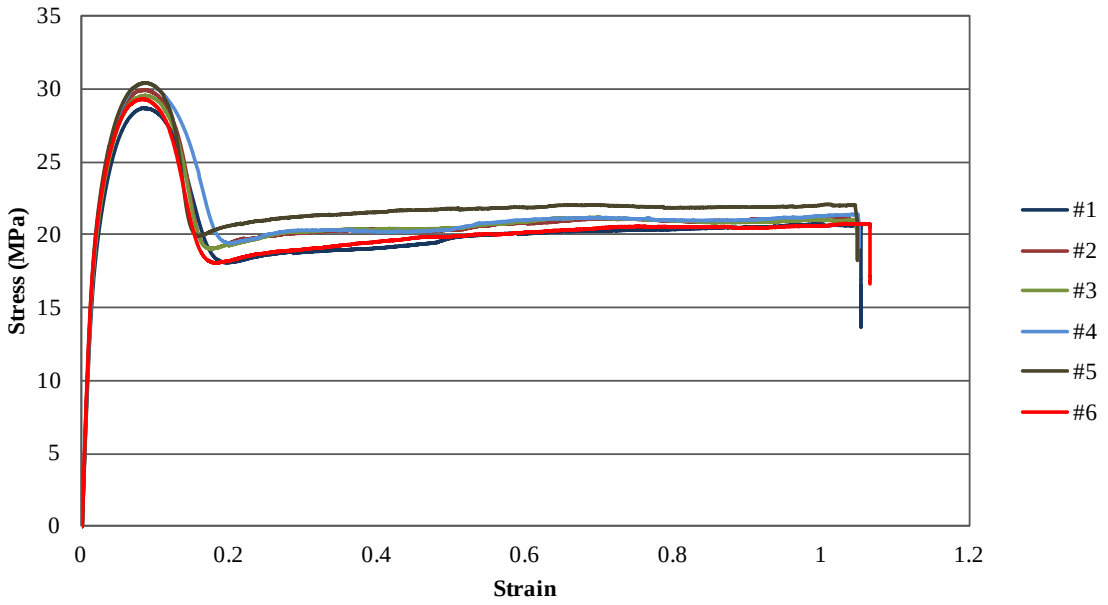


**Figure 3.6** Stress - strain curves of PP 3371 specimens with 1% nanoclay reinforcement

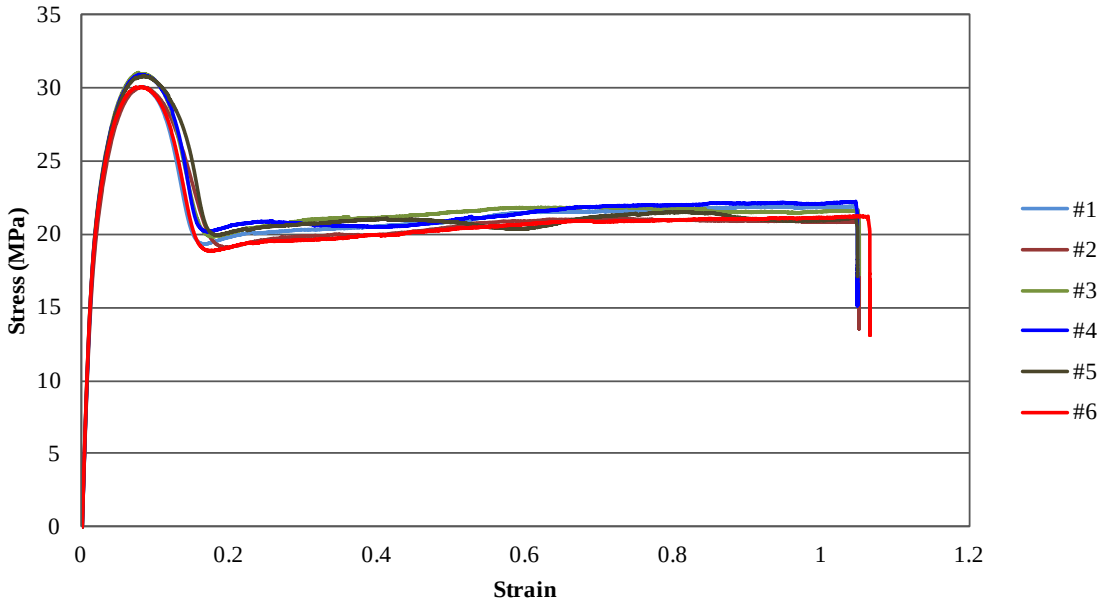


**Figure 3.7** Stress - strain curves of PP 3371 specimens with 3% nanoclay reinforcement

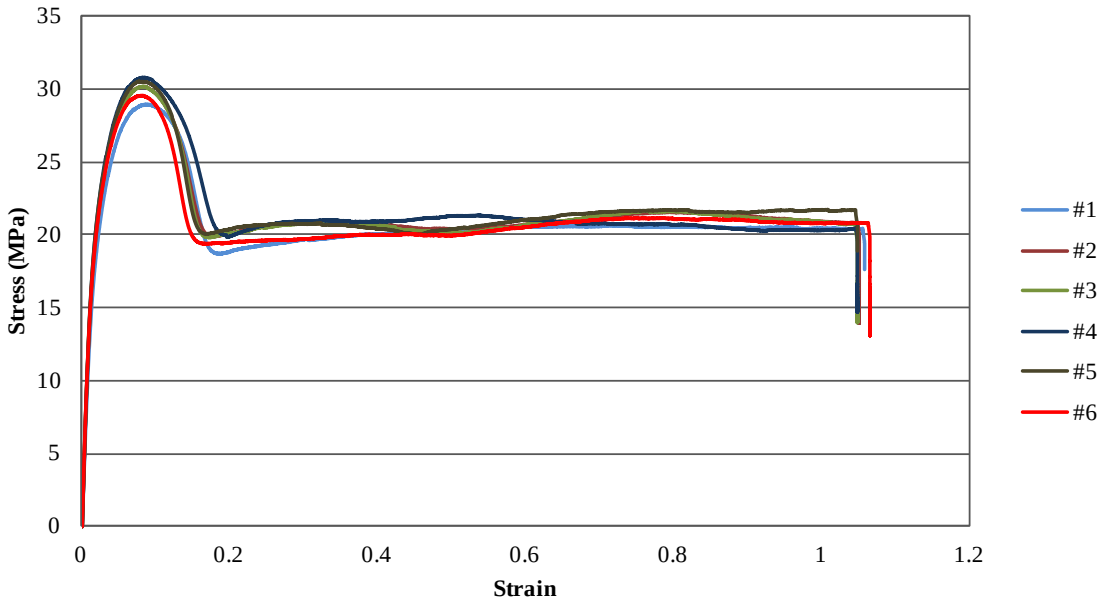


**Figure 3.8** Stress - strain curves of PP 3371 specimens with 6% nanoclay reinforcement

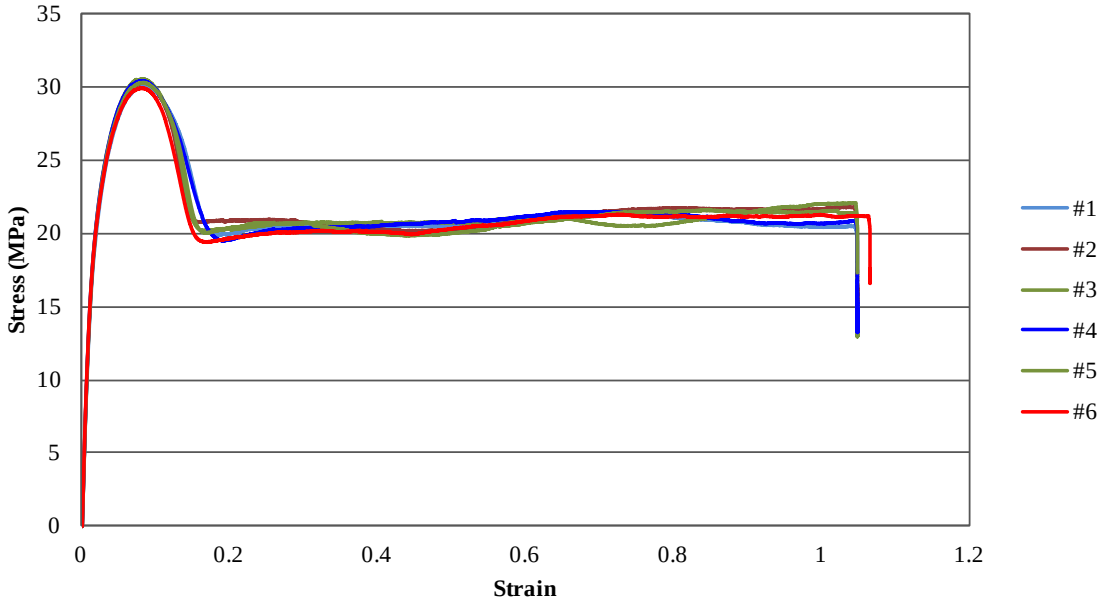


**Figure 3.9** Stress - strain curves of PP 3371 specimens with 10% nanoclay reinforcement

As shown in Figures 3.4 - 3.9, all PP 3371 specimens with various nanoclay reinforcements show the same behavior under tensile loading at room temperature. After the stress reaches its peak value necking occurs and none of the specimens failed at 95% strain.

Various percentages of nanoclay reinforcement were used to ascertain its effect on the mechanical properties of the resulting nanocomposites. Figure 3.10 shows the comparison of the stress - strain curves of PP 3371 specimens with 0%, 0.2%, 1%, 3%, 6% and 10% nanoclay reinforcement.

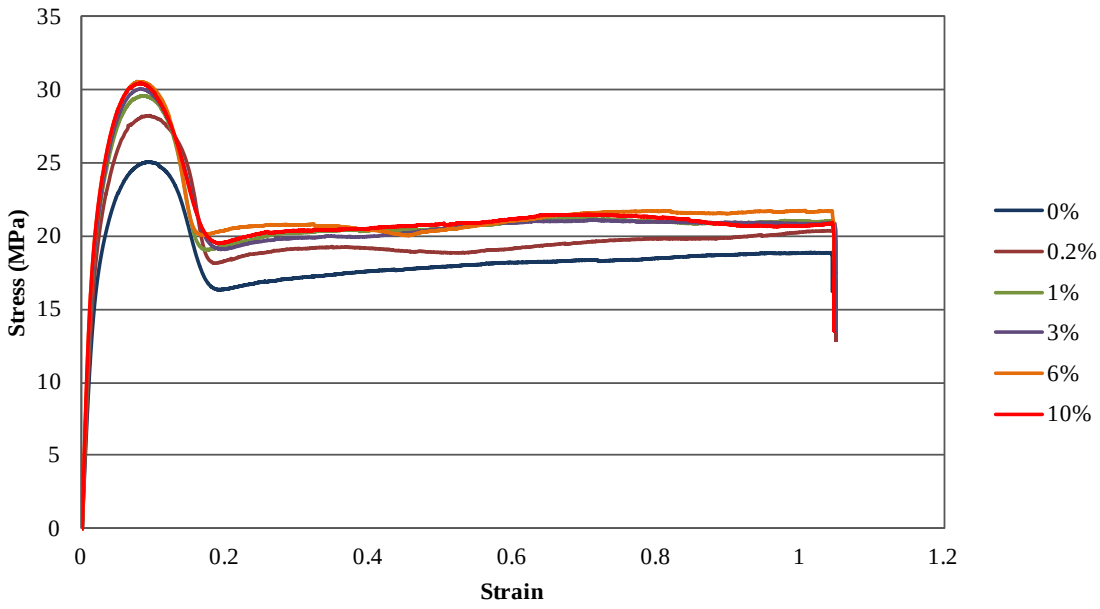


**Figure 3.10** Comparison of stress - strain curves of PP 3371 specimens with various nanoclay reinforcement percentages

The results in Figure 3.10 show that, as the percentage of nanoclay reinforcement increases the Young's modulus and the ultimate tensile stress of the nanocomposite also increase. Thus, the nanocomposite becomes stiffer and stronger with higher percentages of nanoclay. However, this effect becomes less pronounced for percentages above 3%. Average value of key mechanical properties, such as Young's modulus, ultimate tensile strength, strain at failure, etc., are given in Table 3.1.

**Table 3.1** Average values of material properties of PP 3371 specimens with 0%, 0.2%, 1%, 3%, 6% and 10% nanoclay reinforcement at room temperature

| PP 3371 with | Young's Modulus (GPa) (Average) | Poisson's Ratio (Average) | Ultimate Stress (MPa) | Strain at Ultimate Stress | End of Test Strain |
|---|---|---|---|---|---|
| **0%** | 1.200 | 0.3947 | 25.122 | 0.0745 | 1.0233 |
| **0.2%** | 1.317 | 0.4167 | 27.826 | 0.0668 | 1.0258 |
| **1%** | 1.508 | 0.4056 | 29.277 | 0.0661 | 1.0268 |
| **3%** | 1.628 | 0.3852 | 29.900 | 0.0653 | 1.0397 |
| **6%** | 1.646 | 0.3722 | 30.009 | 0.0659 | 1.0332 |
| **10%** | 1.742 | 0.3725 | 30.073 | 0.0658 | 1.0331 |

In addition to using time-history readings from load-cell and crosshead motion, a digital camera was used to capture the surface strain progression. The main reason for using the digital camera was to prove the reliability of the test results obtained from other methods. During the test a picture of the marked specimen was taken every 15 seconds and the strains were calculated by using the displacements obtained from the taken pictures. Figure 3.11 shows a marked specimen mounted in the MTS machine. The optical method was used for pure PP 3371 specimens and PP 3371 specimens with 10% nanoclay reinforcement. The stress - strain curves obtained using the crosshead displacements and the optical method for neat and 10% clay reinforced specimens are given in Figures 3.12 and 3.13 respectively and show remarkable consistency. Thus, one can use the strains calculated from the crosshead motion with some confidence.

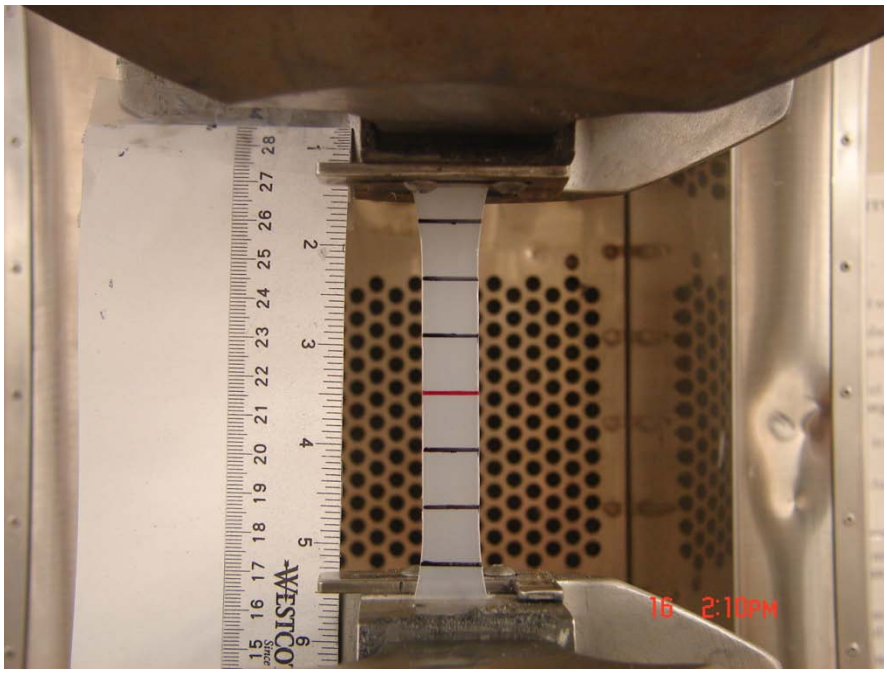

**Figure 3.11** A ruler and a marked specimen under tensile load

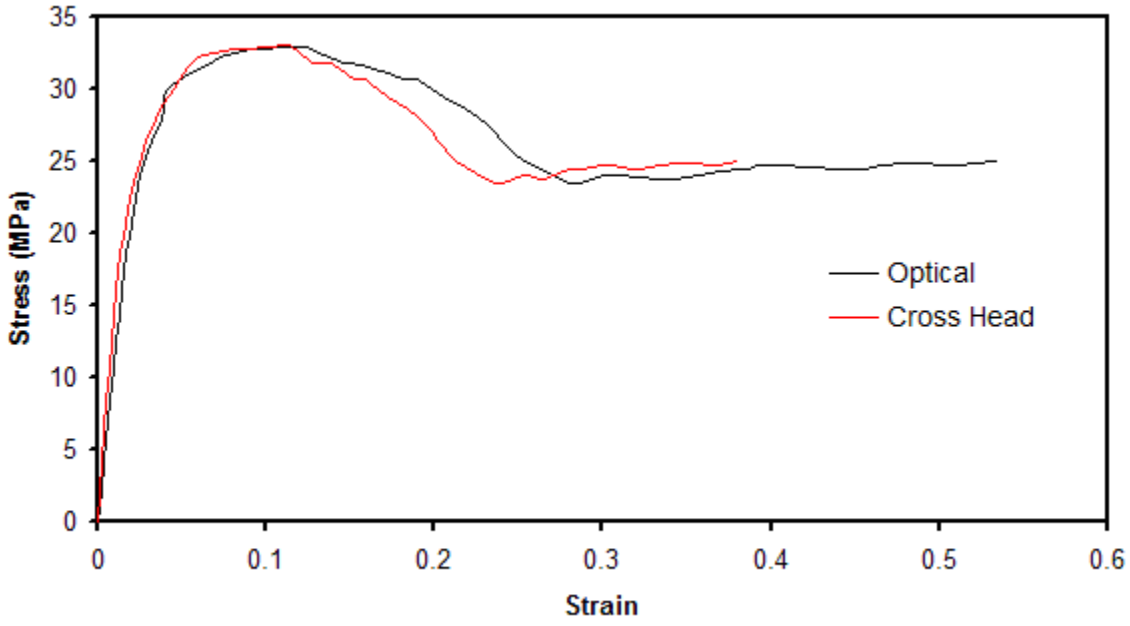


**Figure 3.12** Comparison of crosshead and optical stress-strain curves for neat PP3371 specimens

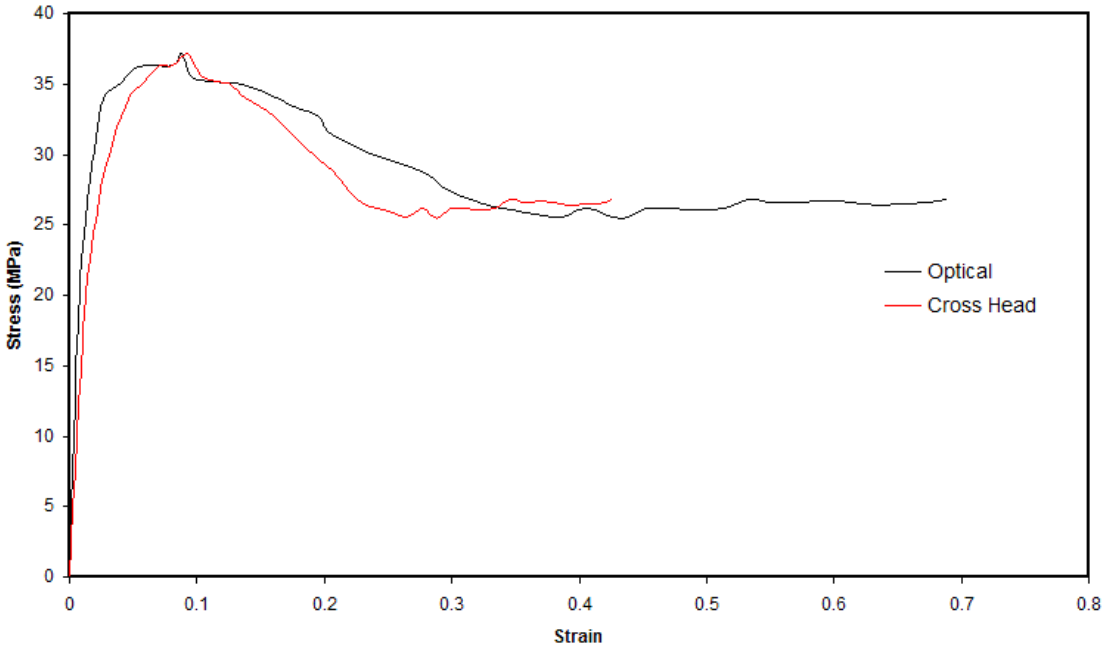


**Figure 3.13** Comparison of crosshead and optical stress-strain curves for PP 3371 specimens reinforced with 10% nanoclay

### 3.2.2 Effect of Temperature

The PP 3371 specimens with various nanoclay reinforcements were then subjected to tensile loading at different temperatures in an MTS machine with a crosshead speed of 5 mm/min. At high temperatures, the environmental chamber was used to perform the tensile tests at 160ºF (71ºC) and at 120ºF (49ºC). At low temperatures, the environmental chamber was cooled with liquid nitrogen to reach -4ºF (-20ºC) and then -65ºF (-54ºC). The stress-strain curves were plotted for each specimen with the strains calculated from the crosshead displacements. Poisson's ratio values were calculated from strain gage data.

3.2.2-a) Tensile test of PP 3371 at 160ºF (71ºC)

To obtain the properties of PP 3371 specimen with 0%, 0.2%, 1%, 3%, 6% and 10% nanoclay reinforcement at high temperatures the specimens were first subjected to tensile test at 160°F.

The stress - strain curves of PP 3371 specimens with various nanoclay reinforcement percentages are shown Figures 3.14 – 3.19.

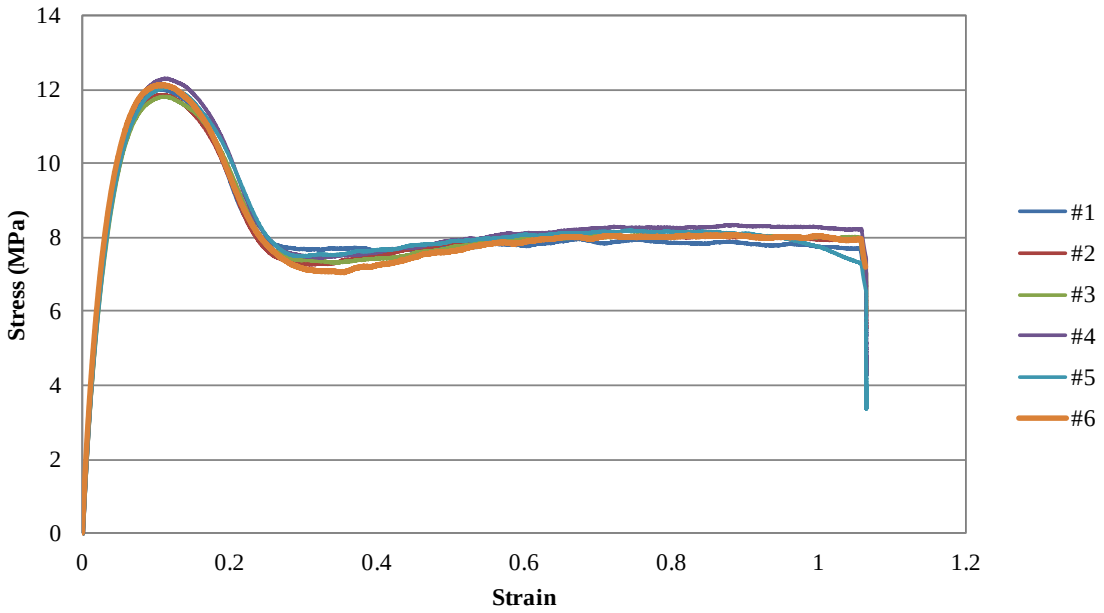


**Figure 3.14** Stress - strain curves of neat PP 3371 specimens at 160°F (71°C)

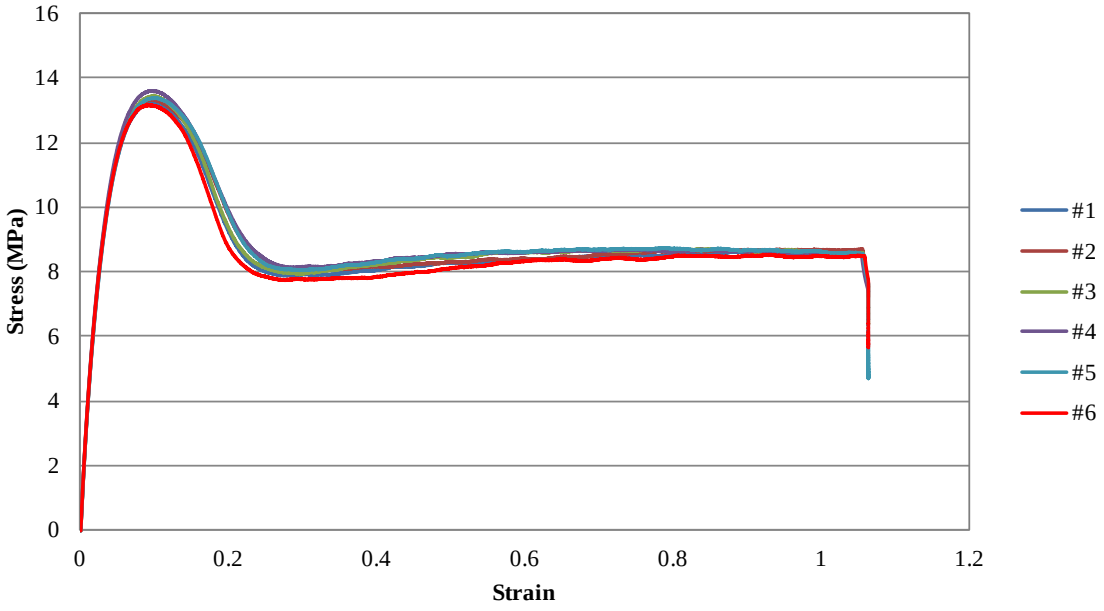


**Figure 3.15** Stress - strain curves of PP 3371 specimens with 0.2% nanoclay reinforcement at 160°F (71°C)

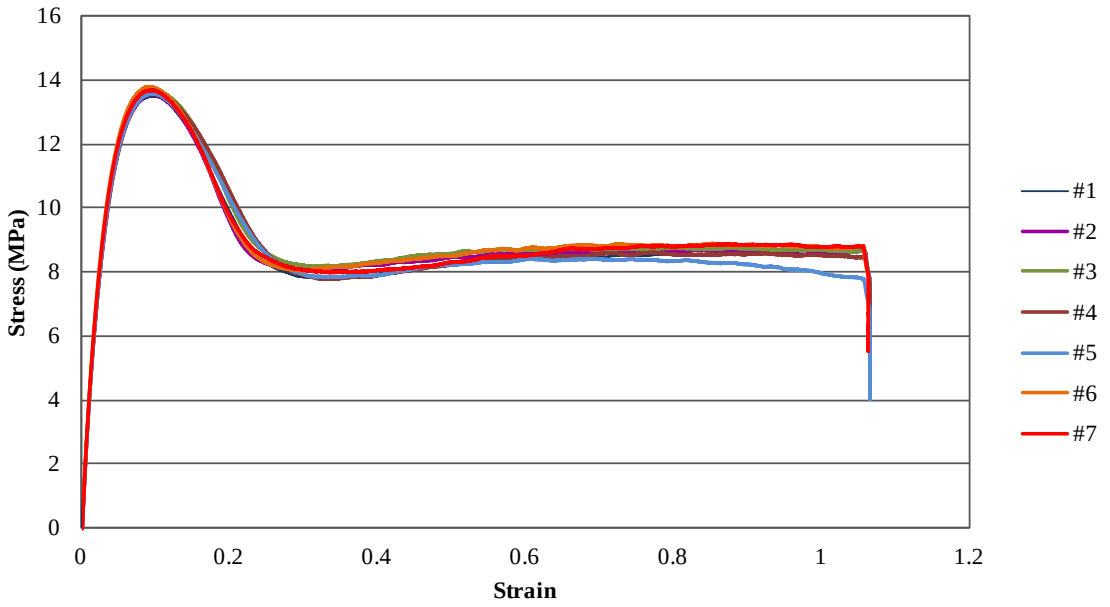


**Figure 3.16** Stress - strain curves of PP 3371 specimens with 1% nanoclay reinforcement at 160°F (71°C)

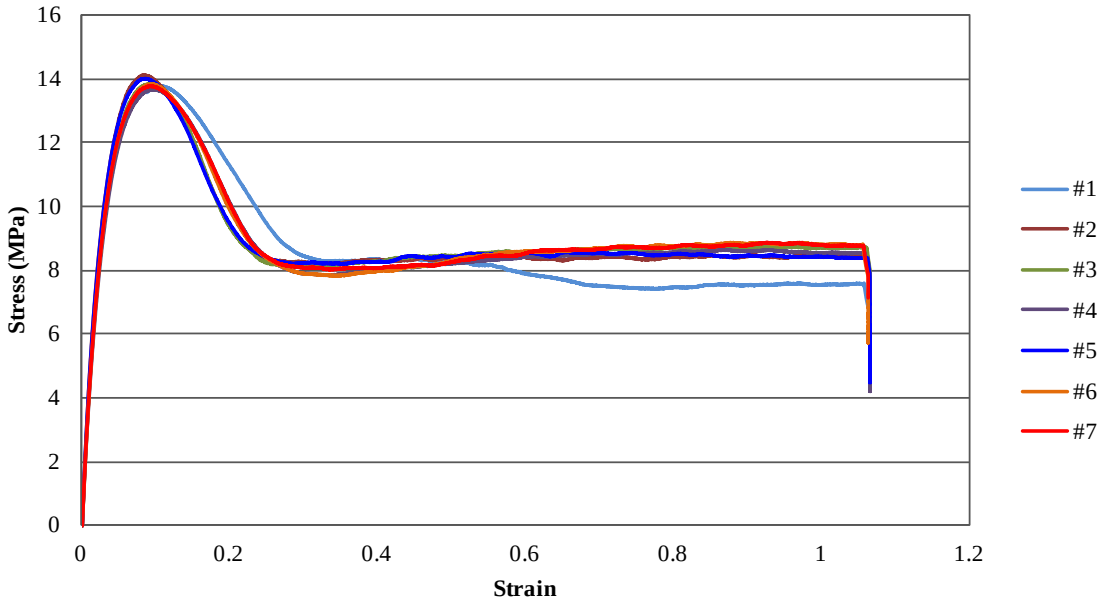


**Figure 3.17** Stress – strain curves of PP 3371 specimens with 3% nanoclay reinforcement at 160°F (71°C)

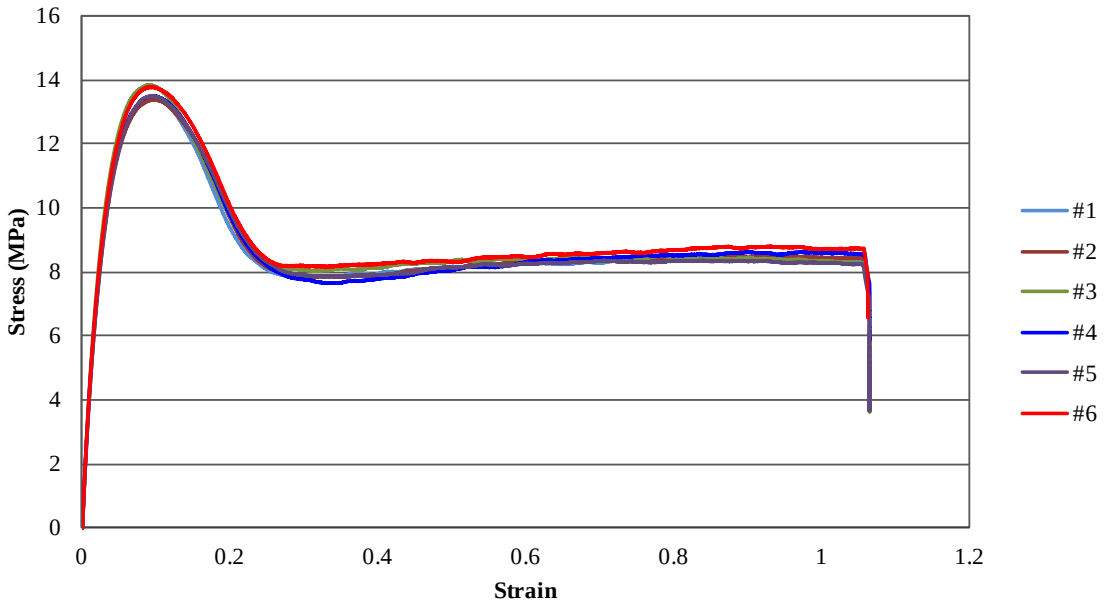


**Figure 3.18** Stress - strain curves of PP 3371 specimens with 6% nanoclay reinforcement at 160°F (71°C)

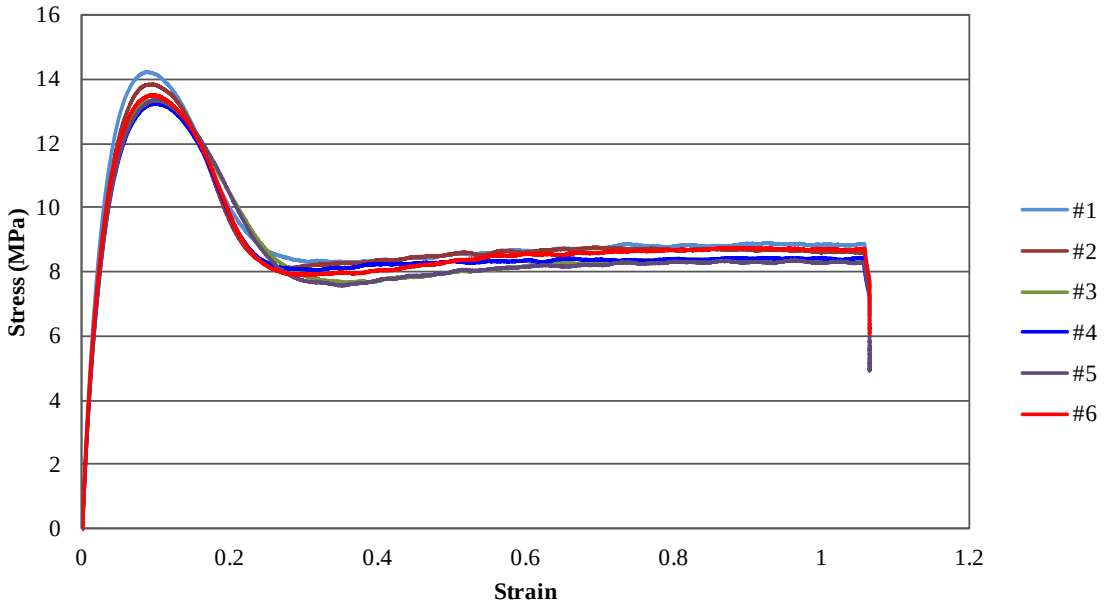


**Figure 3.19** Stress - strain curves of PP 3371 specimens with 10% nanoclay reinforcement at 160°F (71°C)

The results in Figures 3.14 – 3.19 are summarized in Figure 3.20 which depicts the effect of nanoclay reinforcement at 160°F (71°C).

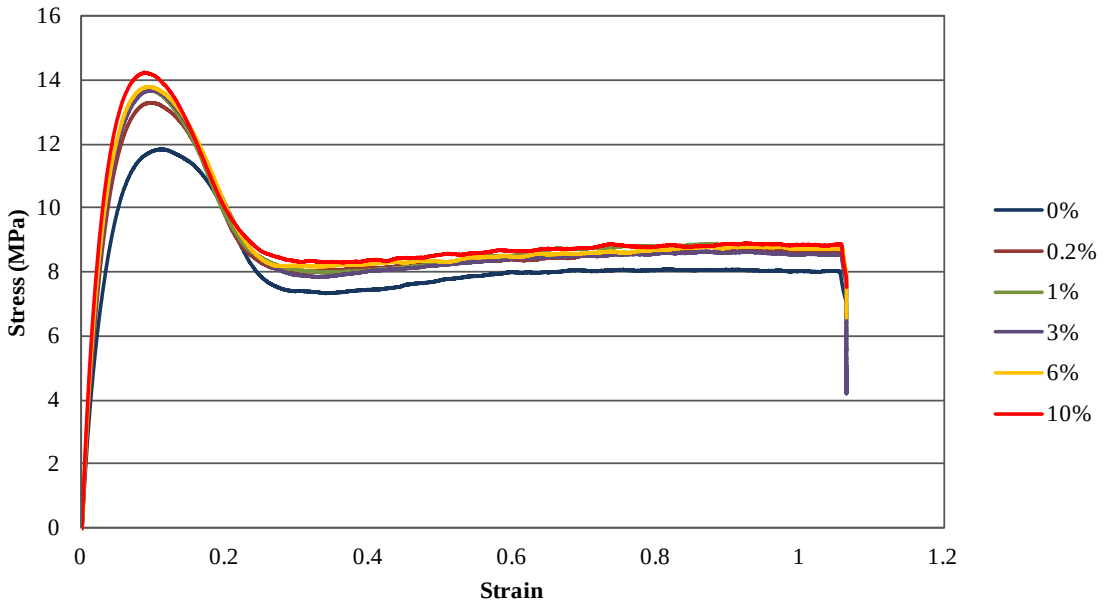


**Figure 3.20** Comparison of stress-strain curves of PP 3371 specimens with 0%, 0.2%, 1%, 3%, 6% and 10% nanoclay reinforcement at 160°F (71°C)

From the results shown in Figure 3.20, it is seen that at 160°F (71°C), an increase in nanoclay reinforcement leads to a higher Young's modulus and ultimate stress as was the case at room temperature.

Mechanical properties, such as Young's modulus, ultimate stress, etc. obtained at 160°F (71°C) are given in Table 3.2.

**Table 3.2** Average values of material properties of PP 3371 specimens with 0%, 0.2%, 1%, 3%, 6% and 10% nanoclay reinforcement at 160°F (71°C)

| PP 3371 with | Young's Modulus (GPa) (Average) | Poisson's Ratio (Average) | Ultimate Stress (MPa) | Strain at Ultimate Stress | End of Test Strain |
|---|---|---|---|---|---|
| **0%** | 0.392 | 0.4256 | 11.730 | 0.0819 | 1.0360 |
| **0.2%** | 0.449 | 0.4782 | 12.997 | 0.0725 | 1.0308 |
| **1%** | 0.465 | 0.4715 | 13.303 | 0.0732 | 1.0341 |
| **3%** | 0.497 | 0.4523 | 13.567 | 0.0713 | 1.0354 |
| **6%** | 0.503 | 0.5077 | 13.396 | 0.0774 | 1.0374 |
| **10%** | 0.515 | 0.4896 | 13.431 | 0.0791 | 1.0338 |

3.2.2-b) Tensile test of PP 3371 at 120ºF (49ºC)

Next the specimens were tested at 120ºF (49ºC). The stress - strain curves of PP 3371 specimens with various nanoclay reinforcement percentages are plotted with strains calculated from the crosshead displacements and shown Figures 3.21 – 3.26.

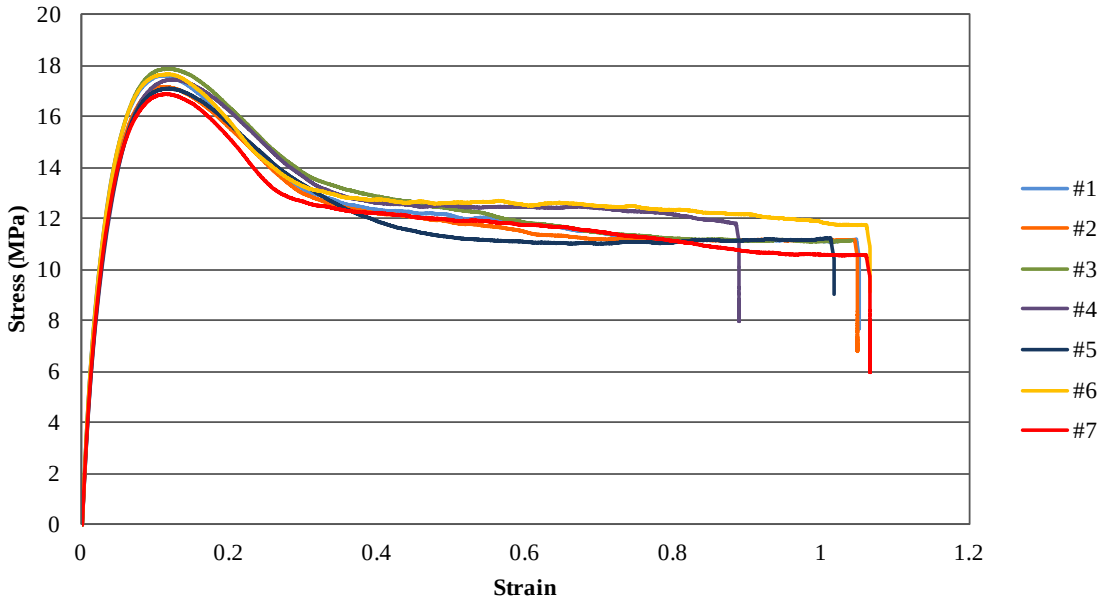


**Figure 3.21** Stress - strain curves of neat PP 3371 specimens at 120°F (49°C)

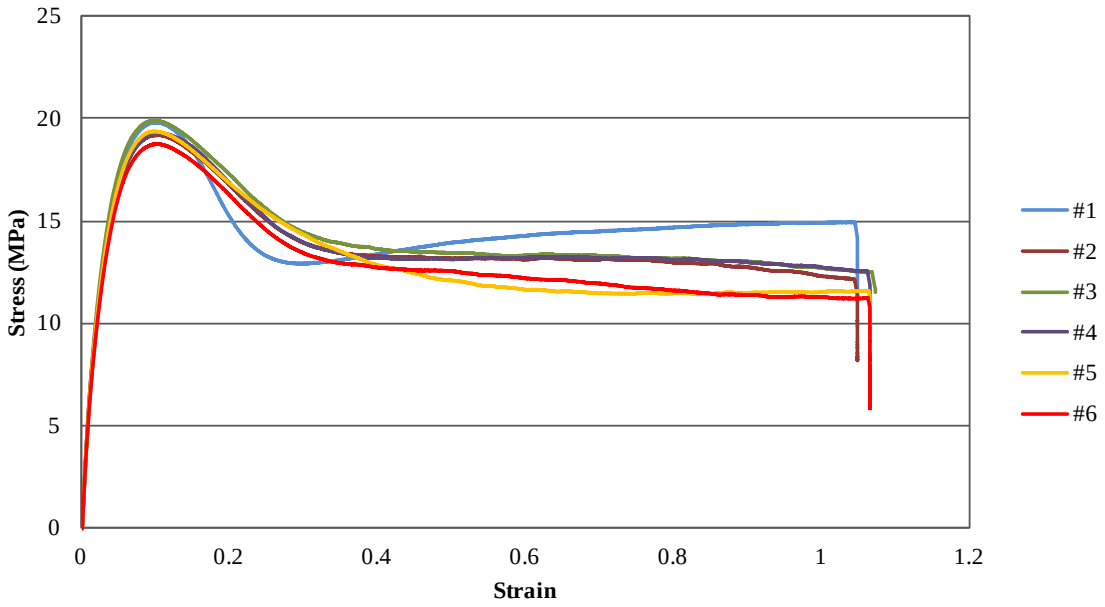


**Figure 3.22** Stress - strain curves of PP 3371 specimens with 0.2% nanoclay reinforcement at 120°F (49°C)

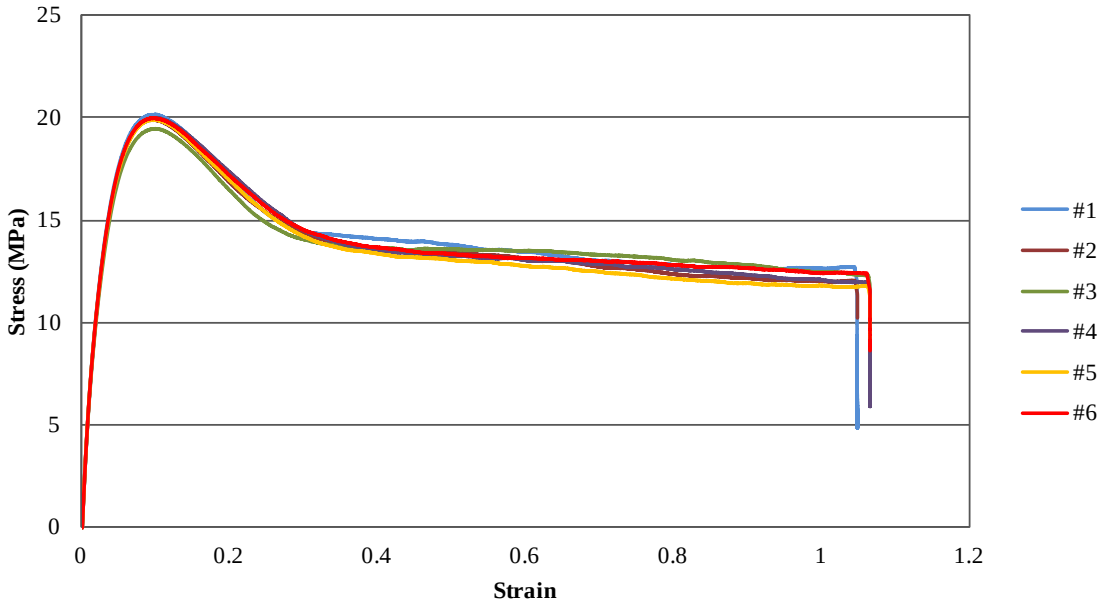


**Figure 3.23** Stress - strain curves of PP 3371 specimens with 1% nanoclay reinforcement at 120°F (49°C)

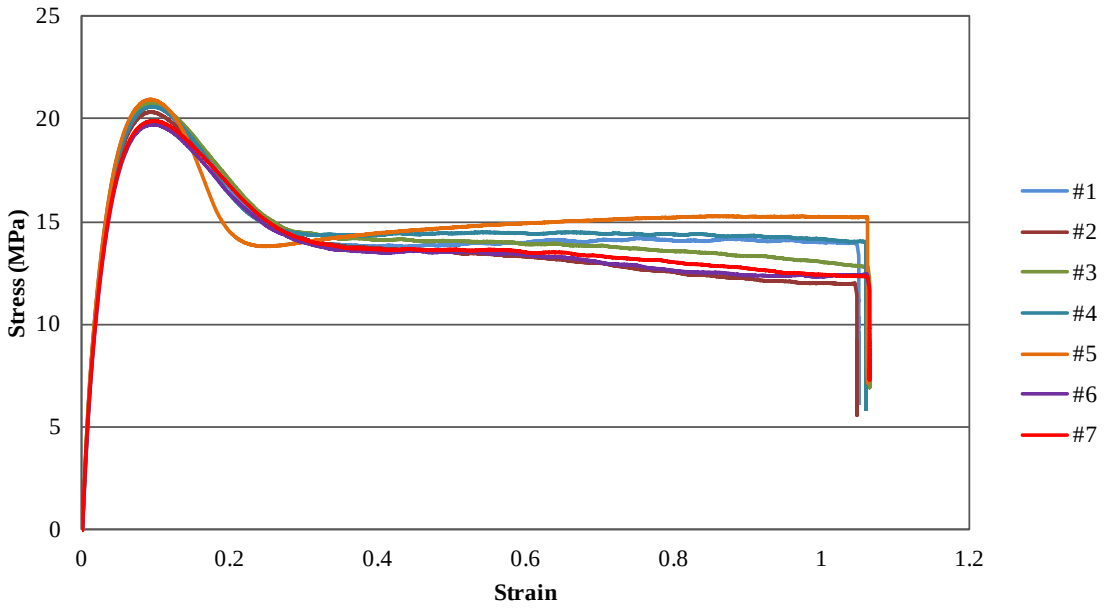


**Figure 3.24** Stress - strain curves of PP 3371 specimens with 3% nanoclay reinforcement at 120°F (49°C)

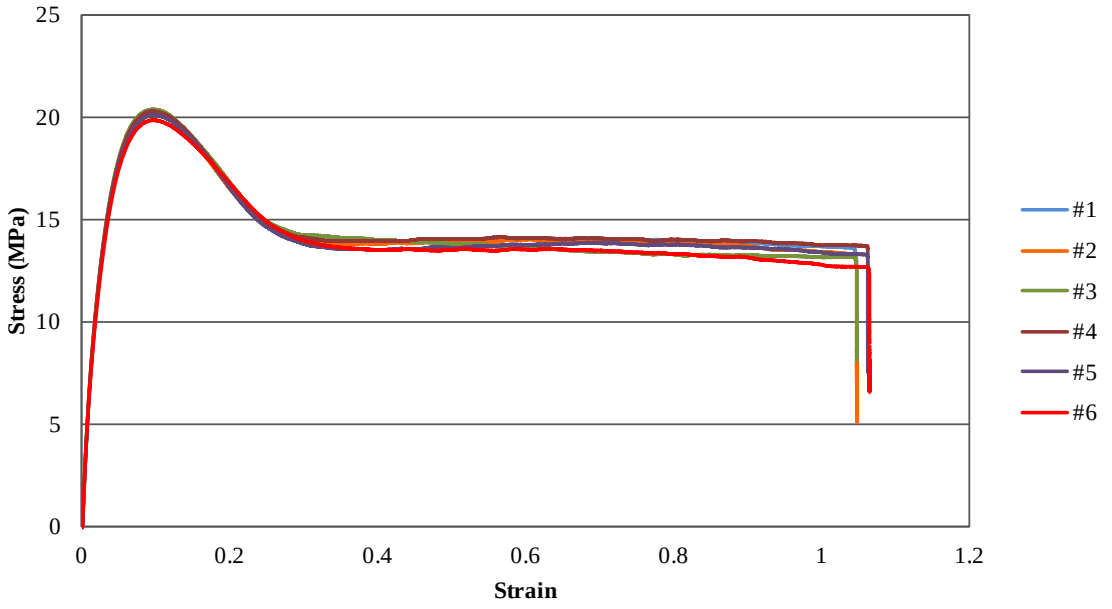


**Figure 3.25** Stress-strain curves of PP 3371 specimens with 6% nanoclay reinforcement at 120°F (49°C)

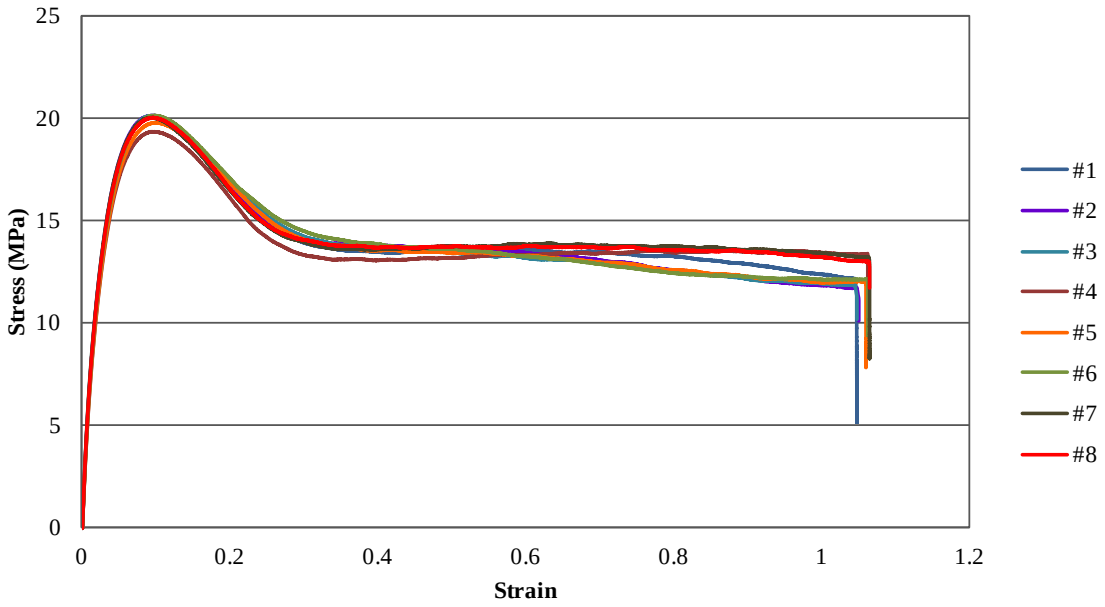


**Figure 3.26** Stress-strain curves of PP 3371 specimens with 10% nanoclay reinforcement at 120°F (49°C)

The results from Figures 3.21 – 3.26 are consolidated in Figure 3.27.

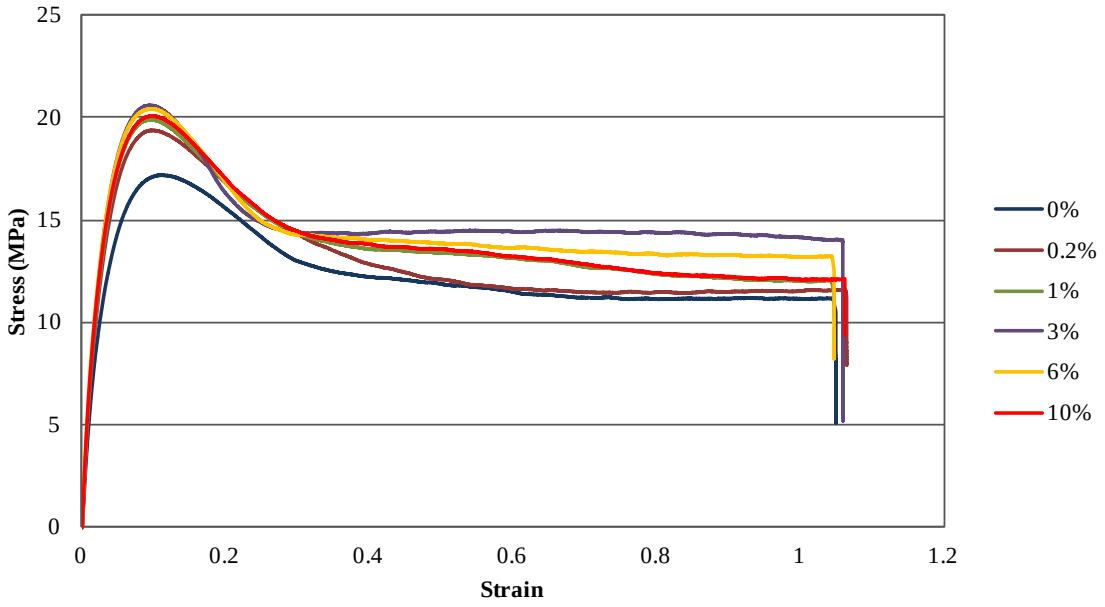


**Figure 3.27** Comparison of stress - strain curves of PP 3371 specimens with 0%, 0.2%, 1%, 3%, 6% and 10% nanoclay reinforcement at 120°F (49°C)

From the results shown in Figure 3.27, it is seen that at 120ºF also an increase in nanoclay reinforcement leads to a higher Young's modulus and ultimate stress as was the case at room temperature. Furthermore, for PP 3371 specimens with 1%, 3% and 6% nanaoclay reinforcement the spread between the curves is very small. Average value of mechanical properties, such as Young's modulus, ultimate stress, etc. obtained at 120°F (4°C) are given in Table 3.3.

**Table 3.3.** Average values of material properties of PP 3371 specimens with 0%, 0.2%, 1%, 3%, 6% and 10% nanoclay reinforcement at 120°F (49ºC)

| PP 3371 with | Young's Modulus (GPa) (Average) | Poisson's Ratio (Average) | Ultimate Stress (MPa) | Strain at Ultimate Stress | End of Test Strain |
|---|---|---|---|---|---|
| **0%** | 0.616 | 0.4038 | 17.166 | 0.0919 | 1.0021 |
| **0.2%** | 0.728 | 0.4350 | 19.087 | 0.0788 | 1.0355 |
| **1%** | 0.765 | 0.4631 | 19.583 | 0.0772 | 1.0345 |
| **3%** | 0.828 | 0.4355 | 19.954 | 0.0789 | 1.0336 |
| **6%** | 0.833 | 0.4334 | 19.863 | 0.0759 | 1.0248 |
| **10%** | 0.866 | 0.4111 | 19.981 | 0.0759 | 1.0353 |

3.2.2-c) Tensile test of PP 3371 at -4ºF (-20ºC)

The nanoclay reinforced PP 3371 specimens were also tested at low temperatures starting with -4ºF (-20ºC). The stress - strain curves of PP 3371 specimens with various percentage of nanoclay reinforcement are plotted in Figures 3.28-3.33.

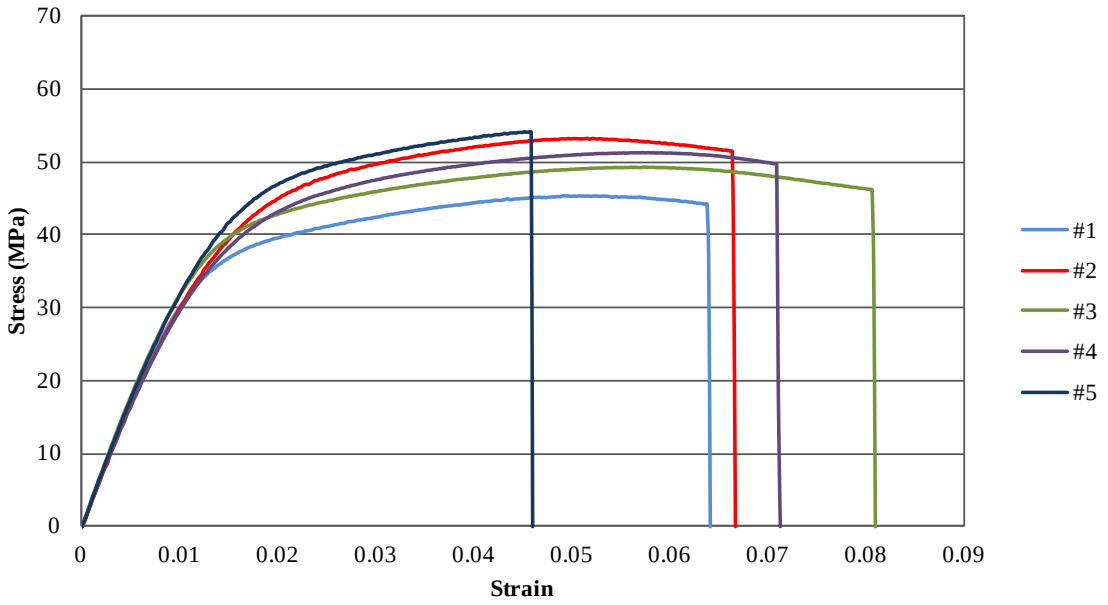


**Figure 3.28** Stress - strain curves of PP 3371 specimens with 0% nanoclay reinforcement at -4°F (-20°C)

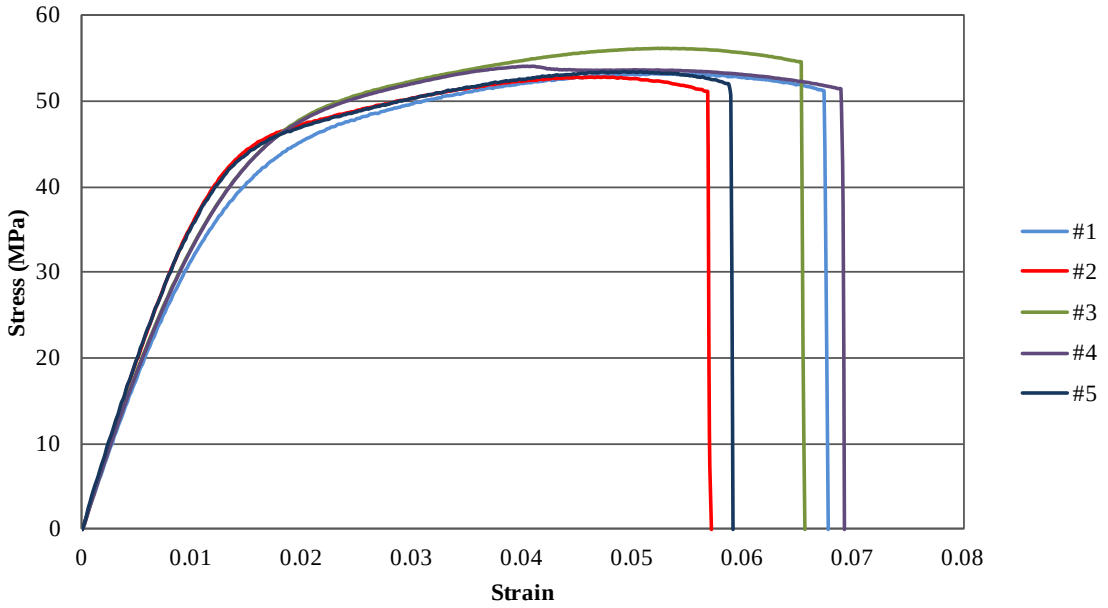


**Figure 3.29** Stress - strain curves of PP 3371 specimens with 0.2% nanoclay reinforcement at -4°F (-20°C)

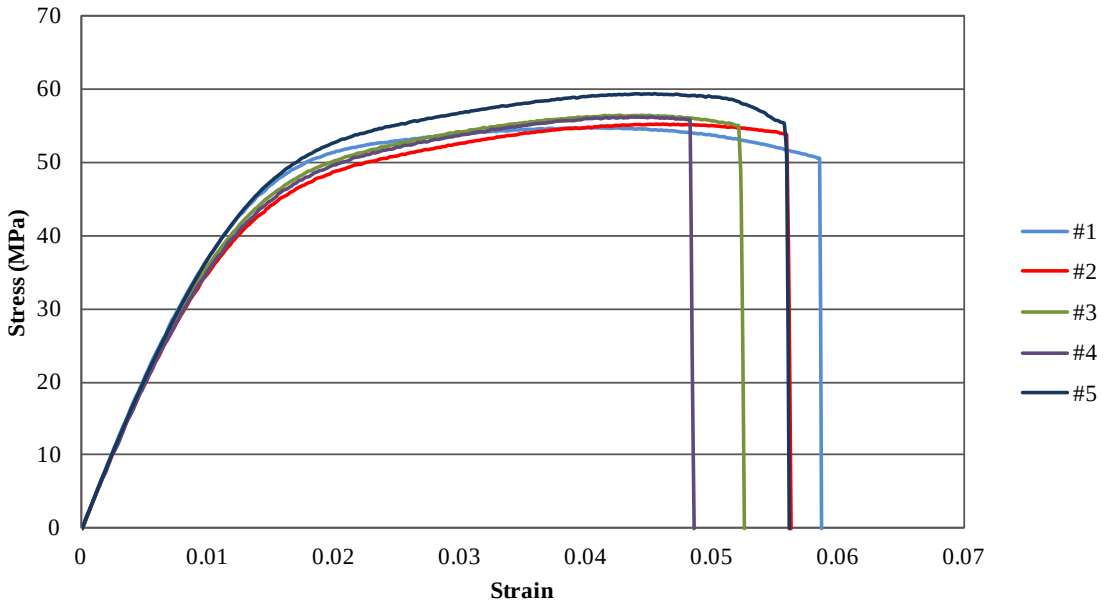


**Figure 3.30** Stress - strain curves of PP 3371 specimens with 1% nanoclay reinforcement at -4°F (-20°C)

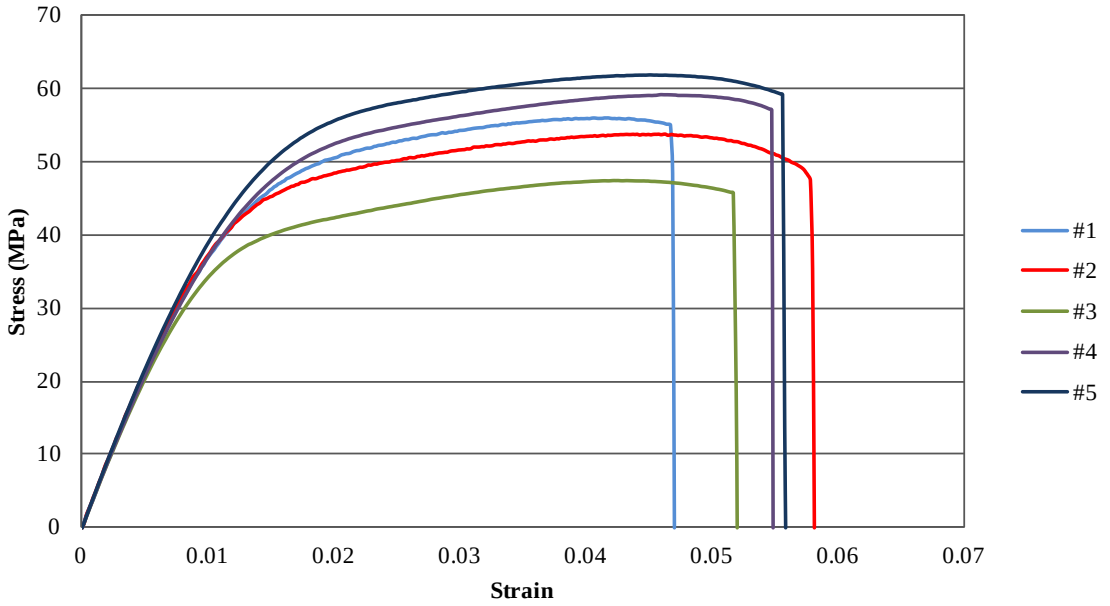


**Figure 3.31** Stress - strain curves of PP 3371 specimens with 3% nanoclay reinforcement at -4°F (-20°C)

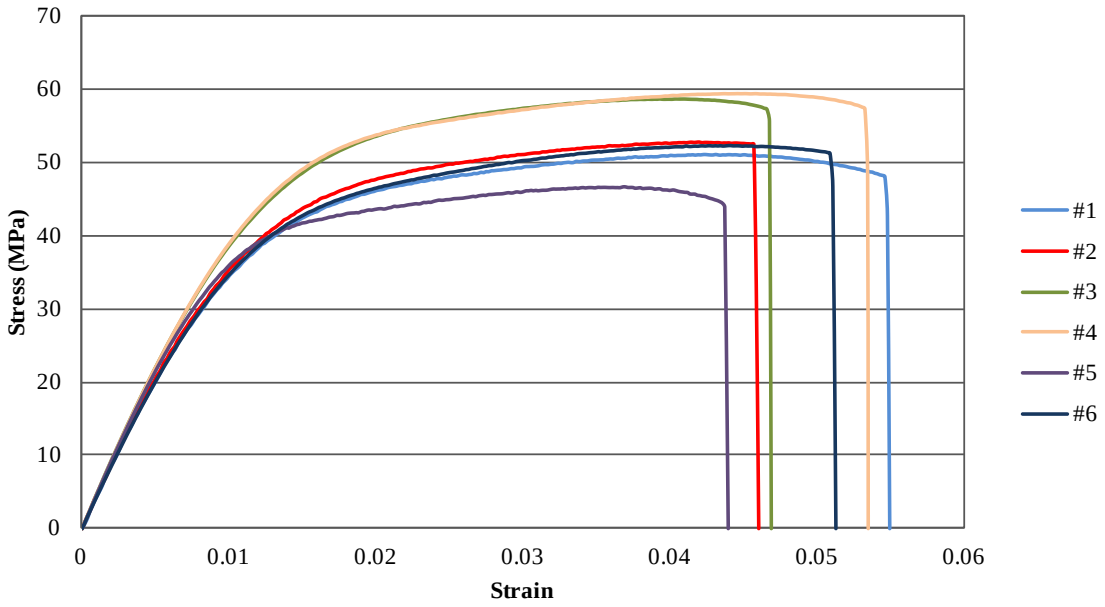


**Figure 3.32** Stress - strain curves of PP 3371 specimens with 6% nanoclay reinforcement at -4°F (-20°C)

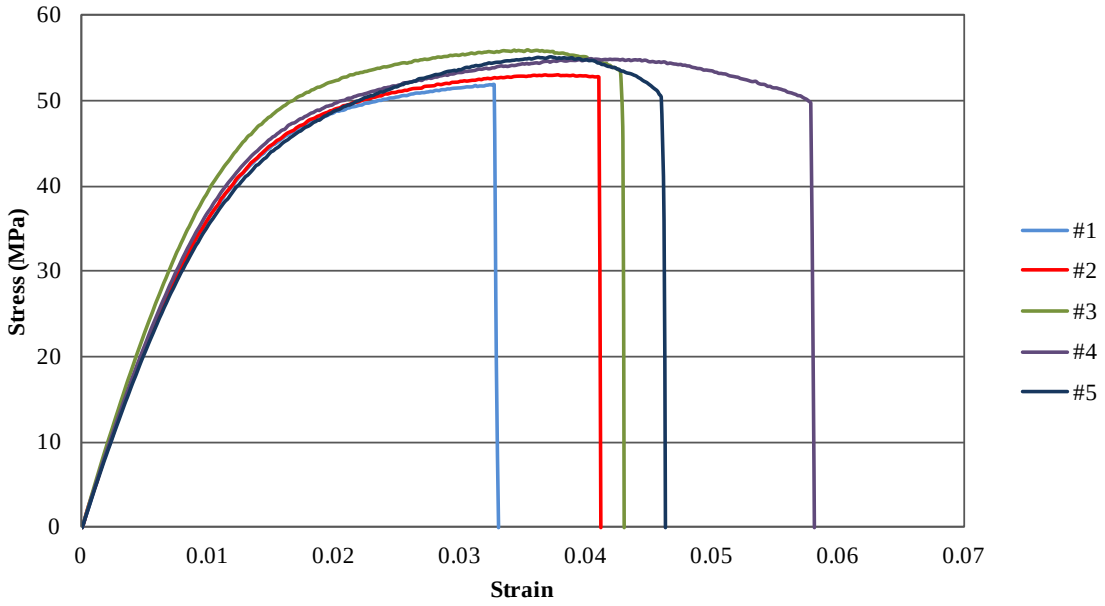


**Figure 3.33** Stress - strain curves of PP 3371 specimens with 10% nanoclay reinforcement at -4°F (-20°C)

Again the results for various nanoclay reinforcement percentages at -4°F (-20°C) are summarized in Figure 3.34.

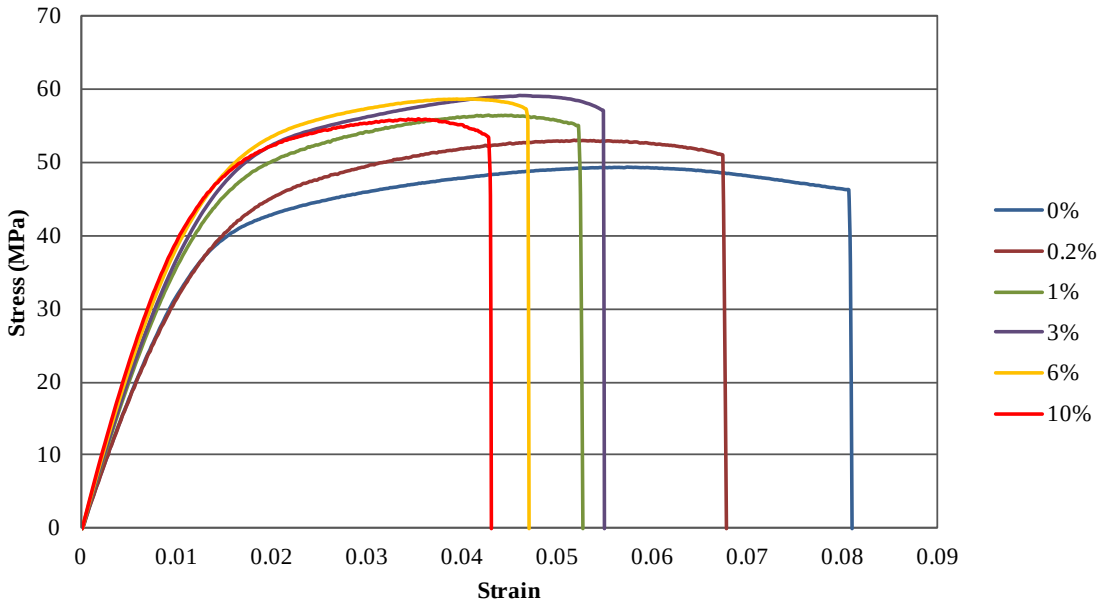


**Figure 3.34** Comparison of stress-strain curves of PP 3371 specimens with 0%, 0.2%,1%, 3%, 6% and 10% nanoclay reinforcement at –4°F (–20°C)

As seen in Figure 3.34, at low temperature all the specimens failed at relatively low strains (4% to 9%) compared to failure strains at room and high temperatures. In general, specimens with a higher percentage of nanoclay reinforcement failed at lower strains. Average values of mechanical properties, such as Young's modulus, ultimate stress, etc. obtained at –4°F (–20°C) are given in Table 3.4.

**Table 3.4.** Average of values of material properties of PP 3371 specimens with 0%, 0.2%, 1%, 3%, 6% and 10% nanoclay reinforcement at –4°F (–20°C)

| PP 3371 with | Young's Modulus (GPa) (Average) | Poisson's Ratio (Average) | Ultimate Stress (MPa) | Strain at Ultimate Stress | End of Test Strain |
|---|---|---|---|---|---|
| **0%** | 3.346 | 0.3438 | 50.607 | 0.0517 | 0.0642 |
| **0.2%** | 3.713 | 0.3307 | 53.8378 | 0.0491 | 0.0619 |
| **1%** | 4.008 | 0.3156 | 56.3626 | 0.0431 | 0.0523 |
| **3%** | 4.179 | 0.3114 | 55.5831 | 0.0433 | 0.0518 |
| **6%** | 4.212 | 0.3056 | 52.3178 | 0.0409 | 0.0471 |
| **10%** | 4.333 | 0.2928 | 54.0557 | 0.0367 | 0.0427 |

3.2.2-d) Tensile test of PP 3371 at -65ºF (-54ºC)

The tensile tests were also performed at the lowest temperature value of -65ºF (-54ºC). The stress vs. strain curves are shown Figures 3.35 – 3.40.

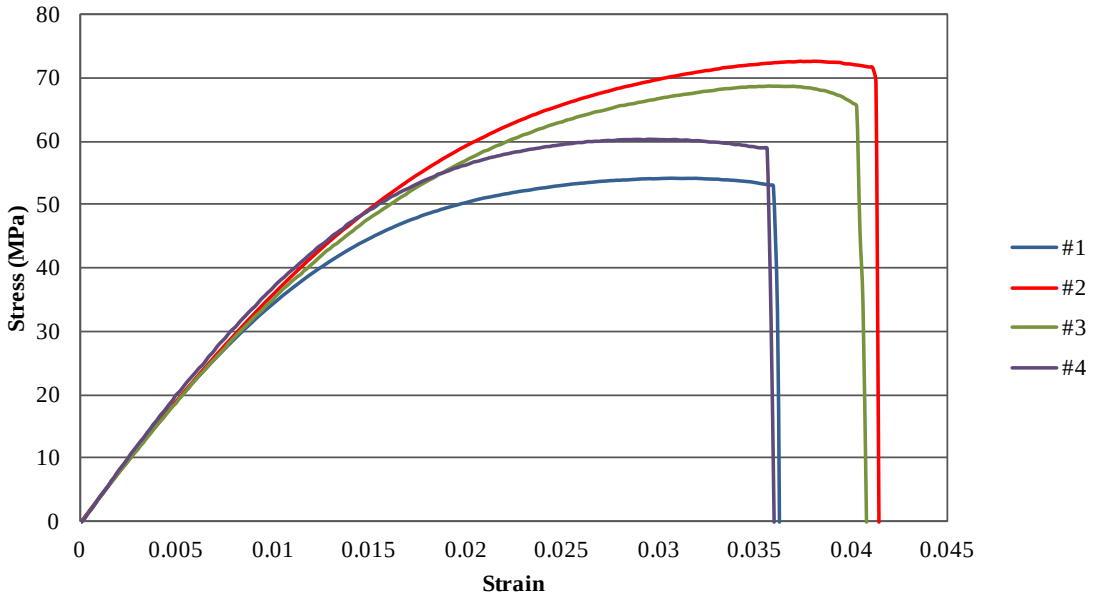


**Figure 3.35** Stress - strain curves of neat PP 3371 specimens at -65°F (-54°C)

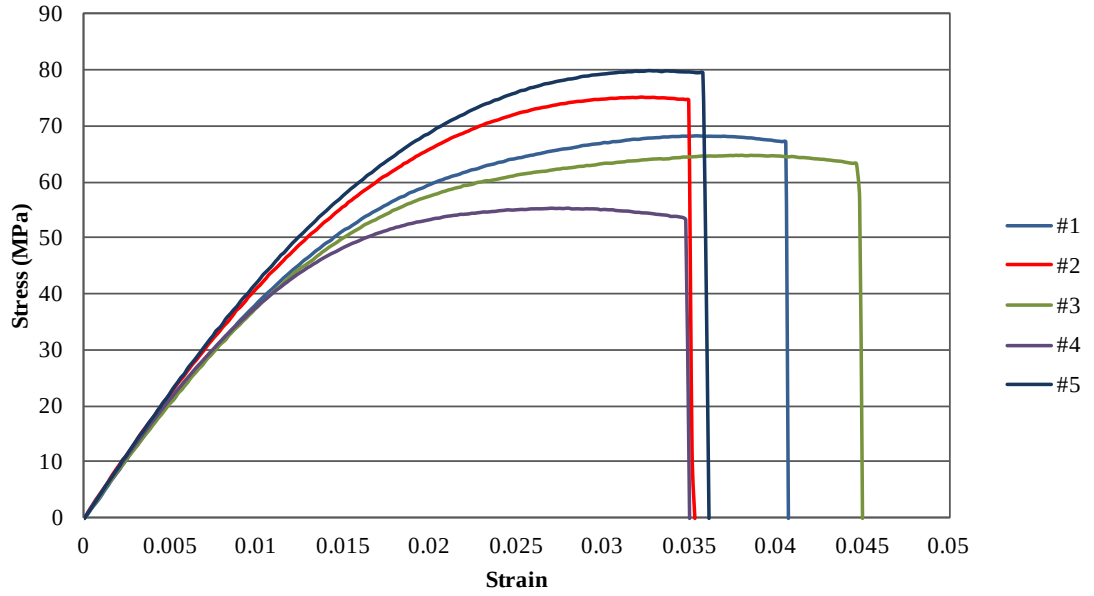


**Figure 3.36** Stress - strain curves of PP 3371 specimens with 0.2% nanoclay reinforcement at -65°F (-54°C)

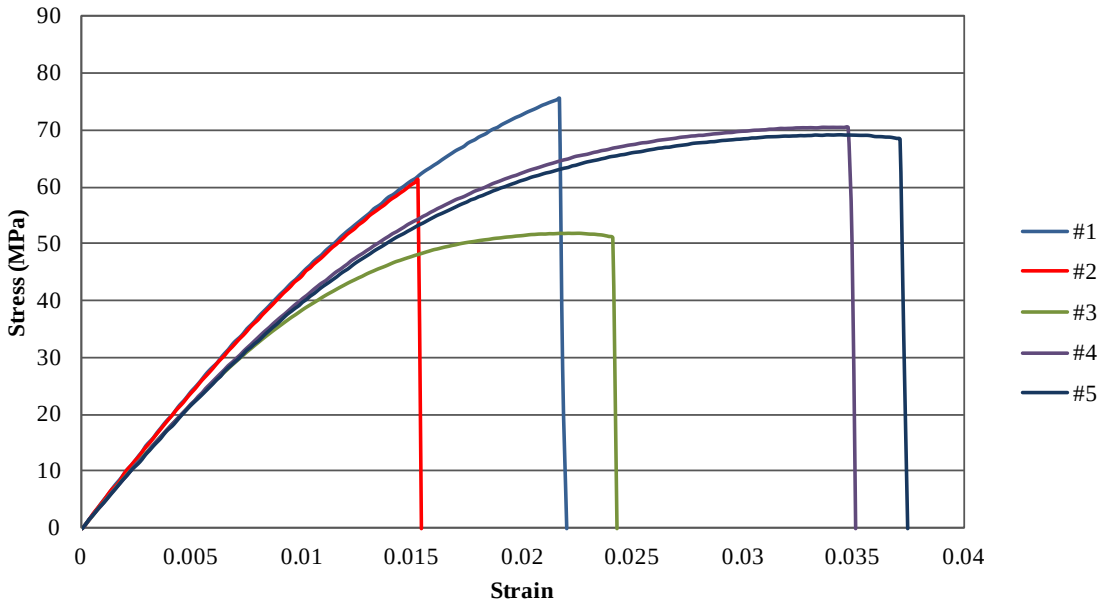


**Figure 3.37** Stress - strain curves of PP 3371 specimens with 1% nanoclay reinforcement at -65°F (-54°C)

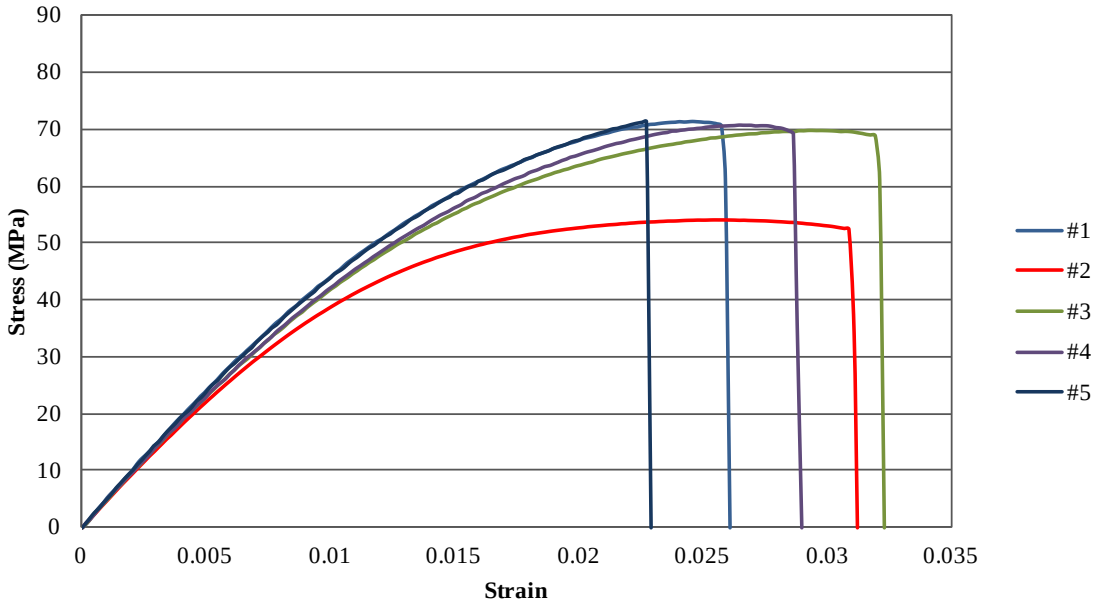


**Figure 3.38** Stress - strain curves of PP 3371 specimens with 3% nanoclay reinforcement at -65°F (-54°C)

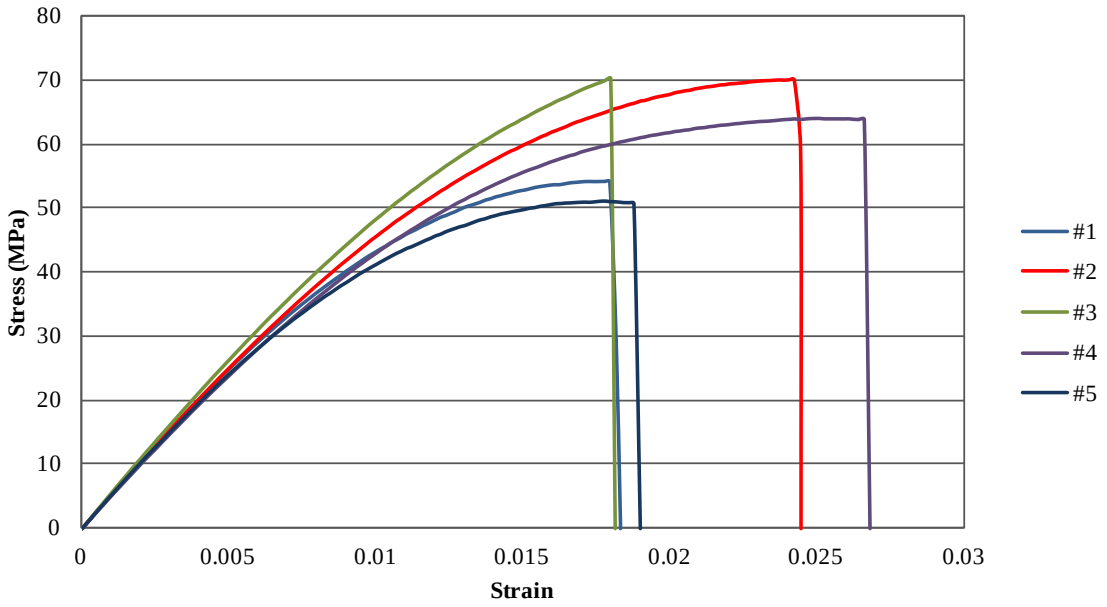


**Figure 3.39** Stress - strain curves of PP 3371 specimens with 6% nanoclay reinforcement at -65°F (-54°C)

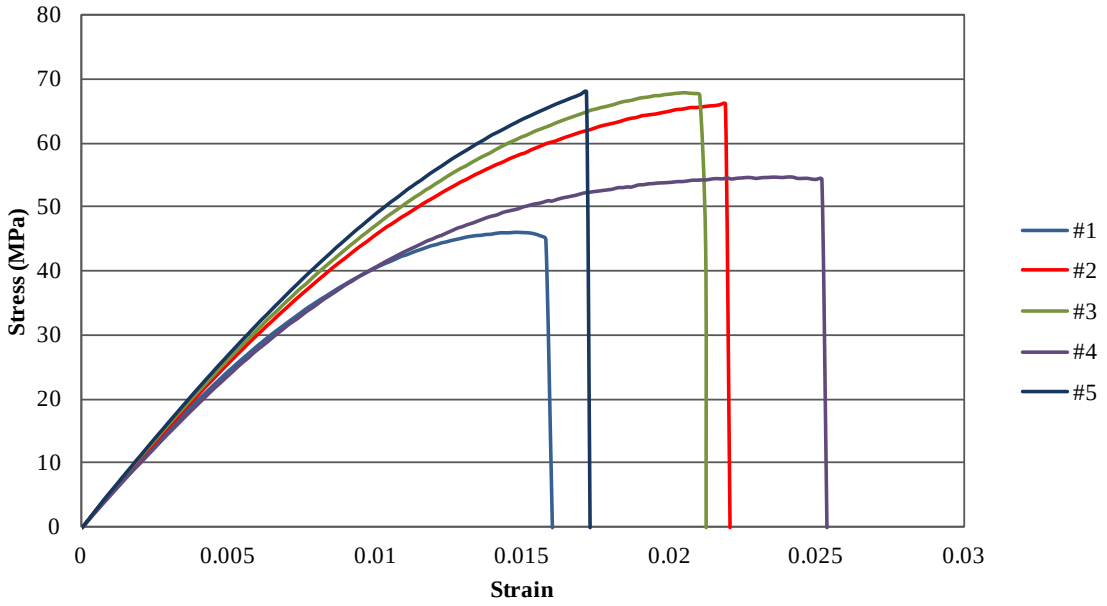


**Figure 3.40** Stress - strain curves of PP 3371 specimens with 10% nanoclay reinforcement at -65°F (-54°C)

The results in Figures 3.35 – 3.40 are summarized in Figure 3.41 which depicts the effect of nanoclay reinforcement at -65°F (-54°C).

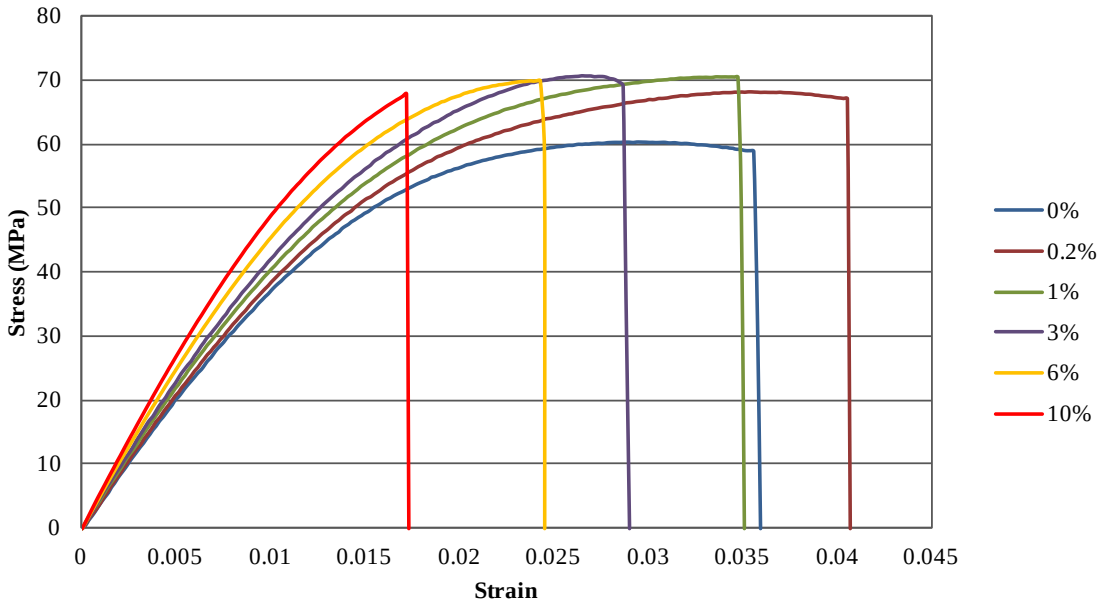


**Figure 3.41** Comparison of stress-strain curves of PP 3371 specimens with 0%, 0.2%, 1%, 3%, 6% and 10% nanoclay reinforcement at -65°F (-54°C)

From the results shown in Figure 3.41, it is seen that at at -65°F (-54°C) an increase in nanoclay reinforcement leads to a higher Young's modulus and ultimate stress as was the case at room temperature. At -65ºF the specimens failed at relatively low strains (1.5% to 4%) in contrast to the specimens tested at room and high temperatures. Mechanical properties, such as Young's modulus, ultimate stress, etc. obtained at -65°F (-54°C) are given in Table 3.5.

**Table 3.5** Average values of material properties of PP 3371 specimens with 0%, 0.2%, 1%, 3%, 6% and 10% nanoclay reinforcement at -65°F (-54ºC)

| PP 3371 with | Young's Modulus (GPa) (Average) | Poisson's Ratio (Average) | Ultimate Stress (MPa) | Strain at Ultimate Stress | End of Test Strain |
|---|---|---|---|---|---|
| **0%** | 3.866 | 0.3429 | 63.9034 | 0.0327 | 0.0357 |
| **0.2%** | 4.284 | 0.3283 | 68.5570 | 0.0325 | 0.0372 |
| **1%** | 4.603 | 0.3193 | 65.1837 | 0.0254 | 0.0259 |
| **3%** | 4.694 | 0.3076 | 67.0177 | 0.0247 | 0.0272 |
| **6%** | 4.973 | 0.3039 | 61.5911 | 0.0203 | 0.0203 |
| **10%** | 5.092 | 0.2983 | 60.2389 | 0.0192 | 0.0194 |

3.2.2-e) Comparison of stress-strain curves of PP 3371specimens at various temperatures for a given nanoclay reinforcement percentage

The stress-strain curves for a given nanoclay reinforcement percentage obtained at -65°F(-54°C), -4°F (-20°C), room temperature, 120°F (49°C) and 160°F (71°C) are plotted on the same graph to showcase the effect of temperature on the nanocomposite. In Figures 3.42-3.47, the stress-strain curves of PP 3371 specimens with 0%, 0.2%, 1%, 3%, 6% and 10% nanoclay reinforcement are shown, respectively.

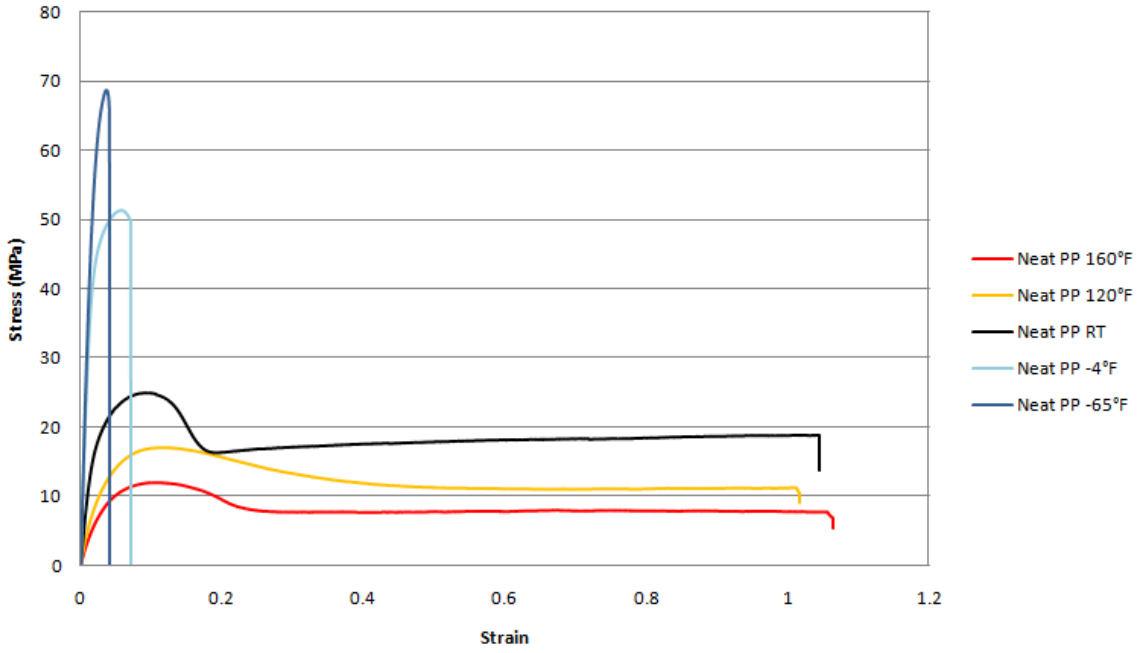


**Figure 3.42** Comparison of stress - strain curves of neat PP 3371 specimens obtained at -65°F (-54°C), -4°F (-20°C), RT, 120°F (49°C) and 160°F (71°C)

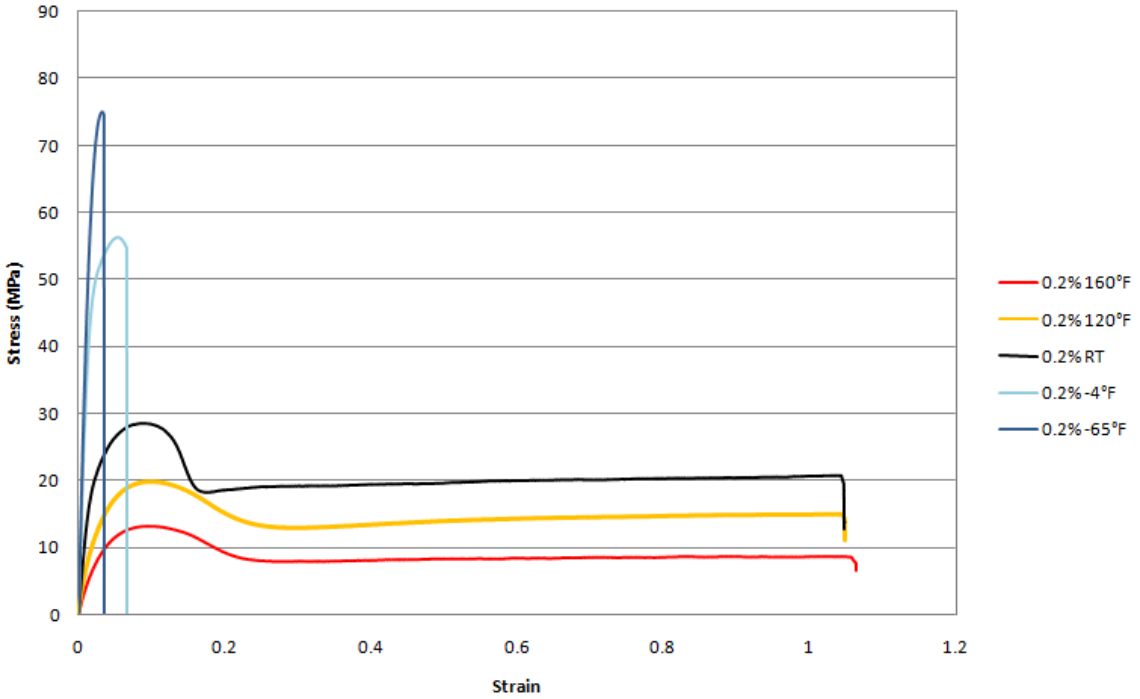


**Figure 3.43** Comparison of stress - strain curves of PP 3371 specimens with 0.2% nanoclay reinforcement obtained at -65°F (-54°C), -4°F (-20°C), RT, 120°F (49°C)

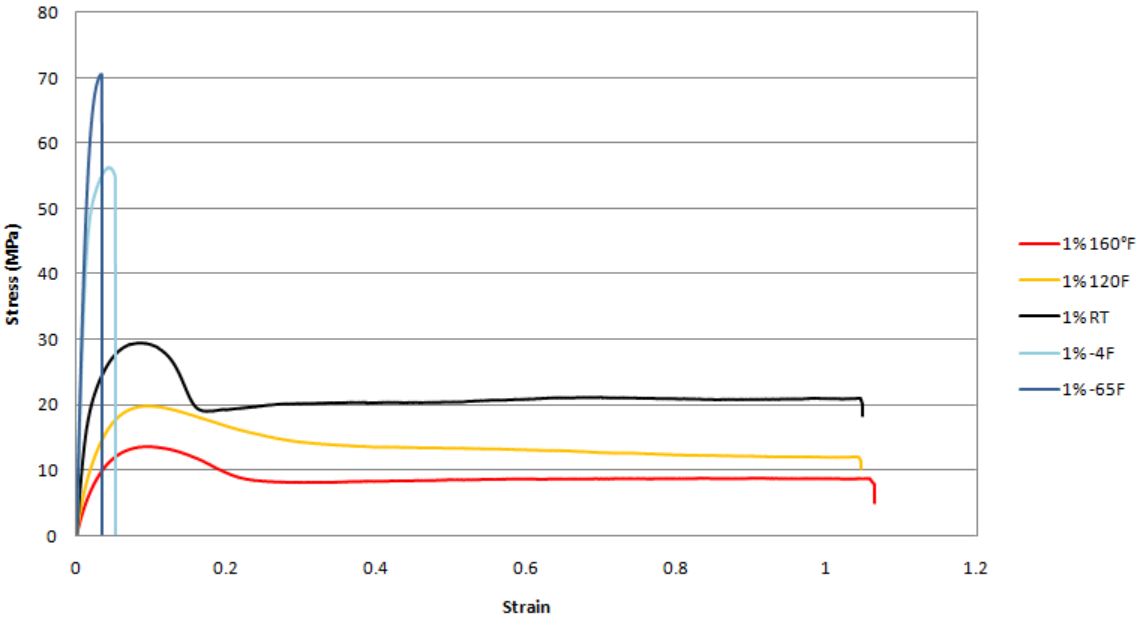


**Figure 3.44** Comparison of stress - strain curves of PP 3371 specimens with 1% nanoclay reinforcement obtained at -65°F (-54°C), -4°F (-20°C), RT, 120°F (49°C)

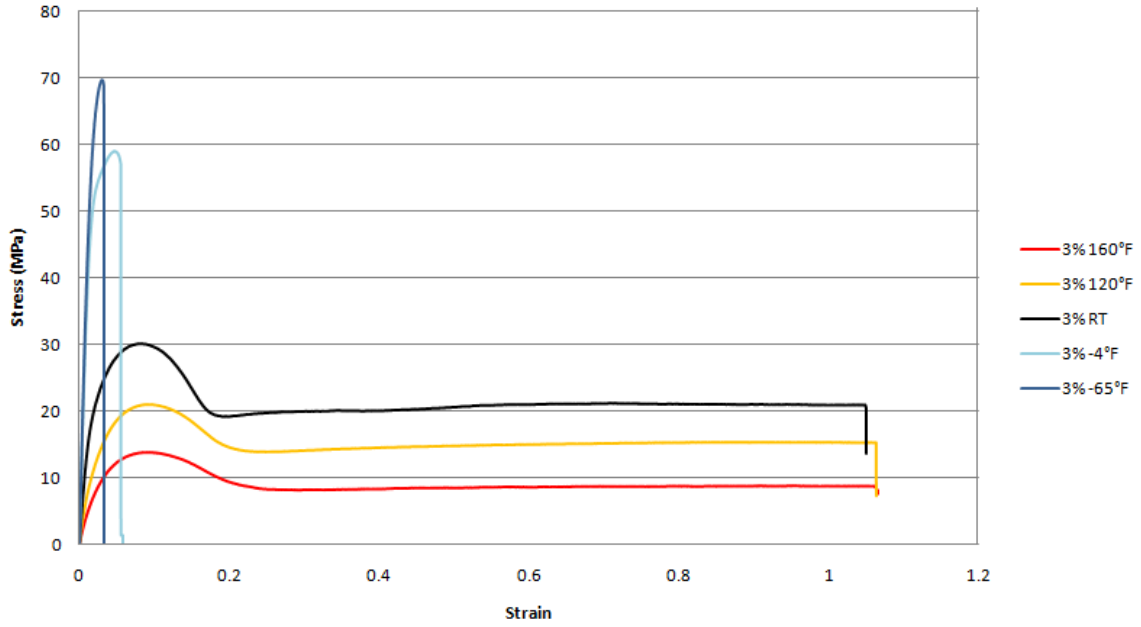


**Figure 3.45** Comparison of stress-strain curves of PP 3371 specimens with 3% nanoclay reinforcement obtained at -65°F (-54°C), -4°F (-20°C), RT, 120°F (49°C)

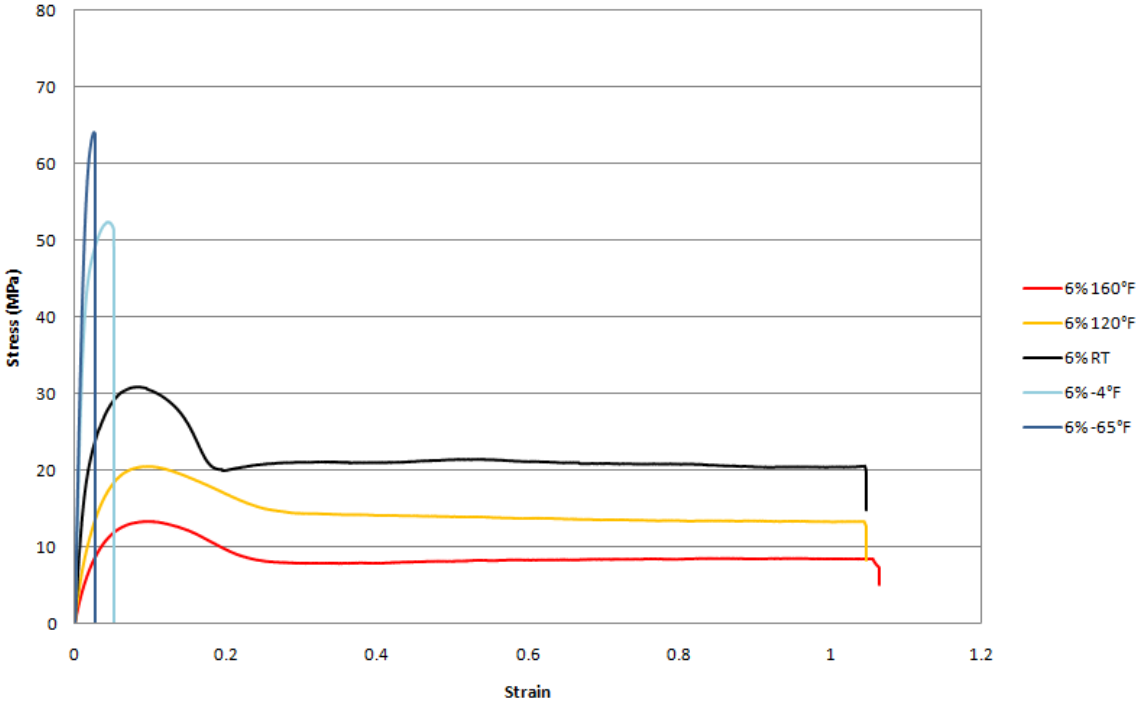


**Figure 3.46** Comparison of stress-strain curves of PP 3371 specimens with 6% nanoclay reinforcement obtained at -65°F (-54°C), -4°F (-20°C), RT, 120°F (49°C)

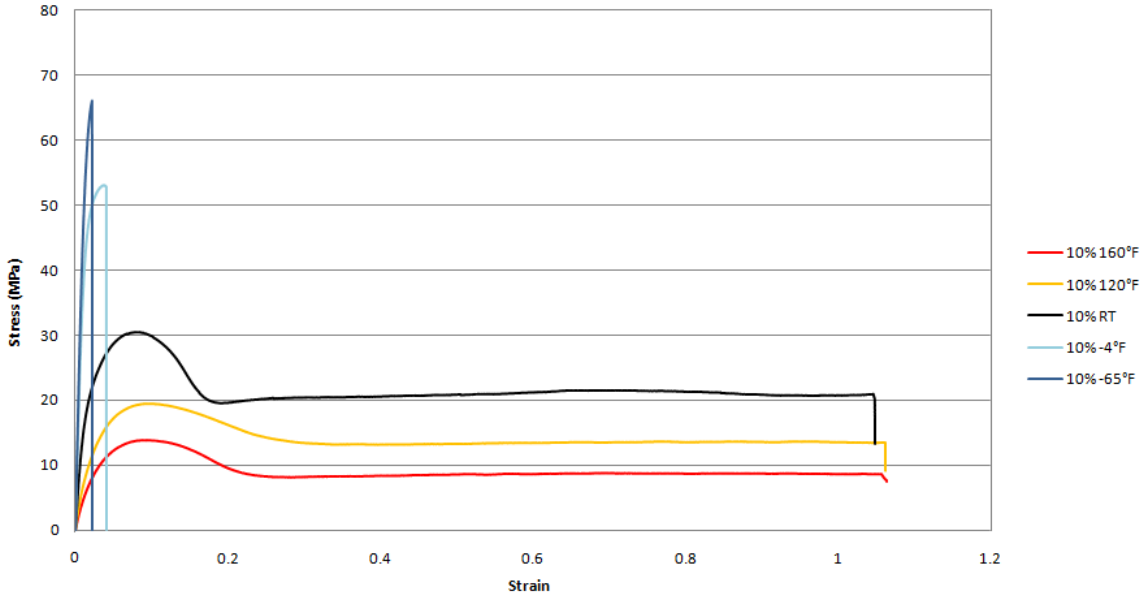


**Figure 3.47** Comparison of stress-strain curves of PP 3371 specimens with 10% nanoclay reinforcement obtained at -65°F (-54°C), -4°F (-20°C), RT, 120°F (49°C)

As can be deduced from the graphs, high temperature has a significant and deleterious effect on the material properties. As the temperature increases, the Young's modulus and the ultimate tensile stress of the nanocomposite decrease. However, as the temperature decreases, the Young's modulus and ultimate tensile stress increase. At low temperatures the material becomes brittle and fails at relatively low strains. The results are summarized in Table 3.6.

**Table 3.6** Material properties of PP 3371 specimens with 0%, 0.2% 1%, 3%, 6% and 10% nanoclay reinforcement at -65°F (-54°C),-4°F (-20°C),room temperature, 120°F (49°C) and 160°F (71°C)

| PP 3371 | Temperature | Young's Modulus (GPa) | Poisson's Ratio | Ultimate Stress (MPa) | Strain at Ultimate Stress | End of Test Strain |
|---|---|---|---|---|---|---|
| **0%** | *-65ºF (-54ºC)* | 3.866 | 0.3429 | 63.9034 | 0.0327 | 0.0357 |
| | *-4 ºF (-20ºC)* | 3.346 | 0.3438 | 50.607 | 0.0517 | 0.0642 |
| | *Room Temp.* | 1.200 | 0.3947 | 25.122 | 0.0745 | 1.0233 |
| | *120 ºF (49ºC)* | 0.616 | 0.4038 | 17.166 | 0.0919 | 1.0021 |
| | *160 ºF (71ºC )* | 0.392 | 0.4256 | 11.730 | 0.0819 | 1.0360 |
| **0.2%** | *-65ºF (-54ºC)* | 4.284 | 0.3283 | 68.5570 | 0.0325 | 0.0372 |
| | *-4 ºF (-20ºC)* | 3.713 | 0.3307 | 53.8378 | 0.0491 | 0.0619 |
| | *Room Temp.* | 1.317 | 0.4167 | 27.826 | 0.0668 | 1.0258 |
| | *120 ºF (49ºC)* | 0.728 | 0.4350 | 19.087 | 0.0788 | 1.0355 |
| | *160 ºF (71ºC )* | 0.449 | 0.4782 | 12.997 | 0.0725 | 1.0308 |
| **1%** | *-65ºF (-54ºC)* | 4.603 | 0.3193 | 65.1837 | 0.0254 | 0.0259 |
| | *-4 ºF (-20ºC)* | 4.008 | 0.3156 | 56.3626 | 0.0431 | 0.0523 |
| | *Room Temp.* | 1.508 | 0.4056 | 29.277 | 0.0661 | 1.0268 |
| | *120 ºF (49ºC)* | 0.765 | 0.4631 | 19.583 | 0.0772 | 1.0345 |
| | *160 ºF (71ºC )* | 0.465 | 0.4715 | 13.303 | 0.0732 | 1.0341 |
| **3%** | *-65ºF (-54ºC)* | 4.694 | 0.3076 | 67.0177 | 0.0247 | 0.0272 |
| | *-4 ºF (-20ºC)* | 4.179 | 0.3114 | 55.5831 | 0.0433 | 0.0518 |
| | *Room Temp.* | 1.628 | 0.3852 | 29.900 | 0.0653 | 1.0397 |
| | *120 ºF (49ºC)* | 0.828 | 0.4355 | 19.954 | 0.0789 | 1.0336 |
| | *160 ºF (71ºC )* | 0.497 | 0.4523 | 13.567 | 0.0713 | 1.0354 |
| **6%** | *-65ºF (-54ºC)* | 4.973 | 0.3039 | 61.5911 | 0.0203 | 0.0203 |
| | *-4 ºF (-20ºC)* | 4.212 | 0.3056 | 52.3178 | 0.0409 | 0.0471 |
| | *Room Temp.* | 1.646 | 0.3722 | 30.009 | 0.0659 | 1.0332 |
| | *120 ºF (49ºC)* | 0.833 | 0.4334 | 19.863 | 0.0759 | 1.0248 |
| | *160 ºF (71ºC )* | 0.503 | 0.5077 | 13.396 | 0.0774 | 1.0374 |
| **10%** | *-65ºF (-54ºC)* | 5.092 | 0.2983 | 60.2389 | 0.0192 | 0.0194 |
| | *-4 ºF (-20ºC)* | 4.333 | 0.2928 | 54.0557 | 0.0367 | 0.0427 |
| | *Room Temp.* | 1.742 | 0.3725 | 30.073 | 0.0658 | 1.0331 |
| | *120 ºF (49ºC)* | 0.866 | 0.4111 | 19.981 | 0.0759 | 1.0353 |
| | *160 ºF (71ºC )* | 0.515 | 0.4896 | 13.431 | 0.0791 | 1.0338 |

3.2.2-f) Variation of Young's Modulus & Poisson's Ratio with Temperature

After analyzing all tensile test results for each nanoclay reinforcement value and temperature, the variation of Young's modulus with temperature is presented for all reinforcement percentages to obtain a better understanding of the behavior of nanoclay reinforced composites. Additionally, the variation of the Poisson's ratio with temperature is presented. Figures 3.48 and 3.49 show the variation of Young's modulus and Poisson's ratio respectively with temperature for each reinforcement percentage.

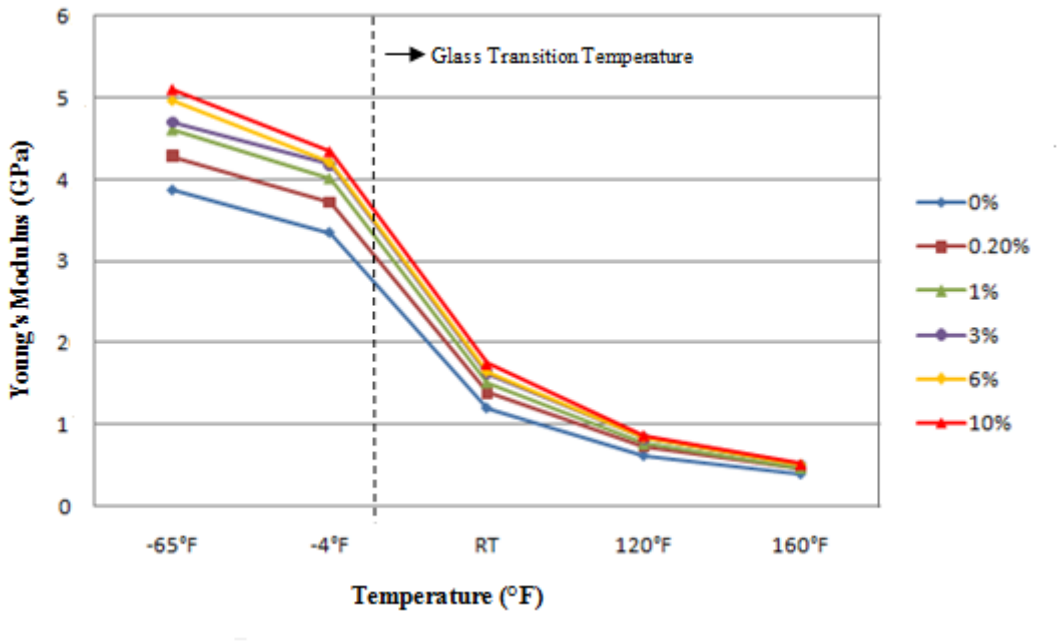


**Figure 3.48** Variation of Young's modulus with temperature

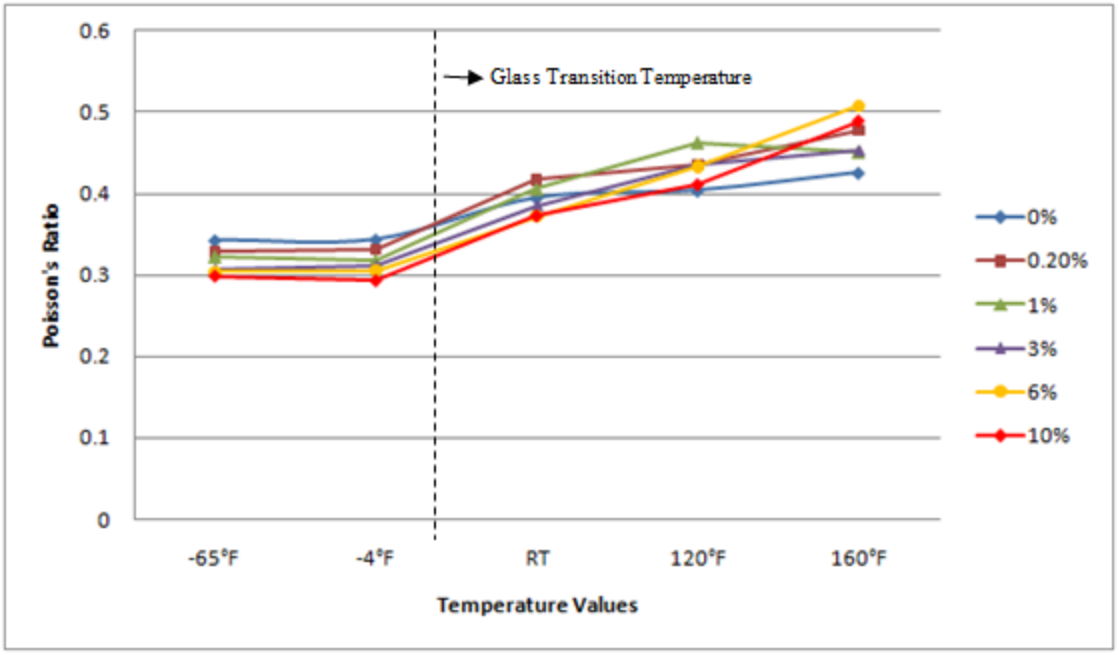


**Figure 3.49** Variation of Poisson's ratio with temperature

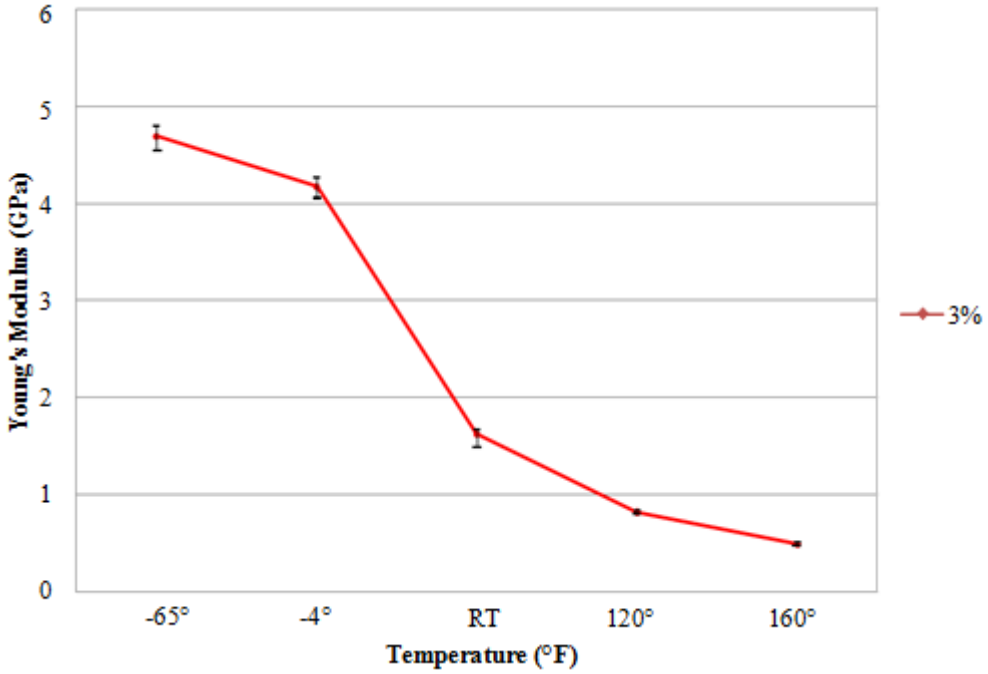


**Figure 3.50** Range of Young's modulus for PP 3371 with 3% nanoclay reinforcement

Figure 3.48 clearly shows that the Young's modulus increases with increasing nanoclay reinforcement percentage and decreases as the temperature increases. However, for the Poisson's ratio Figure 3.49 indicates that while it increases with increasing temperature, its variation with reinforcement percentage is not so obvious.

The same figures also show that as the temperature crosses the glass transition temperature of PP there is significant decrease in the Young's modulus for all test specimens indicating large and rubbery deformations. The jump in Poisson's ratio does not appear to be as significant.

The results are also summarized in Table 3.7 which shows the average values of Young's modulus for each nanoclay reinforcement percentage at each temperature and Table 3.8 which shows the average values of Poisson's ratio for each nanoclay reinforcement percentage at each temperature.

**Table 3.7** Average Young's Moduli (GPa)

| | **-65F** | **-4F** | **RT** | **120F** | **160F** |
|---|---|---|---|---|---|
| **0%** | 3.866 | 3.346 | 1.200 | 0.616 | 0.392 |
| **0.2%** | 4.284 | 3.713 | 1.317 | 0.728 | 0.449 |
| **1%** | 4.603 | 4.008 | 1.508 | 0.765 | 0.465 |
| **3%** | 4.694 | 4.179 | 1.628 | 0.828 | 0.497 |
| **6%** | 4.973 | 4.212 | 1.646 | 0.833 | 0.503 |
| **10%** | 5.092 | 4.333 | 1.742 | 0.866 | 0.515 |

**Table 3.8** Average Poisson's Ratios

| | -65F | -4F | RT | 120F | 160F |
|---|---|---|---|---|---|
| **0%** | 0.3429 | 0.3438 | 0.3947 | 0.4038 | 0.4256 |
| **0.2%** | 0.3283 | 0.3307 | 0.4167 | 0.435 | 0.4782 |
| **1%** | 0.3224 | 0.3176 | 0.4056 | 0.4631 | 0.4516 |
| **3%** | 0.3076 | 0.3114 | 0.3852 | 0.4355 | 0.4523 |
| **6%** | 0.3039 | 0.3056 | 0.3722 | 0.4334 | 0.5077 |
| **10%** | 0.2983 | 0.2928 | 0.3725 | 0.4111 | 0.4896 |

3.2.2-g) Variation of Young's Modulus & Poisson's Ratio with Nanoclay Reinforcement Percentage

The results are also plotted with varying nanoclay reinforcement percentage for each test temperature (Figure 3.51 and 3.52).

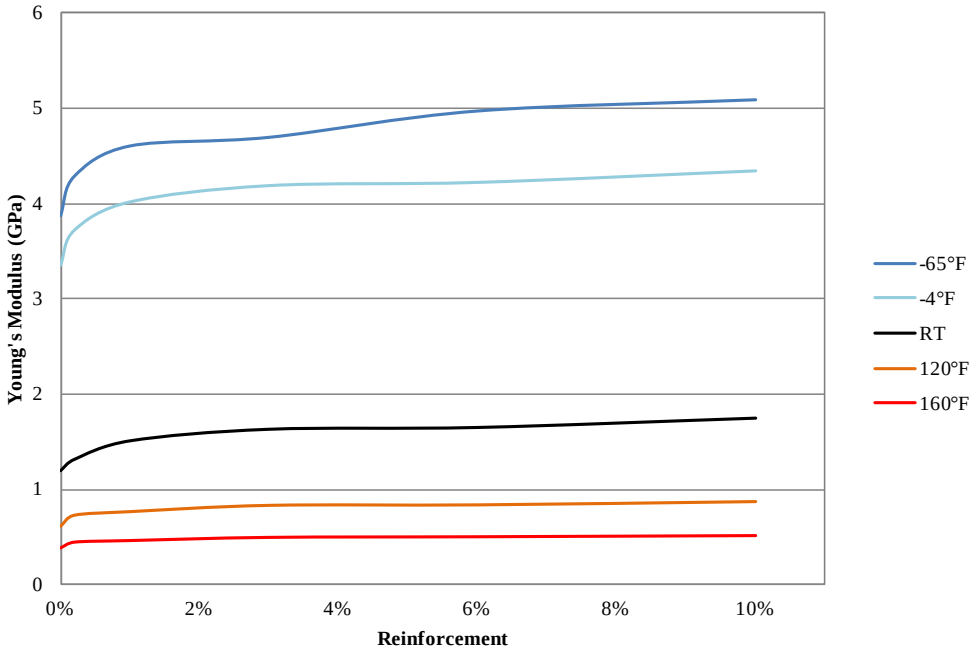


**Figure 3.51** Variation of Young's modulus with nanoclay reinforcement percentage at various test temperatures

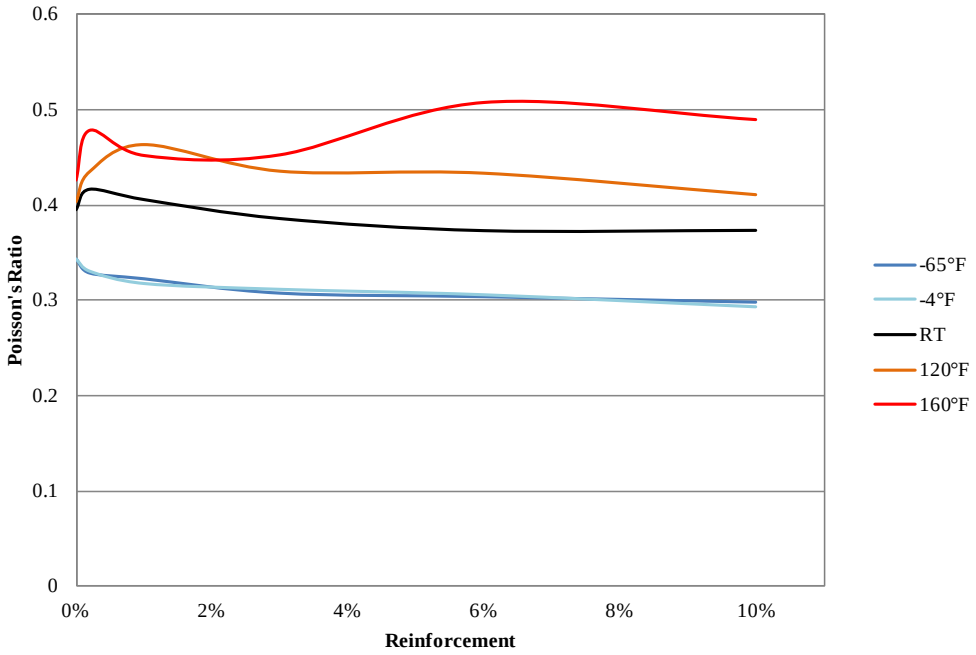


**Figure 3.52** Variation of Poisson's ratio with nanoclay reinforcement percentage at various test temperatures

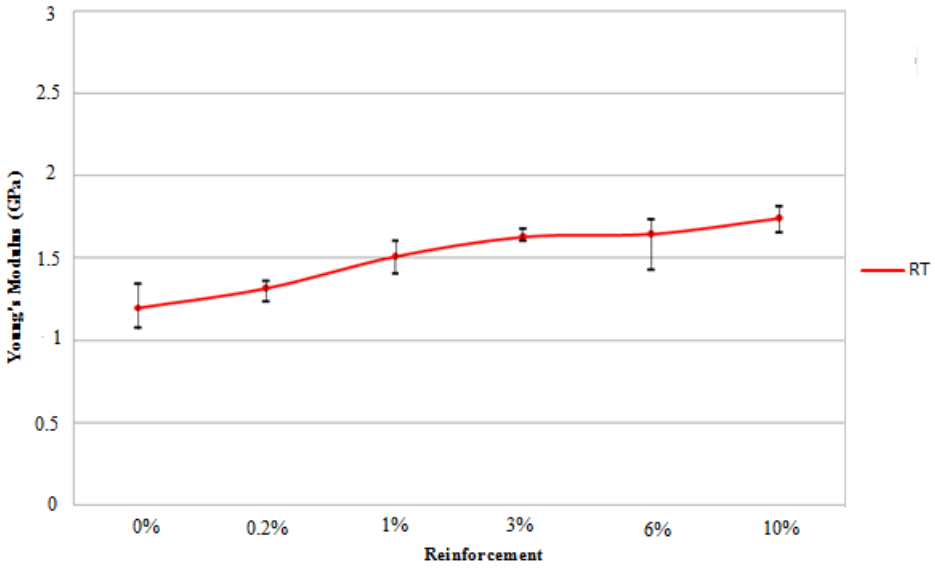


**Figure 3.53** Range of Young's modulus test results vs. reinforcement at room temperature

In Figure 3.51, we can observe the drastic effect of temperature on Young's modulus. When the temperature decreases the Young's modulus shows a dramatic rise at any given reinforcement percentage. However, as was mentioned before, partly because of the glass transition effect and

partly because of the difficulties in obtaining the Poisson's ratio experimentally, as can be seen in Figure 3.52 a consistent trend is difficult to discern.

### 3.2.3 Effect of different resins

In addition to Polypropylene (PP) 3371 resin, we also tested 3% nanoclay reinforced specimens with three different resins, namely, Borealis, Total Petrochemical (TP) 3868 and EPON 828 Epoxy. These specimens were also manufactured by Novus Technologies Corporation.

3.2.3-a) Testing of Borealis specimens with 3% nanoclay reinforcement at -65ºF (-54ºC), -4ºF (-20ºC), room temperature, 120°F (49ºC) and 160°F (71ºC)

Borealis specimens with 3% nanoclay reinforcement were subjected to tensile test at -65ºF (-54ºC), -4ºF (-20ºC), room temperature, 120°F (49ºC) and 160°F (71ºC) and the resulting stress-strain curves are plotted in Figures 3.54 – 3.58 and also summarized in Table 3.9. Borealis specimens with 3% nanoclay reinforcement show large deformation similar to PP 3371 specimens with 3% nanoclay reinforcement at room temperature, 120°F (49ºC) and 160°F (71ºC). Furthermore, these specimens failed too at relatively low strains at low temperatures. The shapes of the curves are also remarkably similar. However, Borealis specimens with 3% nanoclay have higher ultimate tensile stress than PP 3371 specimens.

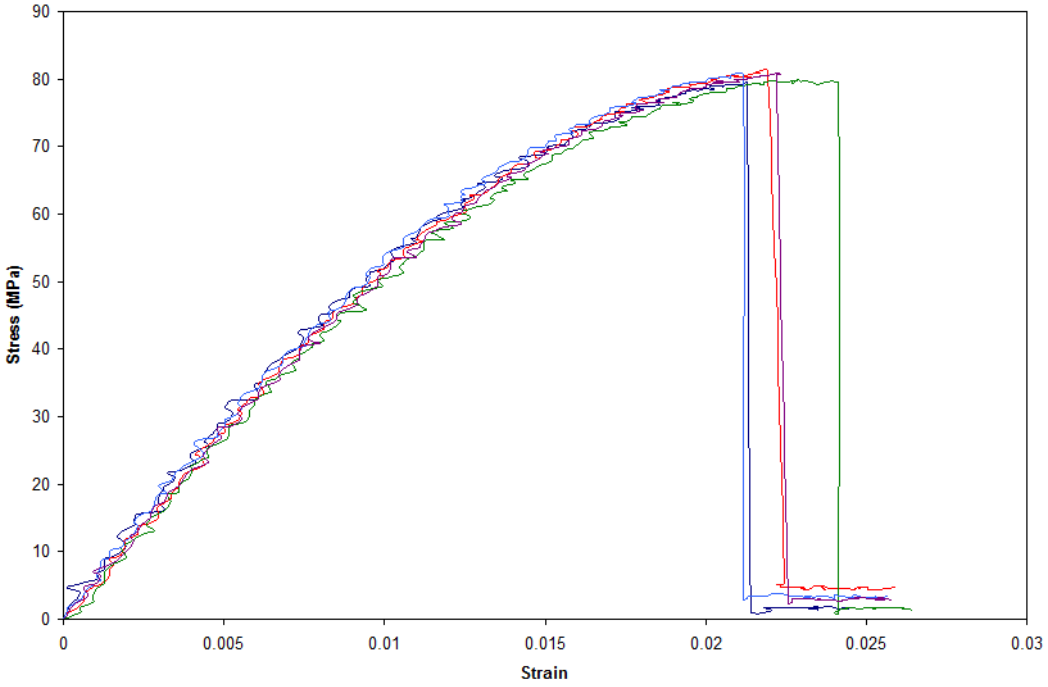


**Figure 3.54** Stress - strain curves of Borealis resin specimens with 3% nanoclay reinforcement at -65ºF (-54ºC)

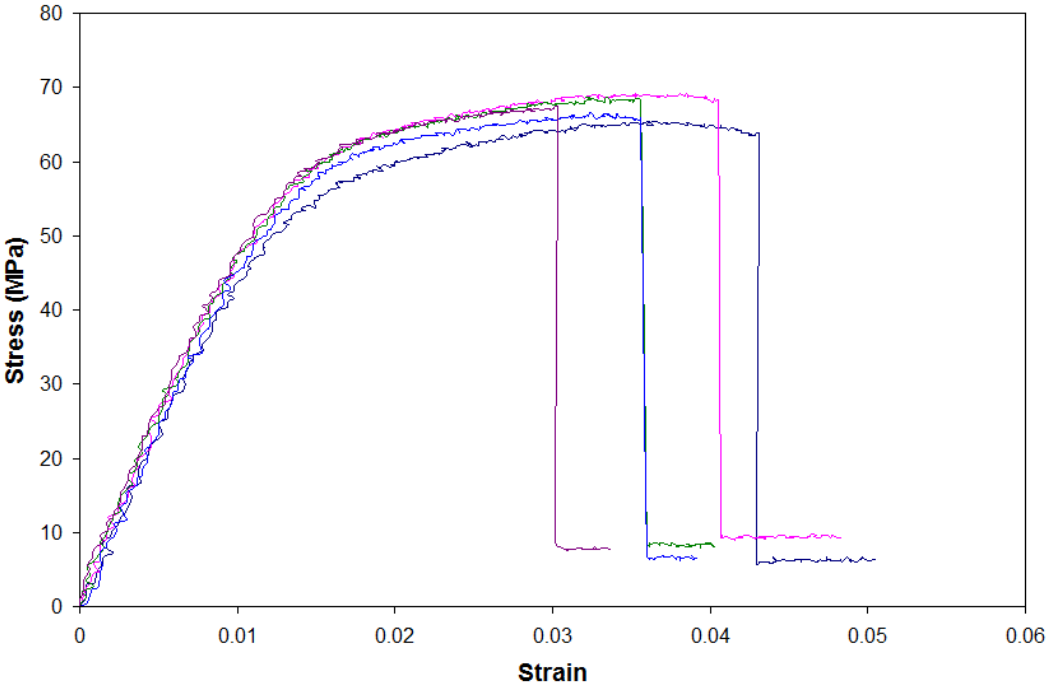


**Figure 3.55** Stress - strain curves of Borealis resin specimens with 3% nanoclay reinforcement at –4ºF (–20ºC)

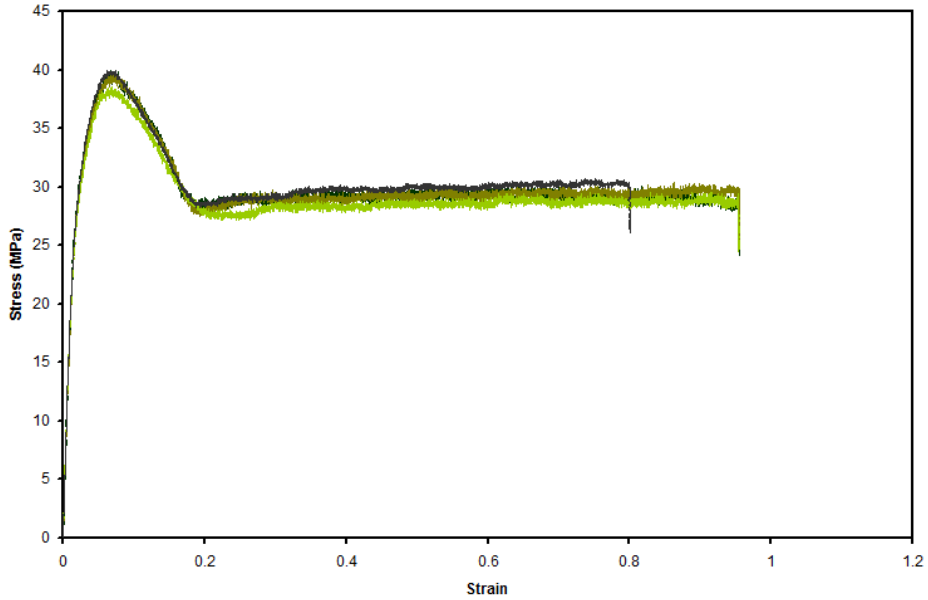


**Figure 3.56** Stress - strain curves of Borealis resin specimens with 3% nanoclay reinforcement at room temperature

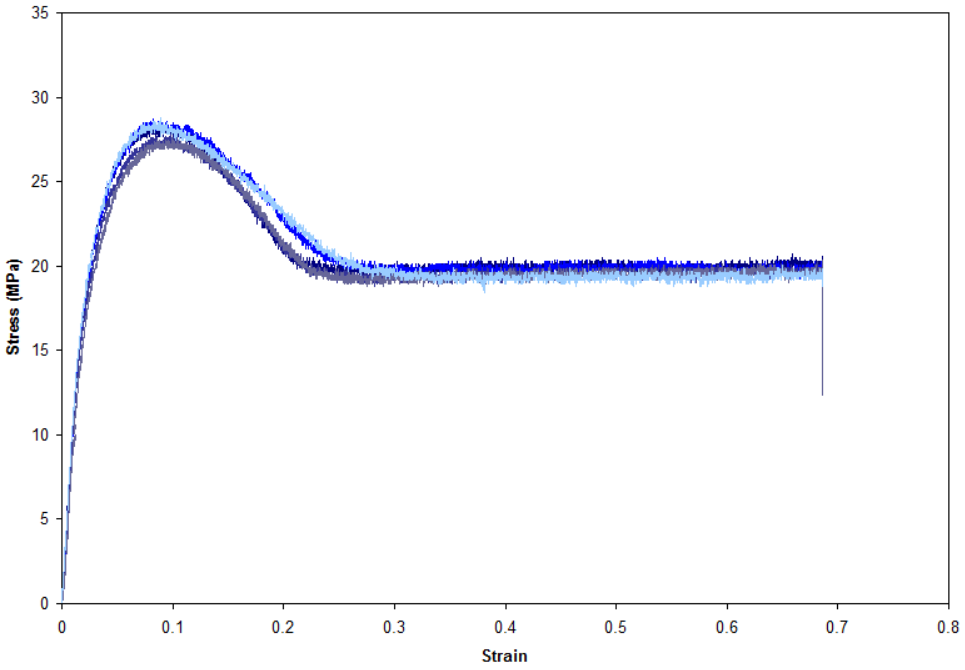


**Figure 3.57** Stress - strain curves of Borealis resin specimens with 3% nanoclay reinforcement at 120ºF (49ºC)

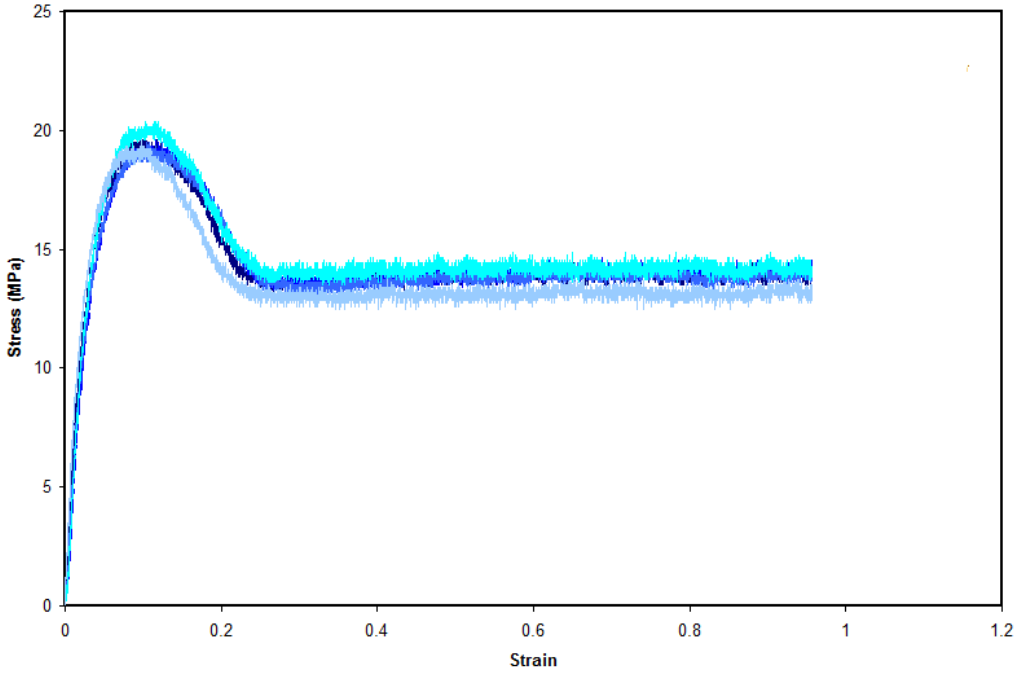


**Figure 3.58** Stress - strain curves of Borealis resin specimens with 3% nanoclay reinforcement at 160ºF (71ºC)

**Table 3.9** Average material properties of Borealis specimens with 3% nanoclay reinforcement at -65ºF (-54ºC),-4ºF (-20ºC), room temperature, 120°F (49ºC) and 160°F (71ºC)

| Borealis Specimens | Temperature | Young's Modulus (GPa) | Ultimate Stress (MPa) | Strain at Ultimate Stress | End of Test Strain |
|---|---|---|---|---|---|
| **3%** | *-65°F* | 5.704 | 80.140 | 0.022 | 0.022 |
| | *-4°F* | 5.109 | 67.173 | 0.033 | 0.037 |
| | *Room Temp.* | 1.965 | 38.944 | 0.073 | 0.954 |
| | *120°F* | 1.020 | 27.914 | 0.091 | 0.951 |
| | *160°F* | 0.569 | 19.405 | 0.106 | 0.951 |

3.2.3-b) Testing of Total Petrochemical 3868 specimens with 3% nanoclay reinforcement at -65°F (-54°C),-4°F (-20°C), room temperature, 120°F (49°C) and 160°F (71°C)

TP 3868 specimens with 3% nanoclay reinforcement were subjected to tensile test to obtain the properties at -65°F (-54°C),-4°F (-20°C), room temperature, 120°F (49°C) and 160°F (71°C). The stress - strain curves of TP 3868 specimens are shown in Figures 3.59 – 3.63 and the results are summarized in Table 3.10. The TP 3868 specimens with 3% nanoclay reinforcement failed at relatively low strains compared to PP 3371 and Borealis specimens at low and room temperatures. However at high temperatures TP 3868 loses its brittleness and behaves like a ductile material.

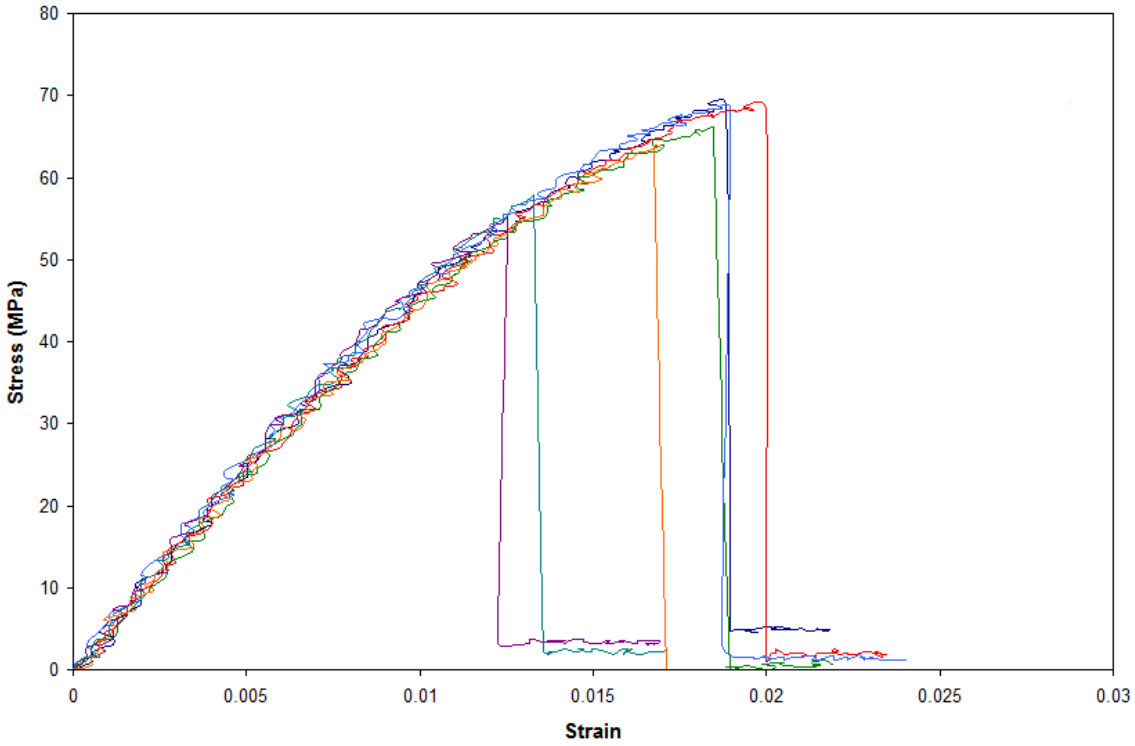


**Figure 3.59** Stress - strain curves of TP 3868 specimens with 3% nanoclay reinforcement at -65ºF (-54ºC)

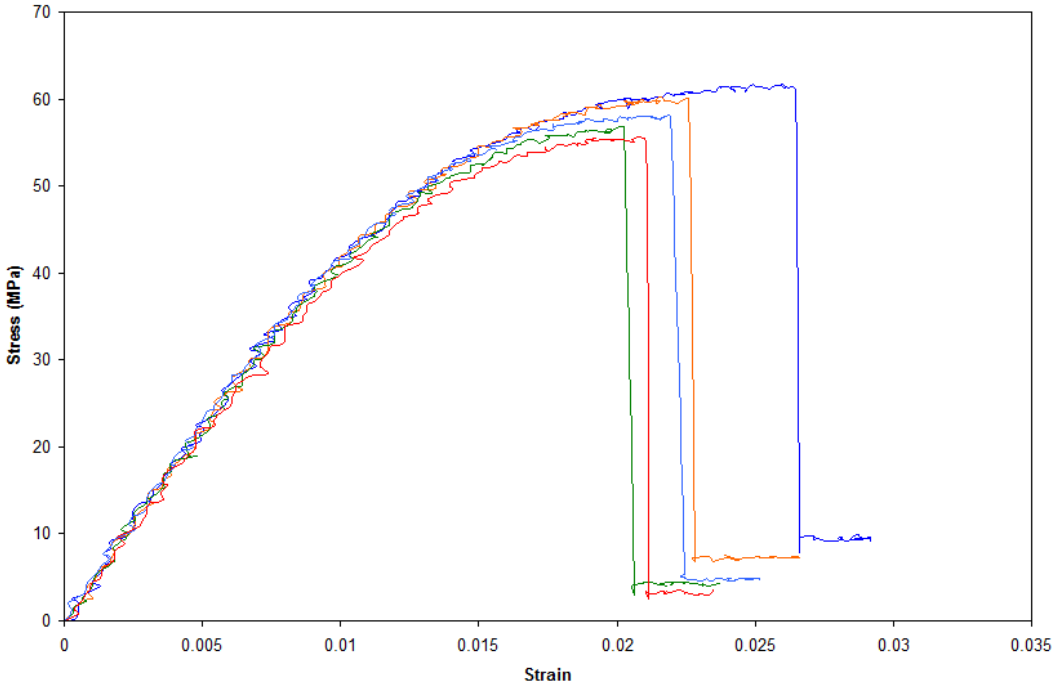


**Figure 3.60** Stress - strain curves of TP 3868 specimens with 3% nanoclay reinforcement at -4ºF (-20ºC)

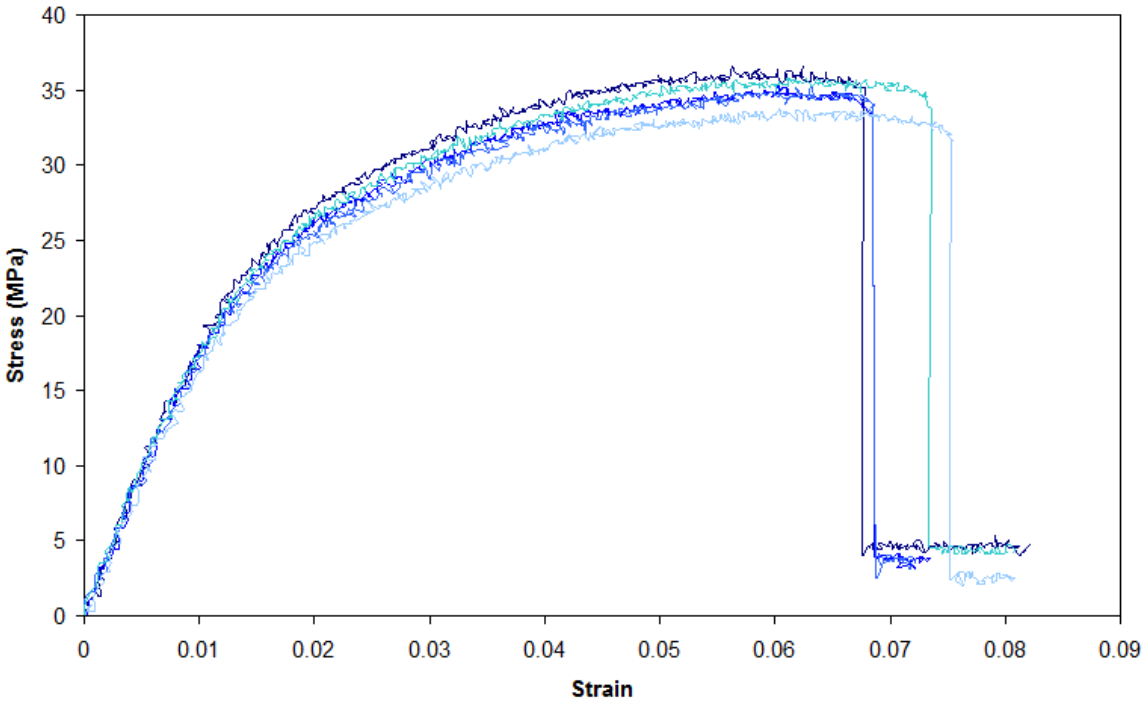


**Figure 3.61** Stress - strain curves of TP 3868 specimens with 3% nanoclay reinforcement at room temperature

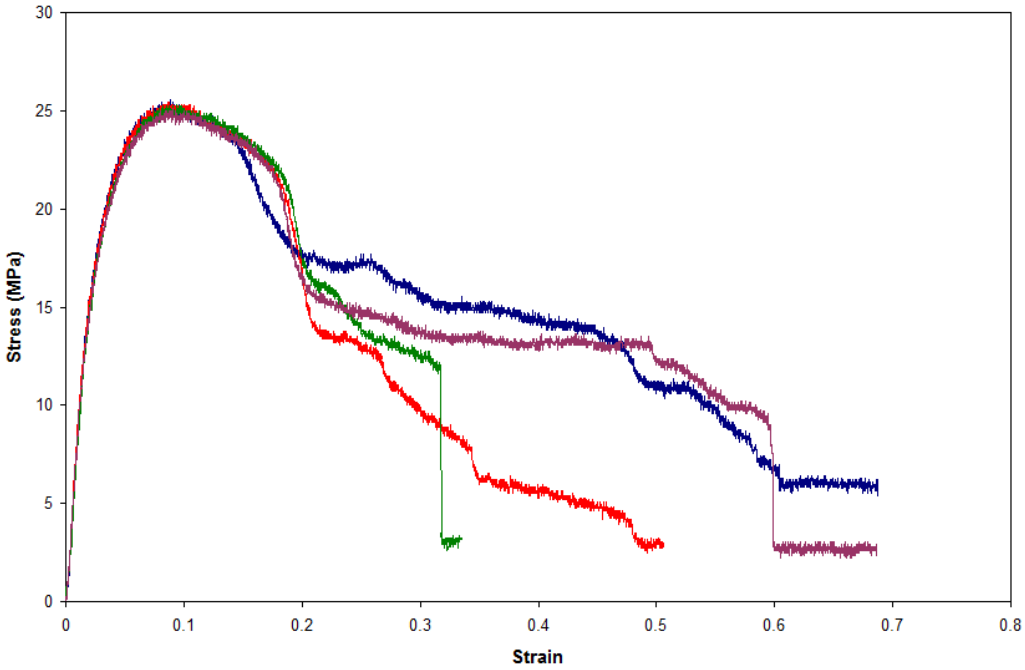


**Figure 3.62** Stress - strain curves of TP 3868 specimens with 3% nanoclay reinforcement at 120ºF (49ºC)

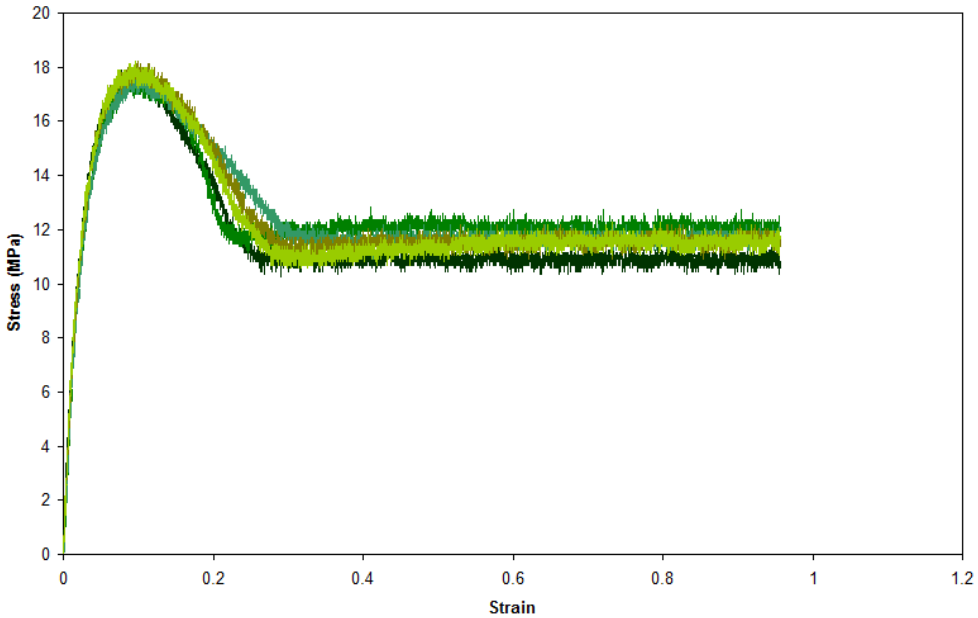


**Figure 3.63** Stress - strain curves of TP 3868 specimens with 3% nanoclay reinforcement at 160ºF (71ºC)

**Table 3.10** Average material properties of TP 3868 specimens with 3% nanoclay reinforcement at -65°F (-54°C),-4°F (-20ºC), room temperature, 120°F (49°C) and 160°F (71°C)

| TP 3868 Specimens | Temperature | Young's Modulus (GPa) | Ultimate Stress (MPa) | Strain at Ultimate Stress | End of Test Strain |
|---|---|---|---|---|---|
| **3%** | *-65°F* | 4.858 | 64.157 | 0.017 | 0.017 |
| | *-4°F* | 4.423 | 58.192 | 0.022 | 0.022 |
| | *Room Temp.* | 1.875 | 34.783 | 0.061 | 0.071 |
| | *120°F* | 0.830 | 25.0997 | 0.093 | 0.526 |
| | *160°F* | 0.587 | 17.671 | 0.099 | 0.945 |

3.2.3-c) Testing of EPON 828 Epoxy specimens with 0%, 1%, 3%, 6% and 10% nanoclay reinforcement at room temperature

The EPON 828 epoxy specimens with various nanoclay reinforcements were subjected to room temperature tensile loading at a crosshead speed of 1 mm/min in an MTS machine. In addition, some specimens were instrumented with strain gages to obtain the Poisson's ratio. The room-temperature stress-strain curves of EPON 828 specimens with various nanoclay reinforcements were then obtained using time-history readings from load-cell for the stresses and crosshead motion, extensometer and strain gages for the strains. The stress-strain curves were then plotted for each EPON 828 specimen. Key mechanical properties, such as Young's modulus, ultimate tensile strength, strain at ultimate stress, Poisson's ratio etc., were then obtained from these curves and tabulated. For tensile tests five specimens were used for each case and the stress-strain curves are given in Figures 3.64- 3.68.

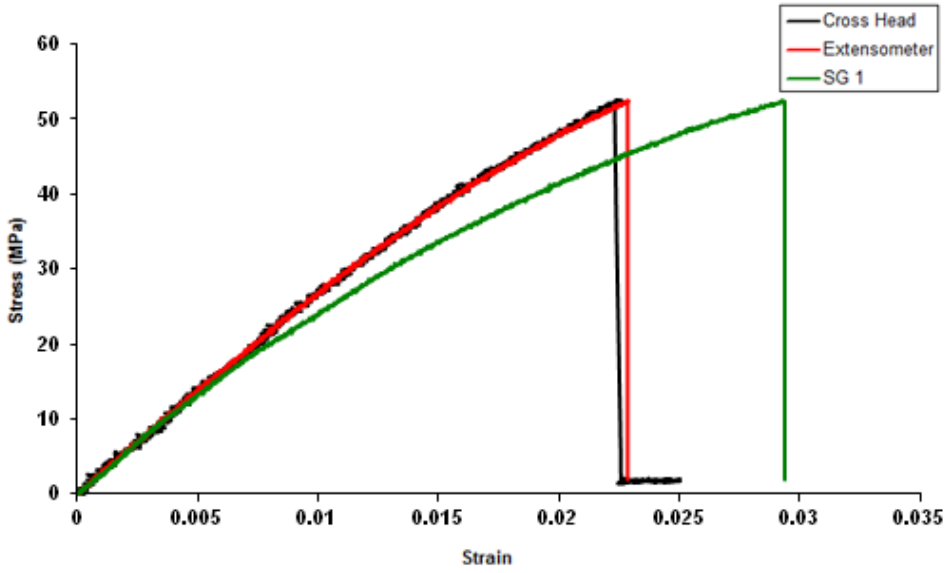


**Figure 3.64** Stress - strain curves of neat EPON 828 specimens at room temperature

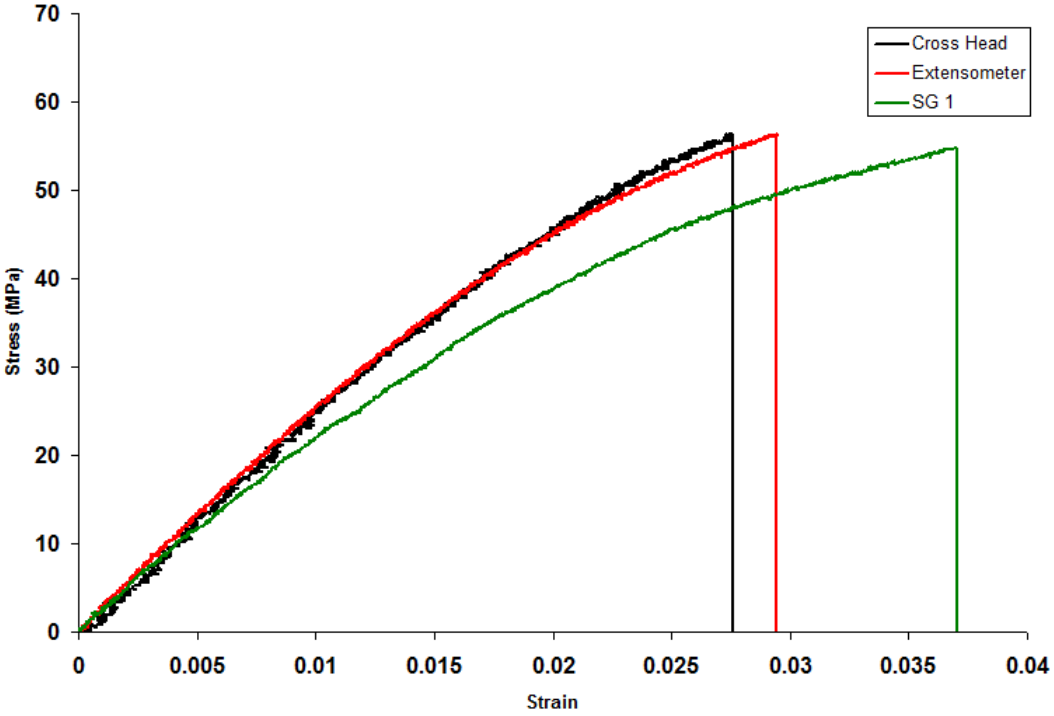


**Figure 3.65** Stress - strain curves of EPON 828 specimens with 1% nanoclay reinforcement

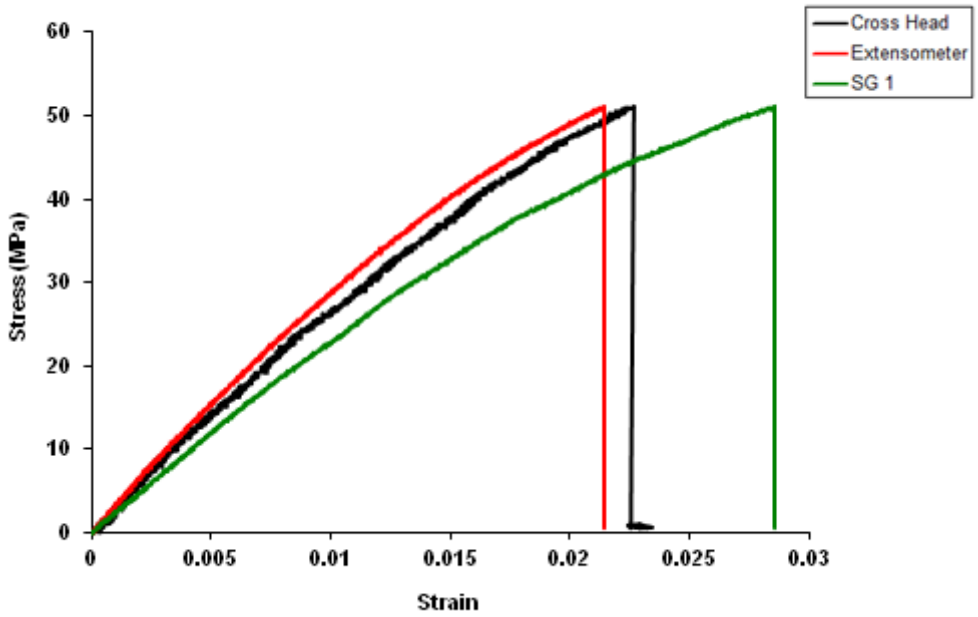


**Figure 3.66** Stress - strain curves of EPON 828 specimens with 3% nanoclay reinforcement

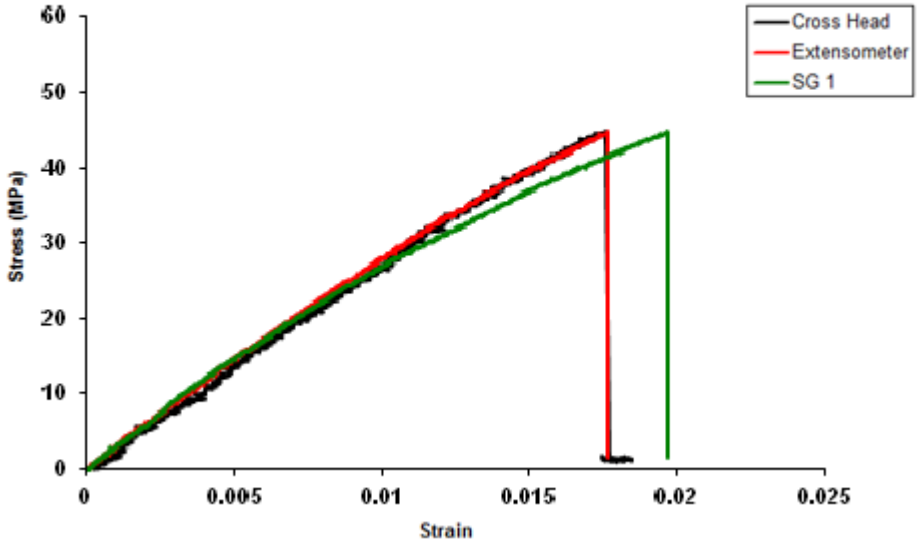


**Figure 3.67** Stress - strain curves of EPON 828 specimens with 6% nanoclay reinforcement

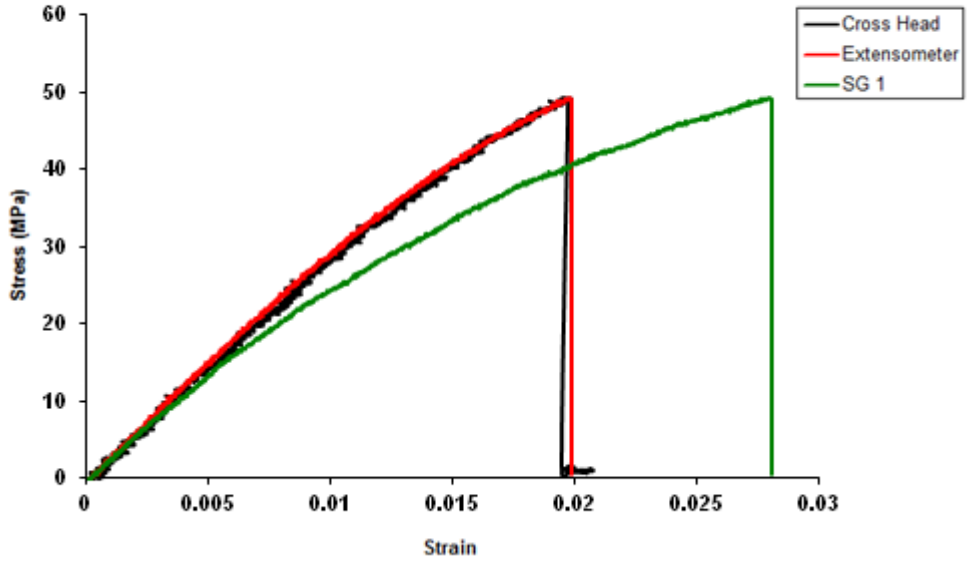


**Figure 3.68** Stress - strain curves of EPON 828 specimens with 10% nanoclay reinforcement

Various percentages of nanoclay reinforcement were used to ascertain its effect on the mechanical properties of the nanocomposite. Figure 3.69 shows the comparison of the stress - strain curves of EPON 828 epoxy specimens with 0%, 1%, 3%, 6% and 10% nanoclay reinforcement. Since the curves obtained with the extensometer were more consistent, they are used in Figure 3.69.

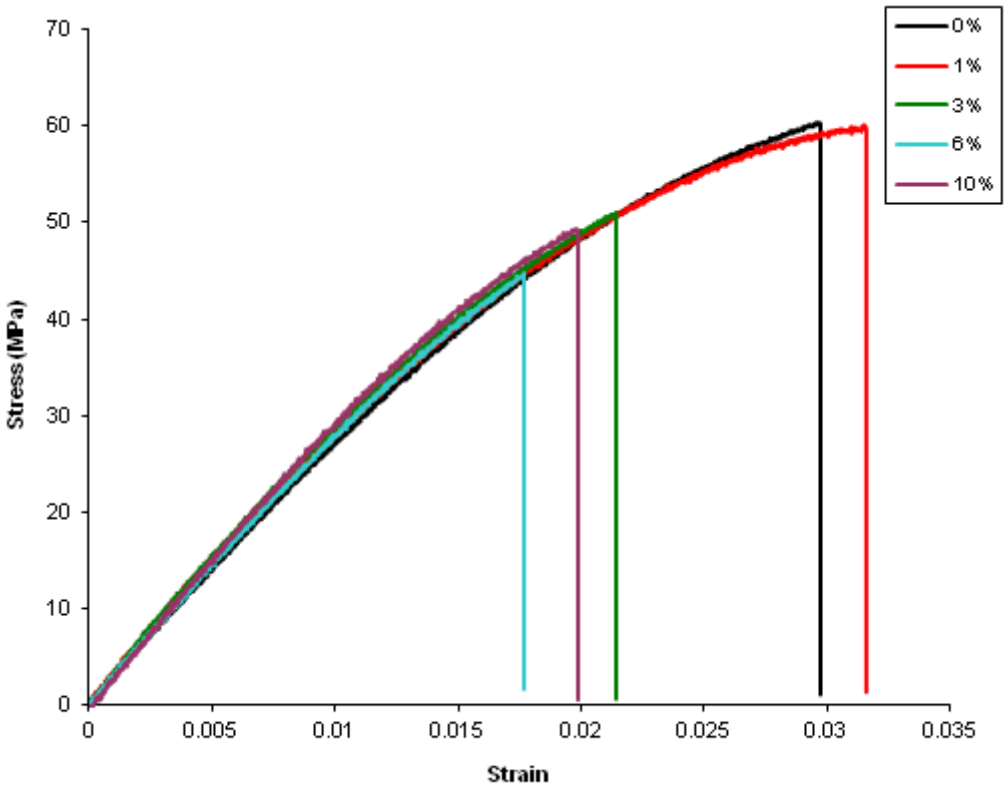


**Figure 3.69** Comparison of stress-strain curves of EPON 828 specimens with various nanoclay reinforcement percentages

The results from Figure 3.69 indicate that in general with increased nanoclay reinforcement, both the failure strain and the failure stress of the nanocomposites decrease.

All the test results and the average material properties are given in Table 3.11 and Table 3.12, respectively. Table 3.12 also includes data available from the manufacturer of the epoxy. As seen in Table 3.11, the average Young's modulus obtained from crosshead, extensometer and strain gage techniques are close to each other, as well as to the manufacturer's data. But since the test results obtained with extensometer are more reliable, they are used in calculating the average Young's modulus for each case.

**Table 3.11** Material properties of EPON 828 specimens with 0%, 1%, 3%, 6% and 10% nanoclay reinforcement at room temperature

| EPON 828 with | # | Young's Modulus (GPa) – Cross Head | Young's Modulus (GPa) – Extensometer | Young's Modulus (GPa) –Strain Gage | NOVUS Test Result (GPa) | Young's Modulus (GPa) (Manufacturer) | Poisson's Ratio |
|---|---|---|---|---|---|---|---|
| **0%** | *1* | 2.673 | - | - | 2.289 | 2.758 | - |
| | *2* | 2.743 | 2.789 | 2.589 | | | 0.2915 |
| | *3* | 2.760 | 2.917 | 2.837 | | | 0.3097 |
| | *4* | 2.725 | 2.747 | 2.695 | | | 0.3303 |
| | | | | | | | |
| **1%** | *1* | 2.672 | - | - | - | - | - |
| | *2* | 2.617 | 2.918 | - | - | - | - |
| | *3* | 2.986 | 2.986 | - | - | - | - |
| | *4* | 2.650 | 3.199 | 2.613 | - | - | 0.3459 |
| | *5* | 2.478 | 2.755 | 2.361 | - | - | 0.3237 |
| | *6* | 2.258 | 2.683 | 2.420 | - | - | 0.3235 |
| | *7* | 2.869 | 2.935 | 2.327 | - | - | 0.3020 |
| | | | | | | | |
| **3%** | *1* | 2.890 | 3.235 | 2.393 | - | - | 0.3407 |
| | *2* | 2.674 | - | 2.508 | - | - | 0.3285 |
| | *3* | 2.614 | 2.995 | 2.391 | - | - | 0.3374 |
| | *4* | 2.292 | 2.410 | 2.256 | - | - | 0.3087 |
| | *5* | 2.838 | 3.296 | - | - | - | - |
| | | | | | | | |
| **6%** | *1* | 2.464 | 2.458 | - | - | - | - |
| | *2* | 2.540 | 2.935 | - | - | - | - |
| | *3* | 2.215 | 3.426 | 2.403 | - | - | - |
| | *4* | 2.645 | 3.020 | 3.063 | - | - | 0.3488 |
| | *5* | 3.064 | 3.383 | 2.630 | - | - | 0.3316 |
| | *6* | 3.290 | 3.357 | 2.613 | - | - | 0.3317 |
| | | | | | | | |
| **10%** | *1* | 3.070 | 3.440 | - | - | - | |
| | *2* | 2.768 | - | - | - | - | |
| | *3* | 2.644 | 2.832 | - | - | - | |
| | *4* | 3.012 | 3.446 | - | - | - | |
| | *5* | 3.147 | 3.438 | - | - | - | |
| | *6* | 2.841 | 4.289 | 2.779 | - | - | 0.3538 |
| | *7* | 3.621 | 3.562 | 2.922 | - | - | 0.3288 |
| | *8* | 2.811 | 2.736 | 2.607 | - | - | 0.3074 |

**Table 3.12** Average material properties of EPON 828 specimens with 0%, 1%, 3%, 6% and 10% nanoclay reinforcement at room temperature

| EPON 828 | Young's Modulus (GPa) (Average) - Extensometer | Maximum Strength (MPa) | Failure Strain ( $\varepsilon_f$ ) | Young's Modulus NOVUS Test Result (GPa) | Young's Modulus (GPa) (Manufacturer) | Poisson's Ratio $\nu_{12}$ |
|---|---|---|---|---|---|---|
| **0%** | 2.8177 | 59.06 | 0.032 | 2.289 | 2.758 | 0.3105 |
| **1%** | 2.9127 | 58.84 | 0.032 | - | - | 0.3238 |
| **3%** | 2.9840 | 50.99 | 0.022 | - | - | 0.3288 |
| **6%** | 3.0965 | 38.97 | 0.014 | - | - | 0.3340 |
| **10%** | 3.3427 | 37.74 | 0.014 | - | - | 0.3348 |

### 3.2.4 Comparison of Test Results for Various Resins

We have the test results for Borealis and TP 3868 specimens with 3% nanoclay reinforcement at various temperatures and also the test results for EPON 828 at room temperature at different nanoclay reinforcement percentages. Figure 3.70 shows the comparison of stress vs. strain curves for the four different resins with 3% nanoclay reinforcement at room temperature.

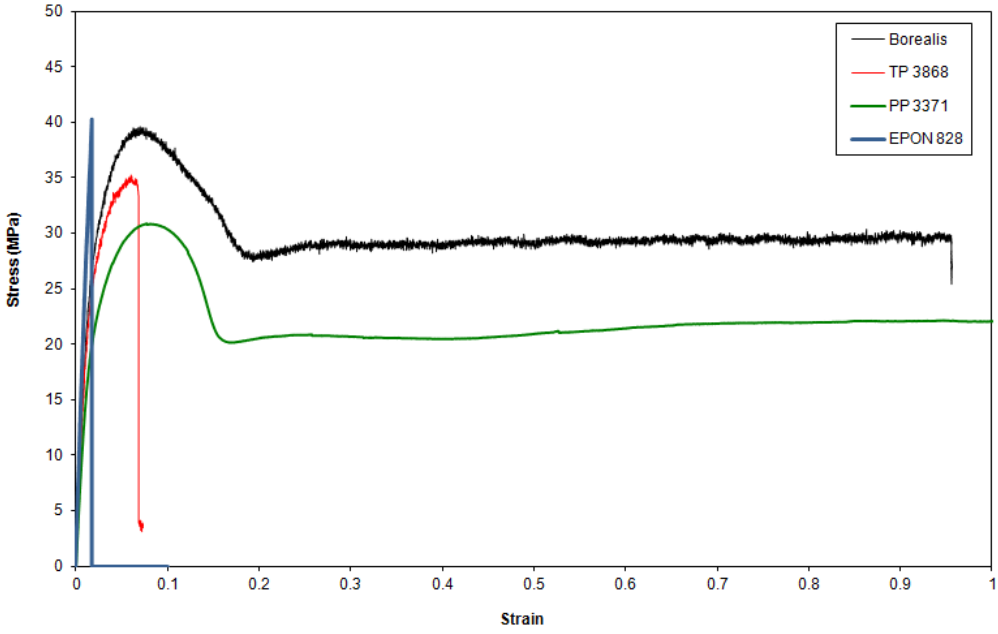


**Figure 3.70** Comparison of stress-strain curves of PP 3371, Borealis, TP 3868 and EPON 828 specimens with 3% nanoclay reinforcement at room temperature

Figure 3.70 indicates that our main resin, PP 3371, is the most ductile material at room temperature when compared with the other resins. Epoxy EPON 828 shows the most brittle behavior at room temperature.

The comparison of the stress-strain curves for the additional PP based resins, namely Borealis and TP 3868, at various temperatures are displayed in Figures 3.71 and 3.72 respectively. It is noted that at low temperatures both resins become brittle and at higher temperatures are more or less ductile. It is also observed that at the same temperature Borealis is relatively more ductile than TP3868.

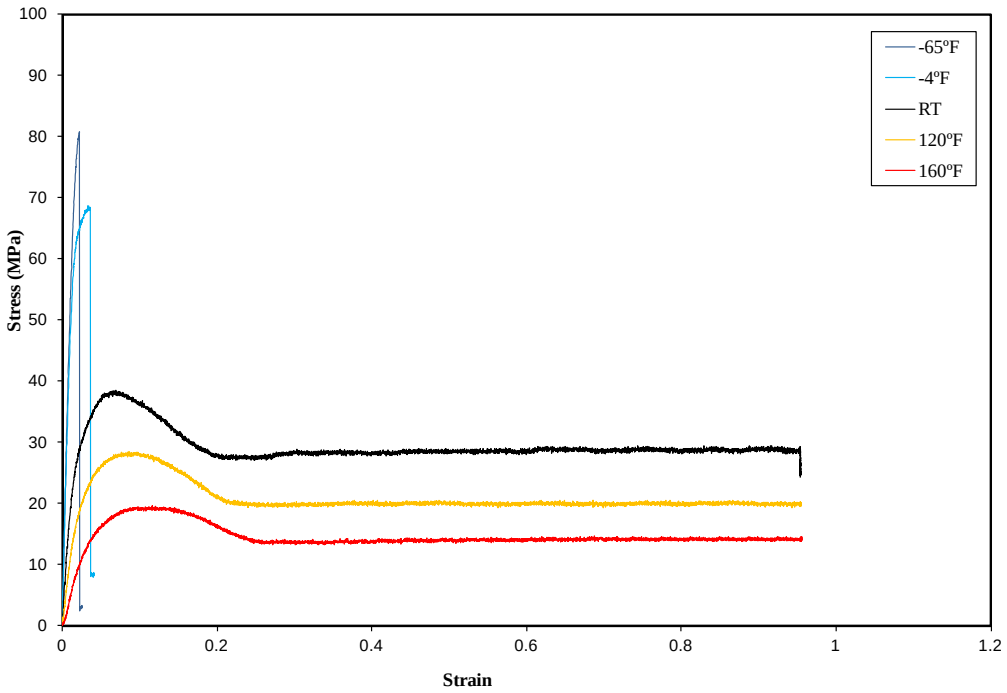


**Figure 3.71** Comparison of stress-strain curves of Borealis specimens with 3% nanoclay reinforcement at various temperatures

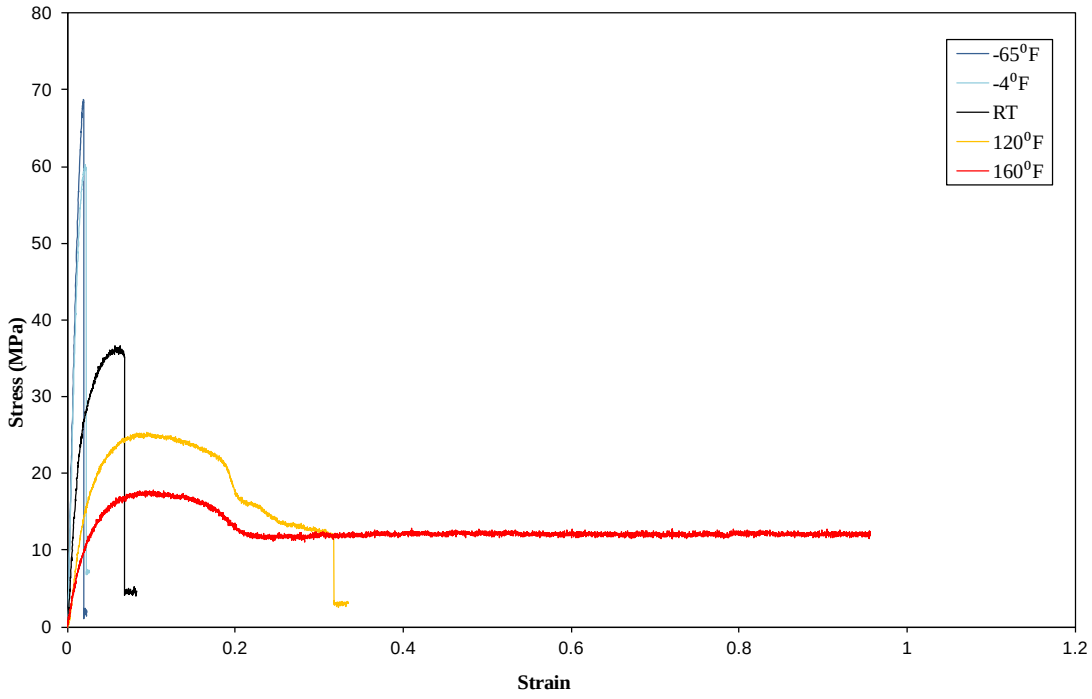


**Figure 3.72** Comparison of stress-strain curves of TP 3868 specimens with 3% nanoclay reinforcement at various temperatures

### 3.3. LOW VELOCITY IMPACT TESTS

Next, low velocity (drop weight) impact tests were carried out at an energy level appropriate for reinforced plastics and various temperatures. PP 3371 specimens with 0%, 0.2%, 1%, 3%, 6% and 10% nanoclay reinforcement were subjected to low velocity impact tests. All specimens had dimensions of 4"x4"×(1/8)". Tests were carried out using an instrumented Instron-Dynatup 8520 drop-weight impact tester.

The results in Table 3.13 show the behavior of specimens at one energy level and -65°F, -4°F, room temperature, 120°F and 160°F. Depending on the drop height, the weight used and the

percentage of nanoclay reinforcement, the following was observed: some specimens were penetrated (P), some cracked (F) and some visually remained virtually intact (NP), that is they were not penetrated. The drop height was 6” and the weight used was 4.126 kg.

**Table 3.13** Drop weight tests results at -65ºF, -4ºF, room temperature, 120°F and 160°F

Drop Height = ~6”

Drop Weight = ~4.126 kg

| Nanoclay Reinforcement Percentage | Specimen | Test Results ( at RT) | Test Results ( at 120°F) | Test Results ( at 160°F) | Test Results ( at -4°F) | Test Results ( at -65°F) |
|---|---|---|---|---|---|---|
| 0% | *1* | NP | NP | NP | P | P |
| | *2* | NP | NP | NP | P | P |
| | *3* | NP | | NP | | |
| | *4* | NP | | | | |
| | *5* | NP | | | | |
| | *6* | NP | | | | |
| | *7* | NP | | | | |
| | *8* | NP | | | | |
| | *9* | NP | | | | |
| | *10* | NP | | | | |
| | | | | | | |
| 0.2% | *1* | NP | NP | NP | P | P |
| | *2* | F | NP | NP | P | P |
| | *3* | P | NP | NP | | |
| | *4* | P | NP | | | |
| | *5* | NP | | | | |
| | *6* | NP | | | | |
| | *7* | F | | | | |
| | *8* | NP | | | | |
| | *9* | P | | | | |
| | *10* | NP | | | | |

**Table 3.13** Continued

| | | | | | | |
|---|---|---|---|---|---|---|
| **1%** | *1* | P | NP | NP | P | P |
| | *2* | F | NP | NP | P | P |
| | *3* | P | | | | |
| | *4* | P | | | | |
| | *5* | P | | | | |
| | *6* | F | | | | |
| | | | | | | |
| **3%** | *1* | P | NP | NP | *Not performed; Penetration assumed* | *Not performed; Penetration assumed* |
| | *2* | P | NP | NP | | |
| | *3* | P | | NP | | |
| | *4* | P | | | | |
| | *5* | F | | | | |
| | | | | | | |
| **6%** | *1* | F | NP | NP | *Not performed; Penetration assumed* | *Not performed; Penetration assumed* |
| | *2* | F | NP | NP | | |
| | *3* | P | | | | |
| | *4* | P | | | | |
| | | | | | | |
| **10%** | *1* | *Not performed; Penetration assumed* | NP | NP | *Not performed- Penetration assumed* | *Not performed; Penetration assumed* |
| | *2* | | NP | NP | | |

P: Penetrated

NP: Virtually intact

F: Some cracked

### 3.3.1 Low Velocity Drop Weight Test Results at Various Temperatures

In Figures 3.73-3.76 we compare the behavior of neat PP specimens at -4°F, -65°F, room temperature, 120°F and 160°F. Neat PP specimens were not penetrated at room temperature and at higher temperatures. However, all were penetrated at the lower temperatures. In case of penetration, the effect is clearly seen in the Force - Displacement and Force – Time (Figures 3.73 and 3.76) curves.

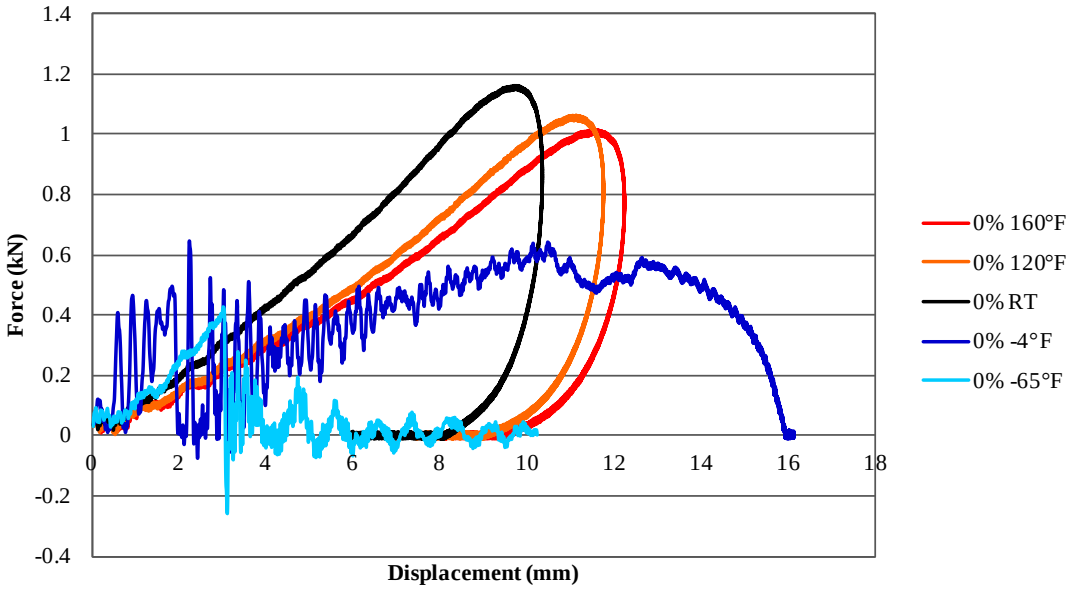


**Figure 3.73** Force vs. displacement curves for neat PP specimens at -4°F, -65°F, room temperature, 120°F and 160°F

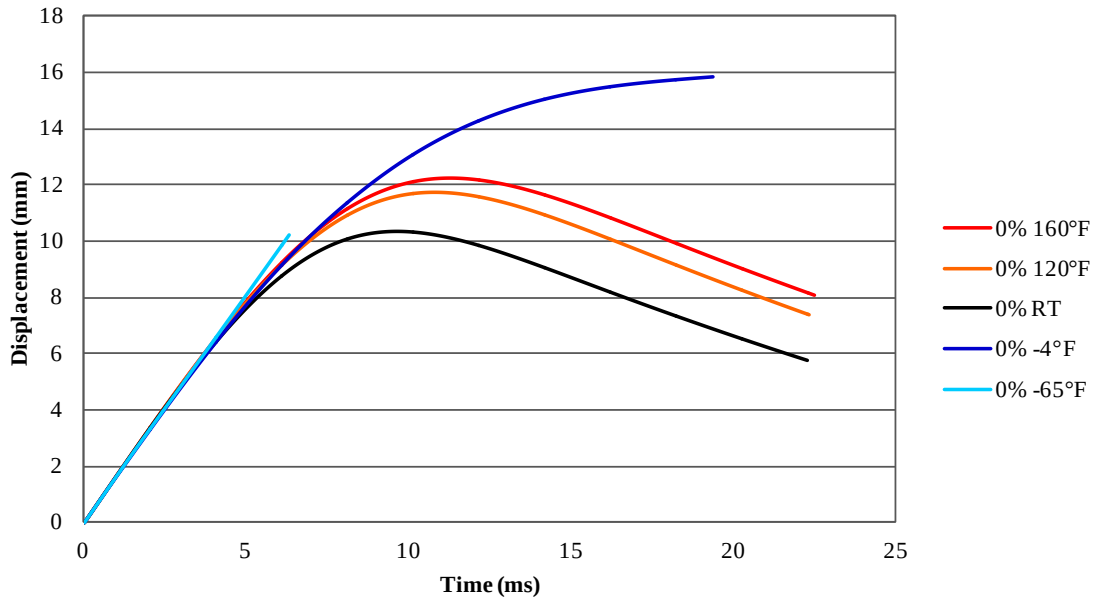


**Figure 3.74** Displacement vs. time curves for neat PP specimens at -4°F, -65°F, room temperature, 120°F and 160°F

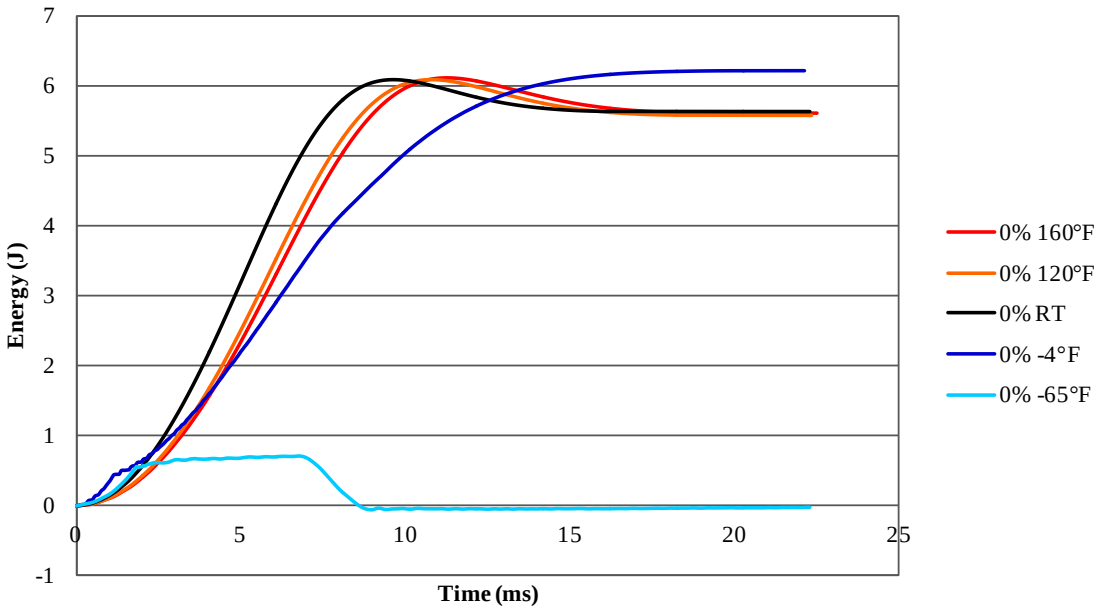


**Figure 3.75** Energy vs. time curves for neat PP specimens at -4°F, -65°F, room temperature, 120°F and 160°F

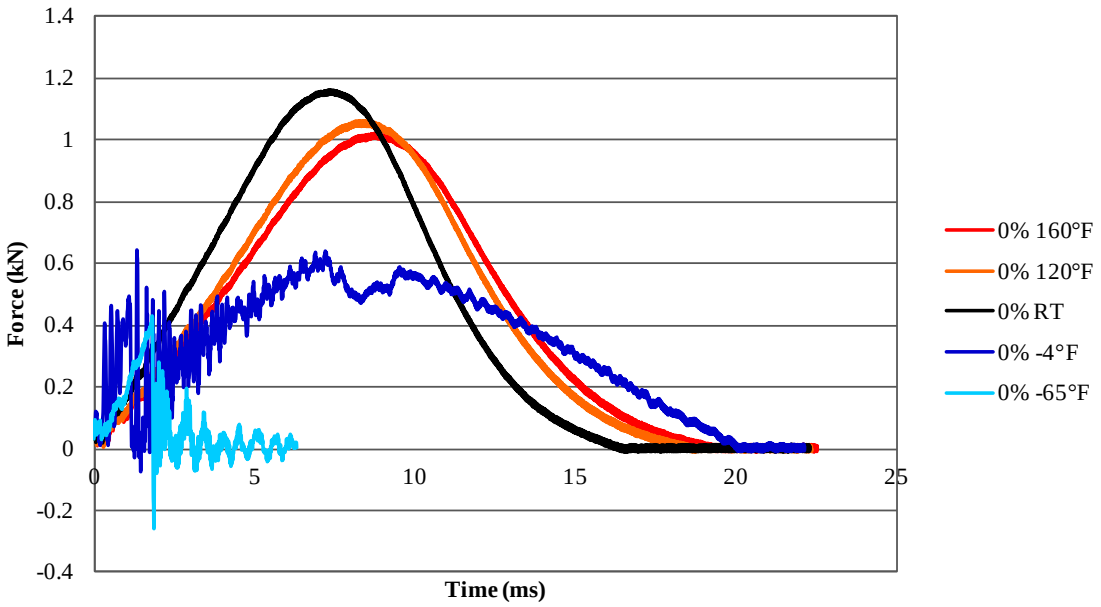


**Figure 3.76** Force vs. time curves for neat PP specimens at -4°F, -65°F, room temperature, 120°F and 160°F

Similarly, in Figures 3.77-3.80 the results for 0.2% nanoclay reinforced specimens at various temperatures are compared. The specimens showed the same behavior at room and high temperatures. However, at low temperatures all specimens were penetrated. Again the evidence of penetration can be seen in Figures 3.77 and 3.80.

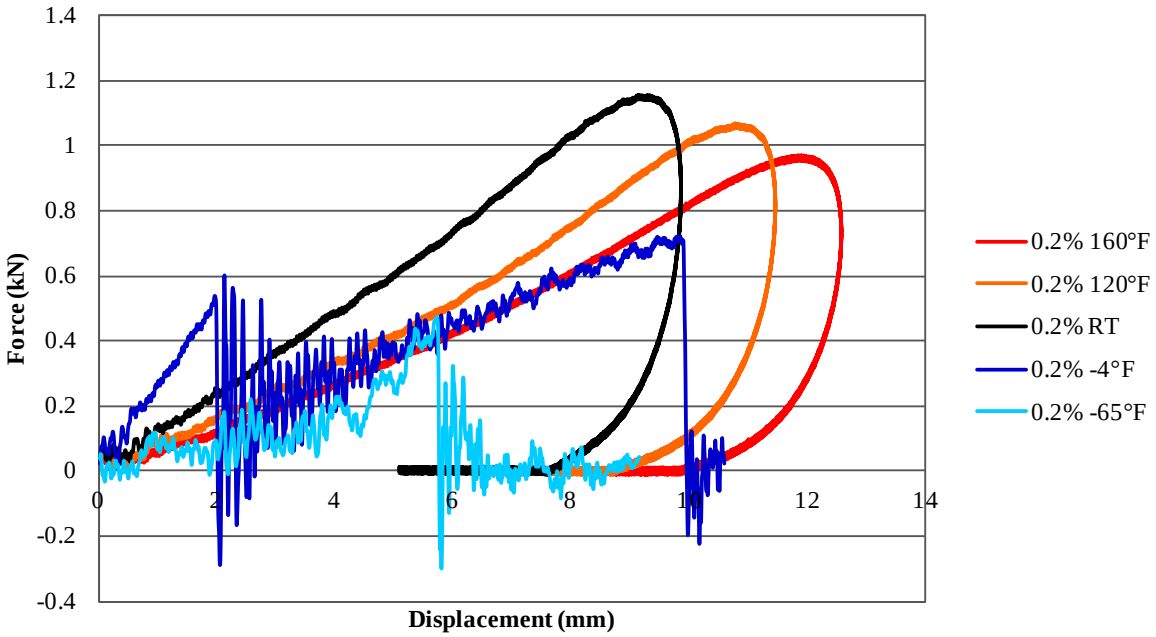


**Figure 3.77** Force vs. displacement curves for PP with 0.2% nanoclay reinforced specimens at -4°F, -65°F, room temperature, 120°F and 160°F

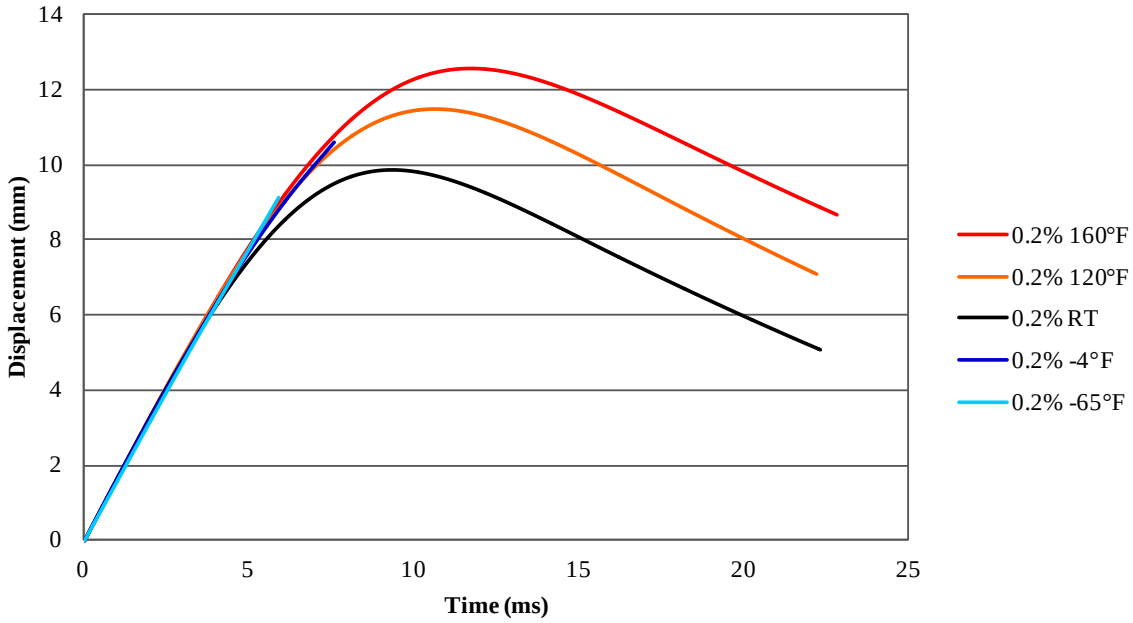


**Figure 3.78** Displacement vs. time curves for PP with 0.2% nanoclay reinforced specimens at -4°F, -65°F, room temperature, 120°F and 160°F

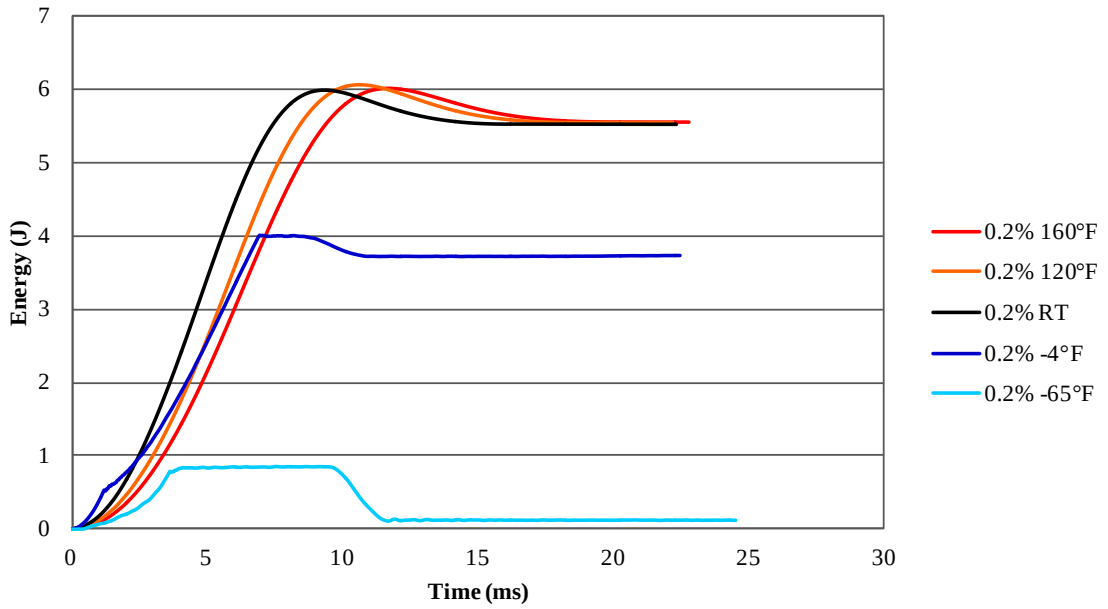


**Figure 3.79** Energy vs. time curves for PP with 0.2% nanoclay reinforced specimens at -4°F, -65°F, room temperature, 120°F and 160°F

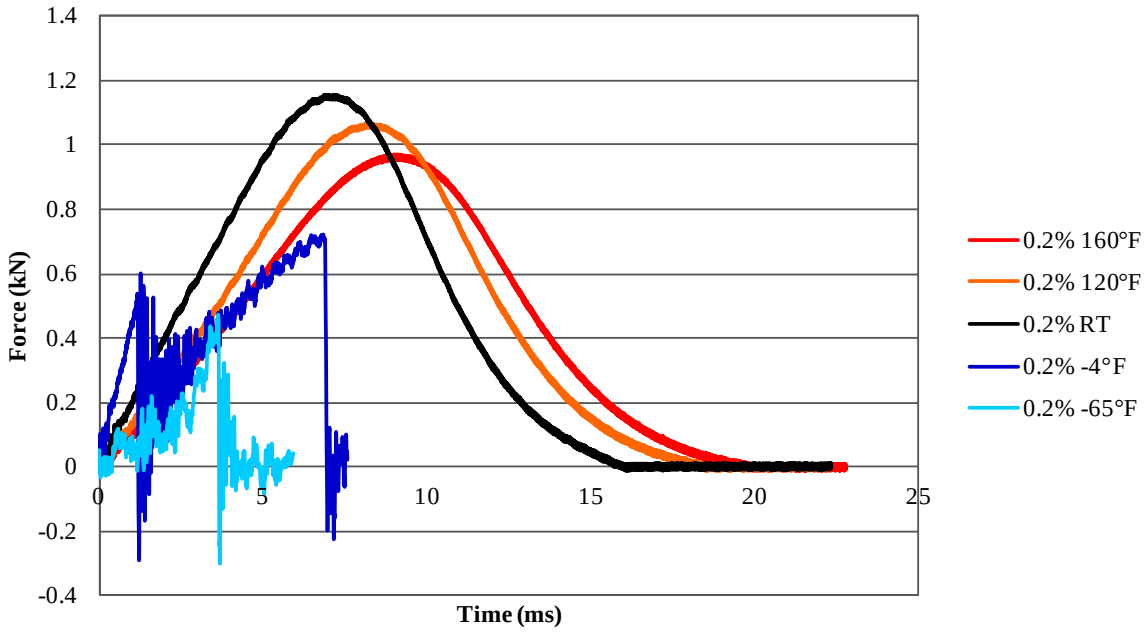


**Figure 3.80** Force vs. time curves for PP with 0.2% nanoclay reinforced specimens at -4°F, -65°F, room temperature, 120°F and 160°F

The results for 1% nanoclay reinforced PP specimens at various temperatures are summarized in Figures 3.81-3.84. Again at low temperatures all the specimens were penetrated. In addition, at room temperature specimens were penetrated and two cracked. This is due to the fact that the increase in nanoclay makes the material more brittle.

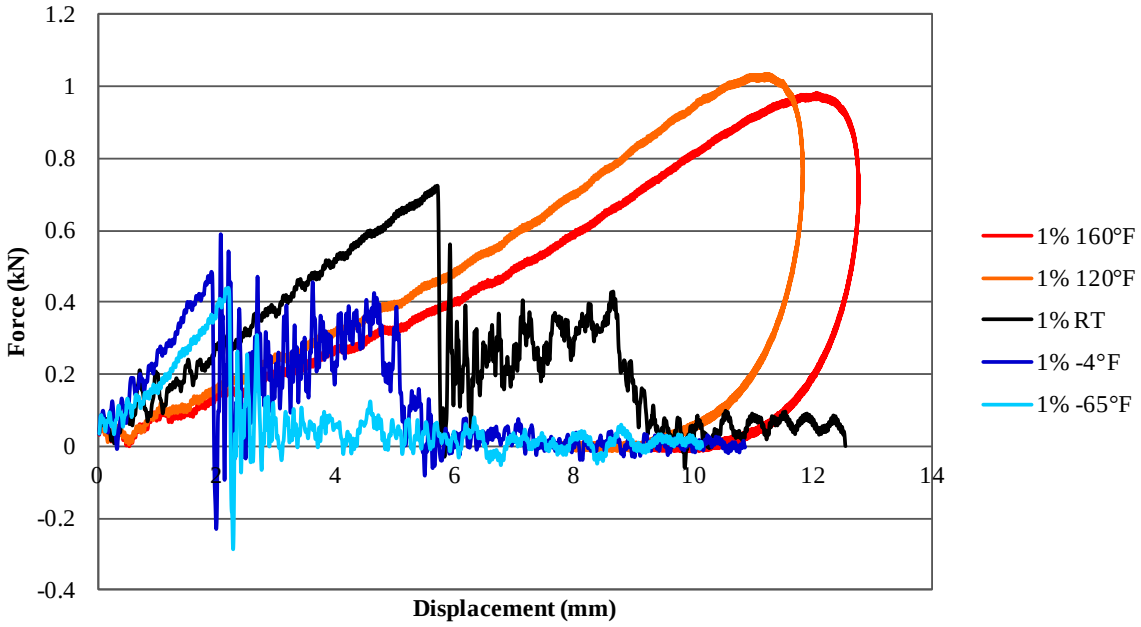


**Figure 3.81** Force vs. displacement curves for PP with 1% nanoclay reinforced specimens at -4°F, -65°F, room temperature, 120°F and 160°F

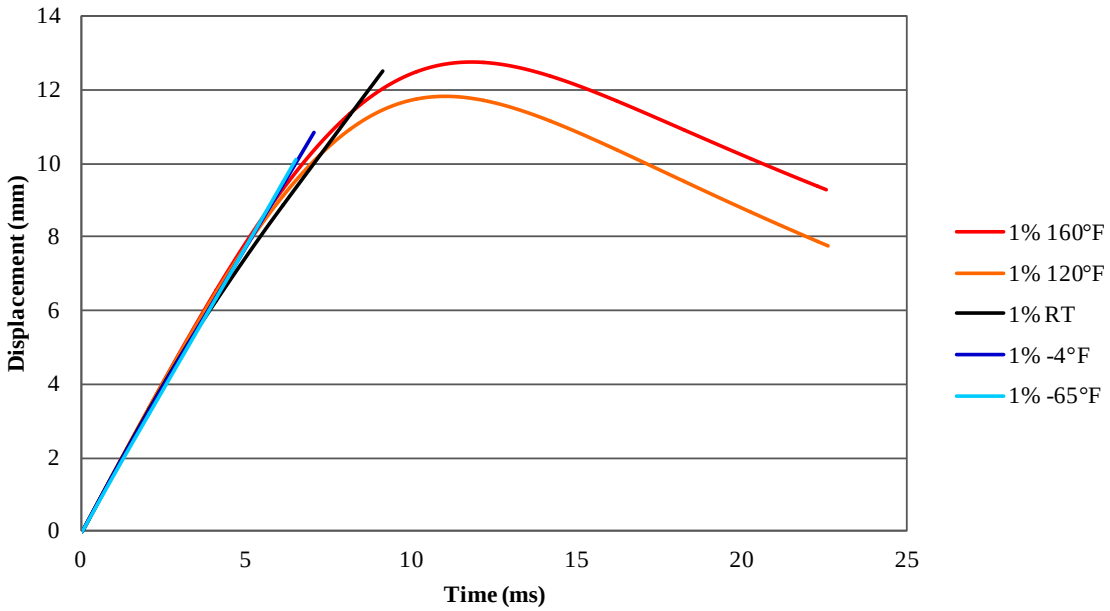


**Figure 3.82** Displacement vs. time curves for PP with 1% nanoclay reinforced specimens at -4°F, -65°F, room temperature, 120°F and 160°F

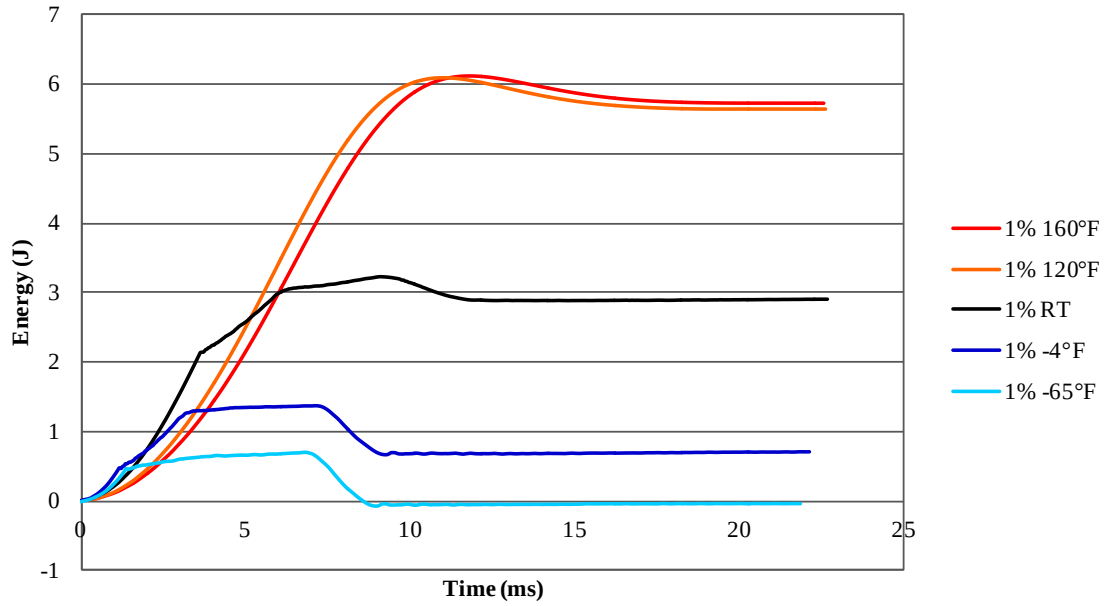


**Figure 3.83** Energy vs. time curves for PP with 1% nanoclay reinforced specimens at -4°F, -65°F, room temperature, 120°F and 160°F

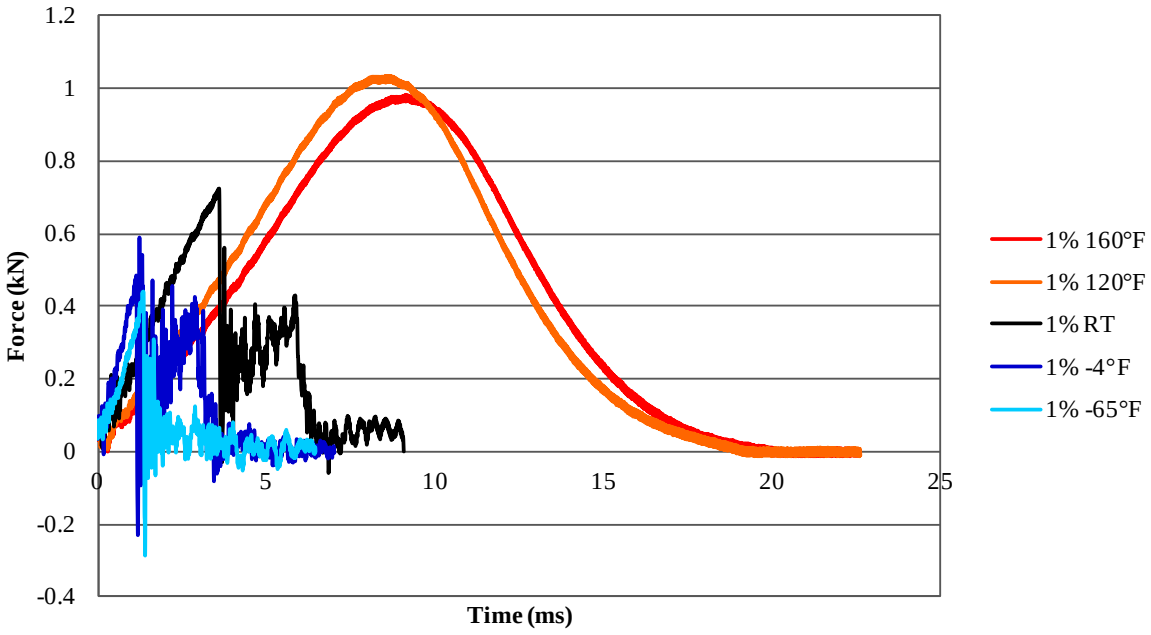


**Figure 3.84** Force vs. time curves for PP with 1% nanoclay reinforced specimens at -4°F, -65°F, room temperature, 120°F and 160°F

The remaninin specimens with 3%, 6% and 10% nanoclay reinforcement were not subjected to low velocity drop weigth tests at low temperatures, because all were expected to be penetrated since a higher percentage of nanoclay makes the material more brittle.

Figures 3.85-3.88 show present the results for 3% nanoclay reinforced specimens at RT, 120°F and 160°F. At this renforcement level at room temperature 4 specimens were penetrated and one cracked. At 120°F and 160°F the specimens were not penetrated.

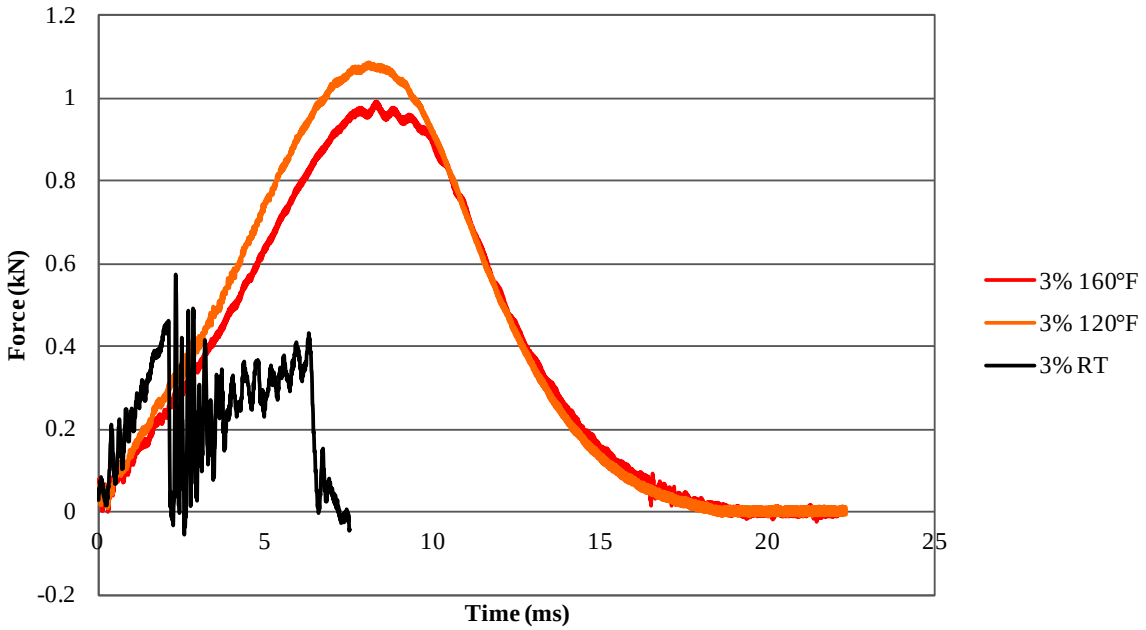


**Figure 3.85** Force vs. displacement curves for PP with 3% nanoclay reinforced specimens at RT, 120°F and 160°F

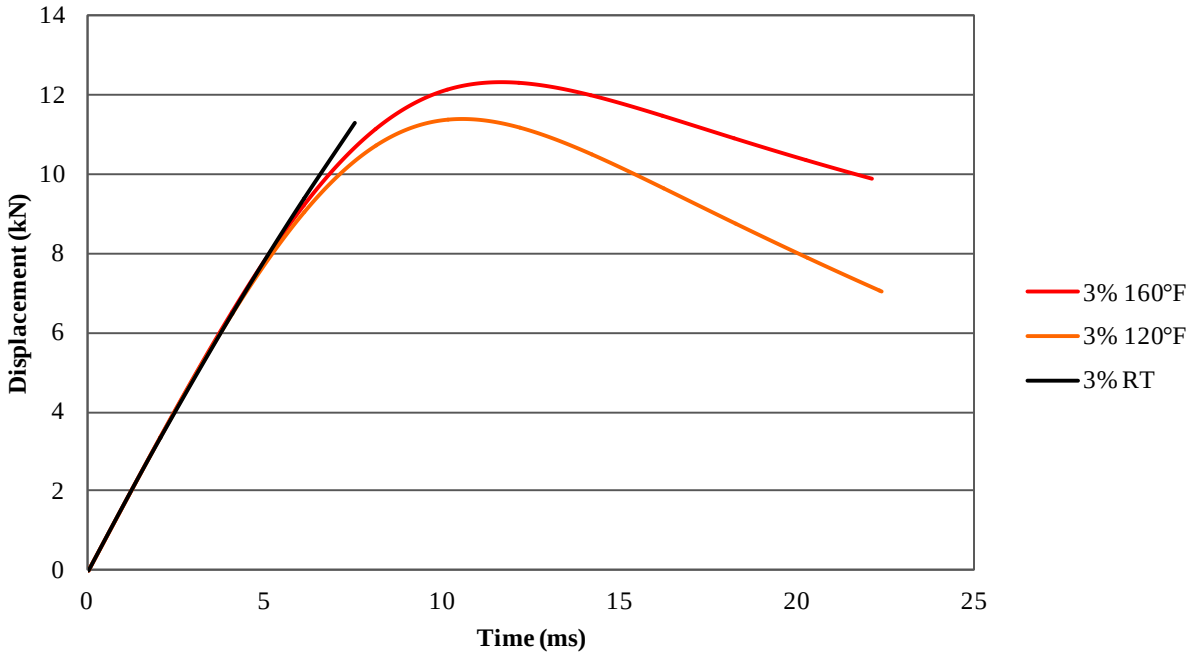


**Figure 3.86** Displacement vs. time curves for PP with 3% nanoclay reinforced specimens at RT, 120°F and 160°F

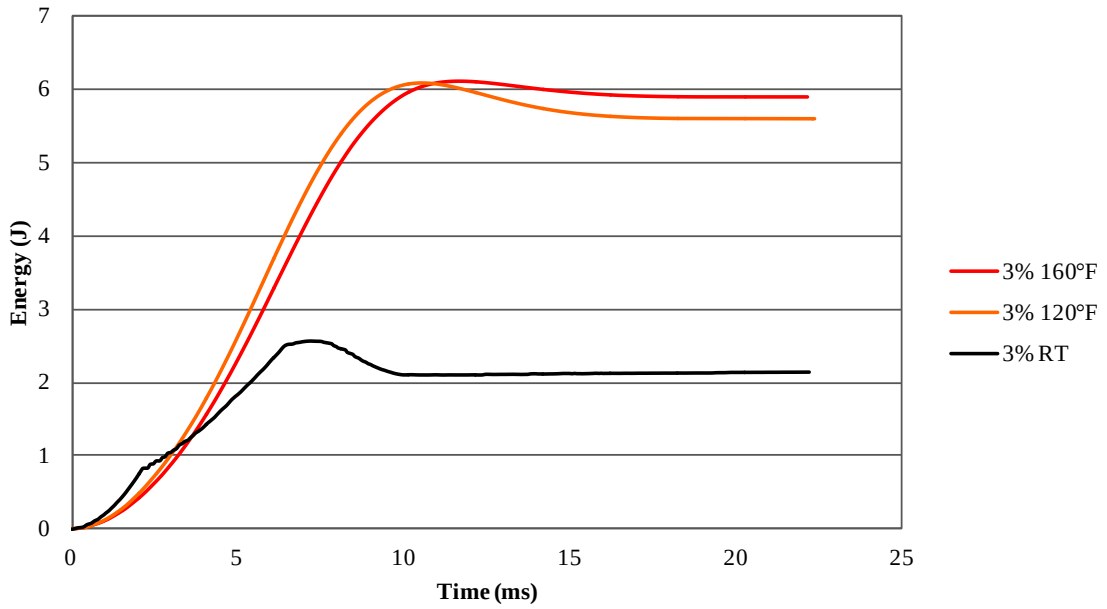


**Figure 3.87** Energy vs. time curves for PP with 3% nanoclay reinforced specimens at RT, 120°F and 160°F

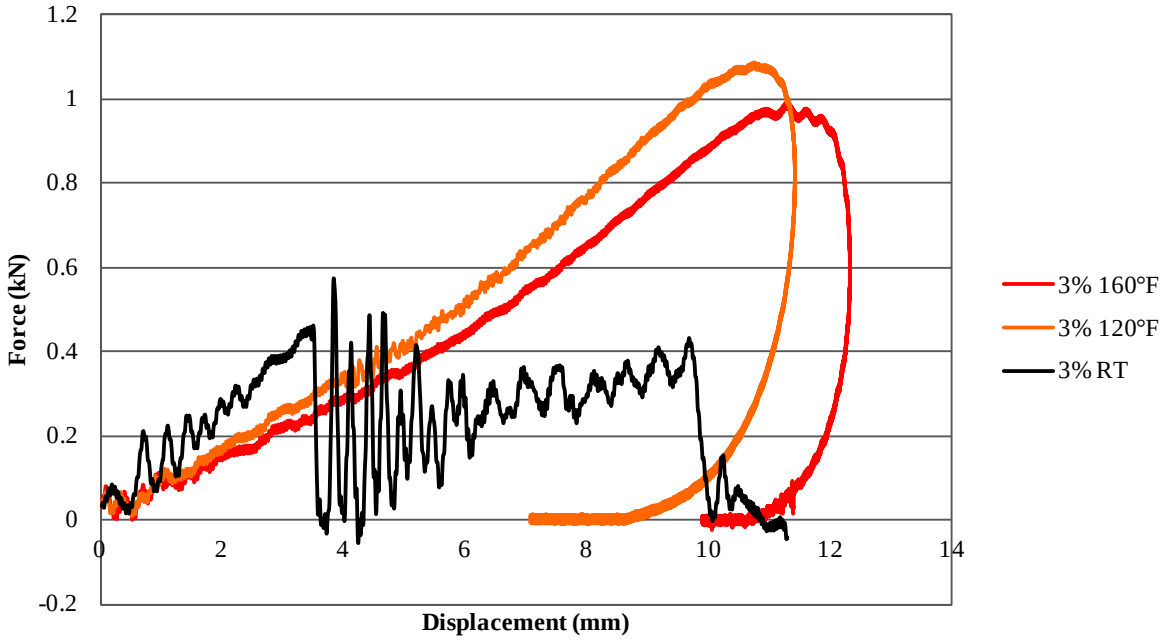


**Figure 3.88** Force vs. time curves for PP with 3% nanoclay reinforced specimens at RT, 120°F and 160°F

The low velocity drop weight test results for PP 3371 specimens with 6% nanoclay reinforcement are depicted in Figures 3.89 –3.93. The behavior was similar to that observed for the 3% specimens. That is at room temperature two specimens were penetrated and two cracked. However, at higher temperatures they were not penetrated.

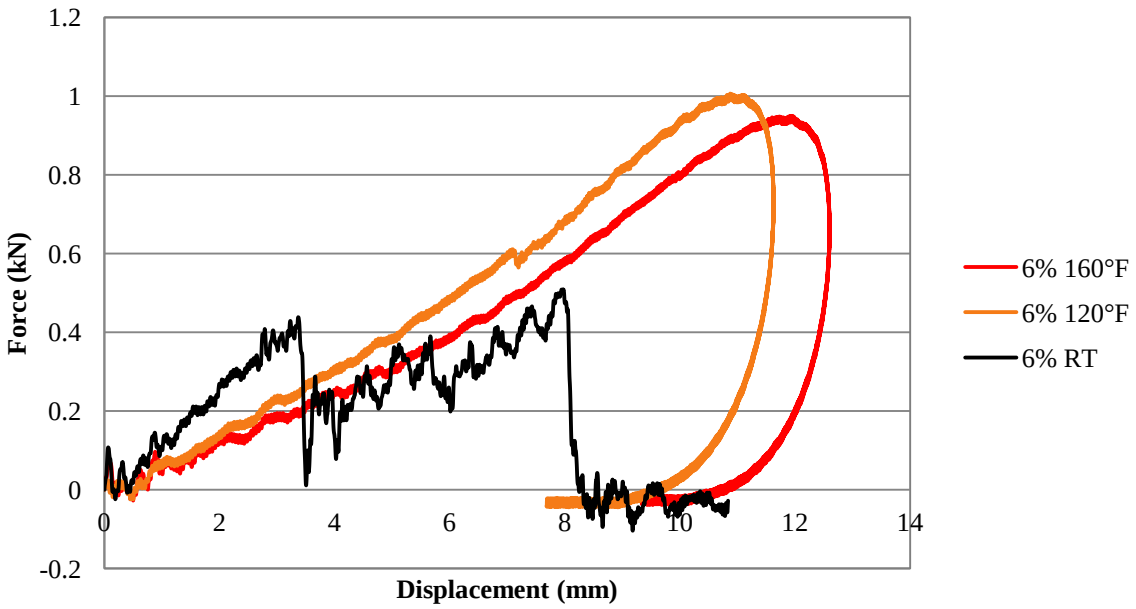


**Figure 3.89** Force vs. displacement curves for PP with 6% nanoclay reinforced specimens at RT, 120°F and 160°F

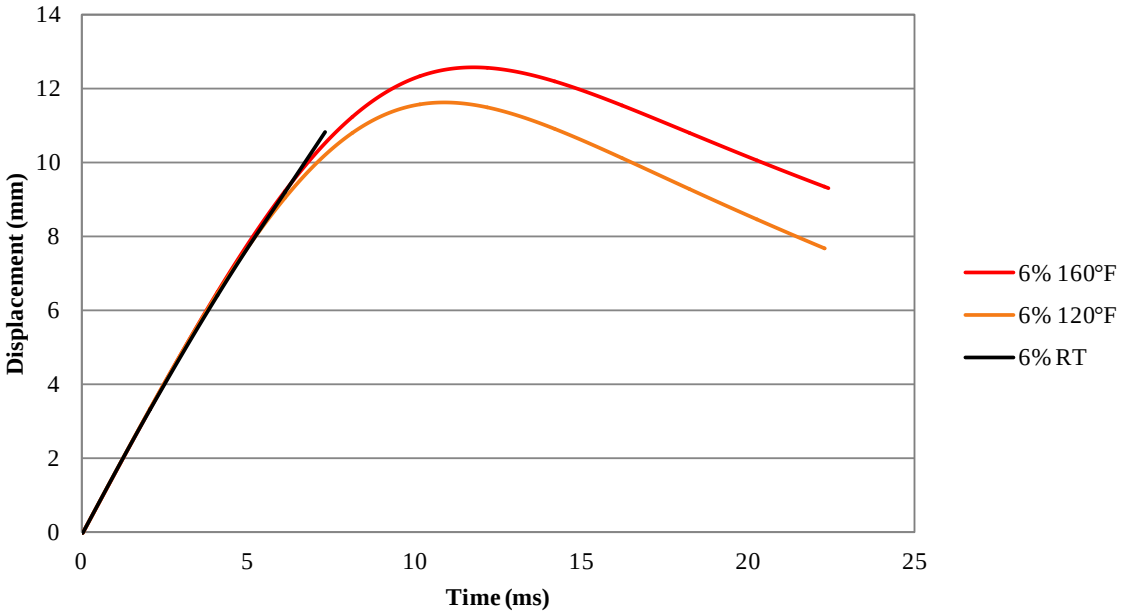


**Figure 3.90** Displacement vs. time curves for PP with 6% nanoclay reinforced specimens at RT, 120°F and 160°F

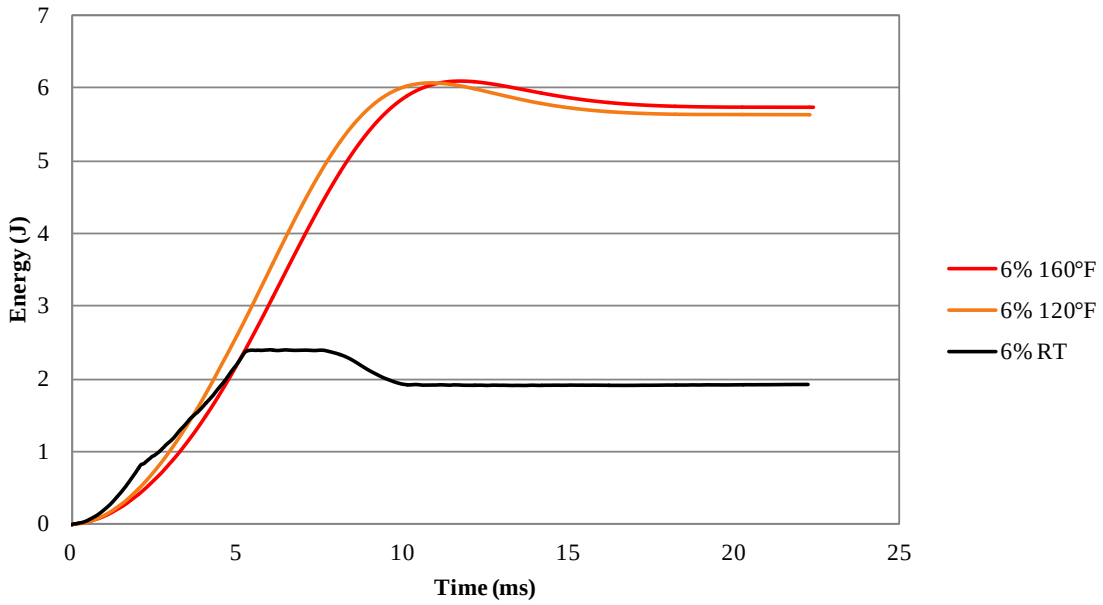


**Figure 3.91** Energy vs. time curves for PP with 6% nanoclay reinforced specimens at RT, 120F and 160F

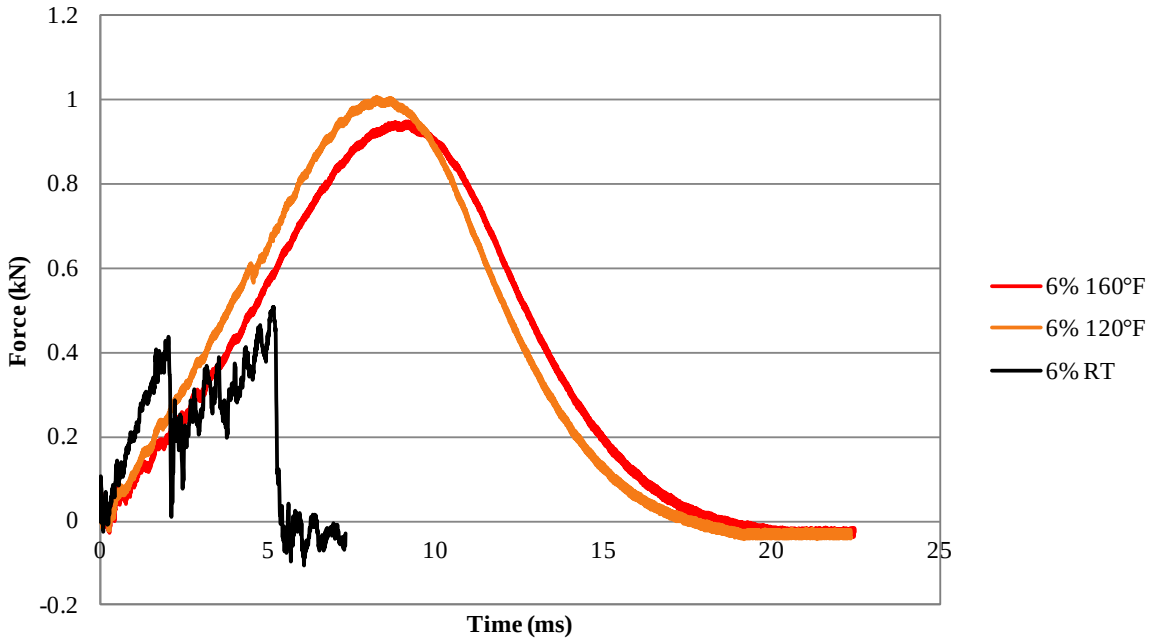


**Figure 3.92** Force vs. time curves for PP with 6% nanoclay reinforced specimens at RT, 120F and 160F

Finally, the 10% nanoclay reinforced PP 3371 specimens were tested at 120°F and 160°F only, because even for 6% reinforcement most of the specimens were penetrated at room temperature. The test results are given at Figures 3.93-3.96.

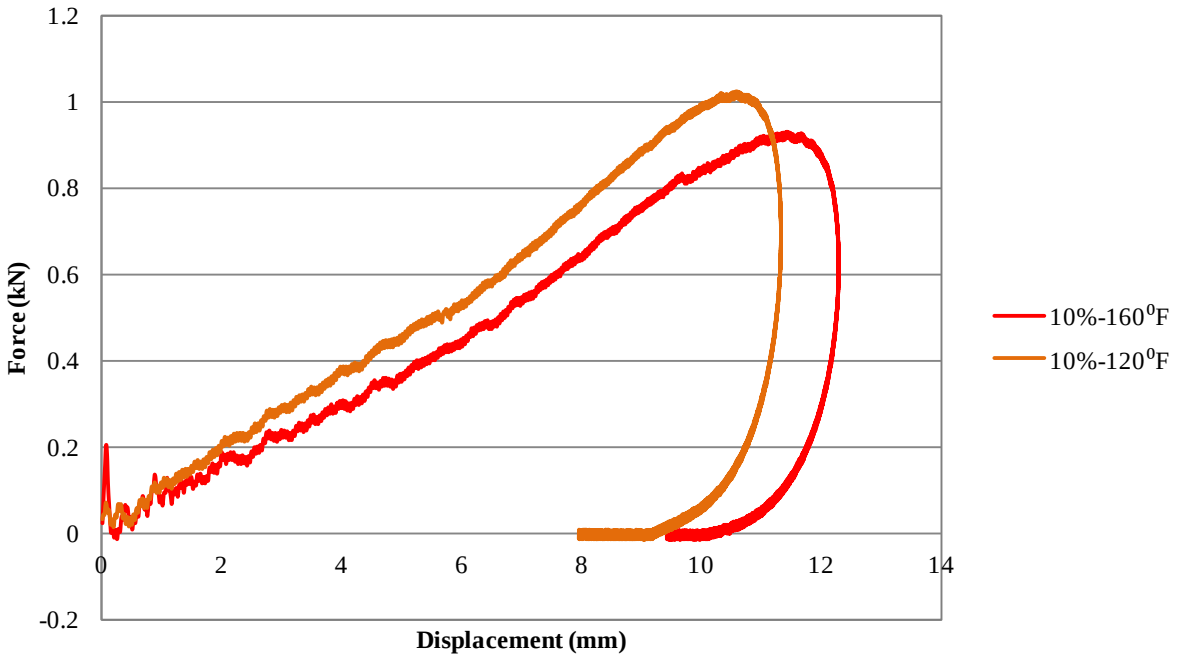


**Figure 3.93** Force vs. displacement curves for PP with 10% nanoclay reinforced specimens at 120°F and 160°F

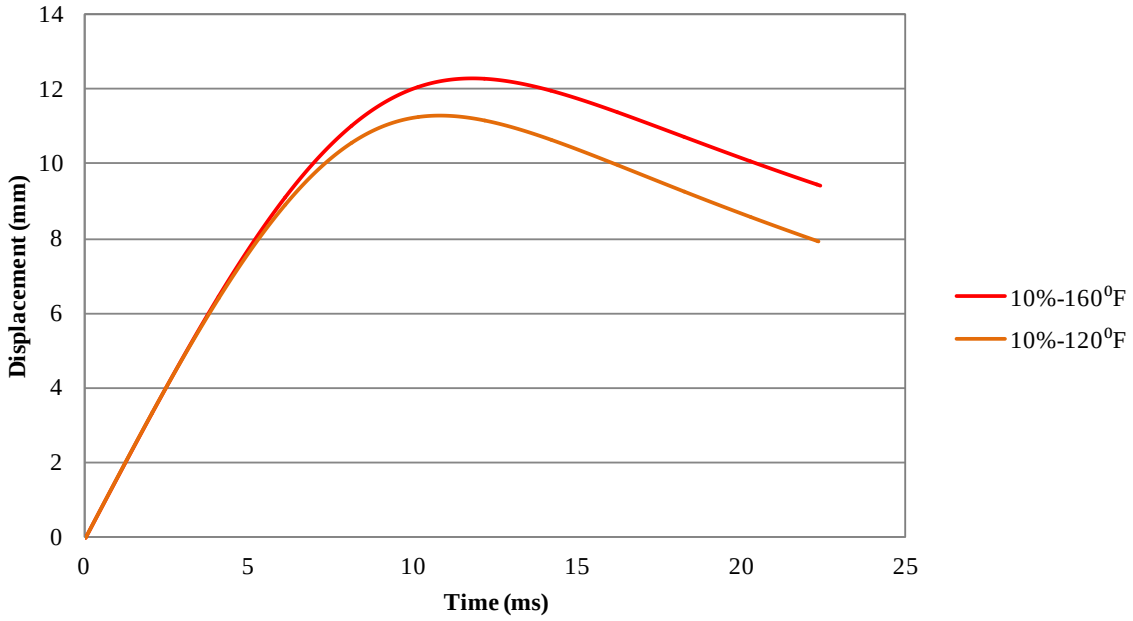


**Figure 3.94** Displacement vs. time curves for PP with 10% nanoclay reinforced specimens at 120°F and 160°F

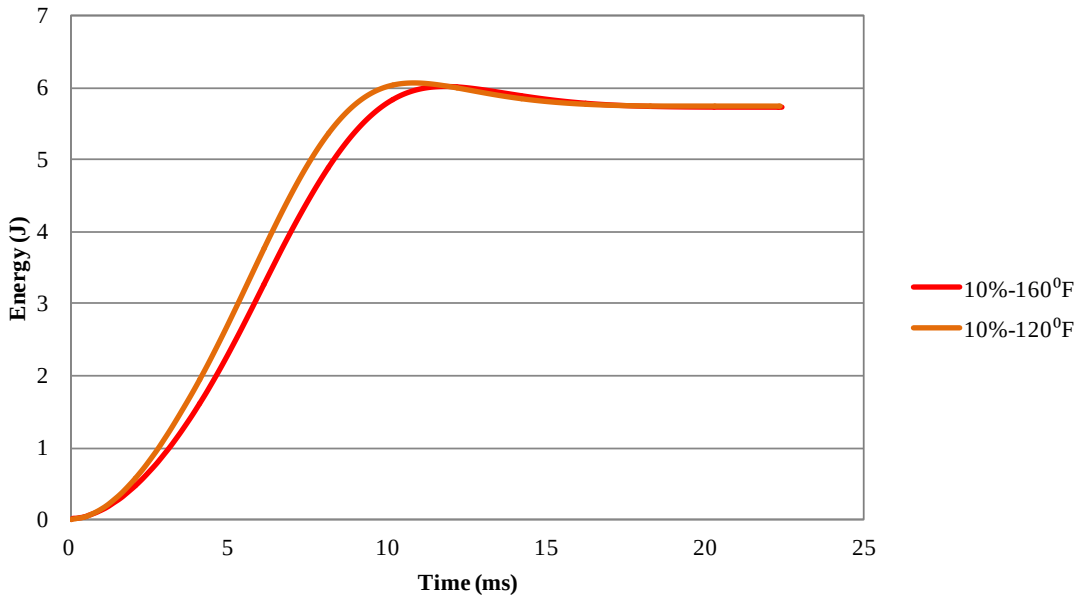


**Figure 3.95** Energy vs. time curves for PP with 10% nanoclay reinforced specimens at 120°F and 160°F

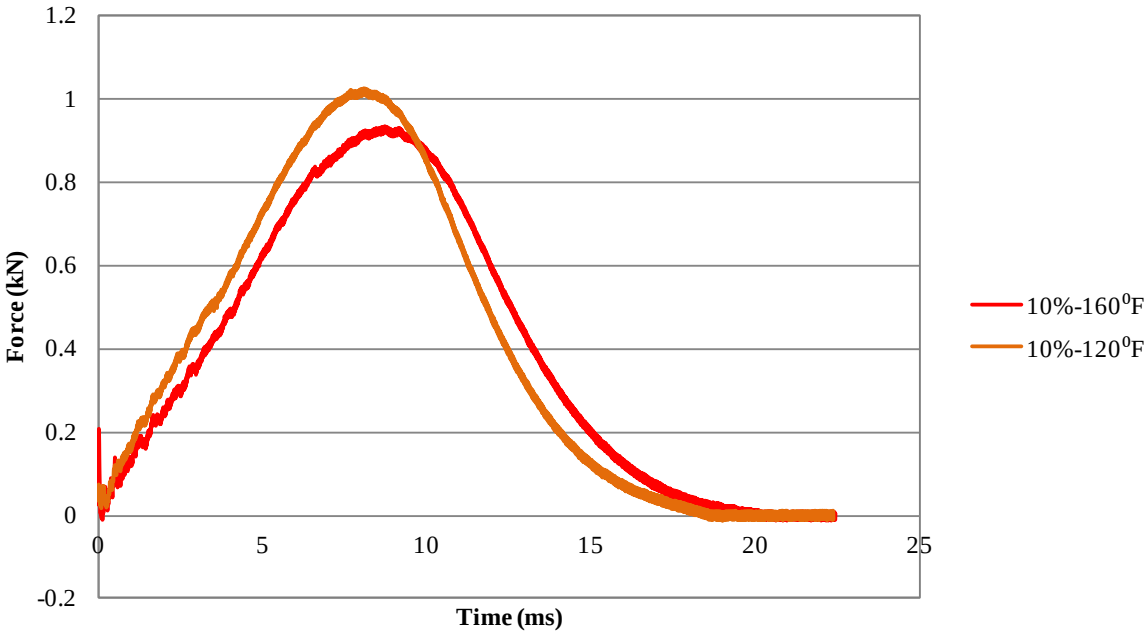


**Figure 3.96** Force vs. time curves for PP with 10% nanoclay reinforced specimens at 120°F and 160°F

### 3.3.2.Comparison of Low Velocity Drop Weight Test Results at a Given Temperature

The test results are replotted at a given temperature to ascertain the effect of nanoclay reinforcement percentage. Figures 3.97-3.100 show the comparison of the results for various nanoclay reinforcement percentages at 160°F. The results for 120°F, RT, -4°F and -65°F are similarly displayed in Figures 3.101-3.104, Figures 3.105-3.108, Figures 3.109-3.112 and Figures 3.113-3.116 respectively.

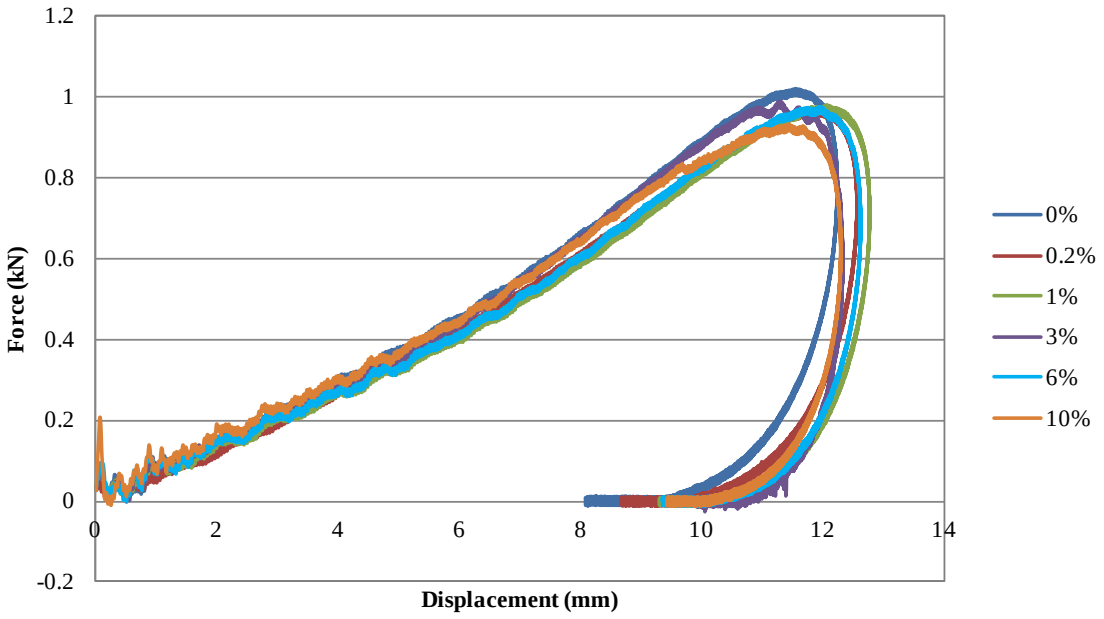


**Figure 3.97** Force vs. displacement curves for PP specimens reinforced with different nanoclay percentages at 160°F

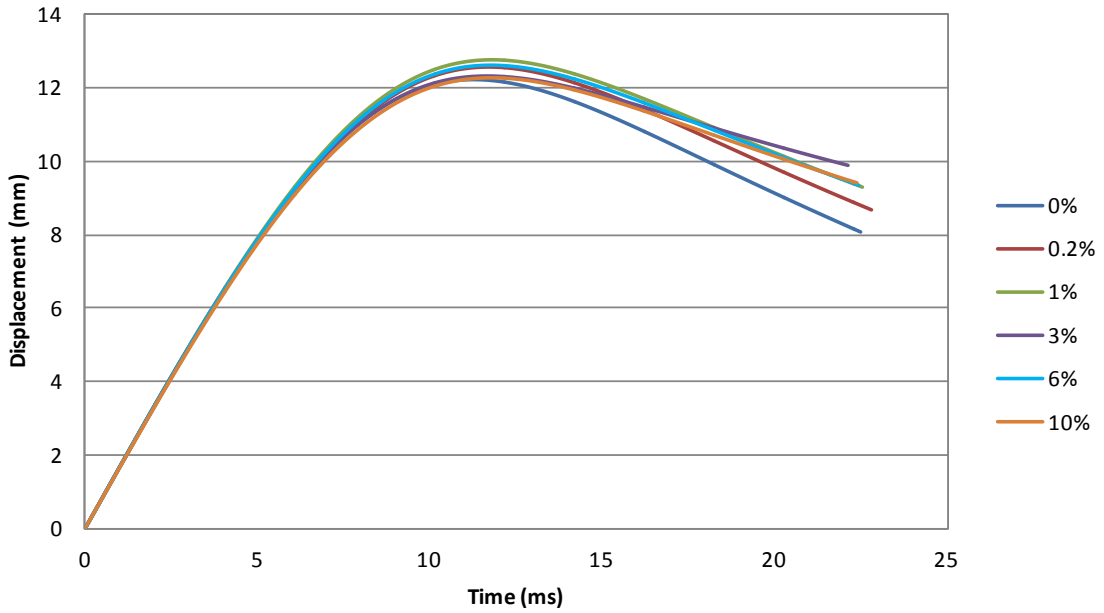


**Figure 3.98** Displacement vs. time curves for PP specimens reinforced with different nanoclay percentages at 160°F

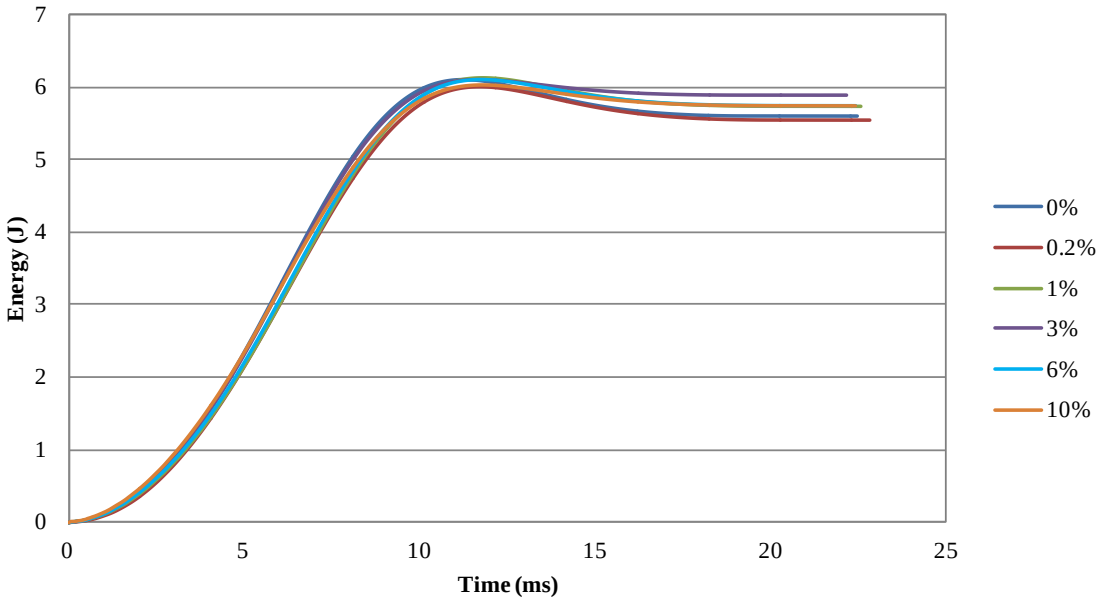


**Figure 3.99** Energy vs. time curves for PP specimens reinforced with different nanoclay percentages at 160°F

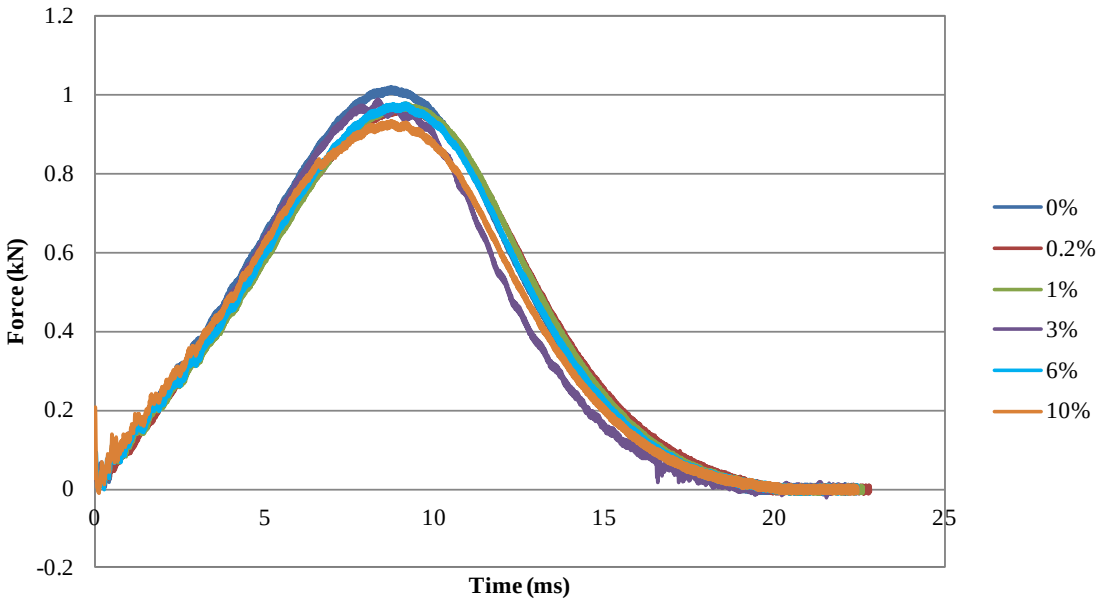


**Figure 3.100** Force vs. time curves for PP specimens reinforced with different nanoclay percentages at 160°F

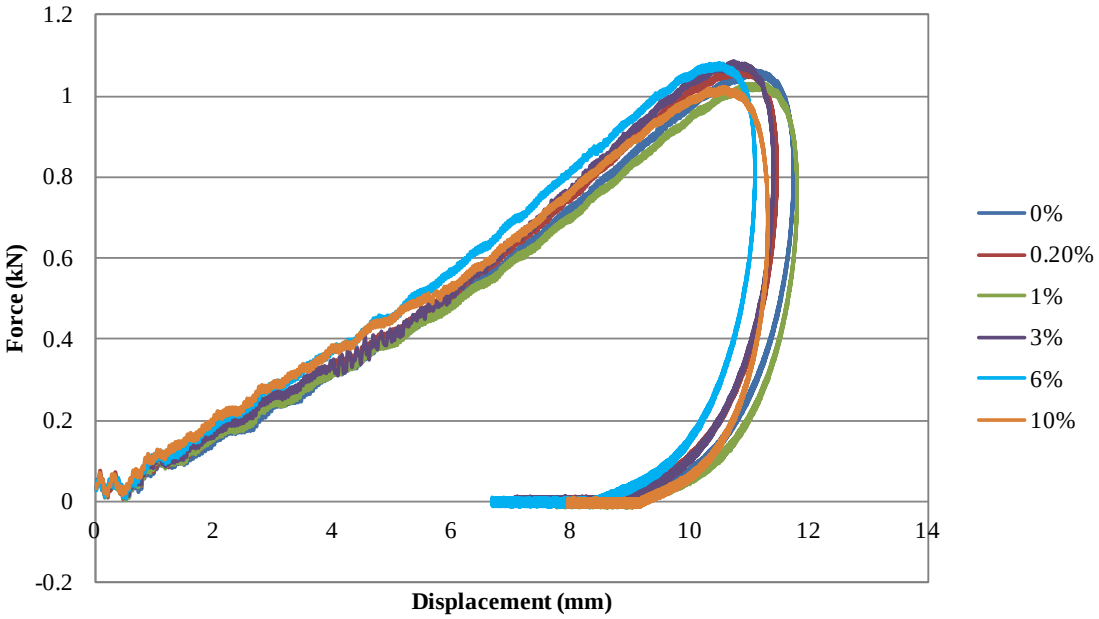


**Figure 3.101** Force vs. displacement curves for PP specimens reinforced with different nanoclay percentages at 120°F

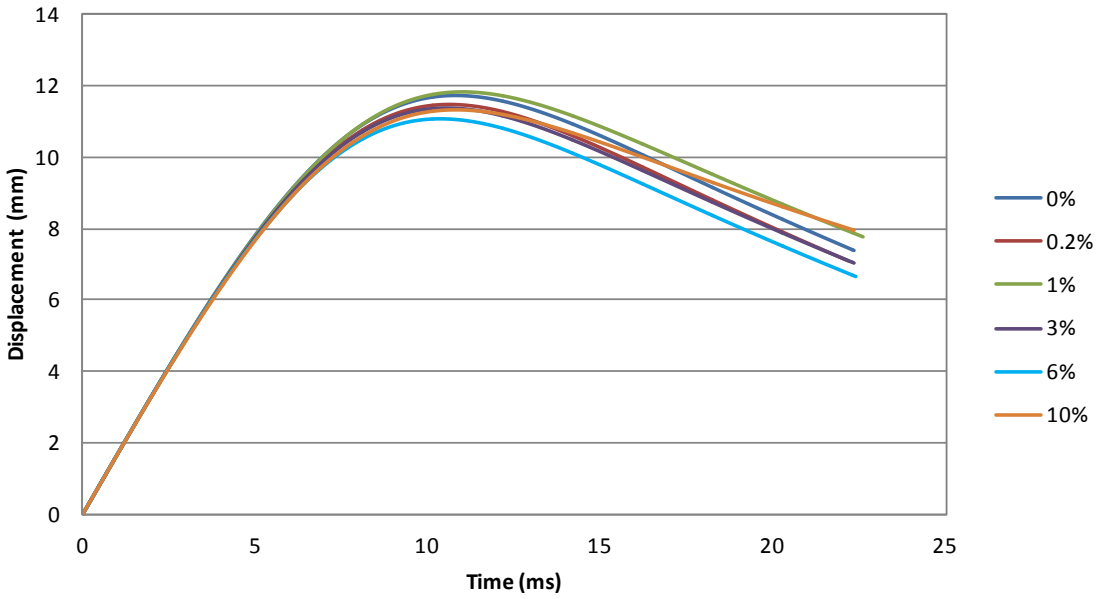


**Figure 3.102** Displacement vs. time curves for PP specimens reinforced with different nanoclay percentages at 120°F

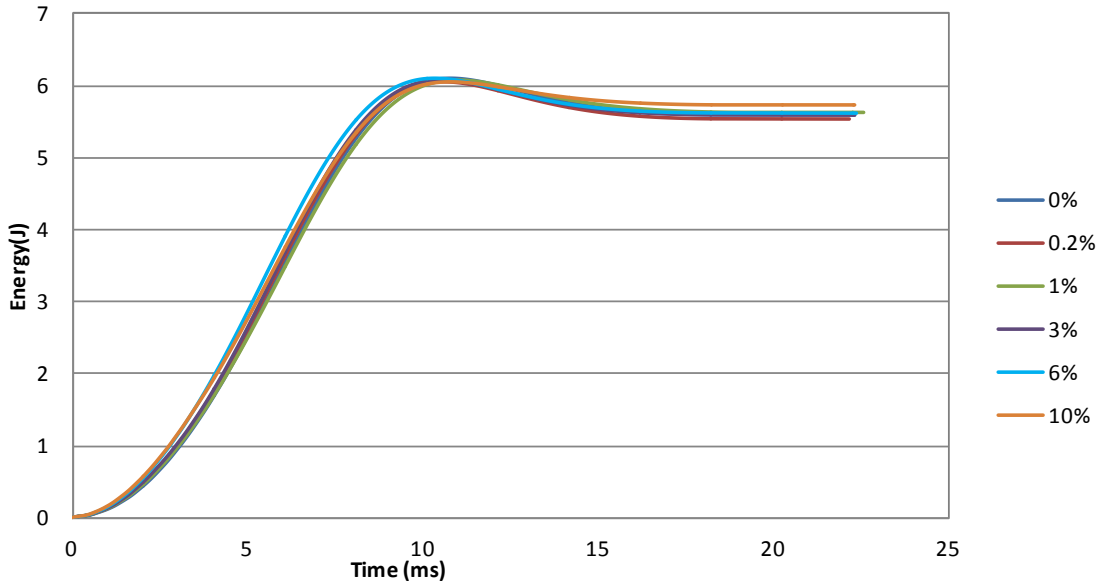


**Figure 3.103** Energy vs. time curves for PP specimens reinforced with different nanoclay percentages at 120°F

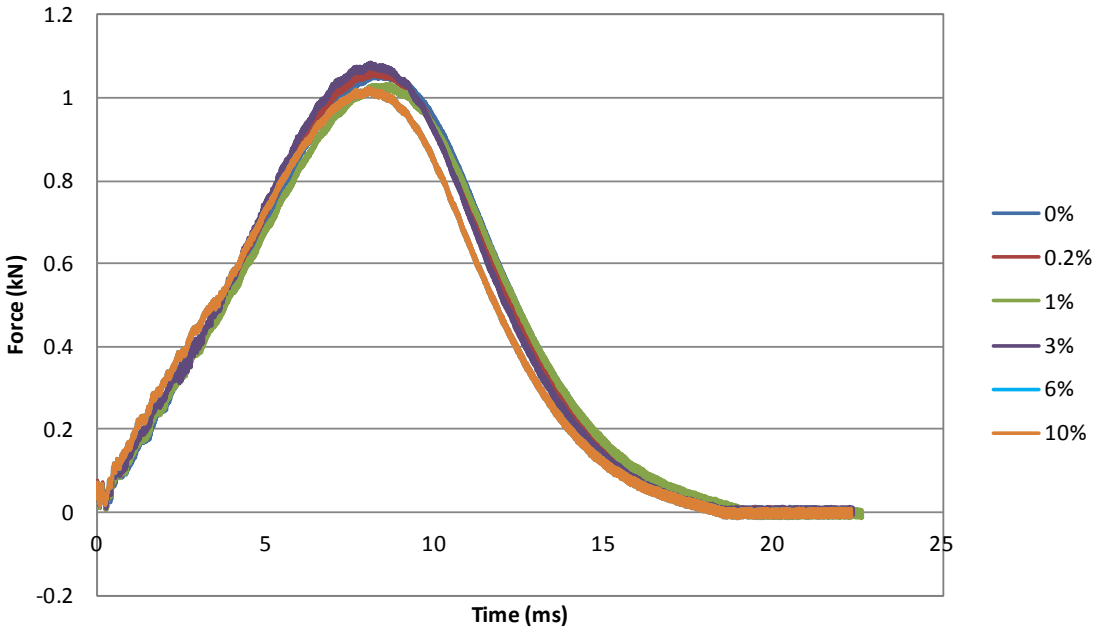


**Figure 3.104** Force vs. time curves for PP specimens reinforced with different nanoclay percentages at 120°F

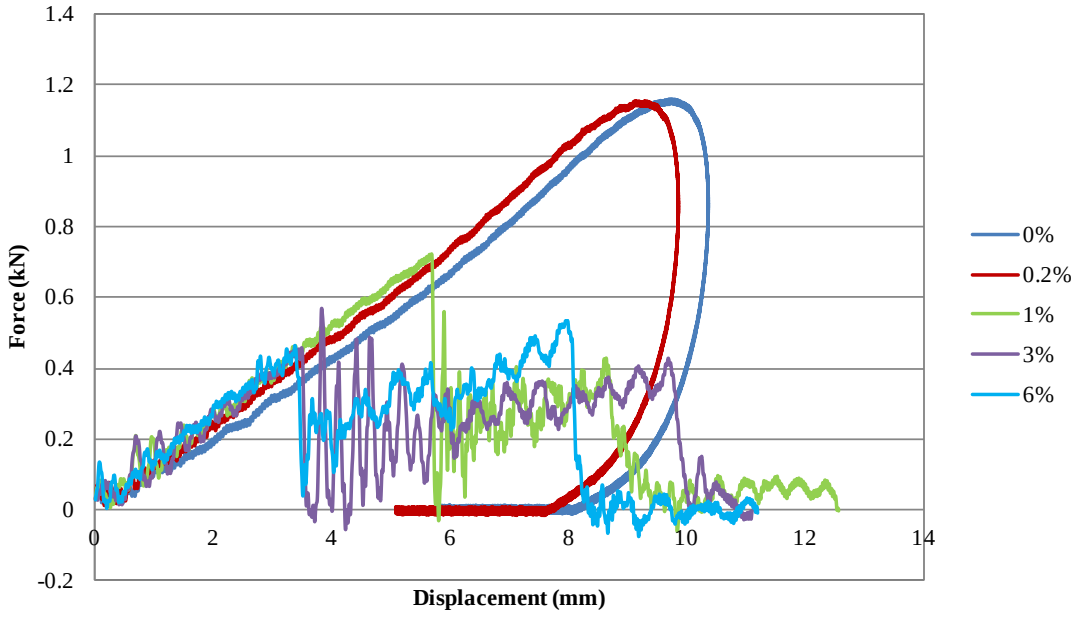


**Figure 3.105** Force vs. displacement curves for PP specimens reinforced with different nanoclay percentages at RT

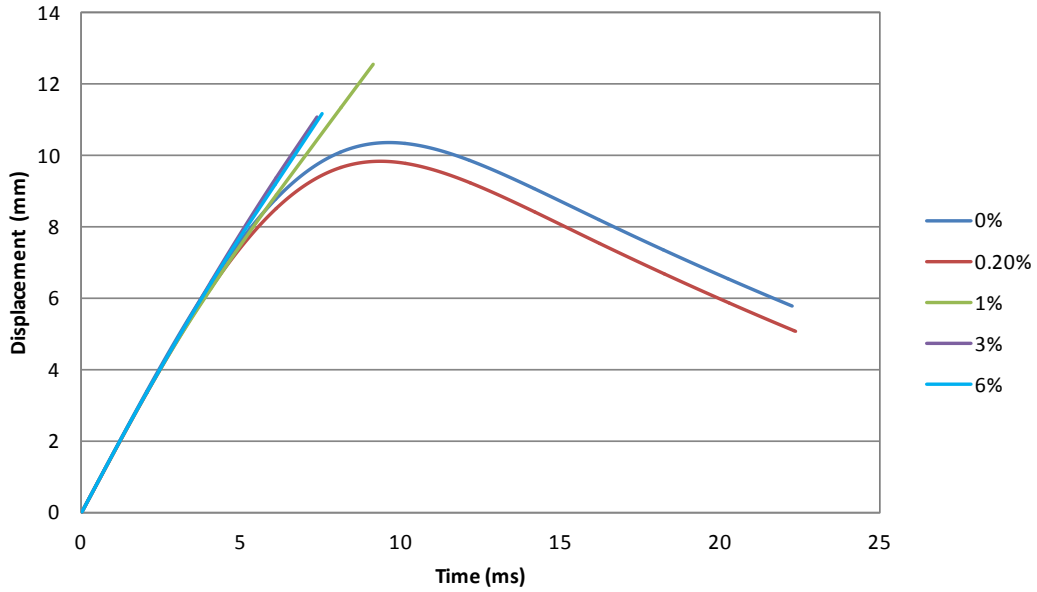


**Figure 3.106** Displacement vs. time curves for PP specimens reinforced with different nanoclay percentages at RT

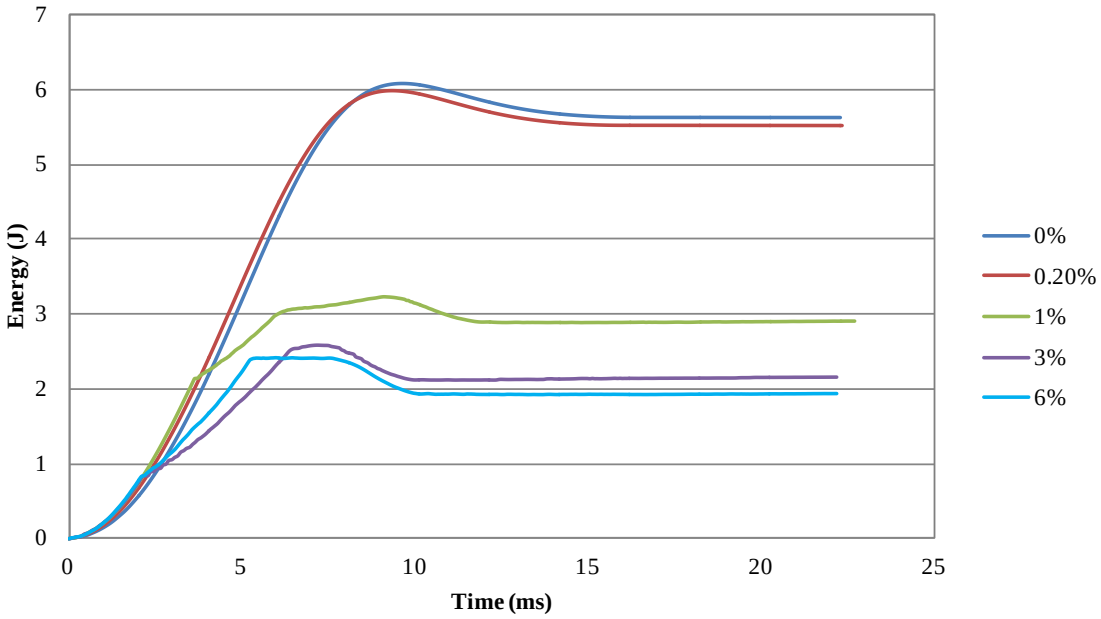


**Figure 3.107** Energy vs. time curves for PP specimens reinforced with different nanoclay percentages at RT

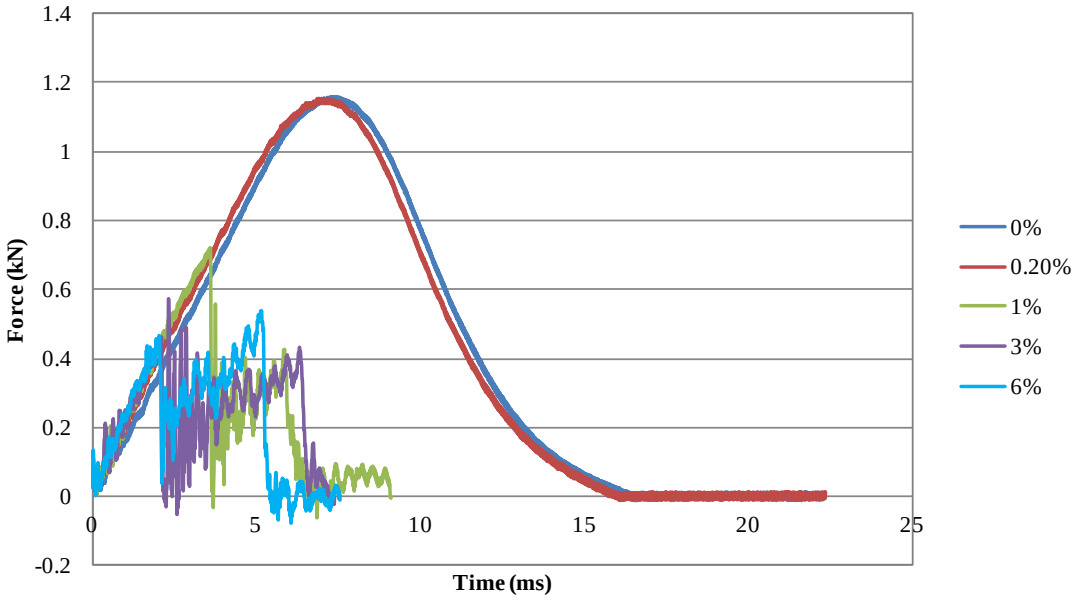


**Figure 3.108** Force vs. time curves for PP specimens reinforced with different nanoclay percentages at RT

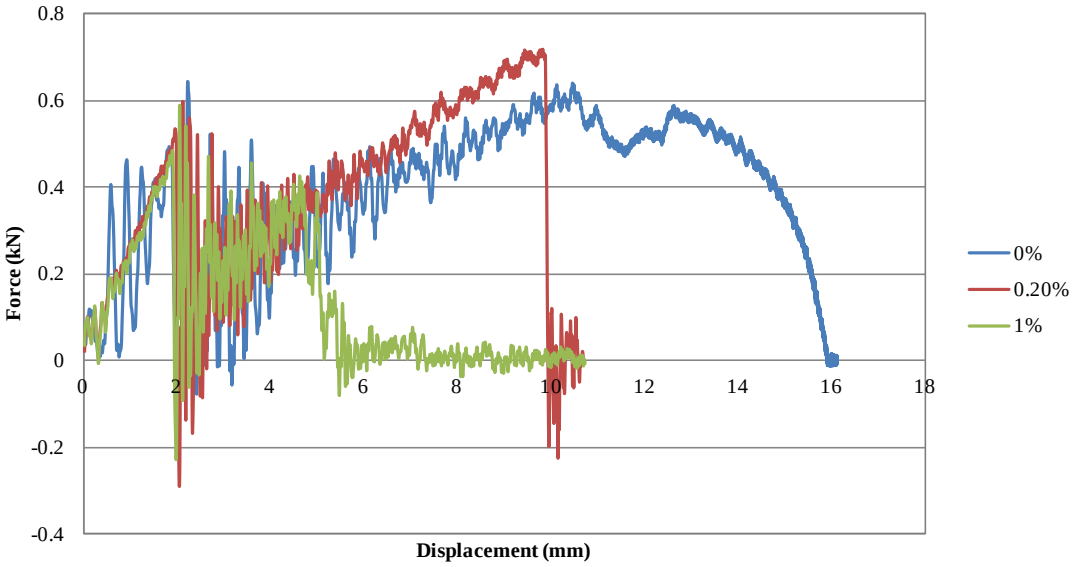


**Figure 3.109** Force vs. displacement curves for PP specimens reinforced with different nanoclay percentages at -4°F

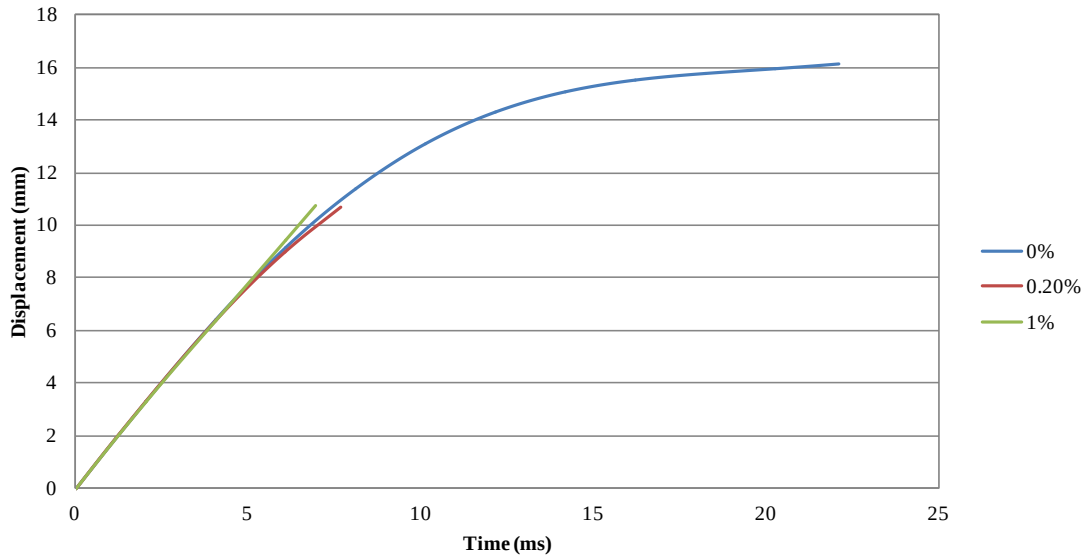


**Figure 3.110** Displacement vs. time curves for PP specimens reinforced with different nanoclay percentages at -4°F

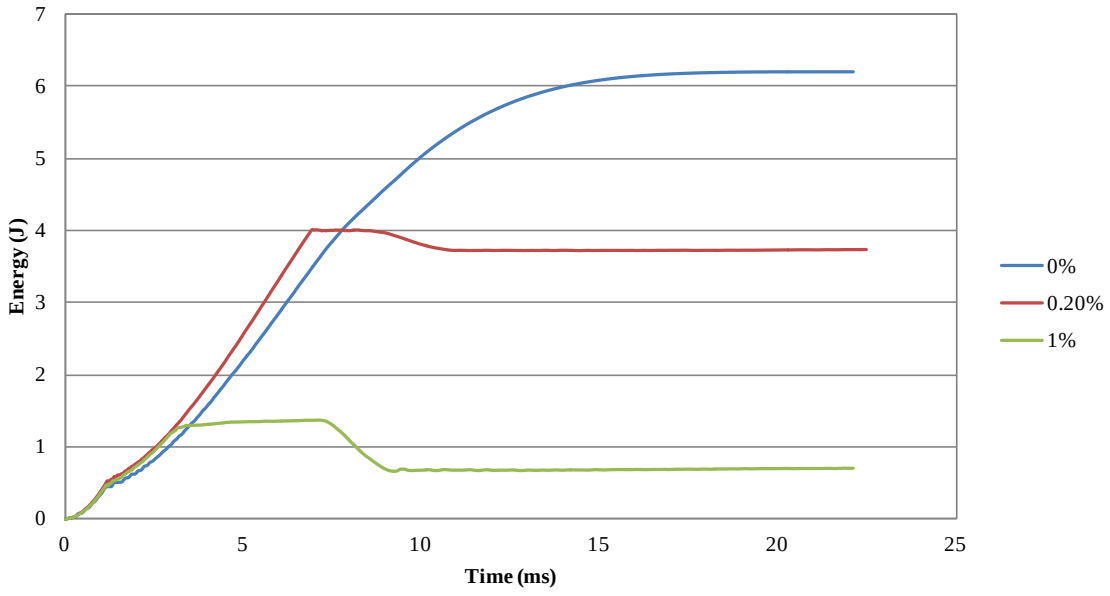


**Figure 3.111** Energy vs. time curves for PP specimens reinforced with different nanoclay percentages at -4°F

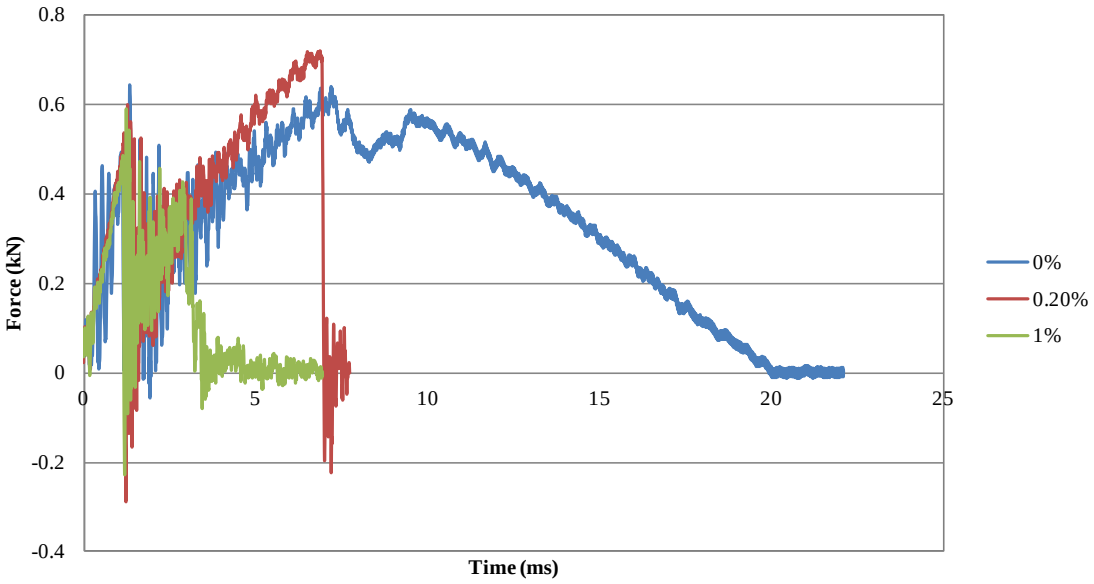


**Figure 3.112** Force vs. time curves for PP specimens reinforced with different nanoclay percentages at -4°F

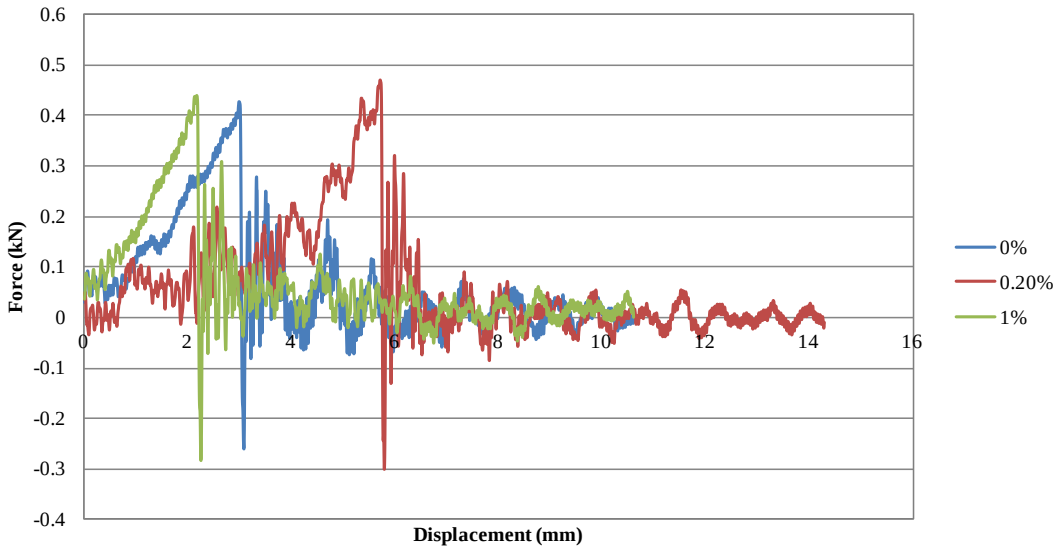


**Figure 3.113** Force vs. displacement curves for PP specimens reinforced with different nanoclay percentages at -65°F

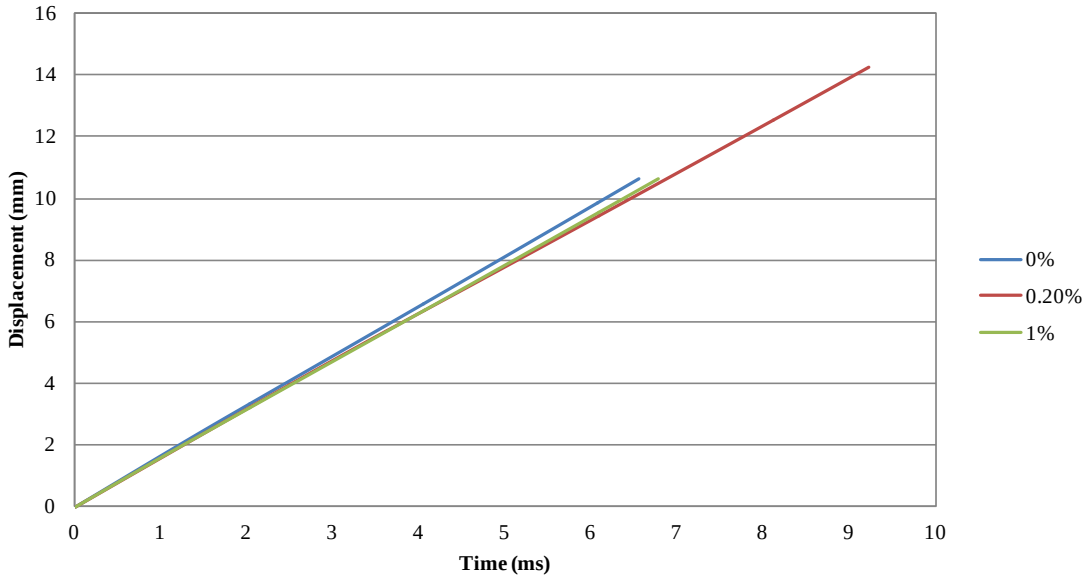


**Figure 3.114** Displacement vs. time curves for PP specimens reinforced with different nanoclay percentages at -65°F

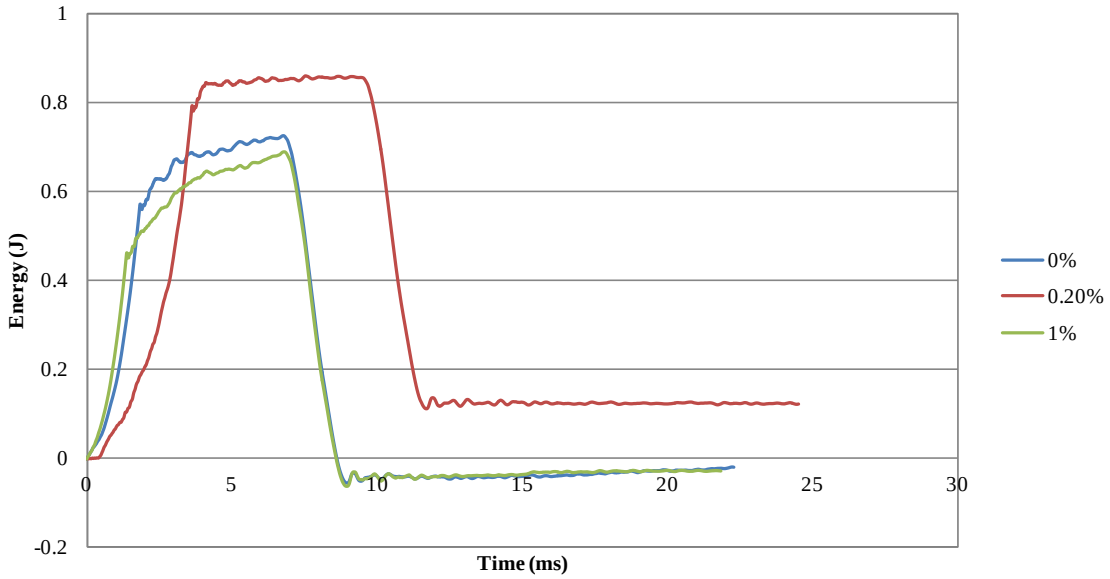


**Figure 3.115** Energy vs. time curves for PP specimens reinforced with different nanoclay percentages at -65°F

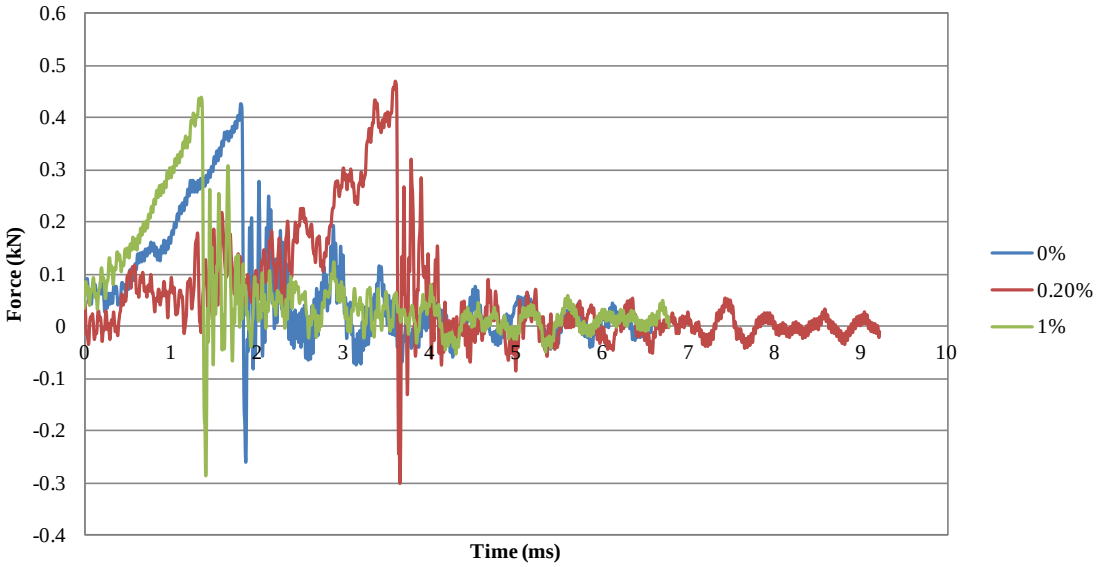


**Figure 3.116** Force vs. time curves for PP specimens reinforced with different nanoclay percentages at -65°F

As a result of the low velocity impact tests, we can state that high temperatures affect polypropylene significantly and practically eliminate the effect of nanoclay reinforcement. The specimens show ductile behavior. However, at room and low temperatures the effect of nanoclay reinforcement is discernable and addition of nanoclay makes the specimens more brittle.

### 3.4. ELECTRON MICROSCOPY

As limited number of the specimens were studied under TEM and SEM. Te purpose of this task is to observe the dispersion of nanoclay in the polypropylene matrix.

A scanning electron microscope (SEM) was used to obtain the imagines presented below. We started working with 10% nanoclay reinforced PP specimens because they have the highest nanoclay percentage and it would be easier to observe nanoclay particles inside PP. We obtained

some good images using SEM. We also tried to get images with a transmission electron microscope (TEM), but since SEM gave better images we continued our work with SEM.

To obtain the SEM images, we had to cut a very thin section of PP specimen. We used a diamond knife and cut a section of 200nm thickness and placed it inside the SEM. Figures 3.117-3.119 depict the images obtained. Red marks show the nanoclay particles.

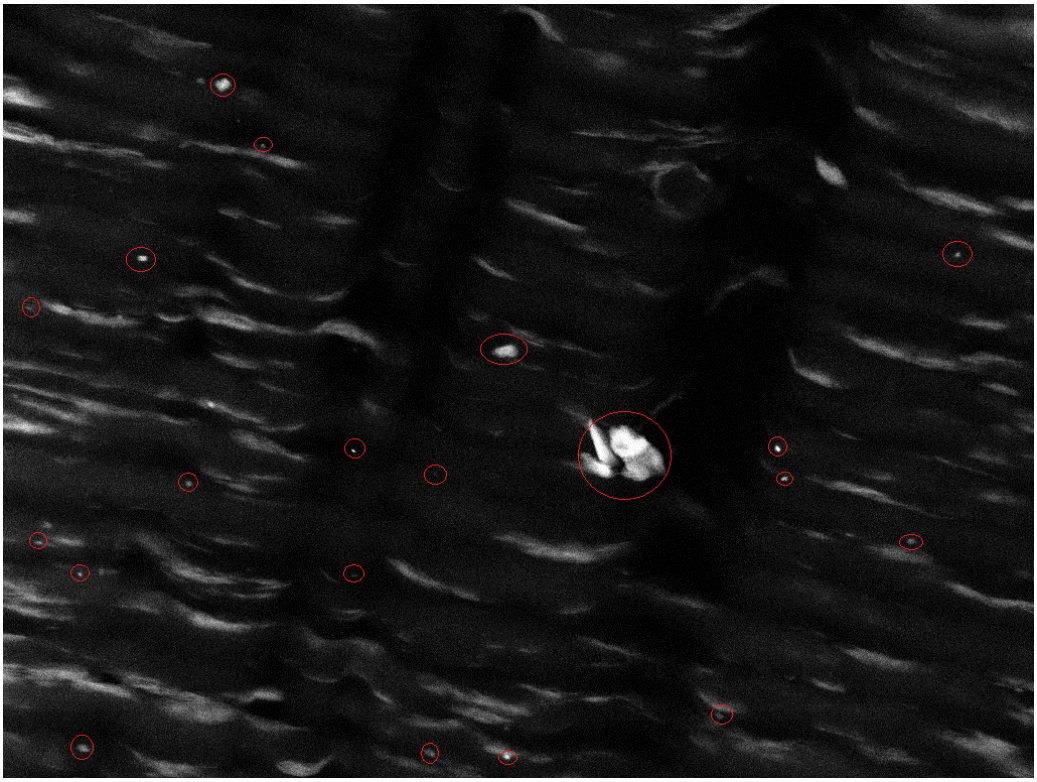

**Figure 3.117** Dispersion of nanoclay particles in 10% nanoclay reinforced PP specimen

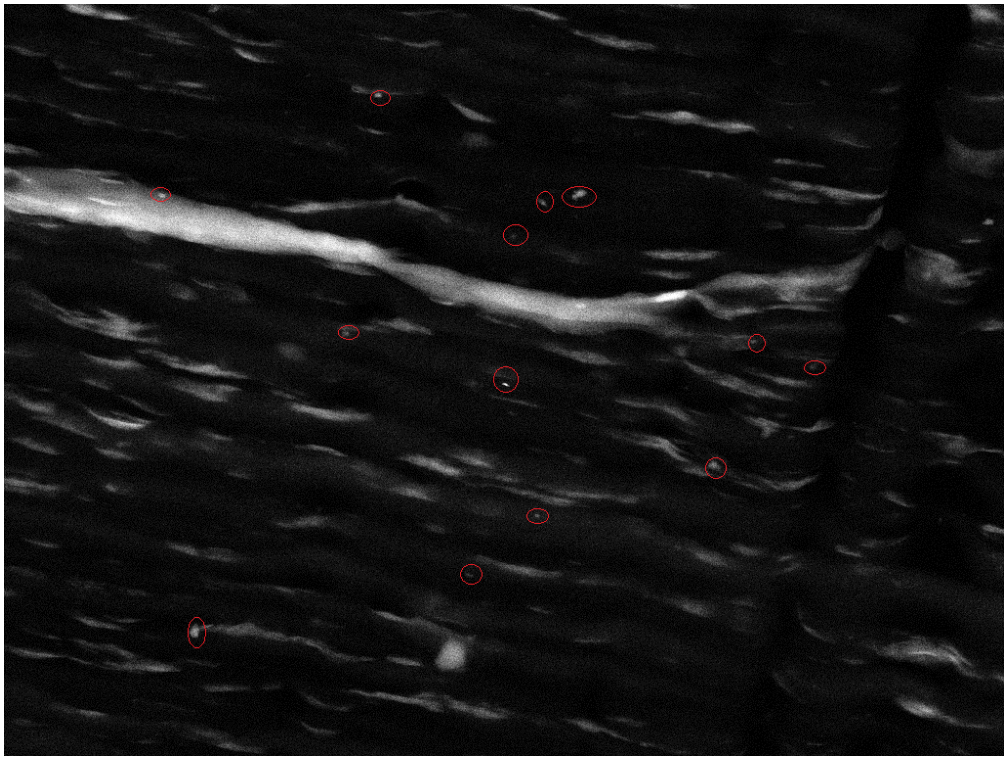

**Figure 3.118** Dispersion of nanoclay particles in 10% nanoclay reinforced PP specimen

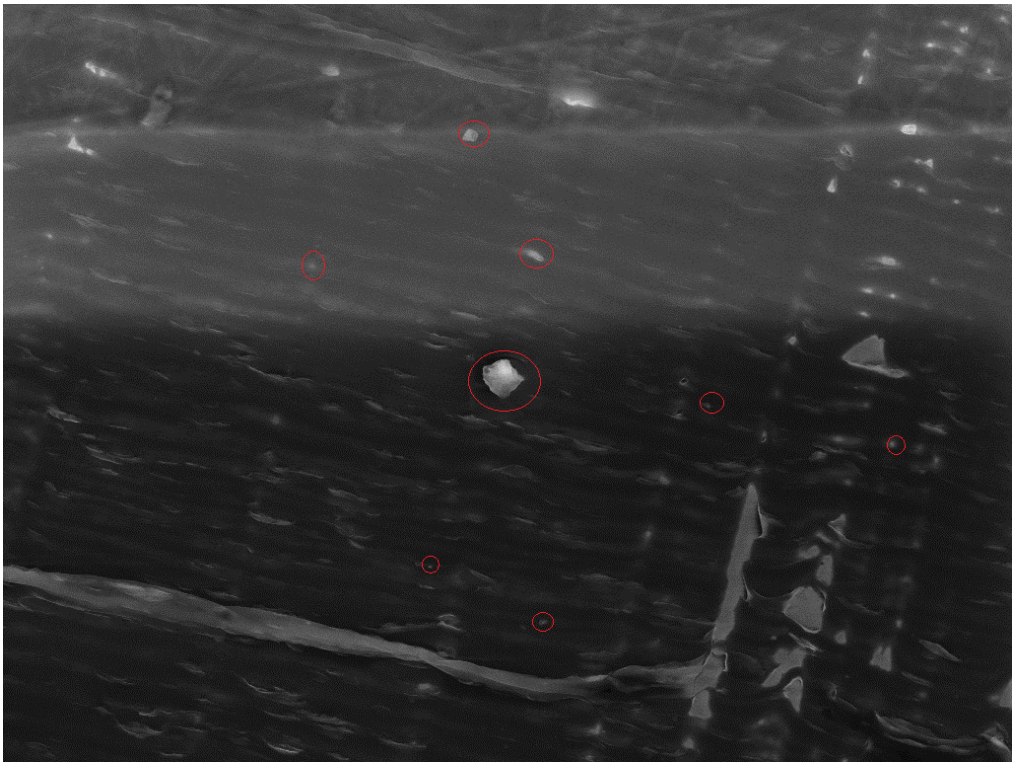

**Figure 3.119** Dispersion of nanoclay particles in 10% nanoclay reinforced PP specimen

Figure 3.120 shows a chunk of nanoclay particle inside the 10% nanoclay reinforced specimen.

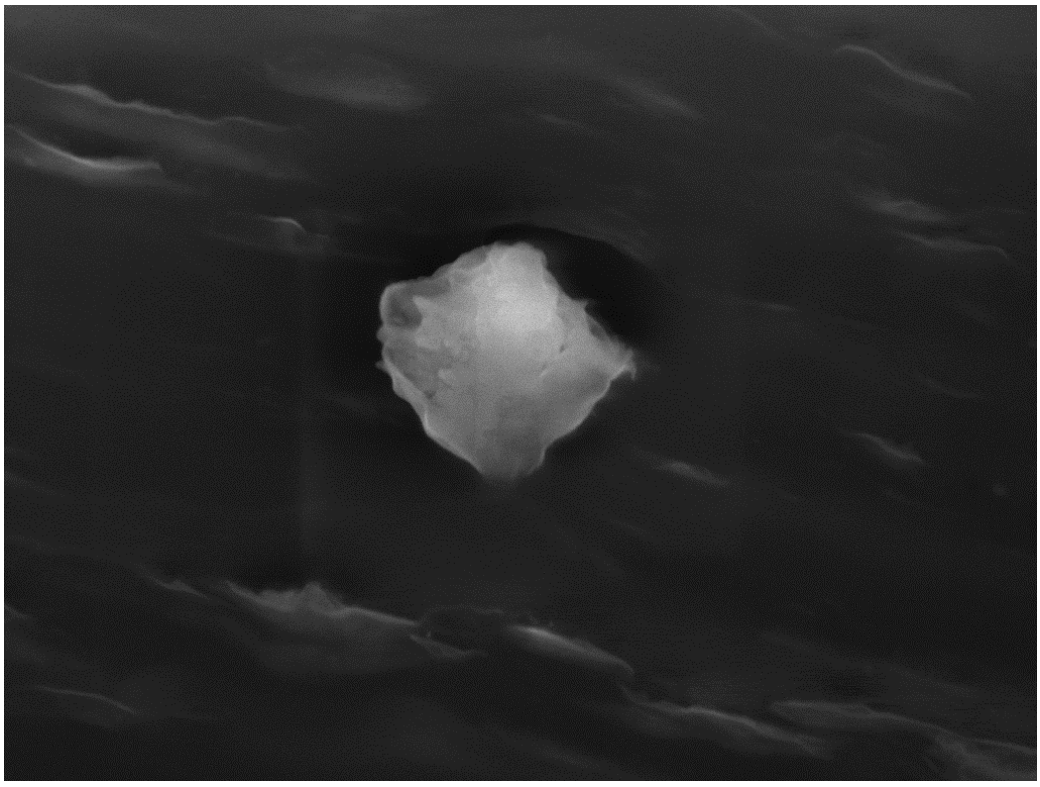

**Figure3.120** Nanoclay particle showing agglomeration of nanoclay flakes.

Additional SEM images of 10% nanoclay reinforced PP specimens (Figures 3.121-3.124) are presented below.

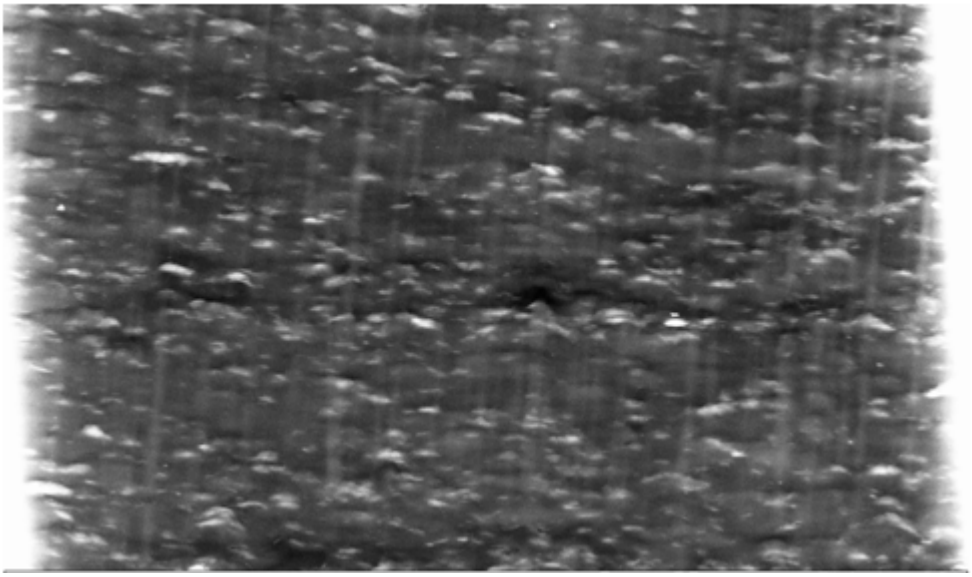

**Figure 3.121** Dispersion of nanoclay particles in 10% nanoclay reinforced PP specimen

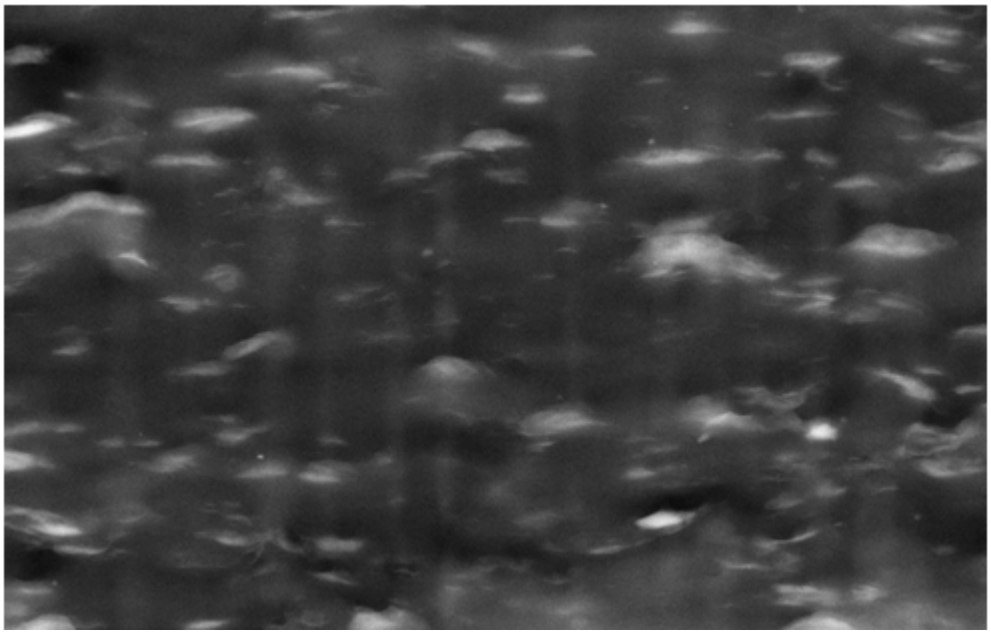

**Figure 3.122** Dispersion of nanoclay particles in 10% nanoclay reinforced PP specimen

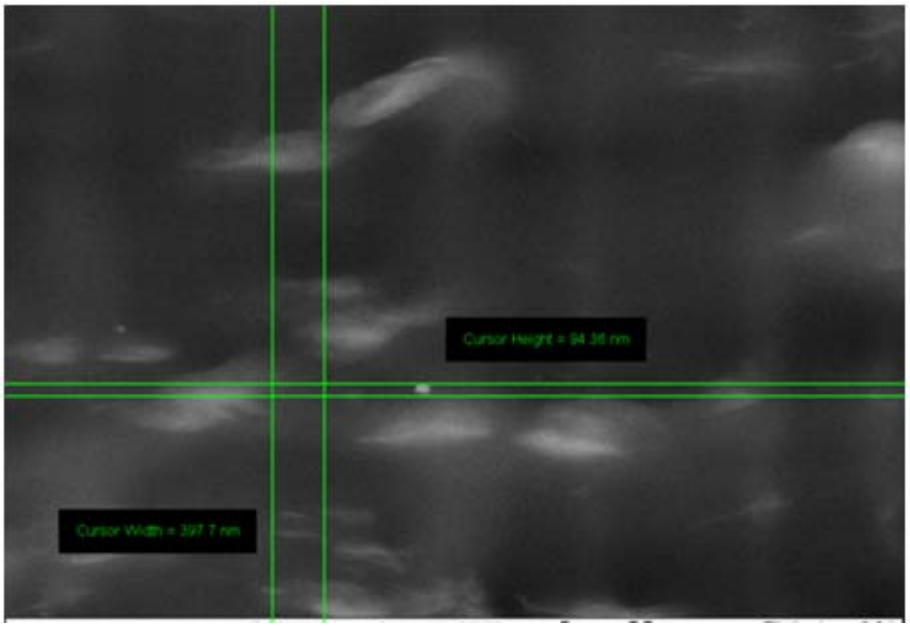


**Figure 3.123** Dispersion of nanoclay particles in 10% nanoclay reinforced PP specimen

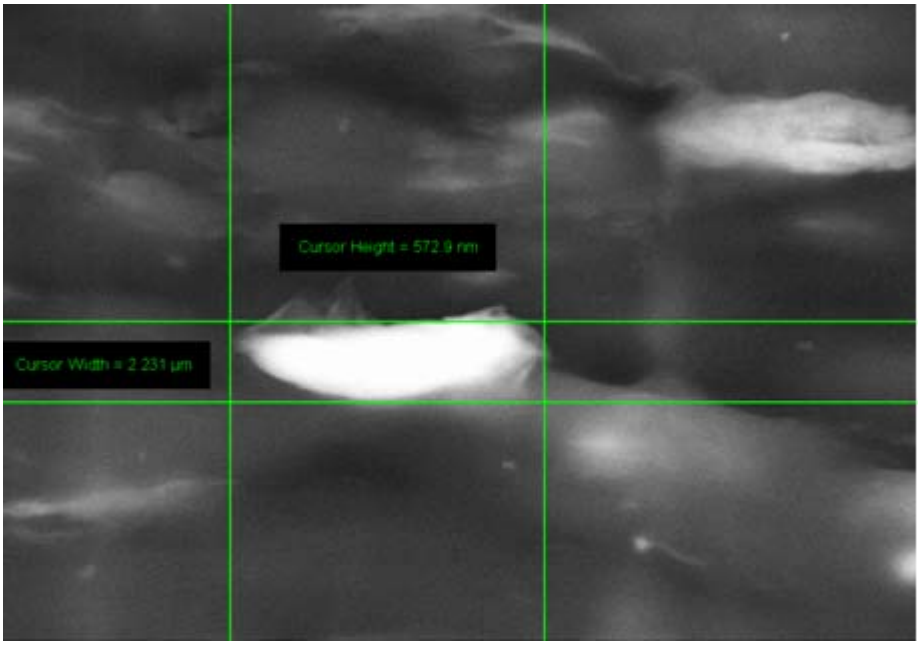


**Figure 3.124** Dispersion of nanoclay particles in 10% nanoclay reinforced PP specimen.

Figure 3.123 and Figure 3.124 show two clay particles with different dimensions.

The SEM images for 1% nanoclay reinforced PP specimens are given below in Figures 3.123-3.125.

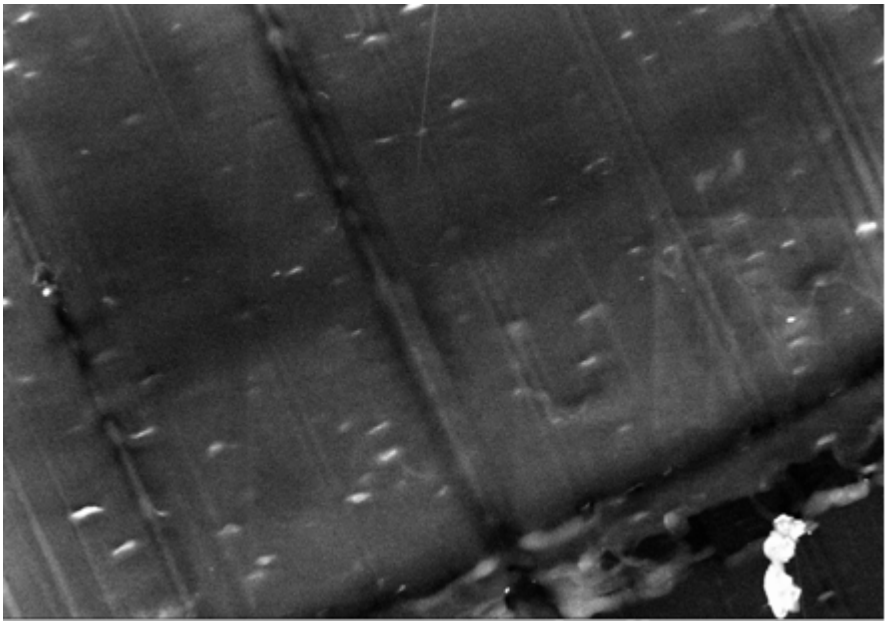

**Figure 3.125** Dispersion of nanoclay particles in 1% nanoclay reinforced PP specimen

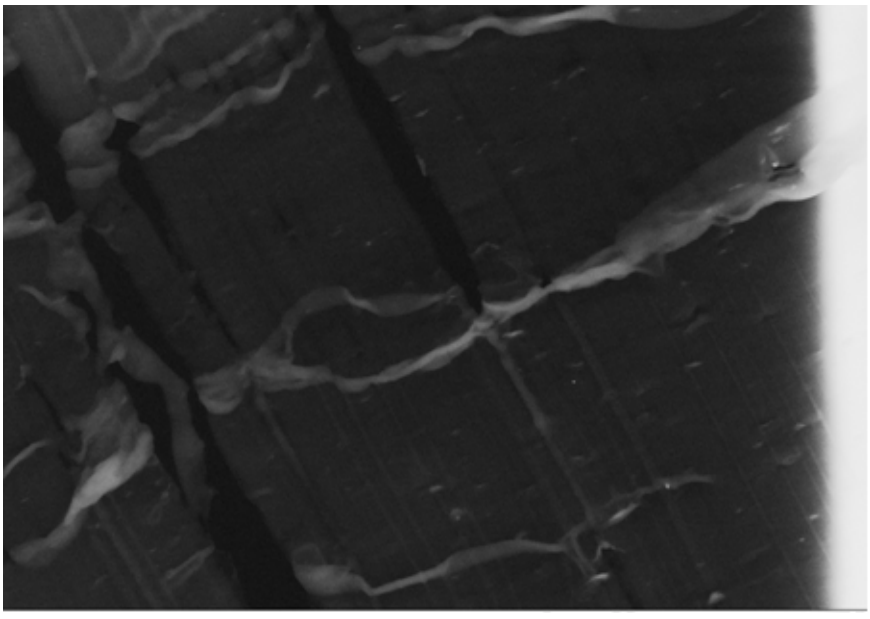

**Figure 3.126** Dispersion of nanoclay particles in 1% nanoclay reinforced PP specimen

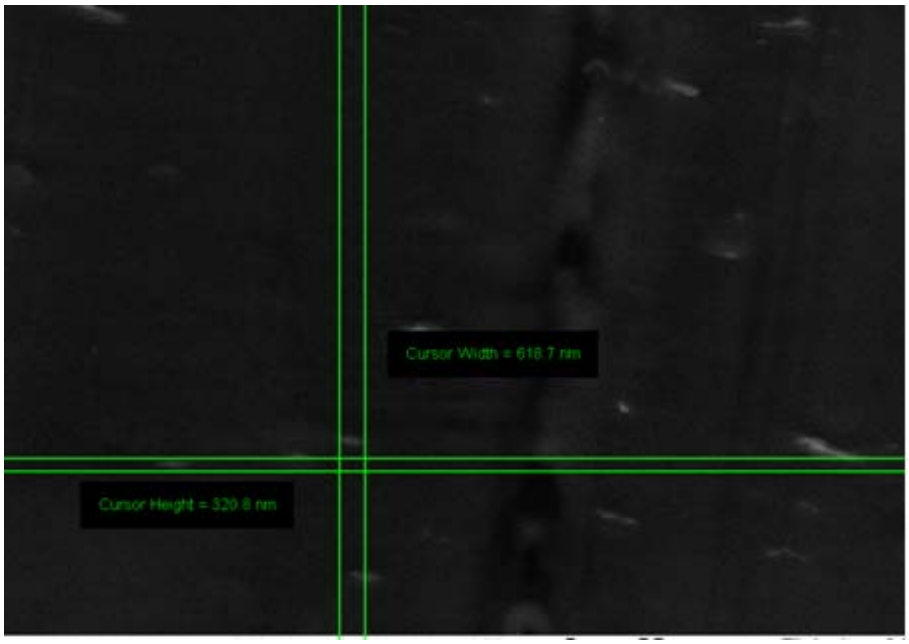


**Figure 3.127** Dispersion of nanoclay particles in 1% nanoclay reinforced PP specimen

Figure 3.127 show the dimension of clay particle in a 1% nanolcay reinforced PP specimen.

The SEM images show that proper nanoclay particle dispersion at high percentages is difficult to achieve. Bad dispersion results in big chucks of nanoclay particles and possible debonding between particle and resin. Also it is observed that the dispersion of particles is more random than oriented.

# 4. MODELING AND SIMULATION

Some modeling and simulation studies also were carried out for this thesis. Testing is expensive and time consuming. Thus, the purpose of modeling and simulation studies is to develop models to predict the properties. If the models are successful, then they can be used to predict the properties for cases where test data are not available. Accordingly, micromechanics modeling and 3-D finite element was carried out to predict some of the mechanical properties obtained though the experimental program.

## 4.1 MICROMECHANICS MODELING

The purpose of micromechanics modeling of polymer/clay nanocomposites is to predict their elastic properties. For multi-scale modeling, intercalated and exfoliated clay systems were studied. A representative volume element consisting of N layers of intercalated or exfoliated clay platelets surrounded by polymer matrix was considered.

### 4.1.1 Application of Mori-Tanaka formulation for tensile testing

The Mori-Tanaka model, which is based on micromechanics and uses Eshelby's solution for inclusions embedded in an infinite matrix, is considered to simulate and predict the elastic properties of two-phase nanoclay reinforced nanocomposites. Here we approximate the nanoclay flakes as thin disks with the aspect ratio $\alpha$ calculated using their thickness and length. For analytical results, three different Mori Tanaka approaches are used. These approaches depend on particle orientation. The three approaches are "Oriented particles", "2-D Randomly distributed particles" and "3-D Randomly distributed partciles".

4.1.1-a) Oriented Nanoclay Particles

Referring to [196], the normalized longitudinal Young's modulus (parallel to the tensile test direction), the normalized transverse Young's modulus, the normalized in plane shear modulus, the normalized out of plane shear modulus, the normalized plane strain bulk modulus and the major Poisson's ratio can be expressed as:

$$\frac{E_{11}}{E_m} = \frac{1}{1 + c\left[-2\nu_m A_3 + (1-\nu_m)A_4 + (1+\nu_m)A_5 A\right]/2A} \tag{1}$$

$$\frac{E_{22}}{E_m} = \frac{1}{1 + c(A_1 + 2\nu_m A_2)A} \tag{2}$$

$$\frac{\mu_{21}}{\mu_m} = 1 + \frac{c}{\frac{\mu_m}{\mu_p - \mu_m} + 2(1-c)S_{1212}} \tag{3}$$

$$\frac{\mu_{13}}{\mu_0} = 1 + \frac{c}{\frac{\mu_m}{\mu_p - \mu_m} + 2(1-c)S_{2323}} \tag{4}$$

$$\frac{K_{13}}{K_m} = \frac{(1+\nu_m)(1-2\nu_m)}{1-\nu_m(1+2\nu_{21}) + c\left\{2(\nu_{21}-\nu_m)A_3 + \left[1-\nu_m(1+2\nu_{21})\right]A_4\right\}/A} \tag{5}$$

where $K_m = \lambda_m + \mu_m$

$$\nu_{21}^2 = \frac{E_{22}}{E_{11}} - \frac{E_{22}}{4}\left(\frac{1}{\mu_{13}} + \frac{1}{K_{13}}\right) \tag{6}$$

and $c$ is the volume fraction of nanoclay and the coefficients $A_1$, $A_2$, $A_3$, $A_4$, $A_5$ and $A$ are given by:

$$A_1 = D_1\left(B_4 + B_5\right) - 2B_2 \tag{7}$$

$$A_2 = \left(1 + D_1\right)B_2 - \left(B_4 + B_5\right) \tag{8}$$

$$A_3 = B_1 - D_1 B_3 \tag{9}$$

$$A_4 = \left(1 + D_1\right)B_1 - 2B_3 \tag{10}$$

$$A_5 = \left(1 - D_1\right)/\left(B_4 - B_5\right) \tag{11}$$

and

$$A = 2B_2B_3 - B_1\left(B_4 + B_5\right) \tag{11.a}$$

with

$$B_1 = cD_1 + D_2 + \left(1-c\right)\left(D_1S_{1111} + 2S_{2211}\right) \tag{12}$$

$$B_2 = c + D_3 + \left(1-c\right)\left(D_1S_{1122} + S_{2222} + S_{2233}\right) \tag{13}$$

$$B_3 = c + D_3 + \left(1-c\right)\left[S_{1111} + \left(1 + D_1\right)S_{2211}\right] \tag{14}$$

$$B_4 = cD_1 + D_2 + \left(1-c\right)\left(S_{1122} + D_1S_{2222} + S_{2233}\right) \tag{15}$$

$$B_5 = c + D_3 + \left(1-c\right)\left(S_{1122} + S_{2222} + D_1S_{2233}\right) \tag{16}$$

and

$$D_1 = 1 + 2\left(\mu_p - \mu_m\right)\Big/\left(\lambda_p - \lambda_m\right) \tag{17}$$

$$D_2 = \left(\lambda_m + 2\mu_m\right)\Big/\left(\lambda_p - \lambda_m\right) \tag{18}$$

$$D_3 = \lambda_m\Big/\left(\lambda_p - \lambda_m\right) \tag{19}$$

The D terms are defined by using $\mu_m$, $\lambda_m$ and $\mu_p$, $\lambda_p$, which are the Lame constants of the matrix and particles, respectively. In the B terms, the components of Eshelby's tensor $S_{ijkl}$ given below are used:

$$S_{1111} = \frac{1}{2\left(1-\nu_m\right)}\left\{1 - 2\nu_m + \frac{3\alpha^2 - 1}{\alpha^2 - 1} - \left[1 - 2\nu_m + \frac{3\alpha^2}{\alpha^2 - 1}\right]g\right\} \tag{20}$$

$$S_{2222} = S_{3333} = \frac{3}{8(1-\nu_m)}\frac{\alpha^2}{\alpha^2-1} + \frac{1}{4(1-\nu_m)}\left[1-2\nu_m - \frac{9}{4(\alpha^2-1)}\right]g \tag{21}$$

$$S_{2233} = S_{3322} = \frac{1}{4(1-\nu_m)}\left\{\frac{\alpha^2}{2(\alpha^2-1)} - \left[1-2\nu_m + \frac{3}{4(\alpha^2-1)}\right]g\right\} \tag{22}$$

$$S_{2211} = S_{3311} = -\frac{1}{2(1-\nu_m)}\frac{\alpha^2}{\alpha^2-1} + \frac{1}{4(1-\nu_m)}\left\{\frac{3\alpha^2}{\alpha^2-1} - (1-2\nu_m)\right\}g \tag{23}$$

$$S_{1122} = S_{1133} = -\frac{1}{2(1-\nu_m)}\left[1-2\nu_m + \frac{1}{\alpha^2-1}\right] + \frac{1}{2(1-\nu_m)}\left[1-2\nu_m + \frac{3}{2(\alpha^2-1)}\right]g \tag{24}$$

$$S_{2323} = S_{3232} = \frac{1}{4(1-\nu_m)}\left\{\frac{\alpha^2}{2(\alpha^2-1)} + \left[1-2\nu_m - \frac{3}{4(\alpha^2-1)}\right]g\right\} \tag{25}$$

$$S_{1212} = S_{1313} = \frac{1}{4(1-\nu_m)}\left\{1-2\nu_m - \frac{\alpha^2+1}{\alpha^2-1} - \frac{1}{2}\left[1-2\nu_m - \frac{3(\alpha^2+1)}{\alpha^2-1}\right]g\right\} \tag{26}$$

Here $\nu_m$ is the Poisson's ratio of the matrix. In Eshelby's tensor, the g term has two different expressions depending on the aspect ratio of the inclusion:

$$g' = \frac{\alpha}{(\alpha^2-1)^{3/2}}\left\{\alpha(\alpha^2-1)^{1/2} - \cosh^{-1}\alpha\right\} \qquad \text{when } \alpha > 1 \tag{27.a}$$

$$g = \frac{\alpha}{(1-\alpha^2)^{3/2}}\left\{\cos^{-1}\alpha - \alpha(1-\alpha^2)^{1/2}\right\} \qquad \text{when } \alpha < 1 \tag{27.b}$$

Before we start the Mori-Tanaka calculations, first we have to determine some material and geometric properties of the constituents, namely matrix and nanoclay.

***Matrix 1:*** PP 3371

$E_m$ = average experimental result at each temperature value

$\nu_m$ = average experimental result at each temperature

$V_m$ = volume fraction of matrix( calculated from weight fraction of matrix)

$W_m$ = weight fraction of matrix

$\gamma_m$ = 8,829N/m$^3$ (specific weight of matrix)

$\mu_m$ = calculated for average experimental result at each temperature value

$\lambda_m$ = calculated for average experimental result at each temperature value

***Matrix 2:*** EPON 828 Epoxy

$E_m$ = 2.8177 GPa (average experimental result at room temperature)

$\nu_m$ = 0. 3105 (average experimental result at room temperature)

$V_m$ = volume fraction of matrix ( calculated from weight fraction of matrix)

$W_m$ = weight fraction of matrix

$\gamma_m$ = 15,696N/m$^3$ (specific weight of matrix)

$\mu_m$ = 1.075 GPa (calculated)

$\lambda_m$ = 1.762 GPa (calculated)

***Particle:*** Nanoclay

$E_{nanoclay}$ = 300 GPa (assumed from molecular dynamics calculations)

$E_p$ = effective Young's modulus of particle = $E_{nanoclay}(N.d_s/t)$ ( Referring to [181] and Figure 4.1)

$\nu_p$ = 0. 2 (assumed)

$V_p = c$ = volume fraction of nanoclay (calculated from weight fraction of nanoclay)

$W_p$ = weight fraction of nanoclay

$\gamma_p$ = 18,639 N/m$^3$ (specific weight of nanoclay)

$\mu_p$ = effective shear modulus calculated for each particle geometry

$\lambda_p$ = effective Lamè constant calculated for each particle geometry

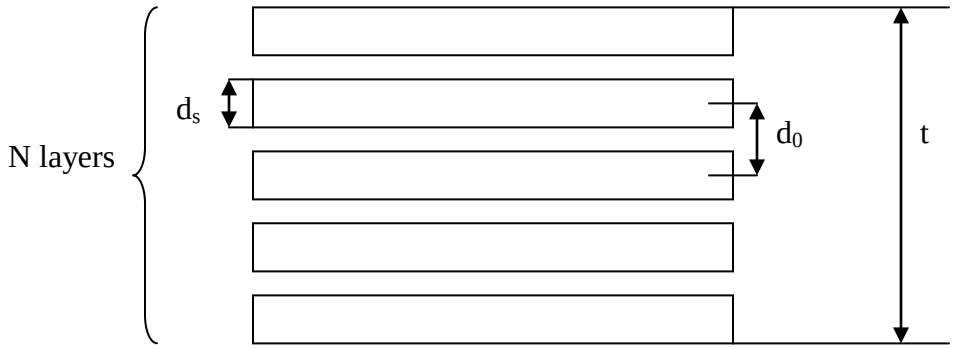


where $t=(N-1)d_0+d_s$

**Figure 4.1** Model of nanoclay particle [181]

First, we calculate the volume fraction of nanoclay to be able to use the Mori-Tanaka formulation. The volume fraction in terms of the weight fraction can be written as:

$$c = \frac{W_p/\gamma_p}{W_p/\gamma_p + (1-W_p)/\gamma_m} \tag{28}$$

For each nanoclay reinforcements, using Eq.28 the volume fraction of nanoclay c is obtained as (Table 4.1):

**Table 4.1** Conversion of weight fractions of nanoclay to volume fractions

| Weight fraction of nanoclay | Volume fraction of nanoclay |
|---|---|
| 0.2% | 0.095% |
| 1% | 0.48 % |
| 3% | 1.44 % |
| 6% | 2.93 % |
| 10% | 5 % |

To determine the aspect ratio of nanoclay flakes, we use for thickness $t = (N-1)d_0 + d_s$ (referring to [181]) where N is the number of nanoclay flakes, $d_0$=2.4 nm, $ds$ = 0.615 nm and the diameter D = 200 nm. Thus, the aspect ratio of nanoclay can be calculated as: $\alpha = \frac{t}{D}$. For the parametric study, 6 different values of N are used and as a consequence 6 different aspect ratios are obtained. But for all cases the aspect ratio of nanoclay is smaller than 1 and thus we use $g$ in Eshelby's tensor for the parametric study. The calculations for various weight fractions (converted to volume fractions), Young's moduli and thicknesses of nanoclay particles were performed using MATLAB R2007b.

4.1.1-b) Results of Parametric Study for Oriented Nanoclay Particles

To obtain the effect of the number of nanoclay flakes in a particle and the effect of the nanoclay's Young's modulus on nanocomposite properties a parametric study was performed. As a result of the parametric study, in the ensuing Mori-Tanaka calculations the number of flakes N in a nanoclay particle was varied from 1 to 6 and the nanoclay Young's modulus $E_{nanoclay}$ =300 GPa was used to calculate the particle thickness t and the effective particle Young's modulus $E_p$. For PP 3371 specimens with nanoclay reinforcement, the Mori-Tanaka calculations were performed using the different Young's modulus values obtained from the tensile tests at various

temperatures. For EPON 828 epoxy specimens with nanoclay reinforcement, the Mori-Tanaka calculations were carried out at room temperature only for N = 6 and $E_{nanoclay}$ =300GPa. The comparison of Mori-Tanaka calculations and experimental results for oriented particles is given in Tables 4.2 - 4.6. The comparison for the epoxy based nanocomposite is shown in Table 4.7.

**Table 4.2** Comparison of Mori-Tanaka calculations and experimental results of PP 3371/clay nanocomposites for oriented particles at 160ºF

| $E_{nanoclay}$ (GPa) | D (nm) | N | $E_p$ (GPa) | t (nm) | Nanoclay Rein. | Young's Modulus (Experimental) (GPa) | $E_{11}$ (GPa) | $E_{22}$ (GPa) | Poisson's Ratio (Experimental) | $\nu_{21}$ |
|---|---|---|---|---|---|---|---|---|---|---|
| 300 | 200 | 1 | 300 | 0.615 | 0% | 0.39204 | 0.39204 | 0.39204 | 0.4256 | 0.4256 |
| | | | | | 0.2% | 0.4499 | 0.4586 | 0.4186 | 0.4782 | 0.4481 |
| | | | | | 1% | 0.4654 | 0.7212 | 0.5081 | 0.4715 | 0.5019 |
| | | | | | 3% | 0.4969 | 1.3800 | 0.6577 | 0.4523 | 0.5522 |
| | | | | | 6% | 0.5031 | 2.4061 | 0.7884 | 0.5077 | 0.5767 |
| | | | | | 10% | 0.5146 | 3.8646 | 0.8934 | 0.4896 | 0.5884 |
| | | | | | | | | | | |
| 300 | 200 | 2 | 122.388 | 3.015 | 0% | 0.39204 | 0.39204 | 0.39204 | 0.4256 | 0.4256 |
| | | | | | 0.2% | 0.4499 | 0.4077 | 0.3986 | 0.4782 | 0.4314 |
| | | | | | 1% | 0.4654 | 0.4704 | 0.4238 | 0.4715 | 0.4515 |
| | | | | | 3% | 0.4969 | 0.6287 | 0.4817 | 0.4523 | 0.4872 |
| | | | | | 6% | 0.5031 | 0.8740 | 0.5574 | 0.5077 | 0.5195 |
| | | | | | 10% | 0.5146 | 1.2213 | 0.6436 | 0.4896 | 0.5442 |
| | | | | | | | | | | |
| 300 | 200 | 3 | 102.216 | 5.415 | 0% | 0.39204 | 0.39204 | 0.39204 | 0.4256 | 0.4256 |
| | | | | | 0.2% | 0.4499 | 0.4013 | 0.3960 | 0.4782 | 0.4290 |
| | | | | | 1% | 0.4654 | 0.4386 | 0.4116 | 0.4715 | 0.4418 |
| | | | | | 3% | 0.4969 | 0.5333 | 0.4490 | 0.4523 | 0.4675 |
| | | | | | 6% | 0.5031 | 0.6804 | 0.5020 | 0.5077 | 0.4952 |
| | | | | | 10% | 0.5146 | 0.8887 | 0.5678 | 0.4896 | 0.5202 |
| | | | | | | | | | | |
| 300 | 200 | 4 | 94.434 | 7.815 | 0% | 0.39204 | 0.39204 | 0.39204 | 0.4256 | 0.4256 |
| | | | | | 0.2% | 0.4499 | 0.3987 | 0.3949 | 0.4782 | 0.4281 |
| | | | | | 1% | 0.4654 | 0.4257 | 0.4065 | 0.4715 | 0.4375 |
| | | | | | 3% | 0.4969 | 0.4945 | 0.4349 | 0.4523 | 0.4576 |
| | | | | | 6% | 0.5031 | 0.6015 | 0.4763 | 0.5077 | 0.4813 |
| | | | | | 10% | 0.5146 | 0.7533 | 0.5300 | 0.4896 | 0.5046 |
| | | | | | | | | | | |

**Table 4.2** Continued

| | | | | | | | | | | |
|---|---|---|---|---|---|---|---|---|---|---|
| 300 | 200 | 5 | 90.308 | 10.215 | 0% | 0.39204 | 0.39204 | 0.39204 | 0.4256 | 0.4256 |
| | | | | | 0.2% | 0.4499 | 0.3973 | 0.3944 | 0.4782 | 0.4275 |
| | | | | | 1% | 0.4654 | 0.4187 | 0.4037 | 0.4715 | 0.4350 |
| | | | | | 3% | 0.4969 | 0.4732 | 0.4269 | 0.4523 | 0.4516 |
| | | | | | 6% | 0.5031 | 0.5583 | 0.4615 | 0.5077 | 0.4722 |
| | | | | | 10% | 0.5146 | 0.6790 | 0.5073 | 0.4896 | 0.4936 |
| | | | | | | | | | | |
| 300 | 200 | 6 | 87.753 | 12.6150 | 0% | 0.39204 | 0.39204 | 0.39204 | 0.4256 | 0.4256 |
| | | | | | 0.2% | 0.4499 | 0.3965 | 0.3940 | 0.4782 | 0.4272 |
| | | | | | 1% | 0.4654 | 0.4143 | 0.4020 | 0.4715 | 0.4334 |
| | | | | | 3% | 0.4969 | 0.4598 | 0.4218 | 0.4523 | 0.4476 |
| | | | | | 6% | 0.5031 | 0.5309 | 0.4518 | 0.5077 | 0.4657 |
| | | | | | 10% | 0.5146 | 0.6320 | 0.4921 | 0.4896 | 0.4854 |

**Table 4.3** Comparison of Mori-Tanaka calculations and experimental results of PP 3371/ clay nanocomposites for oriented particles at 120ºF

| $E_{nanoclay}$ (GPa) | D (nm) | N | $E_p$ (GPa) | t (nm) | Nanoclay Rein. | Young's Modulus (Experimental) (GPa) | $E_{11}$ (GPa) | $E_{22}$ (GPa) | Poisson's Ratio (Experimental) | $\nu_{21}$ |
|---|---|---|---|---|---|---|---|---|---|---|
| 300 | 200 | 1 | 300 | 0.615 | 0% | 0.61595 | 0.61595 | 0.61595 | 0.4038 | 0.4038 |
| | | | | | 0.2% | 0.7285 | 0.7079 | 0.6491 | 0.4350 | 0.4212 |
| | | | | | 1% | 0.7646 | 1.0721 | 0.7585 | 0.4631 | 0.4644 |
| | | | | | 3% | 0.8283 | 1.9875 | 0.9348 | 0.4355 | 0.5070 |
| | | | | | 6% | 0.8332 | 3.4107 | 1.0835 | 0.4334 | 0.5283 |
| | | | | | 10% | 0.8664 | 5.4272 | 1.2016 | 0.4111 | 0.5385 |
| | | | | | | | | | | |
| 300 | 200 | 2 | 122.388 | 3.015 | 0% | 0.61595 | 0.61595 | 0.61595 | 0.4038 | 0.4038 |
| | | | | | 0.2% | 0.7285 | 0.6386 | 0.6246 | 0.4350 | 0.4085 |
| | | | | | 1% | 0.7646 | 0.7296 | 0.6576 | 0.4631 | 0.4249 |
| | | | | | 3% | 0.8283 | 0.9597 | 0.7322 | 0.4355 | 0.4545 |
| | | | | | 6% | 0.8332 | 1.3166 | 0.8274 | 0.4334 | 0.4817 |
| | | | | | 10% | 0.8664 | 1.8211 | 0.9332 | 0.4111 | 0.5027 |
| | | | | | | | | | | |

**Table 4.3** Continued

| | | | | | | | | | | |
|---|---|---|---|---|---|---|---|---|---|---|
| 300 | 200 | 3 | 102.216 | 5.415 | 0% | 0.61595 | 0.61595 | 0.61595 | 0.4038 | 0.4038 |
| | | | | | 0.2% | 0.7285 | 0.6297 | 0.6213 | 0.4350 | 0.4067 |
| | | | | | 1% | 0.7646 | 0.6849 | 0.6422 | 0.4631 | 0.4172 |
| | | | | | 3% | 0.8283 | 0.8251 | 0.6921 | 0.4355 | 0.4388 |
| | | | | | 6% | 0.8332 | 1.0432 | 0.7613 | 0.4334 | 0.4622 |
| | | | | | 10% | 0.8664 | 1.3518 | 0.8457 | 0.4111 | 0.4835 |
| | | | | | | | | | | |
| 300 | 200 | 4 | 94.434 | 7.815 | 0% | 0.61595 | 0.61595 | 0.61595 | 0.4038 | 0.4038 |
| | | | | | 0.2% | 0.7285 | 0.6260 | 0.6199 | 0.4350 | 0.4059 |
| | | | | | 1% | 0.7646 | 0.6663 | 0.6357 | 0.4631 | 0.4138 |
| | | | | | 3% | 0.8283 | 0.7692 | 0.6741 | 0.4355 | 0.4309 |
| | | | | | 6% | 0.8332 | 0.9295 | 0.7295 | 0.4334 | 0.4510 |
| | | | | | 10% | 0.8664 | 1.1566 | 0.8002 | 0.4111 | 0.4709 |
| | | | | | | | | | | |
| 300 | 200 | 5 | 90.308 | 10.215 | 0% | 0.61595 | 0.61595 | 0.61595 | 0.4038 | 0.4038 |
| | | | | | 0.2% | 0.7285 | 0.6239 | 0.6192 | 0.4350 | 0.4055 |
| | | | | | 1% | 0.7646 | 0.6561 | 0.6321 | 0.4631 | 0.4118 |
| | | | | | 3% | 0.8283 | 0.7382 | 0.6639 | 0.4355 | 0.4260 |
| | | | | | 6% | 0.8332 | 0.8664 | 0.7107 | 0.4334 | 0.4435 |
| | | | | | 10% | 0.8664 | 1.0482 | 0.7722 | 0.4111 | 0.4619 |
| | | | | | | | | | | |
| 300 | 200 | 6 | 87.753 | 12.6150 | 0% | 0.61595 | 0.61595 | 0.61595 | 0.4038 | 0.4038 |
| | | | | | 0.2% | 0.7285 | 0.6226 | 0.6187 | 0.4350 | 0.4052 |
| | | | | | 1% | 0.7646 | 0.6496 | 0.6297 | 0.4631 | 0.4105 |
| | | | | | 3% | 0.8283 | 0.7184 | 0.6572 | 0.4355 | 0.4226 |
| | | | | | 6% | 0.8332 | 0.8260 | 0.6983 | 0.4334 | 0.4382 |
| | | | | | 10% | 0.8664 | 0.9789 | 0.7531 | 0.4111 | 0.4551 |

**Table 4.4** Comparison of Mori-Tanaka calculations and experimental results of PP 3371/clay nanocomposites for oriented particles at room temperature

| $E_{nanoclay}$ (GPa) | D (nm) | N | $E_p$ (GPa) | t (nm) | Nanoclay Rein. | Young's Modulus (Experimental) (GPa) | $E_{11}$ (GPa) | $E_{22}$ (GPa) | Poisson's Ratio (Experimental) | $\nu_{21}$ |
|---|---|---|---|---|---|---|---|---|---|---|
| 300 | 200 | 1 | 300 | 0.615 | 0% | 1.2001 | 1.2001 | 1.2001 | 0.3947 | 0.3947 |
| | | | | | 0.2% | 1.3172 | 1.3379 | 1.2487 | 0.4167 | 0.4072 |
| | | | | | 1% | 1.5085 | 1.8857 | 1.4140 | 0.4056 | 0.4411 |
| | | | | | 3% | 1.6278 | 3.2622 | 1.6967 | 0.3852 | 0.4789 |
| | | | | | 6% | 1.6463 | 5.3929 | 1.9512 | 0.3722 | 0.4995 |
| | | | | | 10% | 1.7426 | 8.3927 | 2.1624 | 0.3725 | 0.5092 |
| | | | | | | | | | | |
| 300 | 200 | 2 | 122.388 | 3.015 | 0% | 1.2001 | 1.2001 | 1.2001 | 0.3947 | 0.3947 |
| | | | | | 0.2% | 1.3172 | 1.2374 | 1.2139 | 0.4167 | 0.3984 |
| | | | | | 1% | 1.5085 | 1.3871 | 1.2674 | 0.4056 | 0.4114 |
| | | | | | 3% | 1.6278 | 1.7662 | 1.3893 | 0.3852 | 0.4358 |
| | | | | | 6% | 1.6463 | 2.3531 | 1.5476 | 0.3722 | 0.4592 |
| | | | | | 10% | 1.7426 | 3.1795 | 1.7270 | 0.3725 | 0.4778 |
| | | | | | | | | | | |
| 300 | 200 | 3 | 102.216 | 5.415 | 0% | 1.2001 | 1.2001 | 1.2001 | 0.3947 | 0.3947 |
| | | | | | 0.2% | 1.3172 | 1.2236 | 1.2090 | 0.4167 | 0.3970 |
| | | | | | 1% | 1.5085 | 1.3184 | 1.2443 | 0.4056 | 0.4058 |
| | | | | | 3% | 1.6278 | 1.5592 | 1.3286 | 0.3852 | 0.4239 |
| | | | | | 6% | 1.6463 | 1.9333 | 1.4464 | 0.3722 | 0.4440 |
| | | | | | 10% | 1.7426 | 2.4611 | 1.5914 | 0.3725 | 0.4625 |
| | | | | | | | | | | |
| 300 | 200 | 4 | 94.434 | 7.815 | 0% | 1.2001 | 1.2001 | 1.2001 | 0.3947 | 0.3947 |
| | | | | | 0.2% | 1.3172 | 1.2177 | 1.2069 | 0.4167 | 0.3965 |
| | | | | | 1% | 1.5085 | 1.2887 | 1.2341 | 0.4056 | 0.4031 |
| | | | | | 3% | 1.6278 | 1.4696 | 1.3005 | 0.3852 | 0.4177 |
| | | | | | 6% | 1.6463 | 1.7513 | 1.3966 | 0.3722 | 0.4351 |
| | | | | | 10% | 1.7426 | 2.1495 | 1.5198 | 0.3725 | 0.4525 |
| | | | | | | | | | | |

**Table 4.4** Continued

| | | | | | | | | | | |
|---|---|---|---|---|---|---|---|---|---|---|
| 300 | 200 | 5 | 90.308 | 10.215 | 0% | 1.2001 | 1.2001 | 1.2001 | 0.3947 | 0.3947 |
| | | | | | 0.2% | 1.3172 | 1.2143 | 1.2057 | 0.4167 | 0.3961 |
| | | | | | 1% | 1.5085 | 1.2718 | 1.2283 | 0.4056 | 0.4016 |
| | | | | | 3% | 1.6278 | 1.4184 | 1.2841 | 0.3852 | 0.4138 |
| | | | | | 6% | 1.6463 | 1.6472 | 1.3665 | 0.3722 | 0.4291 |
| | | | | | 10% | 1.7426 | 1.9712 | 1.4747 | 0.3725 | 0.4452 |
| | | | | | | | | | | |
| 300 | 200 | 6 | 87.753 | 12.6150 | 0% | 1.2001 | 1.2001 | 1.2001 | 0.3947 | 0.3947 |
| | | | | | 0.2% | 1.3172 | 1.2121 | 1.2050 | 0.4167 | 0.3959 |
| | | | | | 1% | 1.5085 | 1.2608 | 1.2245 | 0.4056 | 0.4005 |
| | | | | | 3% | 1.6278 | 1.3851 | 1.2733 | 0.3852 | 0.4111 |
| | | | | | 6% | 1.6463 | 1.5793 | 1.3462 | 0.3722 | 0.4247 |
| | | | | | 10% | 1.7426 | 1.8547 | 1.4435 | 0.3725 | 0.4397 |

**Table 4.5** Comparison of Mori-Tanaka calculations and experimental results of PP 3371/clay nanocomposites for oriented particles at -4ºF

| $E_{nanoclay}$ (GPa) | D (nm) | N | $E_p$ (GPa) | t (nm) | Nanoclay Rein. | Young's Modulus (Experimental) (GPa) | $E_{11}$ (GPa) | $E_{22}$ (GPa) | Poisson's Ratio (Experimental) | $\nu_{21}$ |
|---|---|---|---|---|---|---|---|---|---|---|
| 300 | 200 | 1 | 300 | 0.615 | 0% | 3.34644 | 3.34644 | 3.34644 | 0.3438 | 0.3438 |
| | | | | | 0.2% | 3.7128 | 3.5514 | 3.4050 | 0.3307 | 0.3481 |
| | | | | | 1% | 4.0082 | 4.3722 | 3.6122 | 0.3156 | 0.3617 |
| | | | | | 3% | 4.1786 | 6.4451 | 3.9978 | 0.3114 | 0.3811 |
| | | | | | 6% | 4.2123 | 9.6416 | 4.3843 | 0.3056 | 0.3942 |
| | | | | | 10% | 4.3331 | 14.1024 | 4.7373 | 0.2928 | 0.4011 |
| | | | | | | | | | | |
| 300 | 200 | 2 | 122.388 | 3.015 | 0% | 3.34644 | 3.34644 | 3.34644 | 0.3438 | 0.3438 |
| | | | | | 0.2% | 3.7128 | 3.4115 | 3.3667 | 0.3307 | 0.3453 |
| | | | | | 1% | 4.0082 | 3.6732 | 3.4455 | 0.3156 | 0.3507 |
| | | | | | 3% | 4.1786 | 4.3374 | 3.6283 | 0.3114 | 0.3617 |
| | | | | | 6% | 4.2123 | 5.3652 | 3.8730 | 0.3056 | 0.3733 |
| | | | | | 10% | 4.3331 | 6.8037 | 4.1611 | 0.2928 | 0.3833 |
| | | | | | | | | | | |

**Table 4.5** Continued

| | | | | | | | | | | |
|---|---|---|---|---|---|---|---|---|---|---|
| 300 | 200 | 3 | 102.216 | 5.415 | 0% | 3.34644 | 3.34644 | 3.34644 | 0.3438 | 0.3438 |
| | | | | | 0.2% | 3.7128 | 3.3914 | 3.3610 | 0.3307 | 0.3448 |
| | | | | | 1% | 4.0082 | 3.5726 | 3.4185 | 0.3156 | 0.3488 |
| | | | | | 3% | 4.1786 | 4.0335 | 3.5568 | 0.3114 | 0.3574 |
| | | | | | 6% | 4.2123 | 4.7488 | 3.7527 | 0.3056 | 0.3675 |
| | | | | | 10% | 4.3331 | 5.7534 | 3.9981 | 0.2928 | 0.3772 |
| | | | | | | | | | | |
| 300 | 200 | 4 | 94.434 | 7.815 | 0% | 3.34644 | 3.34644 | 3.34644 | 0.3438 | 0.3438 |
| | | | | | 0.2% | 3.7128 | 3.3822 | 3.3584 | 0.3307 | 0.3446 |
| | | | | | 1% | 4.0082 | 3.5260 | 3.4057 | 0.3156 | 0.3479 |
| | | | | | 3% | 4.1786 | 3.8925 | 3.5218 | 0.3114 | 0.3551 |
| | | | | | 6% | 4.2123 | 4.4628 | 3.6906 | 0.3056 | 0.3641 |
| | | | | | 10% | 4.3331 | 5.2656 | 3.9091 | 0.2928 | 0.3734 |
| | | | | | | | | | | |
| 300 | 200 | 5 | 90.308 | 10.215 | 0% | 3.34644 | 3.34644 | 3.34644 | 0.3438 | 0.3438 |
| | | | | | 0.2% | 3.7128 | 3.3765 | 3.3568 | 0.3307 | 0.3445 |
| | | | | | 1% | 4.0082 | 3.4978 | 3.3980 | 0.3156 | 0.3473 |
| | | | | | 3% | 4.1786 | 3.8070 | 3.5001 | 0.3114 | 0.3536 |
| | | | | | 6% | 4.2123 | 4.2890 | 3.6511 | 0.3056 | 0.3618 |
| | | | | | 10% | 4.3331 | 4.9689 | 3.8505 | 0.2928 | 0.3706 |
| | | | | | | | | | | |
| 300 | 200 | 6 | 87.753 | 12.6150 | 0% | 3.34644 | 3.34644 | 3.34644 | 0.3438 | 0.3438 |
| | | | | | 0.2% | 3.7128 | 3.3727 | 3.3557 | 0.3307 | 0.3444 |
| | | | | | 1% | 4.0082 | 3.4784 | 3.3928 | 0.3156 | 0.3469 |
| | | | | | 3% | 4.1786 | 3.7484 | 3.4851 | 0.3114 | 0.3525 |
| | | | | | 6% | 4.2123 | 4.1697 | 3.6233 | 0.3056 | 0.3600 |
| | | | | | 10% | 4.3331 | 4.7650 | 3.8085 | 0.2928 | 0.3683 |

**Table 4.6** Comparison of Mori-Tanaka calculations and experimental results of PP 3371/clay nanocomposites for oriented particles at -65ºF

| $E_{nanoclay}$ (GPa) | D (nm) | N | $E_p$ (GPa) | t (nm) | Nanoclay Rein. | Young's Modulus (Experimental) (GPa) | $E_{11}$ (GPa) | $E_{22}$ (GPa) | Poisson's Ratio (Experimental) | $\nu_{21}$ |
|---|---|---|---|---|---|---|---|---|---|---|
| 300 | 200 | 1 | 300 | 0.615 | 0% | 3.86509 | 3.86509 | 3.86509 | 0.3429 | 0.3429 |
| | | | | | 0.2% | 4.2836 | 4.0780 | 3.9263 | 0.3283 | 0.3467 |
| | | | | | 1% | 4.6031 | 4.9307 | 4.1454 | 0.3193 | 0.3590 |
| | | | | | 3% | 4.6944 | 7.0845 | 4.5646 | 0.3076 | 0.3772 |
| | | | | | 6% | 4.9732 | 10.4035 | 4.9980 | 0.3039 | 0.3900 |
| | | | | | 10% | 5.0920 | 15.0296 | 5.4032 | 0.2983 | 0.3970 |
| | | | | | | | | | | |
| 300 | 200 | 2 | 122.388 | 3.015 | 0% | 3.86509 | 3.86509 | 3.86509 | 0.3429 | 0.3429 |
| | | | | | 0.2% | 4.2836 | 3.9340 | 3.8868 | 0.3283 | 0.3442 |
| | | | | | 1% | 4.6031 | 4.2111 | 3.9715 | 0.3193 | 0.3491 |
| | | | | | 3% | 4.6944 | 4.9146 | 4.1697 | 0.3076 | 0.3591 |
| | | | | | 6% | 4.9732 | 6.0026 | 4.4384 | 0.3039 | 0.3699 |
| | | | | | 10% | 5.0920 | 7.5236 | 4.7590 | 0.2983 | 0.3792 |
| | | | | | | | | | | |
| 300 | 200 | 3 | 102.216 | 5.415 | 0% | 3.86509 | 3.86509 | 3.86509 | 0.3429 | 0.3429 |
| | | | | | 0.2% | 4.2836 | 3.9134 | 3.8809 | 0.3283 | 0.3438 |
| | | | | | 1% | 4.6031 | 4.1078 | 3.9436 | 0.3193 | 0.3474 |
| | | | | | 3% | 4.6944 | 4.6025 | 4.0950 | 0.3076 | 0.3553 |
| | | | | | 6% | 4.9732 | 5.3699 | 4.3111 | 0.3039 | 0.3646 |
| | | | | | 10% | 5.0920 | 6.4462 | 4.5842 | 0.2983 | 0.3737 |
| | | | | | | | | | | |
| 300 | 200 | 4 | 94.434 | 7.815 | 0% | 3.86509 | 3.86509 | 3.86509 | 0.3429 | 0.3429 |
| | | | | | 0.2% | 4.2836 | 3.9038 | 3.8782 | 0.3283 | 0.3437 |
| | | | | | 1% | 4.6031 | 4.0597 | 3.9303 | 0.3193 | 0.3466 |
| | | | | | 3% | 4.6944 | 4.4569 | 4.0584 | 0.3076 | 0.3533 |
| | | | | | 6% | 4.9732 | 5.0743 | 4.2456 | 0.3039 | 0.3616 |
| | | | | | 10% | 5.0920 | 5.9426 | 4.4893 | 0.2983 | 0.3703 |
| | | | | | | | | | | |

**Table 4.6** Continued

| | | | | | | | | | | |
|---|---|---|---|---|---|---|---|---|---|---|
| 300 | 200 | 5 | 90.308 | 10.215 | 0% | 3.86509 | 3.86509 | 3.86509 | 0.3429 | 0.3429 |
| | | | | | 0.2% | 4.2836 | 3.8979 | 3.8765 | 0.3283 | 0.3436 |
| | | | | | 1% | 4.6031 | 4.0302 | 3.9222 | 0.3193 | 0.3461 |
| | | | | | 3% | 4.6944 | 4.3677 | 4.0355 | 0.3076 | 0.3520 |
| | | | | | 6% | 4.9732 | 4.8933 | 4.2037 | 0.3039 | 0.3595 |
| | | | | | 10% | 5.0920 | 5.6339 | 4.4268 | 0.2983 | 0.3677 |
| | | | | | | | | | | |
| 300 | 200 | 6 | 87.753 | 12.6150 | 0% | 3.86509 | 3.86509 | 3.86509 | 0.3429 | 0.3429 |
| | | | | | 0.2% | 4.2836 | 3.8939 | 3.8754 | 0.3283 | 0.3435 |
| | | | | | 1% | 4.6031 | 4.0099 | 3.9166 | 0.3193 | 0.3457 |
| | | | | | 3% | 4.6944 | 4.3062 | 4.0196 | 0.3076 | 0.3510 |
| | | | | | 6% | 4.9732 | 4.7682 | 4.1741 | 0.3039 | 0.3580 |
| | | | | | 10% | 5.0920 | 5.4202 | 4.3817 | 0.2983 | 0.3657 |

**Table 4.7** Comparison of Mori-Tanaka calculations and experimental results of EPON 828 epoxy / clay nanocomposites for oriented particles at room temperature

| $E_{nanoclay}$ (GPa) | D (nm) | N | $E_p$ (GPa) | t (nm) | Nanoclay Rein. | Young's Modulus (Experimental) (GPa) | $E_{11}$ (GPa) | $E_{22}$ (GPa) | Poisson's Ratio (Experimental) | $\nu_{21}$ |
|---|---|---|---|---|---|---|---|---|---|---|
| 300 | 200 | 6 | 87.7525 | 12.6150 | 0% | 2.8177 | 2.8177 | 2.8177 | 0.3105 | 0.3105 |
| | | | | | 1% | 2.9127 | 2.8791 | 3.0247 | 0.3238 | 0.3150 |
| | | | | | 3% | 2.9840 | 2.9977 | 3.4467 | 0.3288 | 0.3236 |
| | | | | | 6% | 3.0965 | 3.1682 | 4.1018 | 0.3340 | 0.3316 |
| | | | | | 10% | 3.3427 | 3.3880 | 5.0218 | 0.3348 | 0.3404 |

4.1.1-c) 2-D Randomly Distributed Nanoclay Particles

Here the nanoclay flakes are in a plane parallel to test direction, but are randomly distributed in the plane. Referring to [197], the normalized in plane Young's modulus, the normalized in plane shear modulus, the normalized out of plane shear modulus and the normalized out of plane Young's modulus for the case of 2-D randomly distributed nanoclay particles can be expressed as:

$$\frac{E_{11}}{E_m} = \left( \frac{1}{1 + cp_{11}} \right) \tag{29}$$

where c is the volume fraction given in equation (28) and $p_{11}$ is:

$$\begin{aligned} p_{11} = {} & \frac{1}{1 + c(b_1 - b_2)} \left\{ \frac{2(a_1 + a_2 - a_3) + a_4 + a_5 a}{16a} - \frac{1}{4\left[ 2S_{1212} + \mu_m / (\mu_p - \mu_m) \right]} \right\} \\ & - \frac{(1 - \nu_m)(1 + cb_5) + 2c\nu_m b_3}{2c^2 b_3 b_4 - (1 + cb_5)\left[ 1 + c(b_1 + b_2) \right]} \frac{2(a_1 - a_2 + a_3) + a_4 + a_5 a}{8a} \\ & + \frac{(1 - \nu_m) cb_4 + \nu_m \left[ 1 + c(b_1 + b_2) \right]}{2c^2 b_3 b_4 - (1 + cb_5)\left[ 1 + c(b_1 + b_2) \right]} \frac{-2a_2 + a_4 - a_5 a}{4a} \end{aligned} \tag{30}$$

$$\frac{\mu_{12}}{\mu_m} = \left( \frac{1}{1 + cp_{12}} \right) \tag{31}$$

with $p_{12}$ given as :

$$\begin{aligned} p_{12} = {} & \left[ 2(a_1 + a_2 - a_3) + a_4 + a_5 a - \frac{4a}{2S_{1212} + \mu_m / (\mu_p - \mu_m)} \right] / \\ & \{ 8a + c[(S_{1122} - S_{2222} + 1)(2a_3 - a_4 - a_5 a) \\ & + 2(S_{1111} - S_{2211} - 1)(a_1 + a_2) + (S_{1122} - S_{2233})(2a_3 - a_4 + a_5 a) \\ & - \frac{4a(2S_{1212} - 1)}{2S_{1212} + \mu_m / (\mu_p - \mu_m)} ] \} \end{aligned} \tag{32}$$

$$\frac{\mu_{13}}{\mu_m} = \left( \frac{1}{1 + cp_{13}} \right) \tag{33}$$

with $p_{13}$

$$p_{13} = -\left[ \frac{1}{2S_{1313} + \mu_m / (\mu_p - \mu_m)} + \frac{1}{2S_{2323} + \mu_m / (\mu_p - \mu_m)} \right] / \left\{ 2 - c \left[ \frac{2S_{1313} - 1}{2S_{1313} + \mu_m / (\mu_p - \mu_m)} + \frac{2S_{2323} - 1}{2S_{2323} + \mu_m / (\mu_p - \mu_m)} \right] \right\} \tag{34}$$

$$\frac{E_{33}}{E_m} = \frac{1}{1 + cp_{33}} \tag{35}$$

where $p_{33}$ is,

$$p_3 = \left\{ \left[ \nu_m (1 + cb_5) + cb_3 \right] (2a_3 + a_4 - a_5 a) - \left[ 1 + c(b_1 + b_2 + 2\nu_0 b_4) \right] (a_4 + a_5 a) \right\} / 2a \left\{ 2c^2 b_3 b_4 - (1 + cb_5) \left[ 1 + c(b_1 + b_2) \right] \right\} \tag{36}$$

The definition of the components of Eshelby's tensor and g were given in section 4.1.1-a). The other constants which are used to calculate the material properties of randomly distributed nanoclay particles are given below:

$$a_1 = 6(\kappa_p - \kappa_m)(\mu_p - \mu_m)(S_{2222} + S_{2233} - 1) - 2(\kappa_m \mu_p - \kappa_p \mu_m) + 6\kappa_p (\mu_p - \mu_m) \tag{37}$$

$$a_2 = 6(\kappa_p - \kappa_m)(\mu_p - \mu_m) S_{1133} + 2(\kappa_m \mu_p - \kappa_p \mu_0) \tag{38}$$

$$a_3 = -6(\kappa_p - \kappa_m)(\mu_p - \mu_m) S_{3311} - 2(\kappa_m \mu_p - \kappa_p \mu_m) \tag{39}$$

$$a_4 = 6(\kappa_p - \kappa_m)(\mu_p - \mu_m)(S_{1111} - 1) + 2(\kappa_m \mu_p - \kappa_p \mu_m) + 6\mu_p (\kappa_p - \kappa_m) \tag{40}$$

$$a_5 = 1 / [S_{3322} - S_{3333} + 1 - \mu_p / (\mu_p - \mu_m)] \tag{41}$$

$$a = 6(\kappa_p - \kappa_m)(\mu_p - \mu_m)[2S_{1133}S_{3311} - (S_{1111} - 1)(S_{3322} + S_{3333} - 1)] + 2(\kappa_m\mu_p - \kappa_p\mu_m)[2(S_{1133} + S_{3311}) + (S_{1111} - S_{3322} - S_{3333})] - 6\kappa_p(\mu_p - \mu_m)(S_{1111} - 1) - 6\mu_p(\kappa_p - \kappa_m)(S_{2222} + S_{2233} - 1) - 6\kappa_p\mu_p \quad (42)$$

$$b_1 = (1/16a)\{2a_3(6S_{1122} + S_{2222} + S_{2233} - 1) + a_4[3(S_{2222} + S_{2233} - 1) + 2S_{1122}] + 3a_5a(S_{2222} - S_{2233} - 1) + 2a_1[3(S_{1111} - 1) + S_{2211}] - 2a_2(S_{1111} + 3S_{2211} - 1) - 4a(2S_{1212} - 1)/[2S_{1212} + \mu_m/(\mu_p - \mu_m)]\} \quad (43)$$

$$b_2 = (1/16a)\{2a_3\left[2S_{1111} + 3(S_{2222} + S_{2233} - 1)\right] + a_4(6S_{1122} + S_{2222} + S_{2233} - 1) + a_5a(S_{2222} - S_{2233} - 1) + 2a_1(S_{1111} + 3S_{2211} - 1) - 2a_2\left[S_{2211} + 3(S_{1111} - 1)\right] + 4a(2S_{1212} - 1)/\left[2S_{1212} + \mu_m/(\mu_p - \mu_m)\right]\} \quad (44)$$

$$b_3 = (1/a)\{-2a_2(S_{1111} + S_{2211} - 1) + a_4(2S_{1122} + S_{2222} + S_{2233} - 1) - a_5a(S_{2222} - S_{2233} - 1)\} \quad (45)$$

$$b_4 = (1/4a)\{2(a_1 - a_2)S_{2211} + (2a_3 + a_4)(S_{2222} + S_{2233} - 1) - a_5a(S_{2222} - S_{2233} - 1)\} \quad (46)$$

$$b_5 = (1/2a)\{-2a_2S_{2211} + a_4(S_{2222} + S_{2233} - 1) + a_5a(S_{2222} - S_{2233} - 1)\} \quad (47)$$

4.1.1-d) Results of Parametric Study for 2-D Randomly Distributed Nanoclay Particles

For the parametric study, in the Mori-Tanaka calculations the number of flakes N in a nanoclay particle was varied from 1 to 6 and the nanoclay Young's modulus $E_{nanoclay}$=300 GPa was used to calculate the particle thickness t and the effective particle Young's modulus Ep. For PP 3371 specimens with nanoclay reinforcement, the Mori-Tanaka calculations were performed with the Young's modulus values obtained from the tensile tests at various temperatures. For EPON 828 epoxy specimens, the Mori-Tanaka calculations were carried out at room temperature only for

N=6 and $E_{nanoclay}$=300GPa. The comparison of Mori-Tanaka calculations and experimental results for 2-D randomly distributed particles in PP 3371 and EPON 828 epoxy is given in Tables 4.8 - 4.12 and Table 4.13 respectively.

**Table 4.8** Comparison of Mori-Tanaka calculations and experimental results of PP 3371/clay nanocomposites for 2-D randomly distributed particles at 160ºF

| $E_{nanoclay}$ (GPa) | D (nm) | N | $E_p$ (GPa) | t (nm) | Nanoclay Rein. | Young's Modulus (Experimental) (GPa) | $E_{11}=E_{22}$ (GPa) | $E_{33}$ (GPa) | Poisson's Ratio (Experimental) | ν |
|---|---|---|---|---|---|---|---|---|---|---|
| 300 | 200 | 1 | 300 | 0.615 | 0% | 0.39204 | 0.39204 | 0.39204 | 0.4256 | 0.4256 |
| | | | | | 0.2% | 0.4499 | 0.4222 | 0.4590 | 0.4782 | 0.4493 |
| | | | | | 1% | 0.4654 | 0.5342 | 0.7280 | 0.4715 | 0.4948 |
| | | | | | 3% | 0.4969 | 0.7950 | 1.4101 | 0.4523 | 0.5086 |
| | | | | | 6% | 0.5031 | 1.1819 | 2.4669 | 0.5077 | 0.4875 |
| | | | | | 10% | 0.5146 | 1.7173 | 3.9562 | 0.4896 | 0.4579 |
| 300 | 200 | 2 | 122.388 | 3.015 | 0% | 0.39204 | 0.39204 | 0.39204 | 0.4256 | 0.4256 |
| | | | | | 0.2% | 0.4499 | 0.3994 | 0.4077 | 0.4782 | 0.4318 |
| | | | | | 1% | 0.4654 | 0.4282 | 0.4709 | 0.4715 | 0.4524 |
| | | | | | 3% | 0.4969 | 0.4983 | 0.6327 | 0.4523 | 0.4839 |
| | | | | | 6% | 0.5031 | 0.6022 | 0.8861 | 0.5077 | 0.5042 |
| | | | | | 10% | 0.5146 | 0.7446 | 1.2461 | 0.4896 | 0.5105 |
| 300 | 200 | 3 | 102.216 | 5.415 | 0% | 0.39204 | 0.39204 | 0.39204 | 0.4256 | 0.4256 |
| | | | | | 0.2% | 0.4499 | 0.3965 | 0.4013 | 0.4782 | 0.4293 |
| | | | | | 1% | 0.4654 | 0.4142 | 0.4388 | 0.4715 | 0.4425 |
| | | | | | 3% | 0.4969 | 0.4579 | 0.5350 | 0.4523 | 0.4671 |
| | | | | | 6% | 0.5031 | 0.5235 | 0.6860 | 0.5077 | 0.4895 |
| | | | | | 10% | 0.5146 | 0.6138 | 0.9013 | 0.4896 | 0.5042 |
| 300 | 200 | 4 | 94.434 | 7.815 | 0% | 0.39204 | 0.39204 | 0.39204 | 0.4256 | 0.4256 |
| | | | | | 0.2% | 0.4499 | 0.3953 | 0.3988 | 0.4782 | 0.4282 |
| | | | | | 1% | 0.4654 | 0.4084 | 0.4259 | 0.4715 | 0.4380 |
| | | | | | 3% | 0.4969 | 0.4411 | 0.4954 | 0.4523 | 0.4578 |
| | | | | | 6% | 0.5031 | 0.4906 | 0.6048 | 0.5077 | 0.4785 |
| | | | | | 10% | 0.5146 | 0.5591 | 0.7610 | 0.4896 | 0.4953 |

**Table 4.8** Continued

| | | | | | | | | | | |
|---|---|---|---|---|---|---|---|---|---|---|
| 300 | 200 | 5 | 90.308 | 10.215 | 0% | 0.39204 | 0.39204 | 0.39204 | 0.4256 | 0.4256 |
| | | | | | 0.2% | 0.4499 | 0.3947 | 0.3973 | 0.4782 | 0.4277 |
| | | | | | 1% | 0.4654 | 0.4052 | 0.4188 | 0.4715 | 0.4354 |
| | | | | | 3% | 0.4969 | 0.4318 | 0.4738 | 0.4523 | 0.4519 |
| | | | | | 6% | 0.5031 | 0.4724 | 0.5605 | 0.5077 | 0.4706 |
| | | | | | 10% | 0.5146 | 0.5287 | 0.6843 | 0.4896 | 0.4875 |
| | | | | | | | | | | |
| 300 | 200 | 6 | 87.753 | 12.6150 | 0% | 0.39204 | 0.39204 | 0.39204 | 0.4256 | 0.4256 |
| | | | | | 0.2% | 0.4499 | 0.3943 | 0.3965 | 0.4782 | 0.4273 |
| | | | | | 1% | 0.4654 | 0.4033 | 0.4143 | 0.4715 | 0.4337 |
| | | | | | 3% | 0.4969 | 0.4259 | 0.4602 | 0.4523 | 0.4479 |
| | | | | | 6% | 0.5031 | 0.4607 | 0.5325 | 0.5077 | 0.4646 |
| | | | | | 10% | 0.5146 | 0.5092 | 0.6359 | 0.4896 | 0.4809 |

**Table 4.9** Comparison of Mori-Tanaka calculations and experimental results of PP 3371/clay nanocomposites for 2-D randomly distributed particles at 120ºF

| $E_{nanoclay}$ (GPa) | D (nm) | N | $E_p$ (GPa) | t (nm) | Nanoclay Rein. | Young's Modulus (Experimental) (GPa) | $E_{11}=E_{22}$ (GPa) | $E_{33}$ (GPa) | Poisson's Ratio (Experimental) | ν |
|---|---|---|---|---|---|---|---|---|---|---|
| 300 | 200 | 1 | 300 | 0.615 | 0% | 0.61595 | 0.61595 | 0.61595 | 0.4038 | 0.4038 |
| | | | | | 0.2% | 0.7285 | 0.6565 | 0.7084 | 0.4350 | 0.4225 |
| | | | | | 1% | 0.7646 | 0.8081 | 1.0795 | 0.4631 | 0.4598 |
| | | | | | 3% | 0.8283 | 1.1627 | 2.0199 | 0.4355 | 0.4721 |
| | | | | | 6% | 0.8332 | 1.6907 | 3.4760 | 0.4334 | 0.4547 |
| | | | | | 10% | 0.8664 | 2.4245 | 5.5244 | 0.4111 | 0.4300 |
| | | | | | | | | | | |
| 300 | 200 | 2 | 122.388 | 3.015 | 0% | 0.61595 | 0.61595 | 0.61595 | 0.4038 | 0.4038 |
| | | | | | 0.2% | 0.7285 | 0.6263 | 0.6387 | 0.4350 | 0.4089 |
| | | | | | 1% | 0.7646 | 0.6672 | 0.7303 | 0.4631 | 0.4259 |
| | | | | | 3% | 0.8283 | 0.7665 | 0.9645 | 0.4355 | 0.4522 |
| | | | | | 6% | 0.8332 | 0.9143 | 1.3308 | 0.4334 | 0.4691 |
| | | | | | 10% | 0.8664 | 1.1171 | 1.8500 | 0.4111 | 0.4739 |
| | | | | | | | | | | |

**Table 4.9** Continued

| | | | | | | | | | | |
|---|---|---|---|---|---|---|---|---|---|---|
| 300 | 200 | 3 | 102.216 | 5.415 | 0% | 0.61595 | 0.61595 | 0.61595 | 0.4038 | 0.4038 |
| | | | | | 0.2% | 0.7285 | 0.6224 | 0.6297 | 0.4350 | 0.4069 |
| | | | | | 1% | 0.7646 | 0.6479 | 0.6851 | 0.4631 | 0.4180 |
| | | | | | 3% | 0.8283 | 0.7111 | 0.8272 | 0.4355 | 0.4388 |
| | | | | | 6% | 0.8332 | 0.8062 | 1.0500 | 0.4334 | 0.4575 |
| | | | | | 10% | 0.8664 | 0.9371 | 1.3670 | 0.4111 | 0.4696 |
| | | | | | | | | | | |
| 300 | 200 | 4 | 94.434 | 7.815 | 0% | 0.61595 | 0.61595 | 0.61595 | 0.4038 | 0.4038 |
| | | | | | 0.2% | 0.7285 | 0.6207 | 0.6260 | 0.4350 | 0.4060 |
| | | | | | 1% | 0.7646 | 0.6398 | 0.6665 | 0.4631 | 0.4144 |
| | | | | | 3% | 0.8283 | 0.6876 | 0.7704 | 0.4355 | 0.4312 |
| | | | | | 6% | 0.8332 | 0.7602 | 0.9336 | 0.4334 | 0.4487 |
| | | | | | 10% | 0.8664 | 0.8605 | 1.1663 | 0.4111 | 0.4627 |
| | | | | | | | | | | |
| 300 | 200 | 5 | 90.308 | 10.215 | 0% | 0.61595 | 0.61595 | 0.61595 | 0.4038 | 0.4038 |
| | | | | | 0.2% | 0.7285 | 0.6198 | 0.6239 | 0.4350 | 0.4056 |
| | | | | | 1% | 0.7646 | 0.6354 | 0.6562 | 0.4631 | 0.4122 |
| | | | | | 3% | 0.8283 | 0.6745 | 0.7389 | 0.4355 | 0.4263 |
| | | | | | 6% | 0.8332 | 0.7343 | 0.8691 | 0.4334 | 0.4422 |
| | | | | | 10% | 0.8664 | 0.8173 | 1.0550 | 0.4111 | 0.4564 |
| | | | | | | | | | | |
| 300 | 200 | 6 | 87.753 | 12.6150 | 0% | 0.61595 | 0.61595 | 0.61595 | 0.4038 | 0.4038 |
| | | | | | 0.2% | 0.7285 | 0.6193 | 0.6226 | 0.4350 | 0.4053 |
| | | | | | 1% | 0.7646 | 0.6325 | 0.6496 | 0.4631 | 0.4108 |
| | | | | | 3% | 0.8283 | 0.6661 | 0.7189 | 0.4355 | 0.4229 |
| | | | | | 6% | 0.8332 | 0.7176 | 0.8280 | 0.4334 | 0.4372 |
| | | | | | 10% | 0.8664 | 0.7895 | 0.9839 | 0.4111 | 0.4510 |

**Table 4.10** Comparison of Mori-Tanaka calculations and experimental results of PP 3371/clay nanocomposites for 2-D randomly distributed particles at RT

| $E_{nanoclay}$ (GPa) | D (nm) | N | $E_p$ (GPa) | t (nm) | Nanoclay Rein. | Young's Modulus (Experimental) (GPa) | $E_{11}=E_{22}$ (GPa) | $E_{33}$ (GPa) | Poisson's Ratio (Experimental) | ν |
|---|---|---|---|---|---|---|---|---|---|---|
| 300 | 200 | 1 | 300 | 0.615 | 0% | 1.2001 | 1.2001 | 1.2001 | 0.3947 | 0.3947 |
| | | | | | 0.2% | 1.3172 | 1.2607 | 1.3384 | 0.4167 | 0.4086 |
| | | | | | 1% | 1.5085 | 1.4898 | 1.8940 | 0.4056 | 0.4404 |
| | | | | | 3% | 1.6278 | 2.0290 | 3.3022 | 0.3852 | 0.4577 |
| | | | | | 6% | 1.6463 | 2.8298 | 5.4780 | 0.3722 | 0.4475 |
| | | | | | 10% | 1.7426 | 3.9392 | 8.5241 | 0.3725 | 0.4275 |
| | | | | | | | | | | |
| 300 | 200 | 2 | 122.388 | 3.015 | 0% | 1.2001 | 1.2001 | 1.2001 | 0.3947 | 0.3947 |
| | | | | | 0.2% | 1.3172 | 1.2171 | 1.2374 | 0.4167 | 0.3988 |
| | | | | | 1% | 1.5085 | 1.2843 | 1.3880 | 0.4056 | 0.4128 |
| | | | | | 3% | 1.6278 | 1.4488 | 1.7726 | 0.3852 | 0.4357 |
| | | | | | 6% | 1.6463 | 1.6943 | 2.3725 | 0.3722 | 0.4520 |
| | | | | | 10% | 1.7426 | 2.0310 | 3.2196 | 0.3725 | 0.4583 |
| | | | | | | | | | | |
| 300 | 200 | 3 | 102.216 | 5.415 | 0% | 1.2001 | 1.2001 | 1.2001 | 0.3947 | 0.3947 |
| | | | | | 0.2% | 1.3172 | 1.2111 | 1.2236 | 0.4167 | 0.3973 |
| | | | | | 1% | 1.5085 | 1.2548 | 1.3188 | 0.4056 | 0.4067 |
| | | | | | 3% | 1.6278 | 1.3636 | 1.5621 | 0.3852 | 0.4246 |
| | | | | | 6% | 1.6463 | 1.5279 | 1.9431 | 0.3722 | 0.4416 |
| | | | | | 10% | 1.7426 | 1.7541 | 2.4834 | 0.3725 | 0.4533 |
| | | | | | | | | | | |
| 300 | 200 | 4 | 94.434 | 7.815 | 0% | 1.2001 | 1.2001 | 1.2001 | 0.3947 | 0.3947 |
| | | | | | 0.2% | 1.3172 | 1.2085 | 1.2177 | 0.4167 | 0.3966 |
| | | | | | 1% | 1.5085 | 1.2420 | 1.2889 | 0.4056 | 0.4038 |
| | | | | | 3% | 1.6278 | 1.3262 | 1.4713 | 0.3852 | 0.4185 |
| | | | | | 6% | 1.6463 | 1.4543 | 1.7574 | 0.3722 | 0.4341 |
| | | | | | 10% | 1.7426 | 1.6316 | 2.1642 | 0.3725 | 0.4471 |
| | | | | | | | | | | |

**Table 4.10** Continued

| | | | | | | | | | | |
|---|---|---|---|---|---|---|---|---|---|---|
| 300 | 200 | 5 | 90.308 | 10.215 | 0% | 1.2001 | 1.2001 | 1.2001 | 0.3947 | 0.3947 |
| | | | | | 0.2% | 1.3172 | 1.2070 | 1.2143 | 0.4167 | 0.3962 |
| | | | | | 1% | 1.5085 | 1.2348 | 1.2719 | 0.4056 | 0.4020 |
| | | | | | 3% | 1.6278 | 1.3047 | 1.4196 | 0.3852 | 0.4144 |
| | | | | | 6% | 1.6463 | 1.4118 | 1.6515 | 0.3722 | 0.4286 |
| | | | | | 10% | 1.7426 | 1.5607 | 1.9817 | 0.3725 | 0.4416 |
| | | | | | | | | | | |
| 300 | 200 | 6 | 87.753 | 12.6150 | 0% | 1.2001 | 1.2001 | 1.2001 | 0.3947 | 0.3947 |
| | | | | | 0.2% | 1.3172 | 1.2060 | 1.2121 | 0.4167 | 0.3960 |
| | | | | | 1% | 1.5085 | 1.2300 | 1.2609 | 0.4056 | 0.4008 |
| | | | | | 3% | 1.6278 | 1.2906 | 1.3859 | 0.3852 | 0.4116 |
| | | | | | 6% | 1.6463 | 1.3839 | 1.5824 | 0.3722 | 0.4244 |
| | | | | | 10% | 1.7426 | 1.5141 | 1.8626 | 0.3725 | 0.4369 |

**Table 4.11** Comparison of Mori-Tanaka calculations and experimental results of PP 3371/clay nanocomposites for 2-D randomly distributed particles at -4ºF

| $E_{nanoclay}$ (GPa) | D (nm) | N | $E_p$ (GPa) | t (nm) | Nanoclay Rein. | Young's Modulus (Experimental) (GPa) | $E_{11}=E_{22}$ (GPa) | $E_{33}$ (GPa) | Poisson's Ratio (Experimental) | ν |
|---|---|---|---|---|---|---|---|---|---|---|
| 300 | 200 | 1 | 300 | 0.615 | 0% | 3.34644 | 3.34644 | 3.34644 | 0.3438 | 0.3438 |
| | | | | | 0.2% | 3.7128 | 3.4325 | 3.5516 | 0.3307 | 0.3495 |
| | | | | | 1% | 4.0082 | 3.7678 | 4.3765 | 0.3156 | 0.3659 |
| | | | | | 3% | 4.1786 | 4.5775 | 6.4694 | 0.3114 | 0.3831 |
| | | | | | 6% | 4.2123 | 5.7895 | 9.7001 | 0.3056 | 0.3866 |
| | | | | | 10% | 4.3331 | 7.4697 | 14.2001 | 0.2928 | 0.3810 |
| | | | | | | | | | | |
| 300 | 200 | 2 | 122.388 | 3.015 | 0% | 3.34644 | 3.34644 | 3.34644 | 0.3438 | 0.3438 |
| | | | | | 0.2% | 3.7128 | 3.3752 | 3.4115 | 0.3307 | 0.3457 |
| | | | | | 1% | 4.0082 | 3.4897 | 3.6737 | 0.3156 | 0.3525 |
| | | | | | 3% | 4.1786 | 3.7749 | 4.3419 | 0.3114 | 0.3653 |
| | | | | | 6% | 4.2123 | 4.2068 | 5.3797 | 0.3056 | 0.3768 |
| | | | | | 10% | 4.3331 | 4.8027 | 6.8353 | 0.2928 | 0.3841 |
| | | | | | | | | | | |

**Table 4.11** Continued

| | | | | | | | | | | |
|---|---|---|---|---|---|---|---|---|---|---|
| 300 | 200 | 3 | 102.216 | 5.415 | 0% | 3.34644 | 3.34644 | 3.34644 | 0.3438 | 0.3438 |
| | | | | | 0.2% | 3.7128 | 3.3669 | 3.3915 | 0.3307 | 0.3451 |
| | | | | | 1% | 4.0082 | 3.4487 | 3.5729 | 0.3156 | 0.3500 |
| | | | | | 3% | 4.1786 | 3.6544 | 4.0359 | 0.3114 | 0.3600 |
| | | | | | 6% | 4.2123 | 3.9684 | 4.7574 | 0.3056 | 0.3707 |
| | | | | | 10% | 4.3331 | 4.4039 | 5.7734 | 0.2928 | 0.3794 |
| | | | | | | | | | | |
| 300 | 200 | 4 | 94.434 | 7.815 | 0% | 3.34644 | 3.34644 | 3.34644 | 0.3438 | 0.3438 |
| | | | | | 0.2% | 3.7128 | 3.3631 | 3.3822 | 0.3307 | 0.3448 |
| | | | | | 1% | 4.0082 | 3.4297 | 3.5262 | 0.3156 | 0.3487 |
| | | | | | 3% | 4.1786 | 3.5981 | 3.8942 | 0.3114 | 0.3571 |
| | | | | | 6% | 4.2123 | 3.8566 | 4.4688 | 0.3056 | 0.3668 |
| | | | | | 10% | 4.3331 | 4.2166 | 5.2802 | 0.2928 | 0.3756 |
| | | | | | | | | | | |
| 300 | 200 | 5 | 90.308 | 10.215 | 0% | 3.34644 | 3.34644 | 3.34644 | 0.3438 | 0.3438 |
| | | | | | 0.2% | 3.7128 | 3.3608 | 3.3765 | 0.3307 | 0.3447 |
| | | | | | 1% | 4.0082 | 3.4182 | 3.4979 | 0.3156 | 0.3479 |
| | | | | | 3% | 4.1786 | 3.5639 | 3.8083 | 0.3114 | 0.3552 |
| | | | | | 6% | 4.2123 | 3.7884 | 4.2935 | 0.3056 | 0.3639 |
| | | | | | 10% | 4.3331 | 4.1022 | 4.9802 | 0.2928 | 0.3725 |
| | | | | | | | | | | |
| 300 | 200 | 6 | 87.753 | 12.6150 | 0% | 3.34644 | 3.34644 | 3.34644 | 0.3438 | 0.3438 |
| | | | | | 0.2% | 3.7128 | 3.3592 | 3.3727 | 0.3307 | 0.3445 |
| | | | | | 1% | 4.0082 | 3.4104 | 3.4785 | 0.3156 | 0.3474 |
| | | | | | 3% | 4.1786 | 3.5405 | 3.7494 | 0.3114 | 0.3538 |
| | | | | | 6% | 4.2123 | 3.7417 | 4.1733 | 0.3056 | 0.3617 |
| | | | | | 10% | 4.3331 | 4.0236 | 4.7742 | 0.2928 | 0.3699 |

**Table 4.12** Comparison of Mori-Tanaka calculations and experimental results of PP 3371/clay nanocomposites for 2-D randomly distributed particles at -65ºF

| $E_{nanoclay}$ (GPa) | D (nm) | N | $E_p$ (GPa) | t (nm) | Nanoclay Rein. | Young's Modulus (Experimental) (GPa) | $E_{11}=E_{22}$ (GPa) | $E_{33}$ (GPa) | Poisson's Ratio (Experimental) | ν |
|---|---|---|---|---|---|---|---|---|---|---|
| 300 | 200 | 1 | 300 | 0.615 | 0% | 3.86509 | 3.86509 | 3.86509 | 0.3429 | 0.3429 |
| | | | | | 0.2% | 4.2836 | 3.9547 | 4.0781 | 0.3283 | 0.3480 |
| | | | | | 1% | 4.6031 | 4.3048 | 4.9347 | 0.3193 | 0.3631 |
| | | | | | 3% | 4.6944 | 5.1529 | 7.1079 | 0.3076 | 0.3803 |
| | | | | | 6% | 4.9732 | 6.4218 | 10.4614 | 0.3039 | 0.3852 |
| | | | | | 10% | 5.0920 | 8.1783 | 15.1285 | 0.2983 | 0.3810 |
| 300 | 200 | 2 | 122.388 | 3.015 | 0% | 3.86509 | 3.86509 | 3.86509 | 0.3429 | 0.3429 |
| | | | | | 0.2% | 4.2836 | 3.8957 | 3.9340 | 0.3283 | 0.3446 |
| | | | | | 1% | 4.6031 | 4.0178 | 4.2117 | 0.3193 | 0.3508 |
| | | | | | 3% | 4.6944 | 4.3225 | 4.9190 | 0.3076 | 0.3628 |
| | | | | | 6% | 4.9732 | 4.7846 | 6.0168 | 0.3039 | 0.3739 |
| | | | | | 10% | 5.0920 | 5.4224 | 7.5549 | 0.2983 | 0.3814 |
| 300 | 200 | 3 | 102.216 | 5.415 | 0% | 3.86509 | 3.86509 | 3.86509 | 0.3429 | 0.3429 |
| | | | | | 0.2% | 4.2836 | 3.8872 | 3.9134 | 0.3283 | 0.3441 |
| | | | | | 1% | 4.6031 | 3.9757 | 4.1081 | 0.3193 | 0.3486 |
| | | | | | 3% | 4.6944 | 4.1983 | 4.6049 | 0.3076 | 0.3580 |
| | | | | | 6% | 4.9732 | 4.5387 | 5.3783 | 0.3039 | 0.3681 |
| | | | | | 10% | 5.0920 | 5.0109 | 6.4662 | 0.2983 | 0.3766 |
| 300 | 200 | 4 | 94.434 | 7.815 | 0% | 3.86509 | 3.86509 | 3.86509 | 0.3429 | 0.3429 |
| | | | | | 0.2% | 4.2836 | 3.8832 | 3.9038 | 0.3283 | 0.3439 |
| | | | | | 1% | 4.6031 | 3.9560 | 4.0599 | 0.3193 | 0.3475 |
| | | | | | 3% | 4.6944 | 4.1400 | 4.4585 | 0.3076 | 0.3553 |
| | | | | | 6% | 4.9732 | 4.4227 | 5.0803 | 0.3039 | 0.3645 |
| | | | | | 10% | 5.0920 | 4.8166 | 5.9575 | 0.2983 | 0.3730 |

**Table 4.12** Continued

| | | | | | | | | | | |
|---|---|---|---|---|---|---|---|---|---|---|
| 300 | 200 | 5 | 90.308 | 10.215 | 0% | 3.86509 | 3.86509 | 3.86509 | 0.3429 | 0.3429 |
| | | | | | 0.2% | 4.2836 | 3.8808 | 3.8979 | 0.3283 | 0.3437 |
| | | | | | 1% | 4.6031 | 3.9441 | 4.0304 | 0.3193 | 0.3468 |
| | | | | | 3% | 4.6944 | 4.1043 | 4.3690 | 0.3076 | 0.3536 |
| | | | | | 6% | 4.9732 | 4.3515 | 4.8979 | 0.3039 | 0.3619 |
| | | | | | 10% | 5.0920 | 4.6971 | 5.6456 | 0.2983 | 0.3701 |
| | | | | | | | | | | |
| 300 | 200 | 6 | 87.753 | 12.6150 | 0% | 3.86509 | 3.86509 | 3.86509 | 0.3429 | 0.3429 |
| | | | | | 0.2% | 4.2836 | 3.8792 | 3.8939 | 0.3283 | 0.3436 |
| | | | | | 1% | 4.6031 | 3.9358 | 4.0101 | 0.3193 | 0.3463 |
| | | | | | 3% | 4.6944 | 4.0797 | 4.3072 | 0.3076 | 0.3523 |
| | | | | | 6% | 4.9732 | 4.3023 | 4.7718 | 0.3039 | 0.3598 |
| | | | | | 10% | 5.0920 | 4.6144 | 5.4297 | 0.2983 | 0.3676 |

**Table 4.13** Comparison of Mori-Tanaka calculations and experimental results of EPON 828/clay nanocomposites for 2-D randomly distributed particles at RT

| $E_{nanoclay}$ (GPa) | D (nm) | N | $E_p$ (GPa) | t (nm) | Nanoclay Rein. | Young's Modulus (Experimental) (GPa) | $E_{11}=E_{22}$ (GPa) | $E_{33}$ (GPa) | Poisson's Ratio (Experimental) | $\nu_{31}$ |
|---|---|---|---|---|---|---|---|---|---|---|
| 300 | 200 | 6 | 87.7525 | 12.6150 | 0% | 2.8177 | 2.8177 | 2.8177 | 0.3105 | 0.3105 |
| | | | | | 1% | 2.9127 | 2.9142 | 3.0249 | 0.3238 | 0.3119 |
| | | | | | 3% | 2.9840 | 3.1089 | 3.4486 | 0.3288 | 0.3399 |
| | | | | | 6% | 3.0965 | 3.4082 | 4.1083 | 0.3340 | 0.4168 |
| | | | | | 10% | 3.3427 | 3.8261 | 5.0367 | 0.3348 | 0.5236 |

4.1.1-e) 3-D Randomly Distributed Nanoclay Particles

Referring to [197], the effective bulk and shear modulus, Young's modulus and Poisson's ratio for the case of 3-D randomly distributed nanoclay particles can be expressed as:

$$p = \frac{p_2}{p_1} \tag{48}$$

$$q = \frac{q_2}{q_1} \tag{49}$$

$$p_1 = 1 + c\frac{\left[2\left(S_{1122}+S_{2222}+S_{2233}-1\right)\left(a_3+a_4\right)+\left(S_{1111}+2S_{2211}-1\right)\left(a_1-2a_2\right)\right]}{3a} \tag{50}$$

$$p_2 = \frac{\left[a_1-2\left(a_2-a_3-a_4\right)\right]}{3a} \tag{51}$$

$$q_1 = 1-c\left\{\frac{2}{5}\frac{2S_{1212}-1}{2S_{1212}+\frac{\mu_0}{\left(\mu_1-\mu_0\right)}}+\frac{1}{3}\frac{2S_{2323}-1}{2S_{2323}+\frac{\mu_0}{\left(\mu_1-\mu_0\right)}}-\frac{1}{15a}\left[\left(S_{1122}-S_{2233}\right)\left(2a_3-a_4+a_5\right.\right.\right. \tag{52}$$

$$\left.\left.\left.+2\left(S_{1111}-S_{2211}-1\right)\left(a_1+a_2\right)+\left(S_{1122}-S_{2222}+1\right)\left(2a_3-a_4-a_5a\right)\right]\right\}$$

$$q_2 = -\frac{2}{5}\frac{1}{2S_{1212}+\frac{\mu_m}{\left(\mu_p-\mu_m\right)}}-\frac{1}{3}\frac{1}{2S_{2323}+\frac{\mu_m}{\left(\mu_p-\mu_m\right)}} \tag{53}$$

$$+\frac{1}{15a}\left[2\left(a_1+a_2-a_3\right)+a_4+a_5a\right]$$

$$\kappa = \frac{\kappa_m}{1+cp} \tag{54}$$

$$\mu = \frac{\mu_m}{1+cp} \tag{55}$$

$$E = \frac{3\mu}{1+\frac{\mu}{3\kappa}} \tag{56}$$

$$\nu = \frac{1}{2} - \frac{E}{6\kappa} \tag{57}$$

4.1.1-f) Results of Parametric Study for 3-D Randomly Distributed Nanoclay Particles

Again the number of flakes N was varied from 1 to 6 and the Young's modulus obtained experimentally for PP 3371 and epoxy were used in the Mori-Tanaka calculations. The comparison of Mori-Tanaka calculations and experimental results for 3-D randomly distributed particles is given in Tables 4.14 - 4.18 for PP 3371 and in Table 4.19 for EPON 828.

**Table 4.14** Comparison of Mori-Tanaka calculations and experimental results of PP 3371/clay nanocomposites for 3-D randomly distributed particles at 160ºF

| $E_{nanoclay}$ (GPa) | D (nm) | N | $E_p$ (GPa) | t (nm) | Nanoclay Rein. | Young's Modulus (Experimental) (GPa) | E (GPa) | κ (GPa) | μ (GPa) | Poisson's Ratio (Experimental) | ν |
|---|---|---|---|---|---|---|---|---|---|---|---|
| 300 | 200 | 1 | 300 | 0.615 | 0% | 0.39204 | 0.39204 | 0.8782 | 0.1375 | 0.4256 | 0.4256 |
| | | | | | 0.2% | 0.4499 | 0.4284 | 0.8957 | 0.1508 | 0.4782 | 0.4203 |
| | | | | | 1% | 0.4654 | 0.5734 | 0.9661 | 0.2046 | 0.4715 | 0.4011 |
| | | | | | 3% | 0.4969 | 0.9353 | 1.1469 | 0.3428 | 0.4523 | 0.3641 |
| | | | | | 6% | 0.5031 | 1.4874 | 1.4318 | 0.5605 | 0.5077 | 0.3269 |
| | | | | | 10% | 0.5146 | 2.2590 | 1.8395 | 0.8720 | 0.4896 | 0.2953 |
| 300 | 200 | 2 | 122.388 | 3.015 | 0% | 0.39204 | 0.39204 | 0.8782 | 0.1375 | 0.4256 | 0.4256 |
| | | | | | 0.2% | 0.4499 | 0.4007 | 0.8828 | 0.1407 | 0.4782 | 0.4244 |
| | | | | | 1% | 0.4654 | 0.4356 | 0.9013 | 0.1534 | 0.4715 | 0.4195 |
| | | | | | 3% | 0.4969 | 0.5244 | 0.9488 | 0.1862 | 0.4523 | 0.4079 |
| | | | | | 6% | 0.5031 | 0.6627 | 1.0238 | 0.2380 | 0.5077 | 0.3921 |
| | | | | | 10% | 0.5146 | 0.8577 | 1.1312 | 0.3122 | 0.4896 | 0.3736 |
| 300 | 200 | 3 | 102.216 | 5.415 | 0% | 0.39204 | 0.39204 | 0.8782 | 0.1375 | 0.4256 | 0.4256 |
| | | | | | 0.2% | 0.4499 | 0.3972 | 0.8812 | 0.1394 | 0.4782 | 0.4249 |
| | | | | | 1% | 0.4654 | 0.4183 | 0.8934 | 0.1471 | 0.4715 | 0.4220 |
| | | | | | 3% | 0.4969 | 0.4720 | 0.9245 | 0.1668 | 0.4523 | 0.4149 |
| | | | | | 6% | 0.5031 | 0.5560 | 0.9737 | 0.1979 | 0.5077 | 0.4048 |
| | | | | | 10% | 0.5146 | 0.6753 | 1.0442 | 0.2425 | 0.4896 | 0.3922 |
| 300 | 200 | 4 | 94.434 | 7.815 | 0% | 0.39204 | 0.39204 | 0.8782 | 0.1375 | 0.4256 | 0.4256 |
| | | | | | 0.2% | 0.4499 | 0.3959 | 0.8806 | 0.1389 | 0.4782 | 0.4251 |
| | | | | | 1% | 0.4654 | 0.4113 | 0.8902 | 0.1445 | 0.4715 | 0.4230 |
| | | | | | 3% | 0.4969 | 0.4507 | 0.9148 | 0.1589 | 0.4523 | 0.4179 |
| | | | | | 6% | 0.5031 | 0.5126 | 0.9536 | 0.1817 | 0.5077 | 0.4104 |
| | | | | | 10% | 0.5146 | 0.6007 | 1.0094 | 0.2144 | 0.4896 | 0.4008 |

**Table 4.14** Continued

| | | | | | | | | | | | |
|---|---|---|---|---|---|---|---|---|---|---|---|
| 300 | 200 | 5 | 90.308 | 10.215 | 0% | 0.39204 | 0.39204 | 0.8782 | 0.1375 | 0.4256 | 0.4256 |
| | | | | | 0.2% | 0.4499 | 0.3951 | 0.8803 | 0.1386 | 0.4782 | 0.4252 |
| | | | | | 1% | 0.4654 | 0.4075 | 0.8885 | 0.1431 | 0.4715 | 0.4236 |
| | | | | | 3% | 0.4969 | 0.4391 | 0.9095 | 0.1547 | 0.4523 | 0.4195 |
| | | | | | 6% | 0.5031 | 0.4889 | 0.9428 | 0.1729 | 0.5077 | 0.4136 |
| | | | | | 10% | 0.5146 | 0.5598 | 0.9905 | 0.1991 | 0.4896 | 0.4058 |
| | | | | | | | | | | | |
| 300 | 200 | 6 | 87.753 | 12.6150 | 0% | 0.39204 | 0.39204 | 0.8782 | 0.1375 | 0.4256 | 0.4256 |
| | | | | | 0.2% | 0.4499 | 0.3946 | 0.8800 | 0.1384 | 0.4782 | 0.4253 |
| | | | | | 1% | 0.4654 | 0.4051 | 0.8874 | 0.1422 | 0.4715 | 0.4239 |
| | | | | | 3% | 0.4969 | 0.4318 | 0.9062 | 0.1520 | 0.4523 | 0.4206 |
| | | | | | 6% | 0.5031 | 0.4739 | 0.9359 | 0.1674 | 0.5077 | 0.4156 |
| | | | | | 10% | 0.5146 | 0.5340 | 0.9786 | 0.1895 | 0.4896 | 0.4091 |

**Table 4.15** Comparison of Mori-Tanaka calculations and experimental results of PP 3371/clay nanocomposites for 3-D randomly distributed particles at 120ºF

| $E_{nanoclay}$ (GPa) | D (nm) | N | $E_p$ (GPa) | t (nm) | Nanoclay Rein. | Young's Modulus (Experimental) (GPa) | E (GPa) | κ (GPa) | μ (GPa) | Poisson's Ratio (Experimental) | ν |
|---|---|---|---|---|---|---|---|---|---|---|---|
| 300 | 200 | 1 | 300 | 0.615 | 0% | 0.61595 | 0.61595 | 1.0671 | 0.2194 | 0.4038 | 0.4038 |
| | | | | | 0.2% | 0.7285 | 0.6656 | 1.0912 | 0.2380 | 0.4350 | 0.3983 |
| | | | | | 1% | 0.7646 | 0.8633 | 1.1882 | 0.3130 | 0.4631 | 0.3789 |
| | | | | | 3% | 0.8283 | 1.3579 | 1.4373 | 0.5057 | 0.4355 | 0.3425 |
| | | | | | 6% | 0.8332 | 2.1149 | 1.8292 | 0.8089 | 0.4334 | 0.3073 |
| | | | | | 10% | 0.8664 | 3.1755 | 2.3892 | 1.2419 | 0.4111 | 0.2785 |
| | | | | | | | | | | | |
| 300 | 200 | 2 | 122.388 | 3.015 | 0% | 0.61595 | 0.61595 | 1.0671 | 0.2194 | 0.4038 | 0.4038 |
| | | | | | 0.2% | 0.7285 | 0.6284 | 1.0736 | 0.2240 | 0.4350 | 0.4024 |
| | | | | | 1% | 0.7646 | 0.6784 | 1.0996 | 0.2428 | 0.4631 | 0.3972 |
| | | | | | 3% | 0.8283 | 0.8058 | 1.1664 | 0.2909 | 0.4355 | 0.3849 |
| | | | | | 6% | 0.8332 | 1.0039 | 1.2718 | 0.3668 | 0.4334 | 0.3684 |
| | | | | | 10% | 0.8664 | 1.2833 | 1.4225 | 0.4754 | 0.4111 | 0.3496 |
| | | | | | | | | | | | |

**Table 4.15** Continued

| | | | | | | | | | | | |
|---|---|---|---|---|---|---|---|---|---|---|---|
| 300 | 200 | 3 | 102.216 | 5.415 | 0% | 0.61595 | 0.61595 | 1.0671 | 0.2194 | 0.4038 | 0.4038 |
| | | | | | 0.2% | 0.7285 | 0.6236 | 1.0714 | 0.2222 | 0.4350 | 0.4030 |
| | | | | | 1% | 0.7646 | 0.6543 | 1.0884 | 0.2337 | 0.4631 | 0.3998 |
| | | | | | 3% | 0.8283 | 0.7329 | 1.1322 | 0.2632 | 0.4355 | 0.3921 |
| | | | | | 6% | 0.8332 | 0.8559 | 1.2012 | 0.3098 | 0.4334 | 0.3812 |
| | | | | | 10% | 0.8664 | 1.0302 | 1.3000 | 0.3765 | 0.4111 | 0.3679 |
| | | | | | | | | | | | |
| 300 | 200 | 4 | 94.434 | 7.815 | 0% | 0.61595 | 0.61595 | 1.0671 | 0.2194 | 0.4038 | 0.4038 |
| | | | | | 0.2% | 0.7285 | 0.6216 | 1.0704 | 0.2215 | 0.4350 | 0.4032 |
| | | | | | 1% | 0.7646 | 0.6444 | 1.0838 | 0.2300 | 0.4631 | 0.4009 |
| | | | | | 3% | 0.8283 | 0.7028 | 1.1182 | 0.2519 | 0.4355 | 0.3952 |
| | | | | | 6% | 0.8332 | 0.7943 | 1.1723 | 0.2863 | 0.4334 | 0.3871 |
| | | | | | 10% | 0.8664 | 0.9245 | 1.2500 | 0.3358 | 0.4111 | 0.3767 |
| | | | | | | | | | | | |
| 300 | 200 | 5 | 90.308 | 10.215 | 0% | 0.61595 | 0.61595 | 1.0671 | 0.2194 | 0.4038 | 0.4038 |
| | | | | | 0.2% | 0.7285 | 0.6205 | 1.0699 | 0.2211 | 0.4350 | 0.4033 |
| | | | | | 1% | 0.7646 | 0.6389 | 1.0813 | 0.2279 | 0.4631 | 0.4015 |
| | | | | | 3% | 0.8283 | 0.6861 | 1.1105 | 0.2456 | 0.4355 | 0.3970 |
| | | | | | 6% | 0.8332 | 0.7603 | 1.1565 | 0.2734 | 0.4334 | 0.3904 |
| | | | | | 10% | 0.8664 | 0.8659 | 1.2225 | 0.3133 | 0.4111 | 0.3819 |
| | | | | | | | | | | | |
| 300 | 200 | 6 | 87.753 | 12.6150 | 0% | 0.61595 | 0.61595 | 1.0671 | 0.2194 | 0.4038 | 0.4038 |
| | | | | | 0.2% | 0.7285 | 0.6198 | 1.0696 | 0.2208 | 0.4350 | 0.4034 |
| | | | | | 1% | 0.7646 | 0.6355 | 1.0797 | 0.2266 | 0.4631 | 0.4019 |
| | | | | | 3% | 0.8283 | 0.6756 | 1.1056 | 0.2416 | 0.4355 | 0.3982 |
| | | | | | 6% | 0.8332 | 0.7386 | 1.1465 | 0.2652 | 0.4334 | 0.3926 |
| | | | | | 10% | 0.8664 | 0.8285 | 1.2051 | 0.2990 | 0.4111 | 0.3854 |

**Table 4.16** Comparison of Mori-Tanaka calculations and experimental results of PP 3371/clay nanocomposites for 3-D randomly distributed particles at room temperature

| $E_{nanoclay}$ (GPa) | D (nm) | N | $E_p$ (GPa) | t (nm) | Nanoclay Rein. | Young's Modulus (Experimental) (GPa) | E (GPa) | κ (GPa) | μ (GPa) | Poisson's Ratio (Experimental) | ν |
|---|---|---|---|---|---|---|---|---|---|---|---|
| 300 | 200 | 1 | 300 | 0.615 | 0% | 1.2001 | 1.2001 | 1.8994 | 0.4302 | 0.3947 | 0.3947 |
| | | | | | 0.2% | 1.3172 | 1.2741 | 1.9358 | 0.4582 | 0.4167 | 0.3903 |
| | | | | | 1% | 1.5085 | 1.5699 | 2.0828 | 0.5711 | 0.4056 | 0.3744 |
| | | | | | 3% | 1.6278 | 2.3124 | 2.4597 | 0.8607 | 0.3852 | 0.3433 |
| | | | | | 6% | 1.6463 | 3.4504 | 3.0515 | 1.3154 | 0.3722 | 0.3115 |
| | | | | | 10% | 1.7426 | 5.0419 | 3.8945 | 1.9630 | 0.3725 | 0.2842 |
| 300 | 200 | 2 | 122.388 | 3.015 | 0% | 1.2001 | 1.2001 | 1.8994 | 0.4302 | 0.3947 | 0.3947 |
| | | | | | 0.2% | 1.3172 | 1.2205 | 1.9100 | 0.4379 | 0.4167 | 0.3935 |
| | | | | | 1% | 1.5085 | 1.3027 | 1.9529 | 0.4690 | 0.4056 | 0.3888 |
| | | | | | 3% | 1.6278 | 1.5122 | 2.0629 | 0.5488 | 0.3852 | 0.3778 |
| | | | | | 6% | 1.6463 | 1.8380 | 2.2360 | 0.6743 | 0.3722 | 0.3630 |
| | | | | | 10% | 1.7426 | 2.2973 | 2.4831 | 0.8535 | 0.3725 | 0.3458 |
| 300 | 200 | 3 | 102.216 | 5.415 | 0% | 1.2001 | 1.2001 | 1.8994 | 0.4302 | 0.3947 | 0.3947 |
| | | | | | 0.2% | 1.3172 | 1.2132 | 1.9066 | 0.4352 | 0.4167 | 0.3940 |
| | | | | | 1% | 1.5085 | 1.2660 | 1.9356 | 0.4551 | 0.4056 | 0.3910 |
| | | | | | 3% | 1.6278 | 1.4009 | 2.0102 | 0.5062 | 0.3852 | 0.3838 |
| | | | | | 6% | 1.6463 | 1.6119 | 2.1275 | 0.5867 | 0.3722 | 0.3737 |
| | | | | | 10% | 1.7426 | 1.9107 | 2.2952 | 0.7018 | 0.3725 | 0.3612 |
| 300 | 200 | 4 | 94.434 | 7.815 | 0% | 1.2001 | 1.2001 | 1.8994 | 0.4302 | 0.3947 | 0.3947 |
| | | | | | 0.2% | 1.3172 | 1.2100 | 1.9052 | 0.4340 | 0.4167 | 0.3941 |
| | | | | | 1% | 1.5085 | 1.2502 | 1.9283 | 0.4491 | 0.4056 | 0.3919 |
| | | | | | 3% | 1.6278 | 1.3529 | 1.9878 | 0.4879 | 0.3852 | 0.3866 |
| | | | | | 6% | 1.6463 | 1.5139 | 2.0815 | 0.5490 | 0.3722 | 0.3788 |
| | | | | | 10% | 1.7426 | 1.7427 | 2.2155 | 0.6365 | 0.3725 | 0.3689 |

**Table 4.16** Continued

| | | | | | | | | | | | |
|---|---|---|---|---|---|---|---|---|---|---|---|
| 300 | 200 | 5 | 90.308 | 10.215 | 0% | 1.2001 | 1.2001 | 1.8994 | 0.4302 | 0.3947 | 0.3947 |
| | | | | | 0.2% | 1.3172 | 1.2082 | 1.9043 | 0.4333 | 0.4167 | 0.3943 |
| | | | | | 1% | 1.5085 | 1.2412 | 1.9242 | 0.4457 | 0.4056 | 0.3925 |
| | | | | | 3% | 1.6278 | 1.3256 | 1.9752 | 0.4775 | 0.3852 | 0.3881 |
| | | | | | 6% | 1.6463 | 1.4581 | 2.0556 | 0.5276 | 0.3722 | 0.3818 |
| | | | | | 10% | 1.7426 | 1.6467 | 2.1706 | 0.5994 | 0.3725 | 0.3736 |
| | | | | | | | | | | | |
| 300 | 200 | 6 | 87.753 | 12.6150 | 0% | 1.2001 | 1.2001 | 1.8994 | 0.4302 | 0.3947 | 0.3947 |
| | | | | | 0.2% | 1.3172 | 1.2071 | 1.9038 | 0.4328 | 0.4167 | 0.3943 |
| | | | | | 1% | 1.5085 | 1.2354 | 1.9216 | 0.4435 | 0.4056 | 0.3929 |
| | | | | | 3% | 1.6278 | 1.3079 | 1.9671 | 0.4707 | 0.3852 | 0.3892 |
| | | | | | 6% | 1.6463 | 1.4218 | 2.0389 | 0.5137 | 0.3722 | 0.3838 |
| | | | | | 10% | 1.7426 | 1.5842 | 2.1417 | 0.5754 | 0.3725 | 0.3767 |

**Table 4.17** Comparison of Mori-Tanaka calculations and experimental results of PP 3371/clay nanocomposites for 3-D randomly distributed particles at -4°F

| $E_{nanoclay}$ (GPa) | D (nm) | N | $E_p$ (GPa) | t (nm) | Nanoclay Rein. | Young's Modulus (Experimental) (GPa) | E (GPa) | κ (GPa) | μ (GPa) | Poisson's Ratio (Experimental) | ν |
|---|---|---|---|---|---|---|---|---|---|---|---|
| 300 | 200 | 1 | 300 | 0.615 | 0% | 3.34644 | 3.34644 | 3.5707 | 1.2451 | 0.3438 | 0.3438 |
| | | | | | 0.2% | 3.7128 | 3.4543 | 3.6263 | 1.2877 | 0.3307 | 0.3412 |
| | | | | | 1% | 4.0082 | 3.8873 | 3.8507 | 1.4595 | 0.3156 | 0.3317 |
| | | | | | 3% | 4.1786 | 4.9843 | 4.4251 | 1.8991 | 0.3114 | 0.3123 |
| | | | | | 6% | 4.2123 | 6.6798 | 5.3244 | 2.5872 | 0.3056 | 0.2909 |
| | | | | | 10% | 4.3331 | 9.0582 | 6.5993 | 3.5628 | 0.2928 | 0.2712 |
| | | | | | | | | | | | |
| 300 | 200 | 2 | 122.388 | 3.015 | 0% | 3.34644 | 3.34644 | 3.5707 | 1.2451 | 0.3438 | 0.3438 |
| | | | | | 0.2% | 3.7128 | 3.3818 | 3.5893 | 1.2591 | 0.3307 | 0.3430 |
| | | | | | 1% | 4.0082 | 3.5240 | 3.6644 | 1.3152 | 0.3156 | 0.3397 |
| | | | | | 3% | 4.1786 | 3.8871 | 3.8569 | 1.4591 | 0.3114 | 0.3320 |
| | | | | | 6% | 4.2123 | 4.4527 | 4.1585 | 1.6847 | 0.3056 | 0.3215 |
| | | | | | 10% | 4.3331 | 5.2507 | 4.5871 | 2.0053 | 0.2928 | 0.3092 |
| | | | | | | | | | | | |

**Table 4.17** Continued

| | | | | | | | | | | | |
|---|---|---|---|---|---|---|---|---|---|---|---|
| 300 | 200 | 3 | 102.216 | 5.415 | 0% | 3.34644 | 3.34644 | 3.5707 | 1.2451 | 0.3438 | 0.3438 |
| | | | | | 0.2% | 3.7128 | 3.3714 | 3.5841 | 1.2549 | 0.3307 | 0.3432 |
| | | | | | 1% | 4.0082 | 3.4718 | 3.6384 | 1.2945 | 0.3156 | 0.3410 |
| | | | | | 3% | 4.1786 | 3.7286 | 3.7776 | 1.3960 | 0.3114 | 0.3355 |
| | | | | | 6% | 4.2123 | 4.1299 | 3.9960 | 1.5552 | 0.3056 | 0.3277 |
| | | | | | 10% | 4.3331 | 4.6978 | 4.3066 | 1.7819 | 0.2928 | 0.3182 |
| | | | | | | | | | | | |
| 300 | 200 | 4 | 94.434 | 7.815 | 0% | 3.34644 | 3.34644 | 3.5707 | 1.2451 | 0.3438 | 0.3438 |
| | | | | | 0.2% | 3.7128 | 3.3666 | 3.5818 | 1.2530 | 0.3307 | 0.3433 |
| | | | | | 1% | 4.0082 | 3.4477 | 3.6267 | 1.2850 | 0.3156 | 0.3416 |
| | | | | | 3% | 4.1786 | 3.6553 | 3.7418 | 1.3668 | 0.3114 | 0.3372 |
| | | | | | 6% | 4.2123 | 3.9803 | 3.9226 | 1.4954 | 0.3056 | 0.3309 |
| | | | | | 10% | 4.3331 | 4.4413 | 4.1800 | 1.6786 | 0.2928 | 0.3229 |
| | | | | | | | | | | | |
| 300 | 200 | 5 | 90.308 | 10.215 | 0% | 3.34644 | 3.34644 | 3.5707 | 1.2451 | 0.3438 | 0.3438 |
| | | | | | 0.2% | 3.7128 | 3.3637 | 3.5804 | 1.2519 | 0.3307 | 0.3434 |
| | | | | | 1% | 4.0082 | 3.4331 | 3.6197 | 1.2792 | 0.3156 | 0.3419 |
| | | | | | 3% | 4.1786 | 3.6110 | 3.7205 | 1.3492 | 0.3114 | 0.3382 |
| | | | | | 6% | 4.2123 | 3.8898 | 3.8789 | 1.4592 | 0.3056 | 0.3329 |
| | | | | | 10% | 4.3331 | 4.2858 | 4.1046 | 1.6161 | 0.2928 | 0.3260 |
| | | | | | | | | | | | |
| 300 | 200 | 6 | 87.753 | 12.6150 | 0% | 3.34644 | 3.34644 | 3.5707 | 1.2451 | 0.3438 | 0.3438 |
| | | | | | 0.2% | 3.7128 | 3.3617 | 3.5795 | 1.2511 | 0.3307 | 0.3435 |
| | | | | | 1% | 4.0082 | 3.4232 | 3.6150 | 1.2752 | 0.3156 | 0.3422 |
| | | | | | 3% | 4.1786 | 3.5808 | 3.7062 | 1.3371 | 0.3114 | 0.3390 |
| | | | | | 6% | 4.2123 | 3.8280 | 3.8495 | 1.4345 | 0.3056 | 0.3343 |
| | | | | | 10% | 4.3331 | 4.1795 | 4.0538 | 1.5734 | 0.2928 | 0.3282 |

**Table 4.18** Comparison of Mori-Tanaka calculations and experimental results of PP 3371/clay nanocomposites for 3-D randomly distributed particles at -65ºF

| $E_{nanoclay}$ (GPa) | D (nm) | N | $E_p$ (GPa) | t (nm) | Nanoclay Rein. | Young's Modulus (Experimental) (GPa) | E (GPa) | κ (GPa) | μ (GPa) | Poisson's Ratio (Experimental) | ν |
|---|---|---|---|---|---|---|---|---|---|---|---|
| 300 | 200 | 1 | 300 | 0.615 | 0% | 3.86509 | 3.86509 | 4.1005 | 1.4391 | 0.3429 | 0.3429 |
| | | | | | 0.2% | 4.2836 | 3.9772 | 4.1585 | 1.4834 | 0.3283 | 0.3406 |
| | | | | | 1% | 4.6031 | 4.4276 | 4.3926 | 1.6620 | 0.3193 | 0.3320 |
| | | | | | 3% | 4.6944 | 5.5692 | 4.9915 | 2.1191 | 0.3076 | 0.3140 |
| | | | | | 6% | 4.9732 | 7.3344 | 5.9288 | 2.8344 | 0.3039 | 0.2938 |
| | | | | | 10% | 5.0920 | 9.8096 | 7.2568 | 3.8478 | 0.2983 | 0.2747 |
| 300 | 200 | 2 | 122.388 | 3.015 | 0% | 3.86509 | 3.86509 | 4.1005 | 1.4391 | 0.3429 | 0.3429 |
| | | | | | 0.2% | 4.2836 | 3.9026 | 4.1203 | 1.4539 | 0.3283 | 0.3421 |
| | | | | | 1% | 4.6031 | 4.0538 | 4.2003 | 1.5136 | 0.3193 | 0.3391 |
| | | | | | 3% | 4.6944 | 4.4397 | 4.4053 | 1.6665 | 0.3076 | 0.3320 |
| | | | | | 6% | 4.9732 | 5.0409 | 4.7264 | 1.9062 | 0.3039 | 0.3222 |
| | | | | | 10% | 5.0920 | 5.8887 | 5.1822 | 2.2466 | 0.2983 | 0.3106 |
| 300 | 200 | 3 | 102.216 | 5.415 | 0% | 3.86509 | 3.86509 | 4.1005 | 1.4391 | 0.3429 | 0.3429 |
| | | | | | 0.2% | 4.2836 | 3.8920 | 4.1150 | 1.4497 | 0.3283 | 0.3424 |
| | | | | | 1% | 4.6031 | 4.0002 | 4.1736 | 1.4923 | 0.3193 | 0.3403 |
| | | | | | 3% | 4.6944 | 4.2770 | 4.3238 | 1.6017 | 0.3076 | 0.3351 |
| | | | | | 6% | 4.9732 | 4.7094 | 4.5593 | 1.7733 | 0.3039 | 0.3278 |
| | | | | | 10% | 5.0920 | 5.3212 | 4.8940 | 2.0174 | 0.2983 | 0.3188 |
| 300 | 200 | 4 | 94.434 | 7.815 | 0% | 3.86509 | 3.86509 | 4.1005 | 1.4391 | 0.3429 | 0.3429 |
| | | | | | 0.2% | 4.2836 | 3.8870 | 4.1126 | 1.4477 | 0.3283 | 0.3425 |
| | | | | | 1% | 4.6031 | 3.9753 | 4.1615 | 1.4825 | 0.3193 | 0.3408 |
| | | | | | 3% | 4.6944 | 4.2013 | 4.2868 | 1.5716 | 0.3076 | 0.3367 |
| | | | | | 6% | 4.9732 | 4.5549 | 4.4834 | 1.7115 | 0.3039 | 0.3307 |
| | | | | | 10% | 5.0920 | 5.0563 | 4.7632 | 1.9108 | 0.2983 | 0.3231 |

**Table 4.18** Continued

| | | | | | | | | | | | |
|---|---|---|---|---|---|---|---|---|---|---|---|
| 300 | 200 | 5 | 90.308 | 10.215 | 0% | 3.86509 | 3.86509 | 4.1005 | 1.4391 | 0.3429 | 0.3429 |
| | | | | | 0.2% | 4.2836 | 3.8840 | 4.1111 | 1.4465 | 0.3283 | 0.3425 |
| | | | | | 1% | 4.6031 | 3.9602 | 4.1542 | 1.4764 | 0.3193 | 0.3411 |
| | | | | | 3% | 4.6944 | 4.1552 | 4.2647 | 1.5532 | 0.3076 | 0.3376 |
| | | | | | 6% | 4.9732 | 4.4607 | 4.4380 | 1.6738 | 0.3039 | 0.3325 |
| | | | | | 10% | 5.0920 | 4.8945 | 4.6849 | 1.8458 | 0.2983 | 0.3259 |
| | | | | | | | | | | | |
| 300 | 200 | 6 | 87.753 | 12.6150 | 0% | 3.86509 | 3.86509 | 4.1005 | 1.4391 | 0.3429 | 0.3429 |
| | | | | | 0.2% | 4.2836 | 3.8819 | 4.1102 | 1.4457 | 0.3283 | 0.3426 |
| | | | | | 1% | 4.6031 | 3.9497 | 4.1493 | 1.4723 | 0.3193 | 0.3413 |
| | | | | | 3% | 4.6944 | 4.1235 | 4.2496 | 1.5406 | 0.3076 | 0.3383 |
| | | | | | 6% | 4.9732 | 4.3959 | 4.4072 | 1.6479 | 0.3039 | 0.3338 |
| | | | | | 10% | 5.0920 | 4.7831 | 4.6318 | 1.8010 | 0.2983 | 0.3279 |

**Table 4.19** Comparison of Mori-Tanaka calculations and experimental results of EPON 828/clay nanocomposites for 3-D randomly distributed particles at room temperature

| $E_{nanoclay}$ (GPa) | D (nm) | N | $E_p$ (GPa) | $E_{nanoclay}$ (GPa) | Nanoclay Rein. | Young's Modulus (Experimental) (GPa) | E (GPa) | κ (GPa) | μ (GPa) | Poisson's Ratio (Experimental) | ν |
|---|---|---|---|---|---|---|---|---|---|---|---|
| 300 | 200 | 6 | 87.7525 | 12.6150 | 0% | 2.8177 | 2.8177 | 2.4782 | 1.0750 | 0.3105 | 0.3105 |
| | | | | | 1% | 2.9127 | 2.9363 | 2.5451 | 1.1227 | 0.3238 | 0.3077 |
| | | | | | 3% | 2.9840 | 3.1794 | 2.6824 | 1.2205 | 0.3288 | 0.3025 |
| | | | | | 6% | 3.0965 | 3.5594 | 2.8976 | 1.3740 | 0.3340 | 0.2953 |
| | | | | | 10% | 3.3427 | 4.0978 | 3.2034 | 1.5922 | 0.3348 | 0.2868 |

### 4.1.2. Results Obtained From Various Mori-Tanaka Calculations

Before starting the Mori-Tanaka calculations, we first analyzed the electron microscopy images showing the distribution of nanoclay particles. The SEM images show that as the nanoclay reinforcement percentage increases more agglomeration of nanoclay particles occurs and bigger particles are evident. Based on this observation, we assumed a different N composition for each percentage. As a consequence, at high percentages larger N values and at low percentage smaller N values were used in the calculations.

Table 4.20 shows the composition of nanoclay particles depending on the reinforcement percentage.

**Table 4.20** Nanoclay flakes number composition for each percentage

| Nanoclay Reinforcement | Composition of Flakes Number |
|---|---|
| 0.2% | 100% N=1 |
| 1% | 40% N=1<br>30% N=2<br>30% N=3 |
| 3% | 40% N=2<br>30% N=3<br>30% N=4 |
| 6% | 100% N=5 |
| 10% | 100% N=6 |

Using this composition we recalculated the Mori-Tanaka results for the three formulations outlined above, namely “oriented particles”, “2-D randomly distributed particles” and “3-D randomly distributed particles”.

4.1.2-a) Comparison of Experimental Results with Mori-Tanaka Calculations

The Mori-Tanaka results for the three types of assumed distributions are compared with the experimental results. In Figures 4.2-4.11 the experimental and numerical results obtained for Young's modulus and Poisson's ratio are compared for the various nanoclay reinforcement percentages. As explained previously, the numerical results are obtained from Mori-Tanaka calculations for oriented. 2-D randomly distributed and 3-D randomly distributed particles.

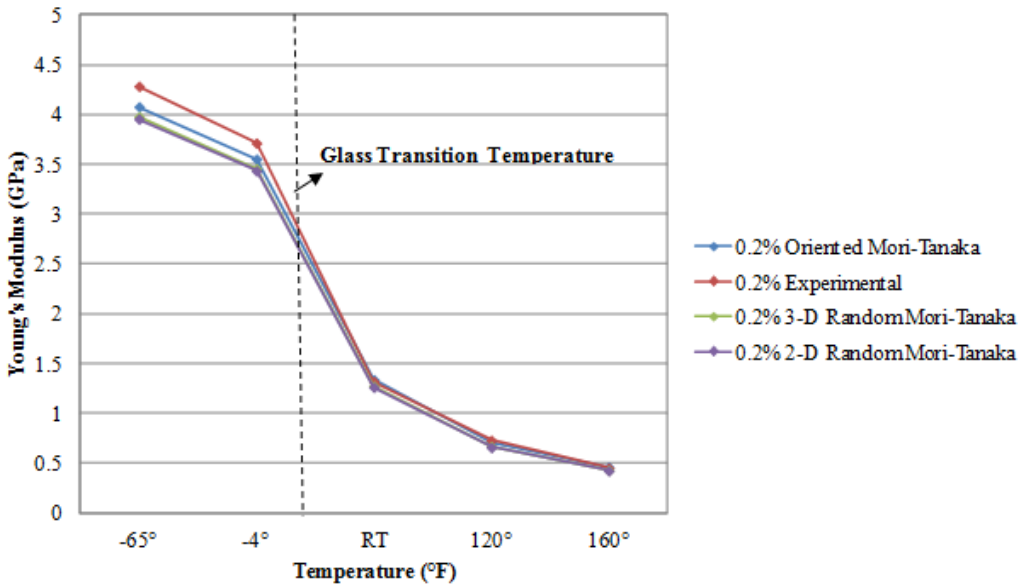


**Figure 4.2** Comparison of Young's modulus obtained from Mori-Tanaka and experimental results for 0.2% nanoclay reinforced PP 3371 specimens at various temperatures

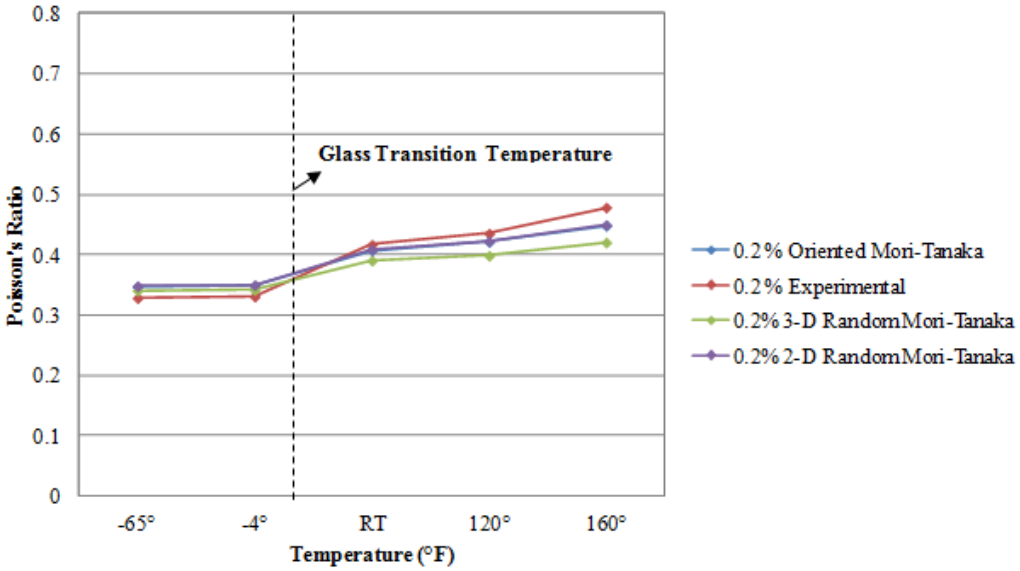


**Figure 4.3** Comparison of Poisson's ratio obtained from Mori-Tanaka and experimental results for 0.2% nanoclay reinforced PP 3371 specimens at various temperatures

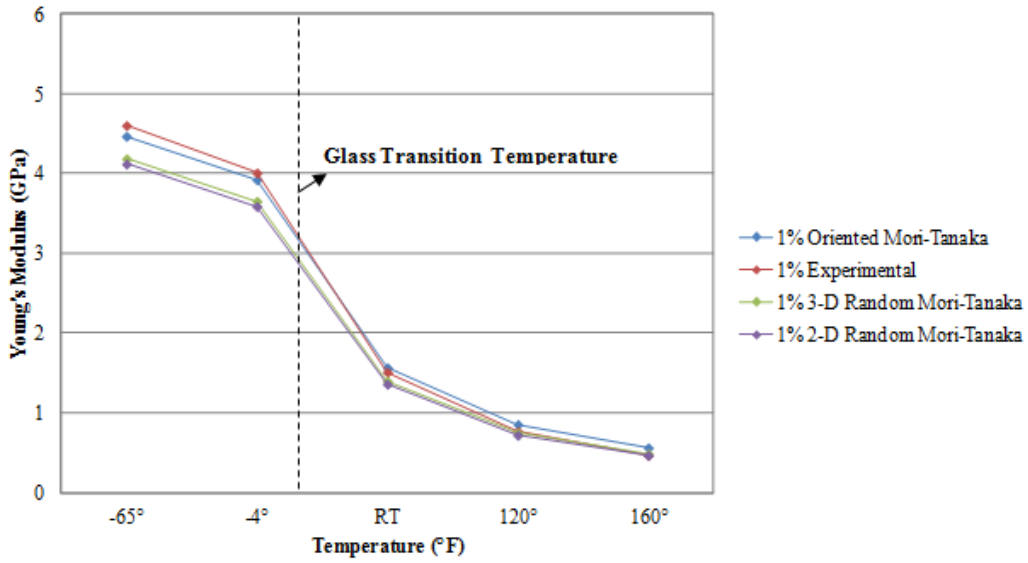


**Figure 4.4** Comparison of Young's modulus obtained from Mori-Tanaka and experimental results for 1% nanoclay reinforced PP 3371 specimens at various temperatures

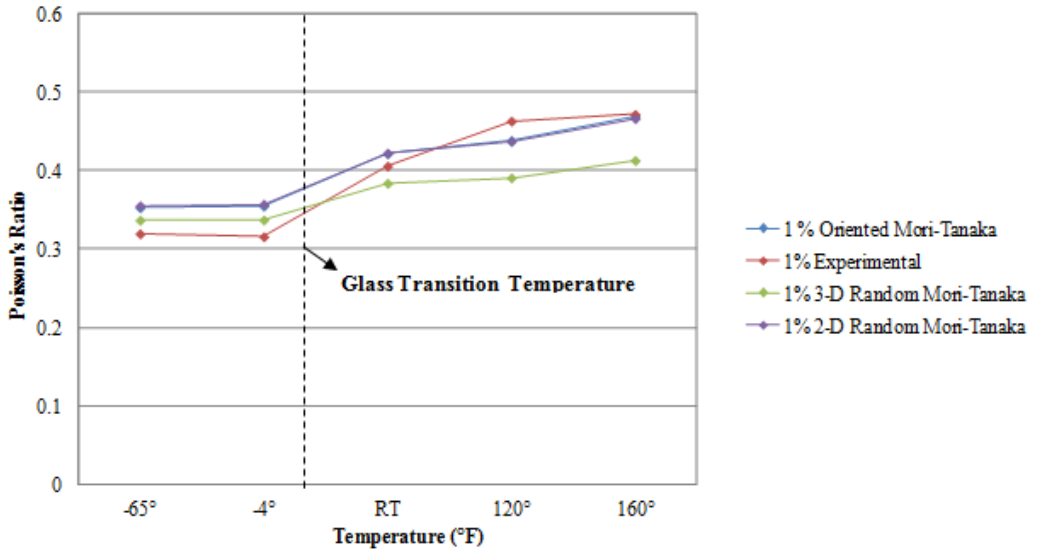


**Figure 4.5** Comparison of Poisson's ratio obtained from Mori-Tanaka and experimental results for 1% nanoclay reinforced PP 3371 specimens at various temperatures

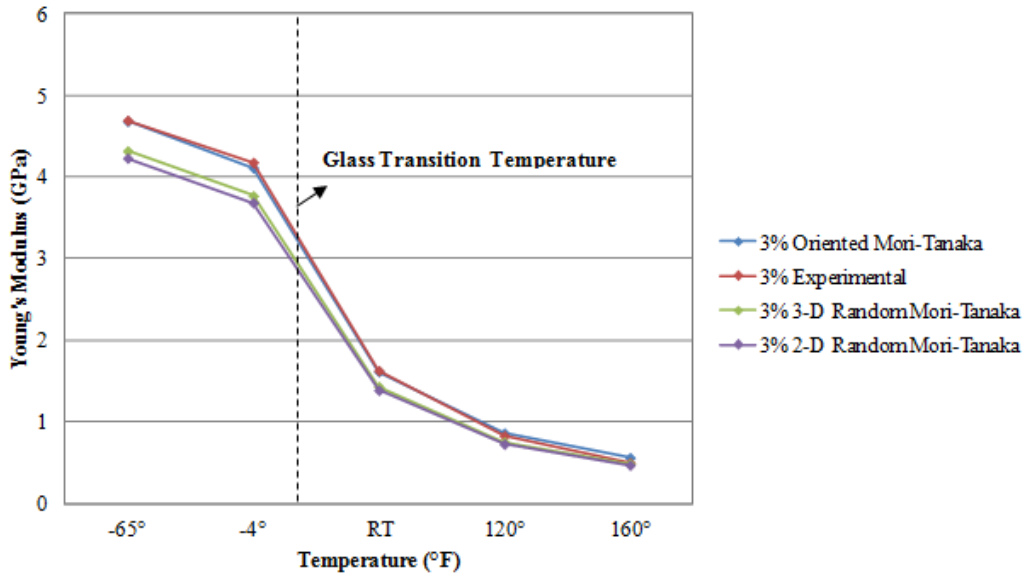


**Figure 4.6** Comparison of Young's modulus obtained from Mori-Tanaka and experimental results for 3% nanoclay reinforced PP 3371 specimens at various temperatures

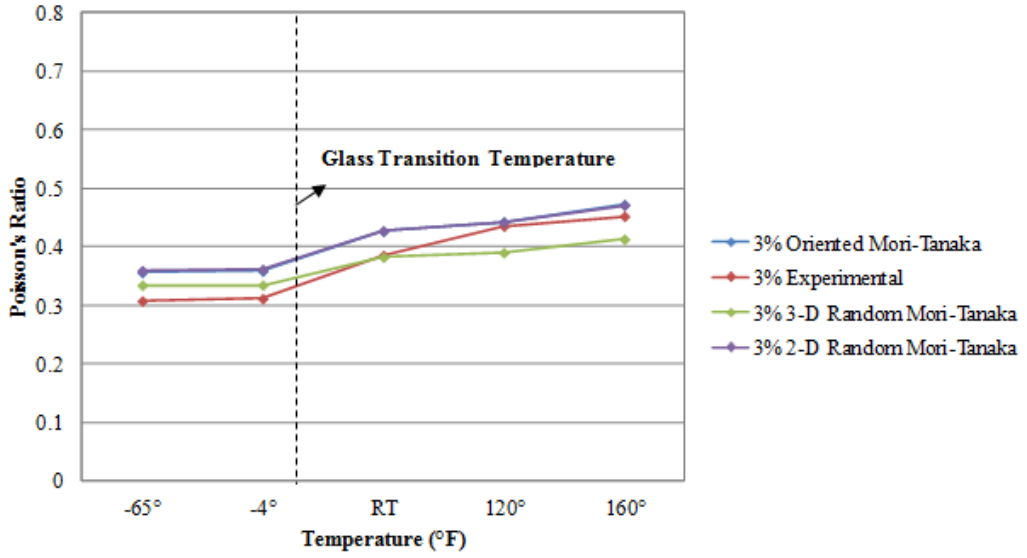


**Figure 4.7** Comparison of Poisson's ratio obtained from Mori-Tanaka and experimental results for 3% nanoclay reinforced PP 3371 specimens at various temperatures

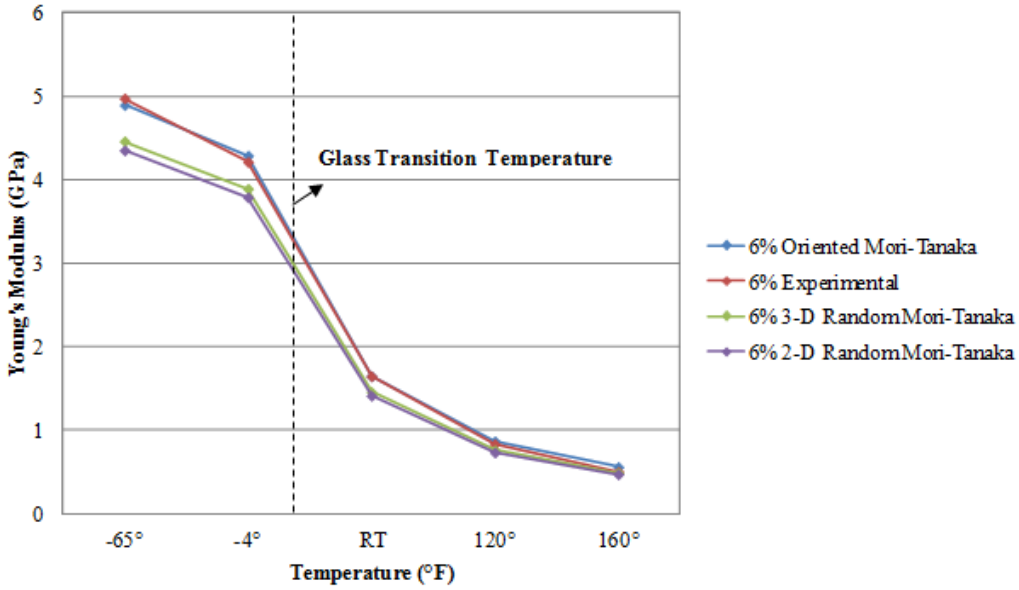


**Figure 4.8** Comparison of Young's modulus obtained from Mori-Tanaka and experimental results for 6% nanoclay reinforced PP 3371 specimens at various temperatures

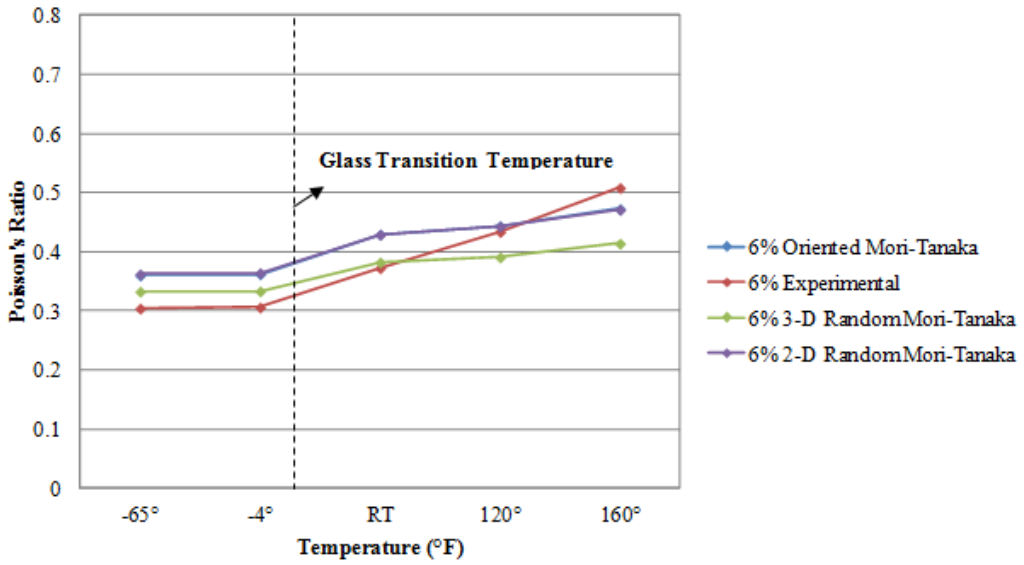


**Figure 4.9** Comparison of Poisson's ratio obtained from Mori-Tanaka and experimental results for 6% nanoclay reinforced PP 3371 specimens at various temperatures

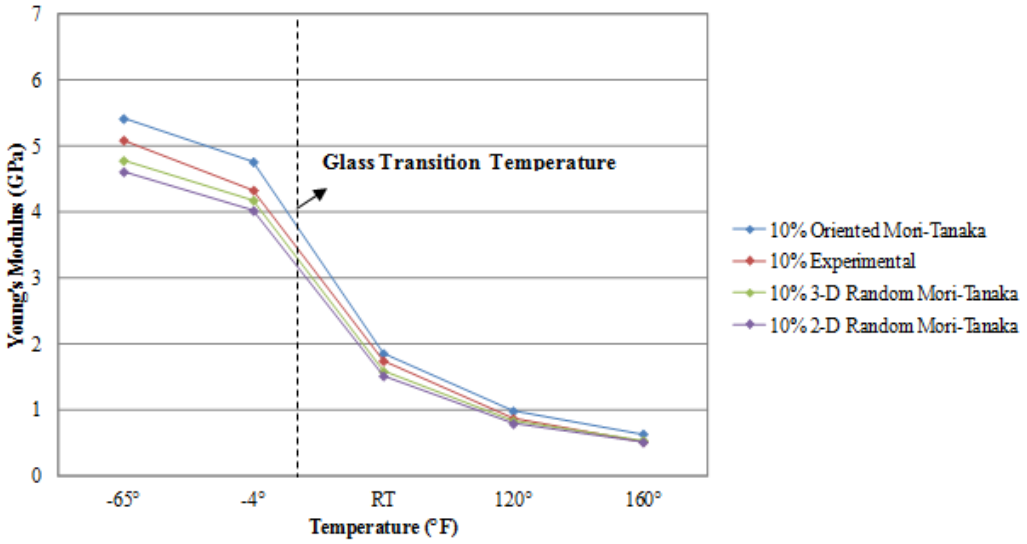


**Figure 4.10** Comparison of Young's modulus obtained from Mori-Tanaka and experimental results for 10% nanoclay reinforced PP 3371 specimens at various temperatures

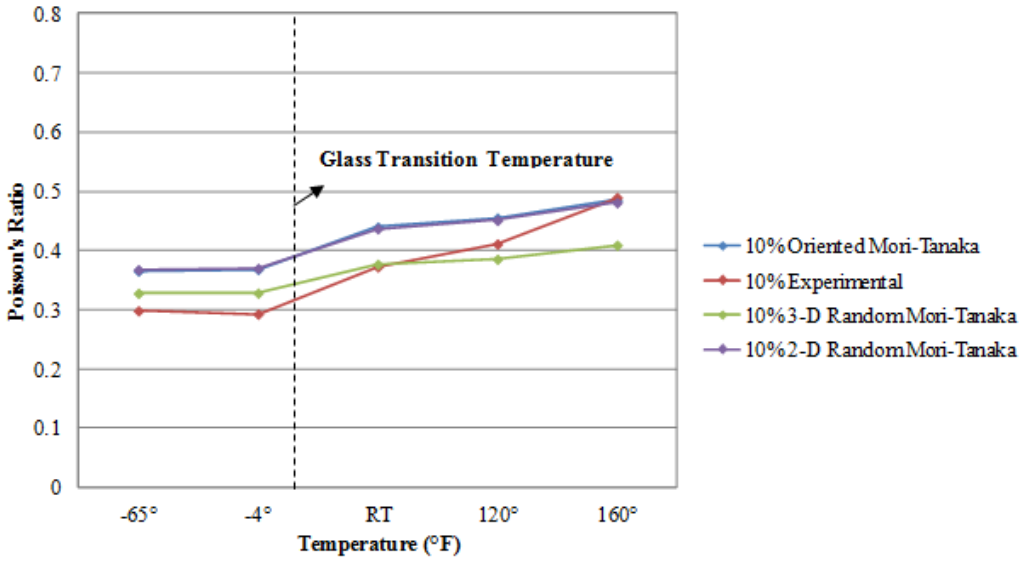


**Figure 4.11** Comparison of Poisson's ratio obtained from Mori-Tanaka and experimental results for 10% nanoclay reinforced PP 3371 specimens at various temperatures

Figures 4.12-4.21 show the comparison of experimental and analytical results for each temperature as a function of the reinforcement percentage.

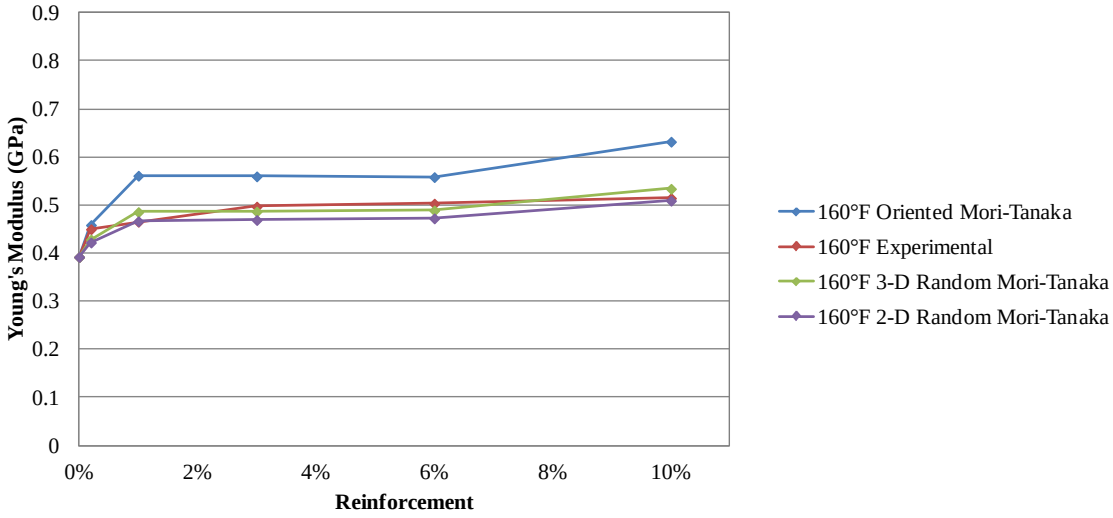


**Figure 4.12** Comparison of Young's modulus obtained from experiments and oriented, 2-D and 3-D random Mori - Tanaka calculations at 160°F

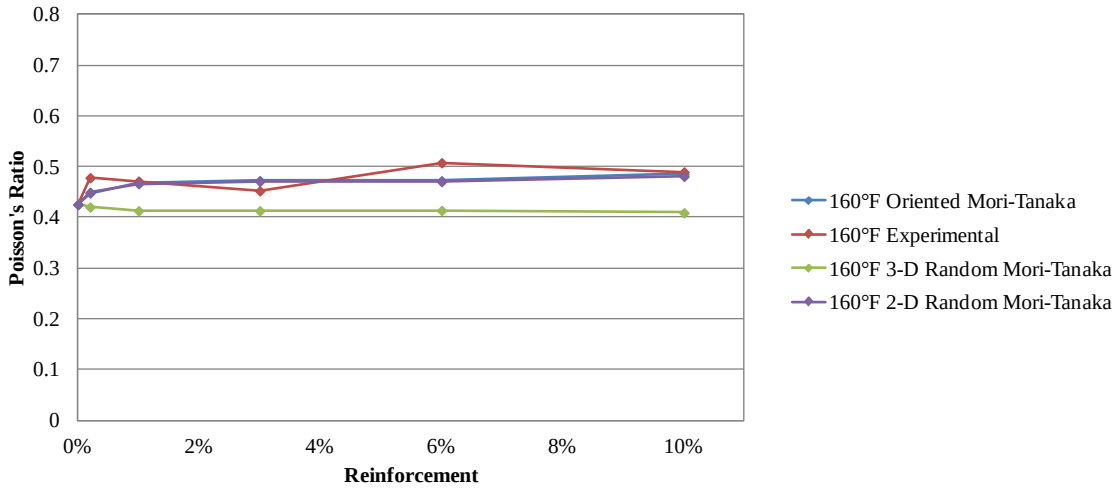


**Figure 4.13** Comparison of Poisson's ratio obtained from experiments and oriented, 2-D and 3-D random Mori - Tanaka calculations at 160°F

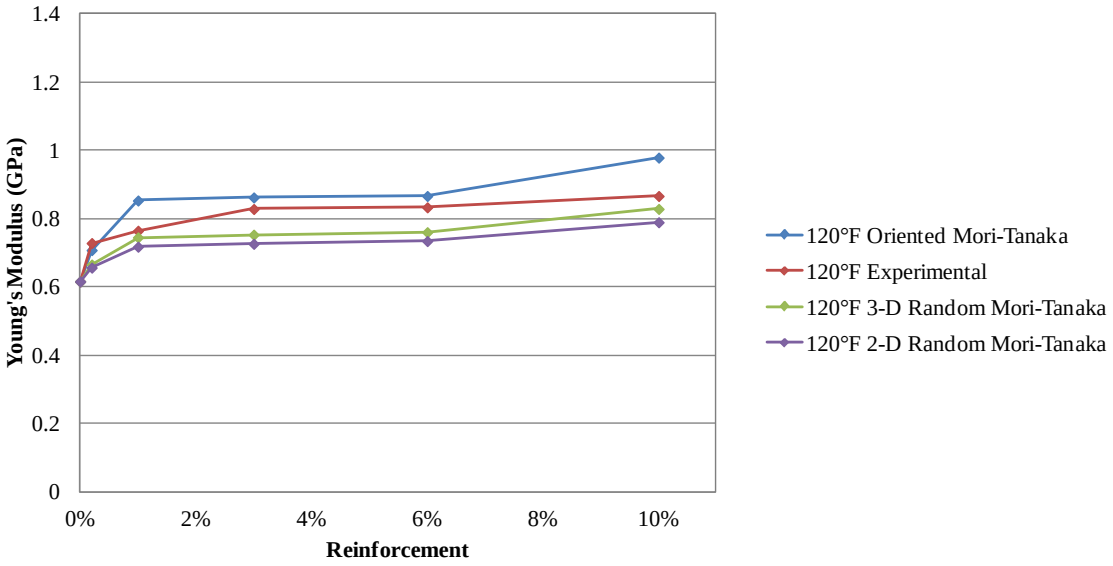


**Figure 4.14** Comparison of Young's modulus obtained from experiments and oriented, 2-D and 3-D random Mori - Tanaka calculations at 120°F

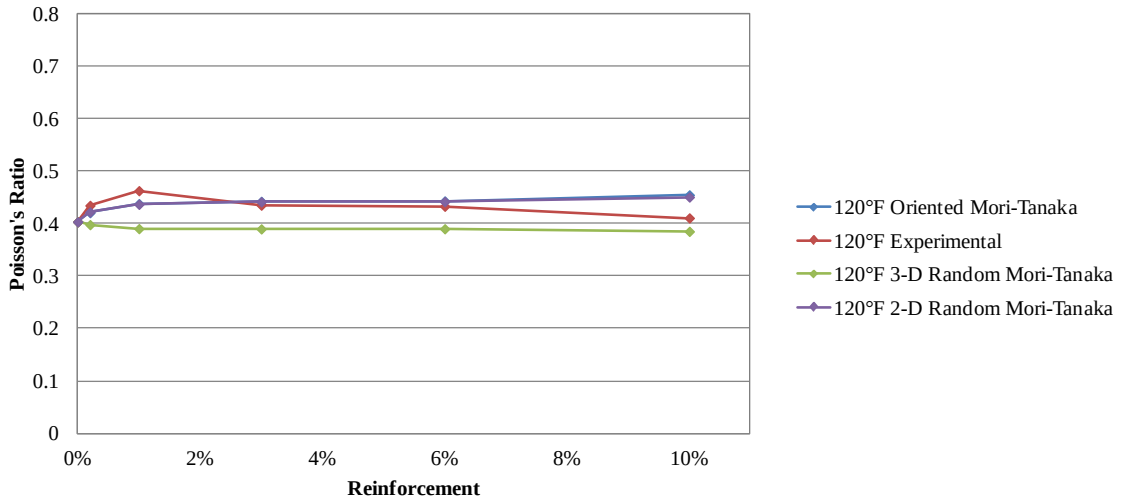


**Figure 4.15** Comparison of Poisson's ratio obtained from experiments and oriented, 2-D and 3-D random Mori - Tanaka calculations at 120°F

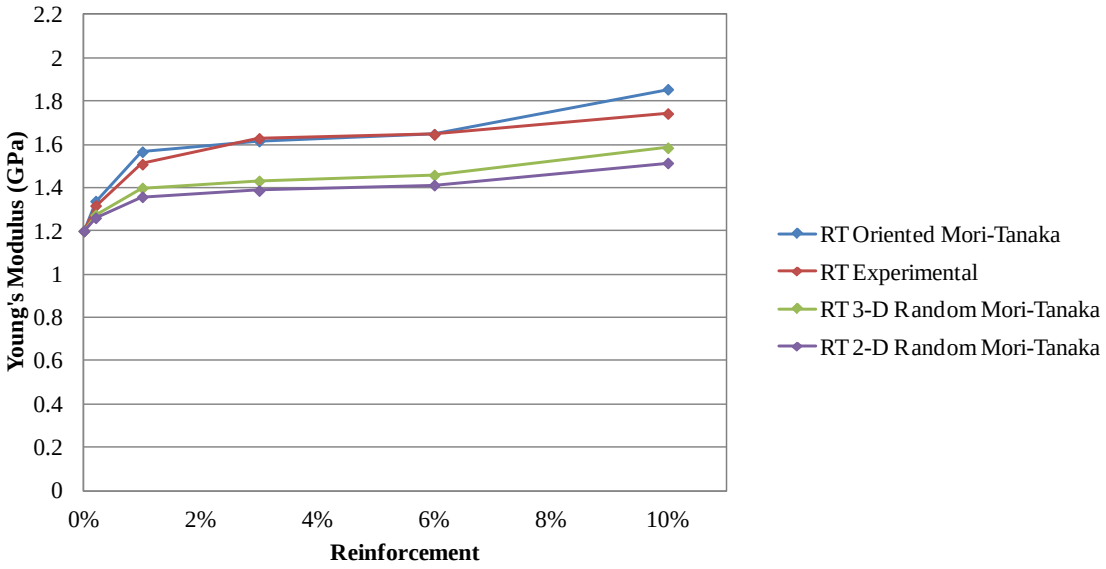


**Figure 4.16** Comparison of Young's modulus obtained from experiments and oriented, 2-D and 3-D random Mori - Tanaka calculations at RT

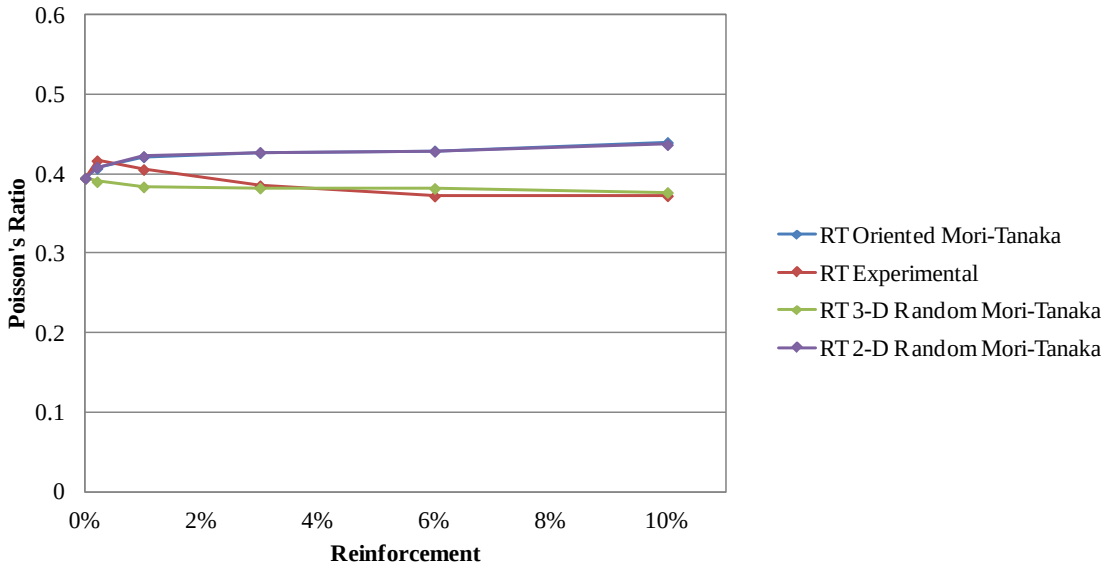


**Figure 4.17** Comparison of Poisson's ratio obtained from experiments and oriented, 2-D and 3-D random Mori - Tanaka calculations at RT

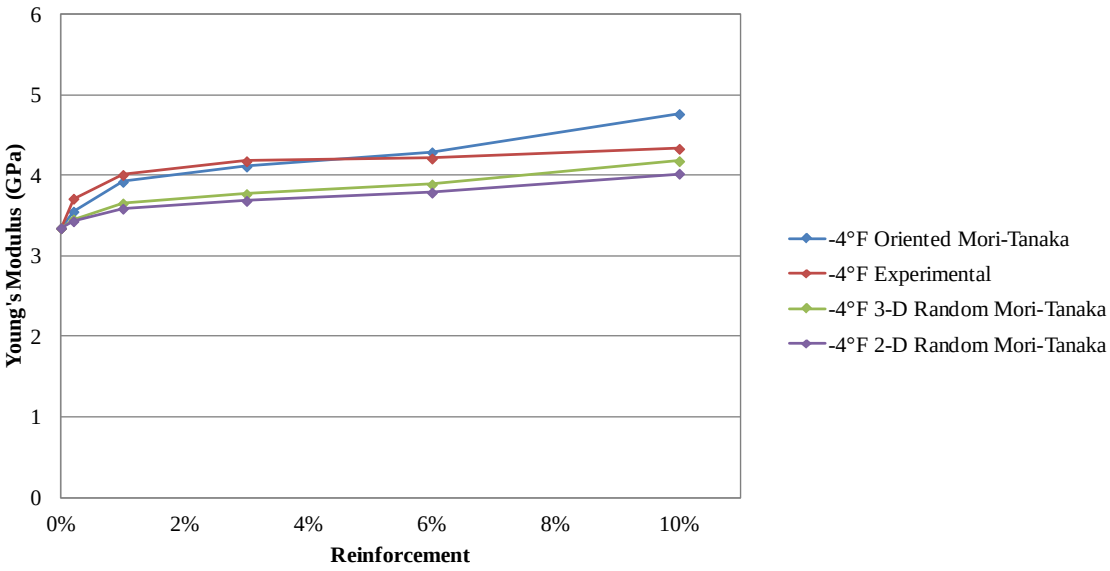


**Figure 4.18** Comparison of Young's modulus obtained from experiments and oriented, 2-D and 3-D random Mori - Tanaka calculations at -4°F

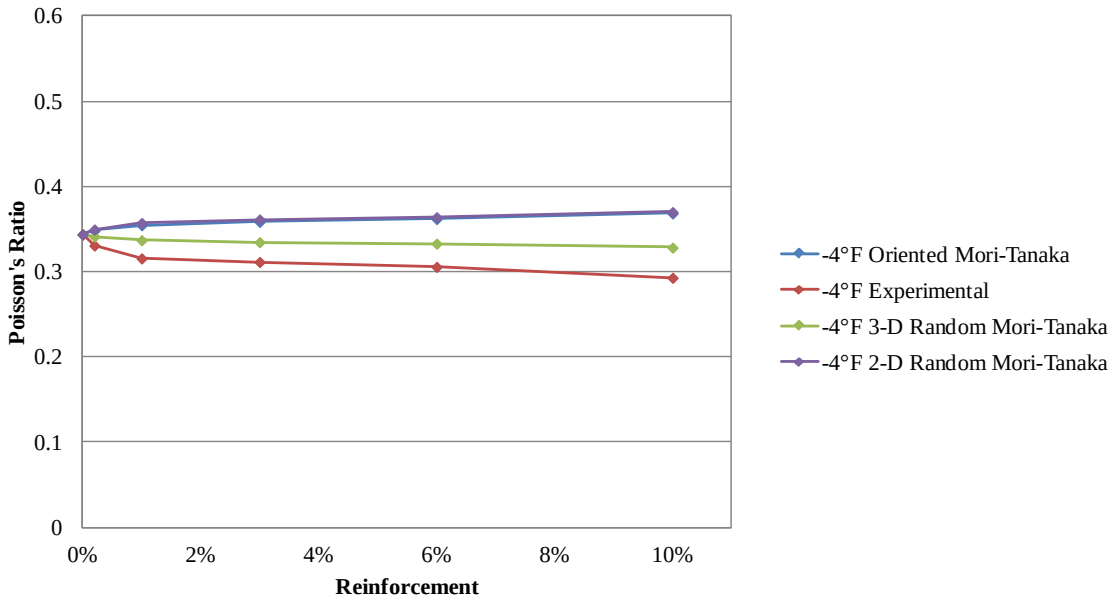


**Figure 4.19** Comparison of Poisson's ratio obtained from experiments and oriented, 2-D and 3-D random Mori - Tanaka calculations at -4°F

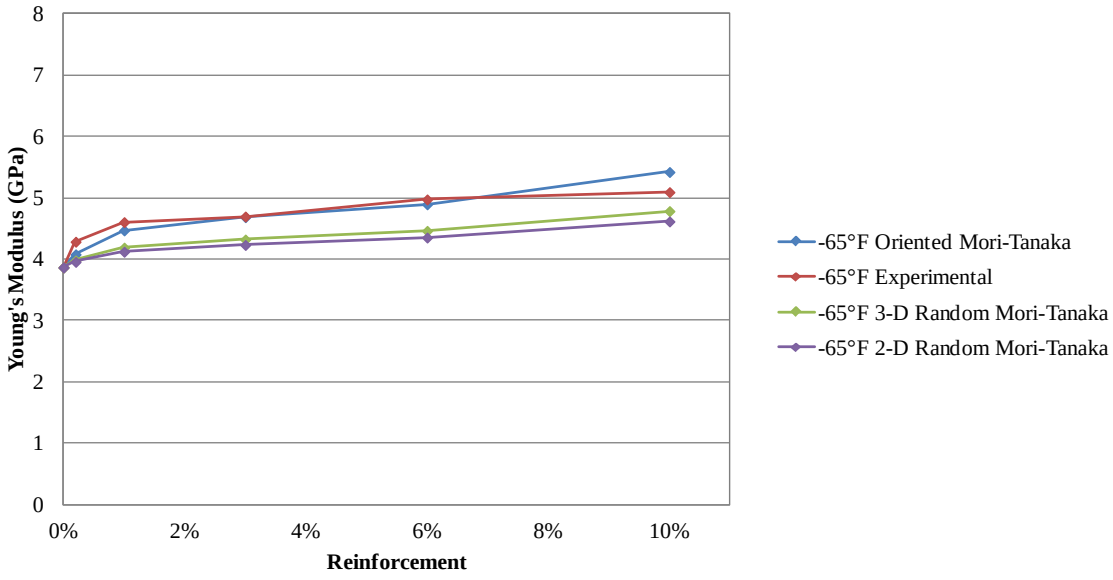


**Figure 4.20** Comparison of Young's modulus obtained from experiments and oriented, 2-D and 3-D random Mori - Tanaka calculations at -65°F

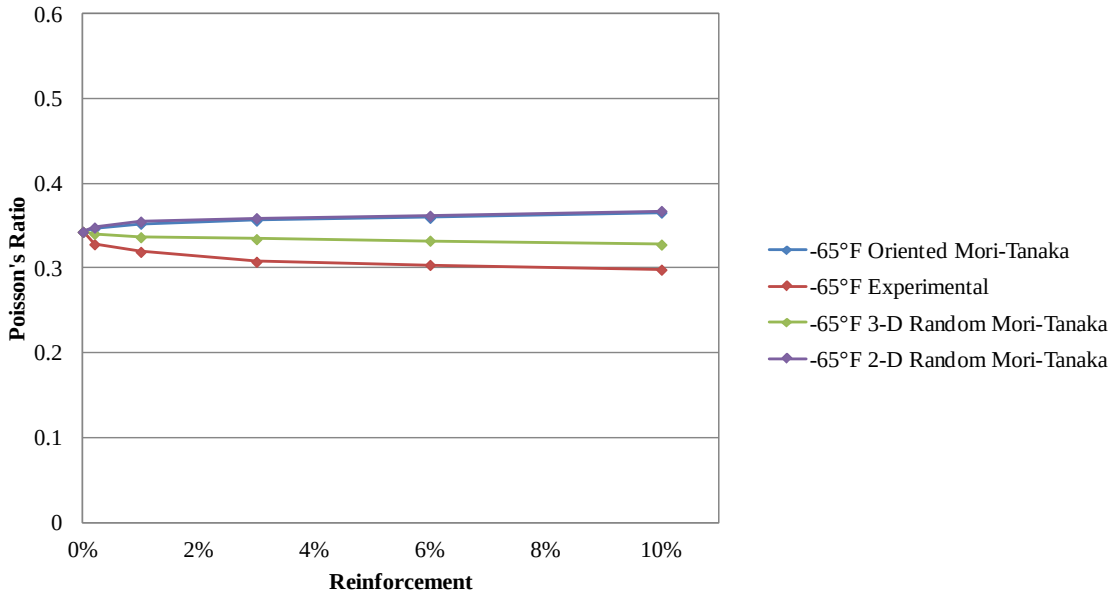


**Figure 4.21** Comparison of Poisson's ratio obtained from experiments and oriented, 2-D and 3-D random Mori - Tanaka calculations at -65°F

As we mentioned before, the results indicate that the agreement between the experimental data and the modified Mori-Tanaka calculations in general is very good, except at higher temperatures and higher reinforcement percentages.

At high temperatures and high percentage values 3 different approaches of Mori Tanaka calculations do not provide a good match with experimental results. We believe that at high temperatures PP material behaves differently than at room or low temperatures and as a consequence the Mori Tanaka approach does not provide good results. This is also confirmed by the fact that for temperatures above the glass transition temperature of PP, there is a steep drop in the values of Young's modulus ( Figures 4.2, 4.4, 4.6, 4.8 and 4.10). Also for high reinforcement percentages as was observed in the SEM pictures, the nanoclay particles do not disperse very well and there may be voids at the nanoclay/matrix interface. This may explain the divergence of results between experimental and calculated values at the higher percentages. To remedy the

situation, the Mori-Tanaka formulation was modified to take into account the effect of voids and temperature (see sections 4.2.3 and 4.2.4).

4.1.2-b) Comparison of Experimental Results with Mori-Tanaka Calculations for Epoxy Based Nanocomposites

Figures 4.22-4.23 show the comparison of Young's modulus and Poisson's ratio obtained from experiments and Mori-Tanaka calculations for EPON 828 epoxy nanoclay reinforced specimens at room temperature. For epoxy there is divergence between experimental and calculated results. This may be due to the fact that more agglomeration of nanoclay particles may occur because of the higher viscosity of epoxy relative to PP.

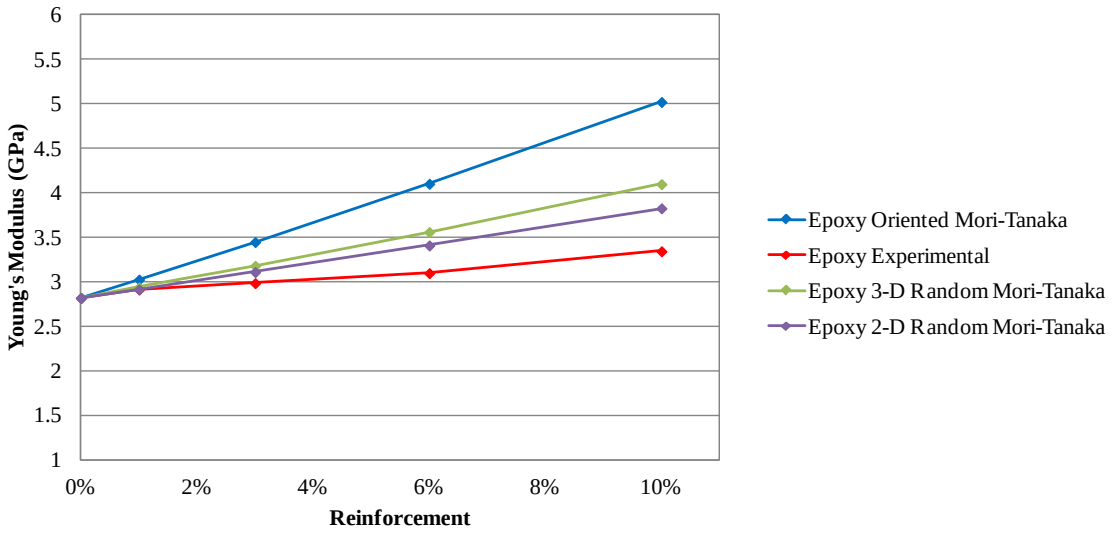


**Figure 4.22** Comparison of Young's modulus obtained from experiments and oriented, 2-D and 3-D random Mori - Tanaka calculations at room temperature

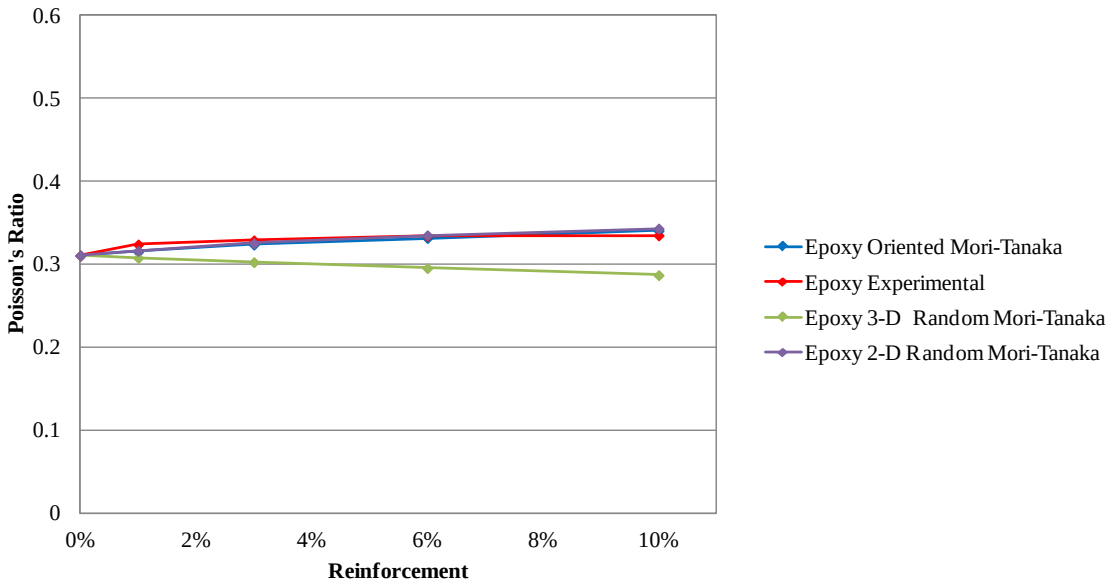


**Figure 4.23** Comparison of Poisson's ratio obtained from experiments and oriented, 2-D and 3-D random Mori - Tanaka calculations at room temperature

### 4.1.3. Mori-Tanaka Calculations with Effect of Voids

When the SEM pictures are analyzed, it is observed that at high reinforcement percentages (contrary to low percentages) there may be voids between the particles and matrix. Because of this observation it was decided to modify the Mori Tanaka calculations by including the effect of voids.

We assume a parabolic distribution of voids as a function of reinforcement percentage since there are fewer voids at lower percentages than at higher percentages. With this assumption the volume fraction of particles can be calculated as follows:

Define:

$V_d$ : max void percentage

$w_p$: nanoclay weight percentage

$v_d$: void fraction at each percentage

The parabolic void distribution can be expressed as:

$$v_d = A w_p^2 \tag{58}$$

Assuming maximum void percentage occurs at $w_p$=10% the unknown A can be obtained from:

$$V_d = A(0.1)^2$$
$$\rightarrow A = 100 V_d$$

Thus, Eq. (58) becomes

$$v_d = 100 V_d \left(w_p\right)^2 \tag{59}$$

The total volume V and total weight are:

$$V = V_p + V_m + V_v \tag{60}$$

$$W = W_p + W_m \tag{61}$$

where,

$V_p$: total volume of particles

$V_m$: total volume of matrix

$V_v$: total volume of voids

$W_p$: total weight of particles

$W_m$: total weight of matrix

From,

$$V_p + V_m = \frac{W_p}{\gamma_p} + \frac{\left(W - W_p\right)}{\gamma_m} \tag{62}$$

$$V_v = V v_d \tag{63}$$

where $\gamma_p$ and $\gamma_m$ are the specific weights of nanoclay and matrix respectively.

The total volume V is obtained as:

$$V = \frac{W_p}{\gamma_p} + \frac{\left(W - W_p\right)}{\gamma_m} + V v_d$$

or

$$V = \frac{\left(\frac{W_p}{\gamma_p} + \frac{\left(W - W_p\right)}{\gamma_m}\right)}{\left(1 - v_d\right)} \tag{64}$$

With the new total volume V, we redefine the volume fraction c of particles in the presence of voids as:

$$c = \frac{\left(\frac{W_p}{\gamma_p}\right)\left(1 - v_d\right)}{\frac{W_p}{\gamma_p} + \frac{\left(1 - W_p\right)}{\gamma_0}} \tag{65}$$

In the ensuing sections, the Young's modulus and the Poisson's ratio are recalculated using the 3 different Mori Tanaka approaches with the new volume fraction c. For all cases the maximum void fraction $V_d$ is assumed to be 6%.

4.1.3-a) Oriented Nanoclay Particles with Effect of Voids

Figures 4.24-4.33 show the comparison of experimental results and oriented Mori Tanaka calculations with and without voids at various temperatures.

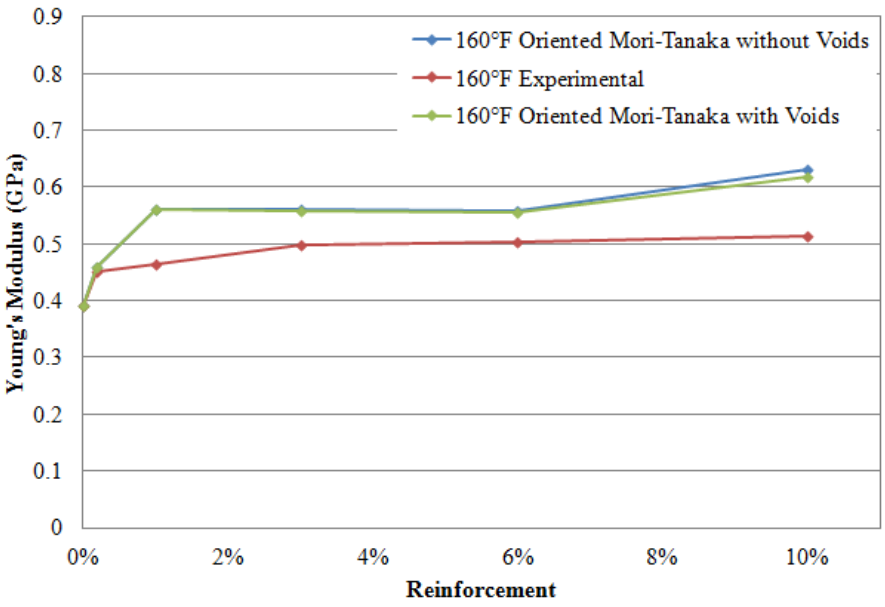


**Figure 4.24** Comparison of Young's modulus obtained from experiments and oriented Mori - Tanaka calculations with and without voids at 160°F

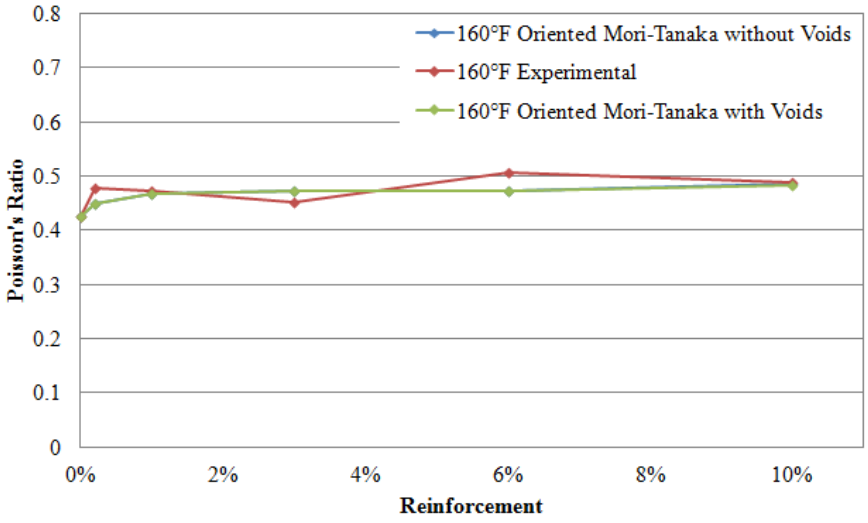


**Figure 4.25** Comparison of Poisson's ratio obtained from experiments and oriented Mori - Tanaka calculations with and without voids at 160°F

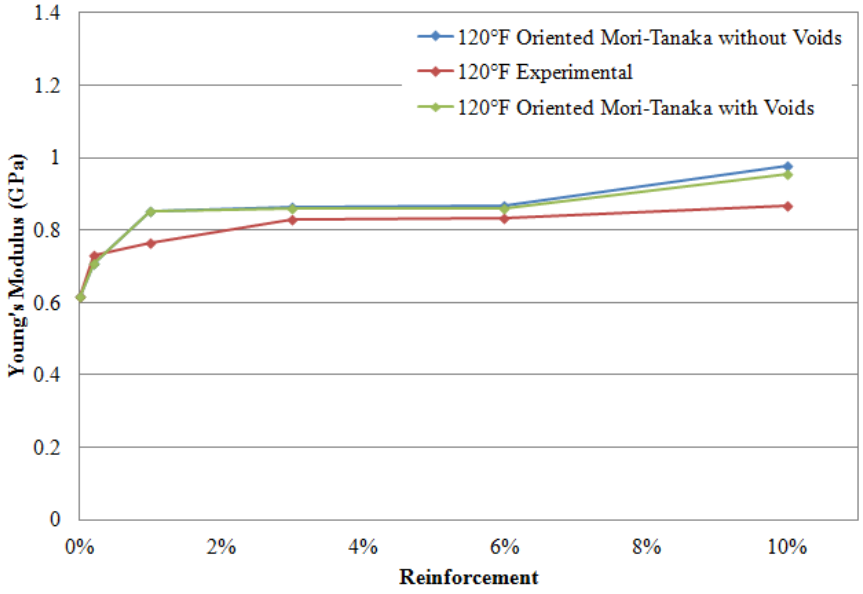


**Figure 4.26** Comparison of Young's modulus obtained from experiments and oriented Mori - Tanaka calculations with and without voids at 120°F

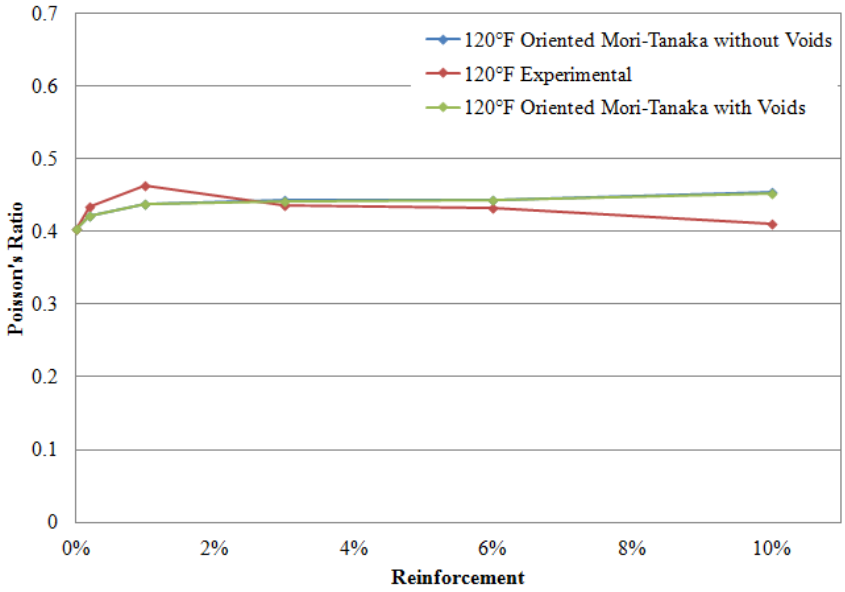


**Figure 4.27** Comparison of Poisson's ratio obtained from experiments and oriented Mori - Tanaka calculations with and without voids at 120°F

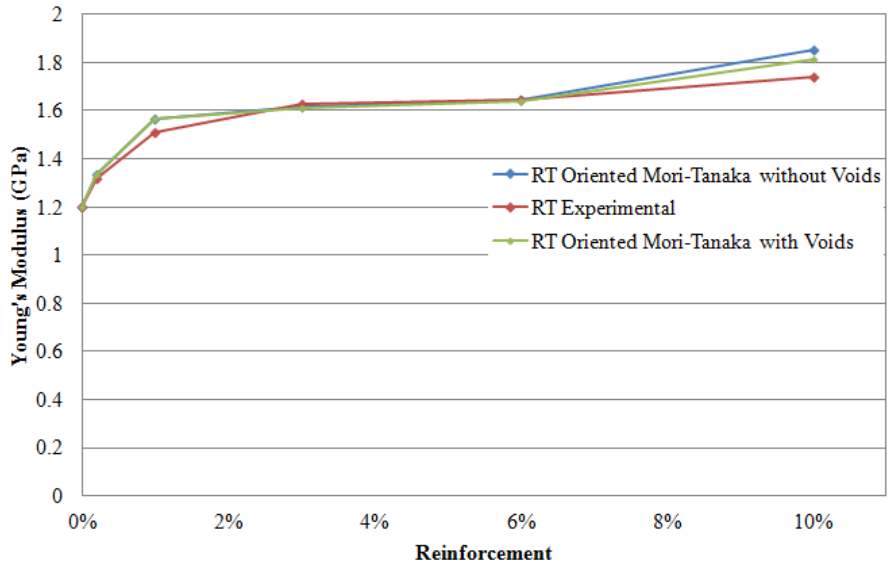


**Figure 4.28** Comparison of Young's modulus obtained from experiments and oriented Mori - Tanaka calculations with and without voids at RT

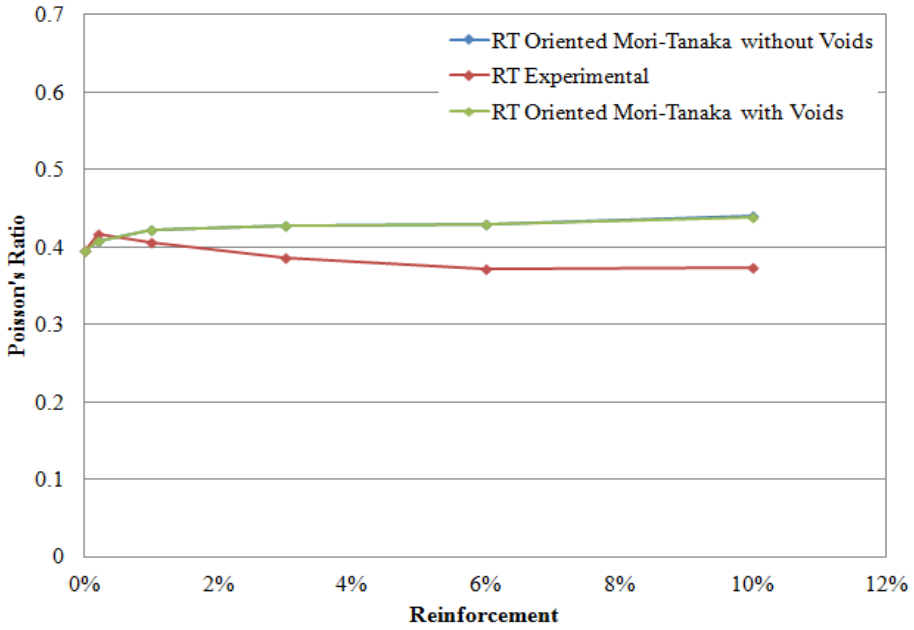


**Figure 4.29** Comparison of Poisson's ratio obtained from experiments and oriented Mori - Tanaka calculations with and without voids at RT

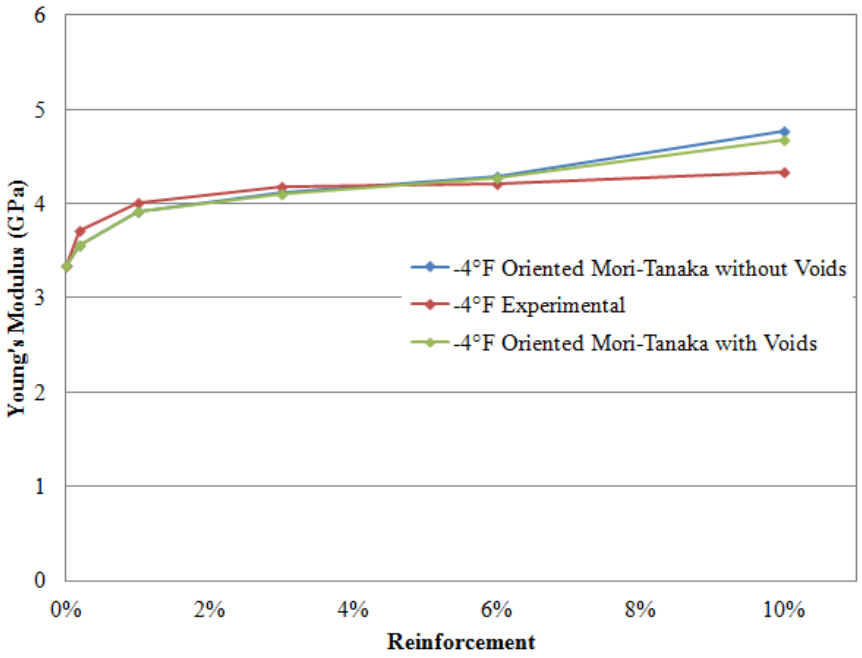


**Figure 4.30** Comparison of Young's modulus obtained from experiments and oriented Mori - Tanaka calculations with and without voids at -4°F

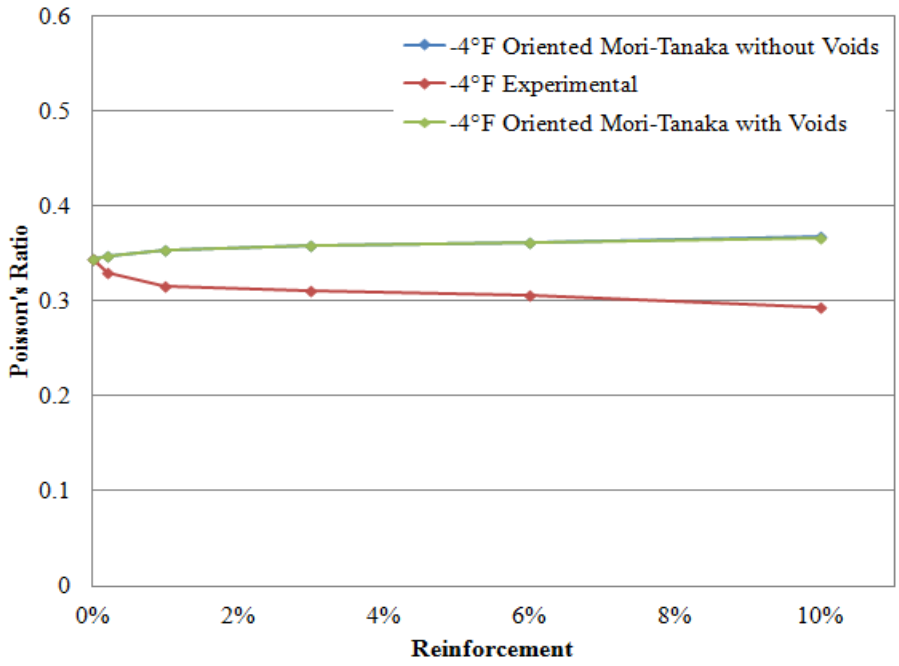


**Figure 4.31** Comparison of Poisson's ratio obtained from experiments and oriented Mori - Tanaka calculations with and without voids at -4°F

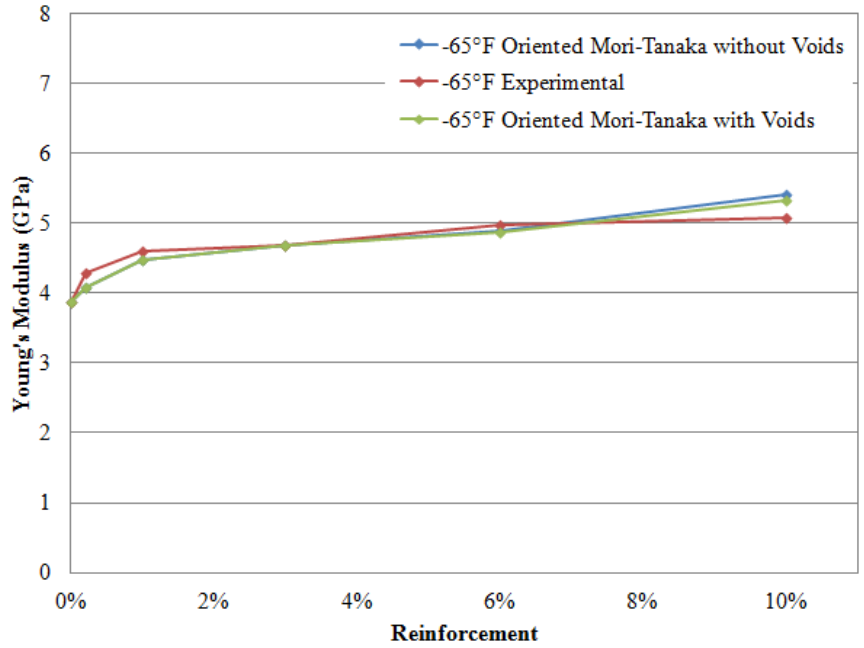


**Figure 4.32** Comparison of Young's modulus obtained from experiments and oriented Mori - Tanaka calculations with and without voids at -65°F

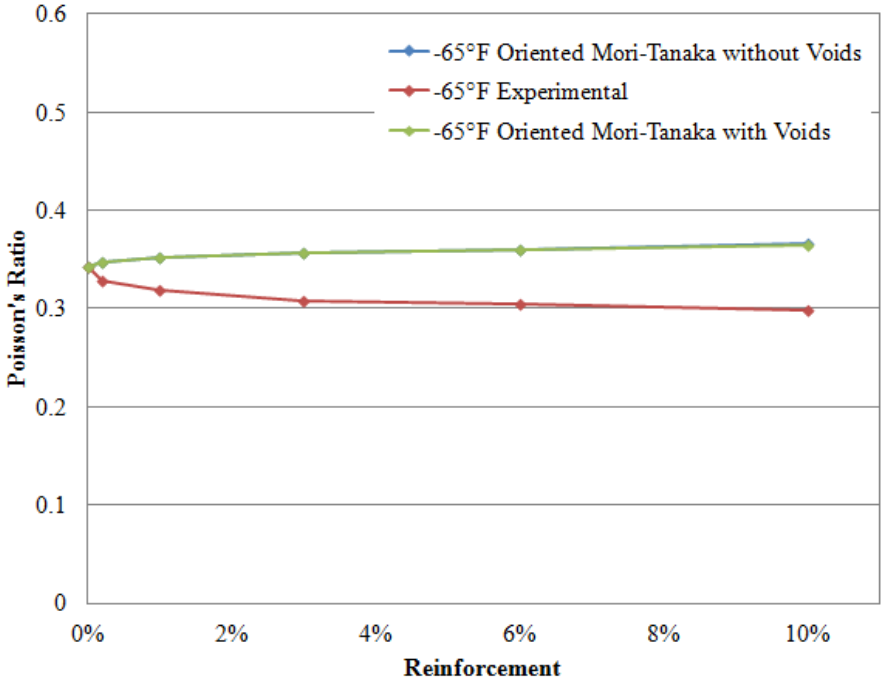


**Figure 4.33** Comparison of Poisson's ratio obtained from experiments and oriented Mori - Tanaka calculations with and without voids at -65°F

As the results given in the previous Figures indicate the inclusion of voids in the calculations affects the value of Young's modulus mainly at 10% but it does not affect the Poisson's ratio significantly. The results obtained by including the effect of voids in general give a better match with experimental data.

4.1.3-b) 2-D Randomly Distributed Nanoclay Particles with Effect of Voids

We recalculated the Mori Tanaka results for the 2-D random cases by including the effect of voids and compared the results with experimental and 2-D random calculations without voids. Figures 4.34-4.43 show these comparisons at each temperature.

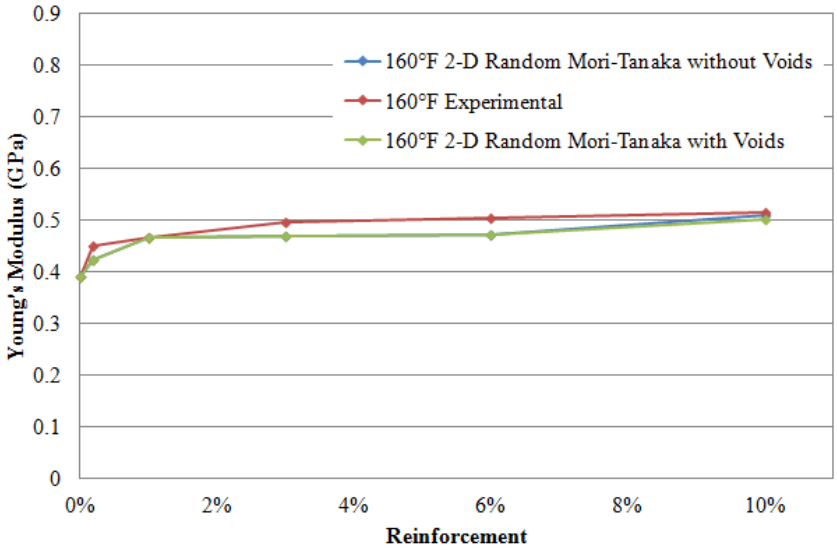


**Figure 4.34** Comparison of Young's modulus obtained from experiments and 2-D random Mori - Tanaka calculations with and without voids at 160°F

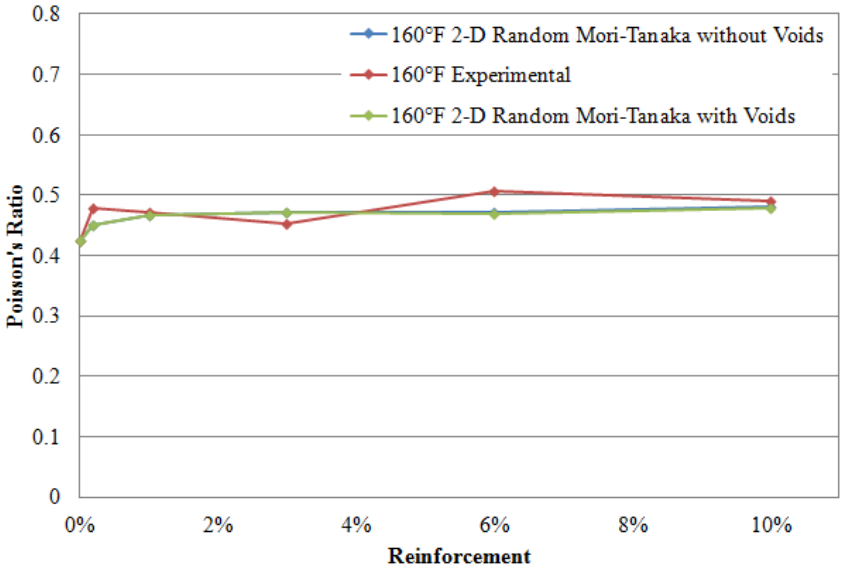


**Figure 4.35** Comparison of Poisson's ratio obtained from experiments and 2-D random Mori - Tanaka calculations with and without voids at 160°F

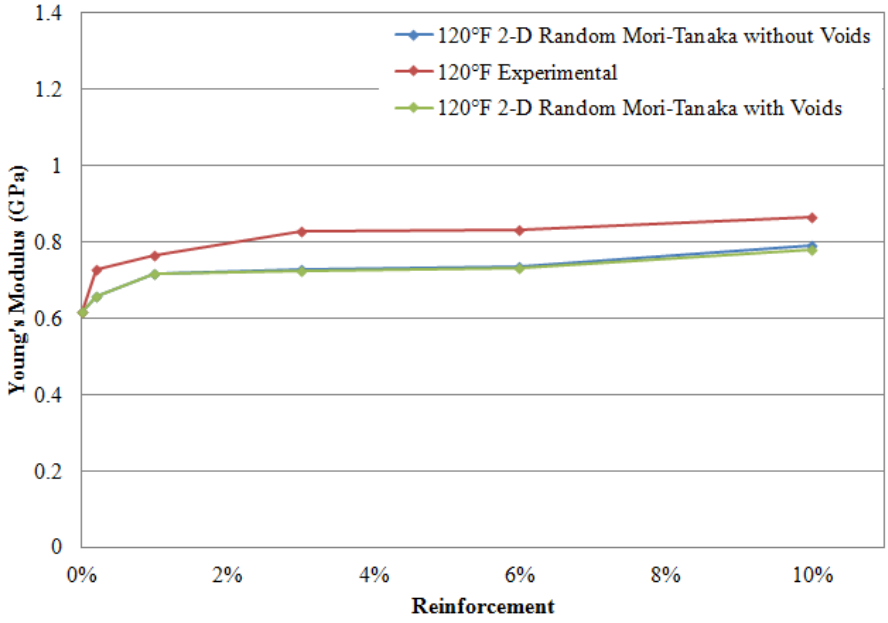


**Figure 4.36** Comparison of Young's modulus obtained from experiments and 2-D random Mori - Tanaka calculations with and without voids at 120°F

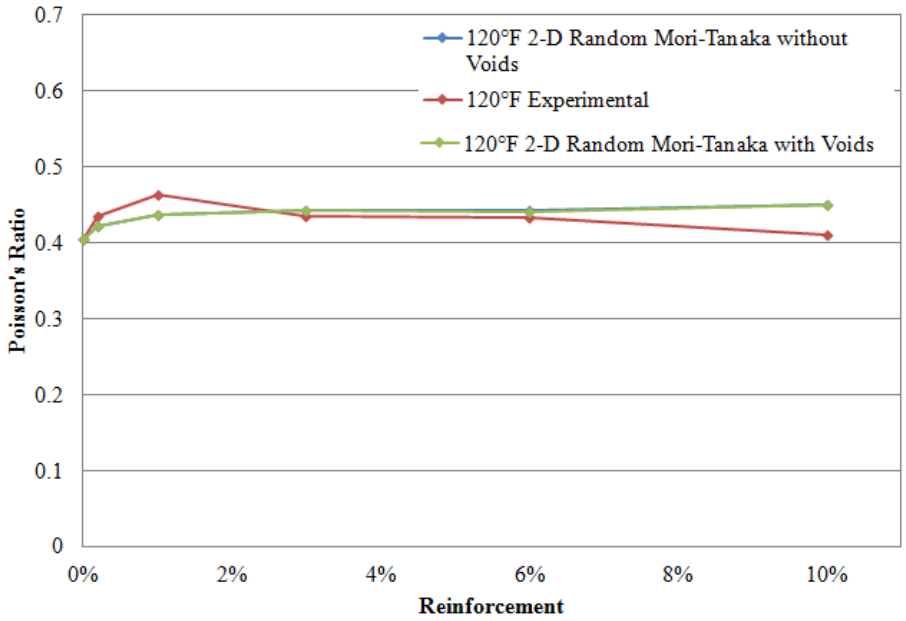


**Figure 4.37** Comparison of Poisson's ratio obtained from experiments and 2-D random Mori - Tanaka calculations with and without voids at 120°F

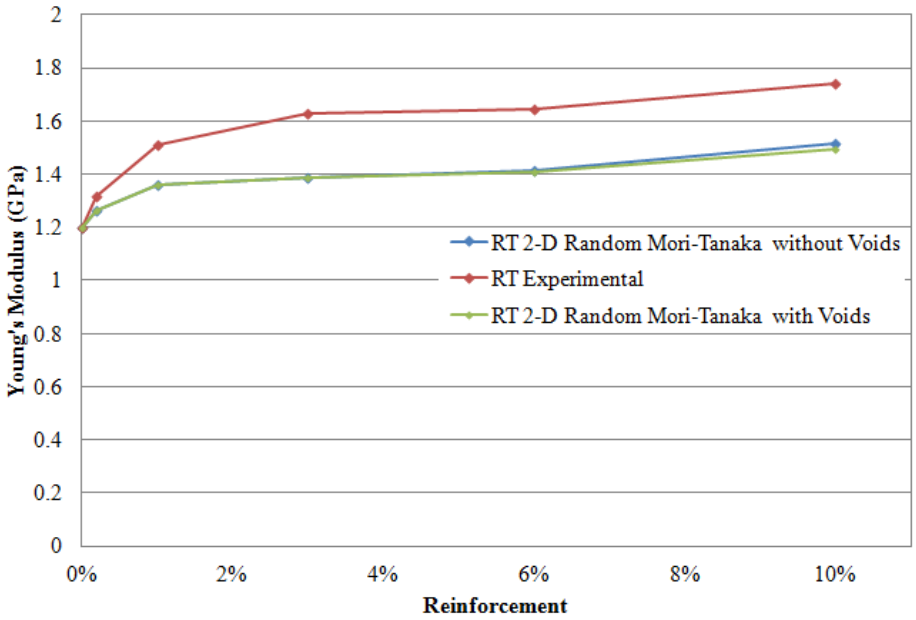


**Figure 4.38** Comparison of Young's modulus obtained from experiments and 2-D random Mori - Tanaka calculations with and without voids at RT

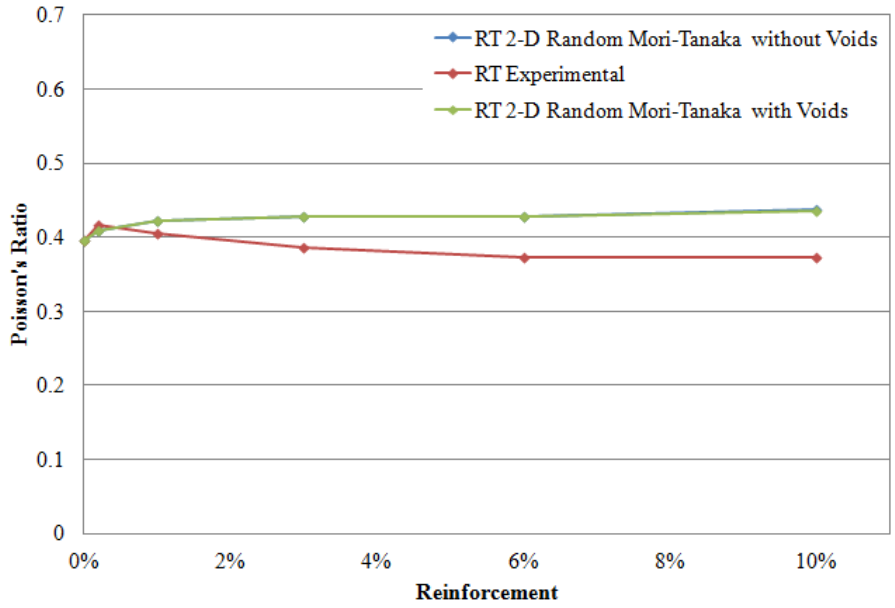


**Figure 4.39** Comparison of Poisson's ratio obtained from experiments and 2-D random Mori - Tanaka calculations with and without voids at RT

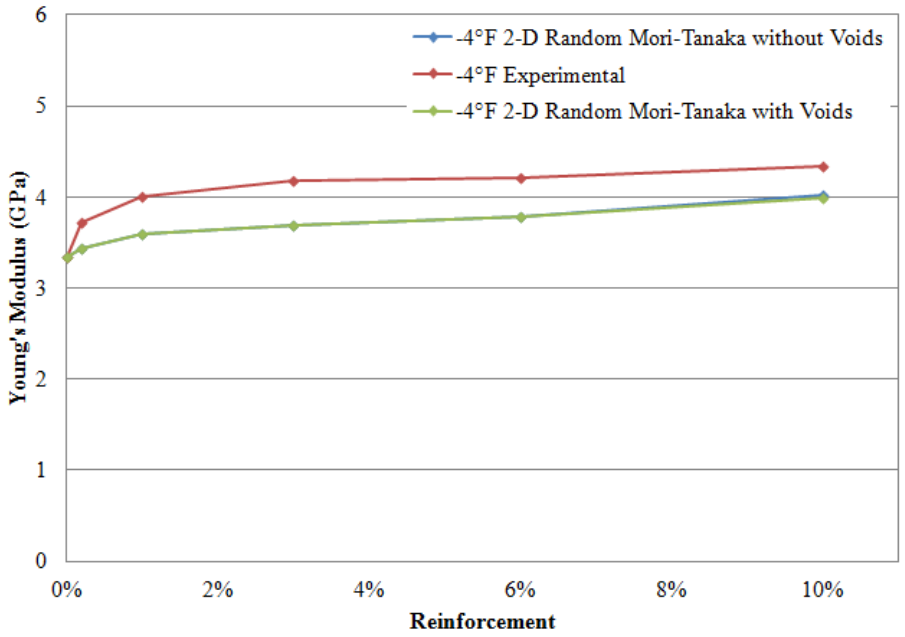


**Figure 4.40** Comparison of Young's modulus obtained from experiments and 2-D random Mori - Tanaka calculations with and without voids at -4°F

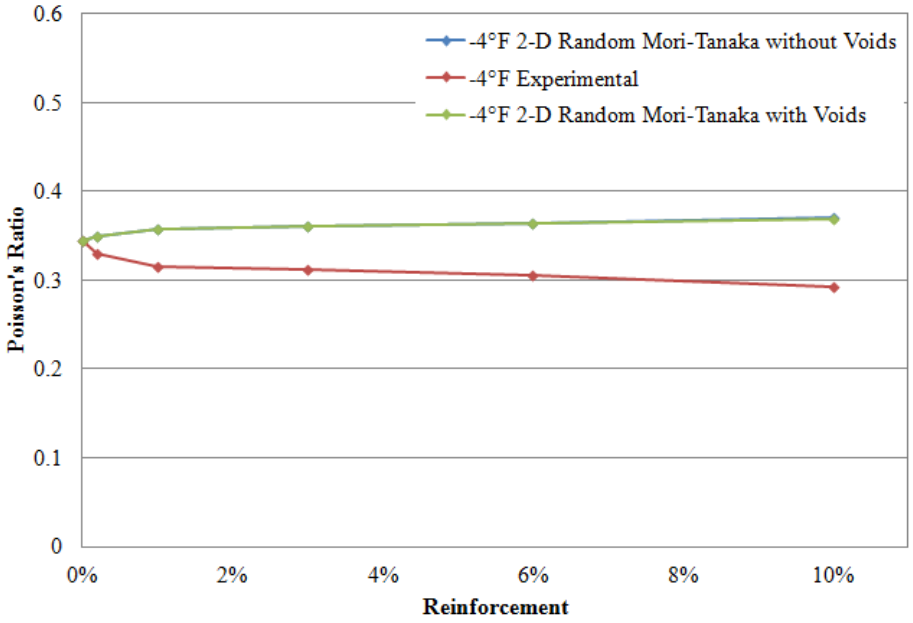


**Figure 4.41** Comparison of Poisson's ratio obtained from experiments and 2-D random Mori - Tanaka calculations with and without voids at -4°F

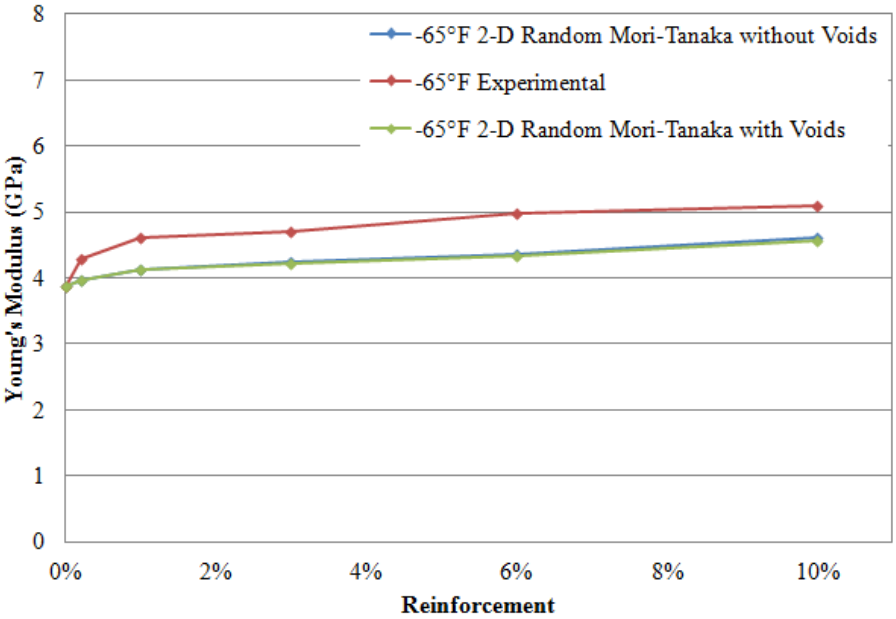


**Figure 4.42** Comparison of Young's modulus obtained from experiments and 2-D random Mori - Tanaka calculations with and without voids at -65°F

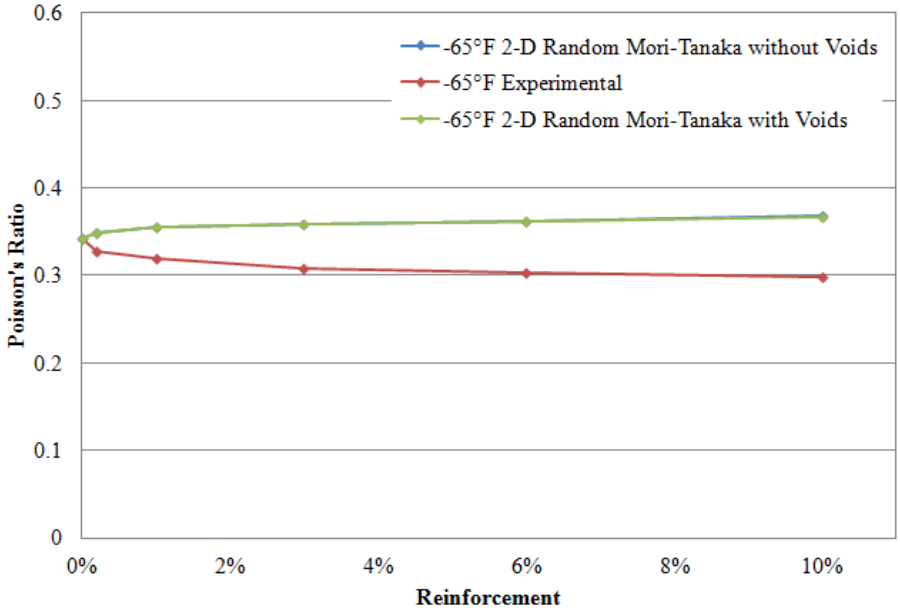


**Figure 4.43** Comparison of Poisson's ratio obtained from experiments and 2-D random Mori - Tanaka calculations with and without voids at -65°F

In the Figures one may observe that, the Young's modulus values are lower than the experimental results and the Poisson's ratio values are not affected significantly. There is improvement in matching the experimental results for higher percentages of reinforcement at room and lower temperatures. At higher temperatures the improvement is not evident.

4.1.3-c) 3-D Randomly Distributed Nanoclay Particles with Effect of Voids

Finally, we performed Mori -Tanaka calculations for 3-D random cases by including the effect of voids and compared the results with experimental and 3D random calculations without voids. Figures 4.44-4.53 show the comparison at each temperature.

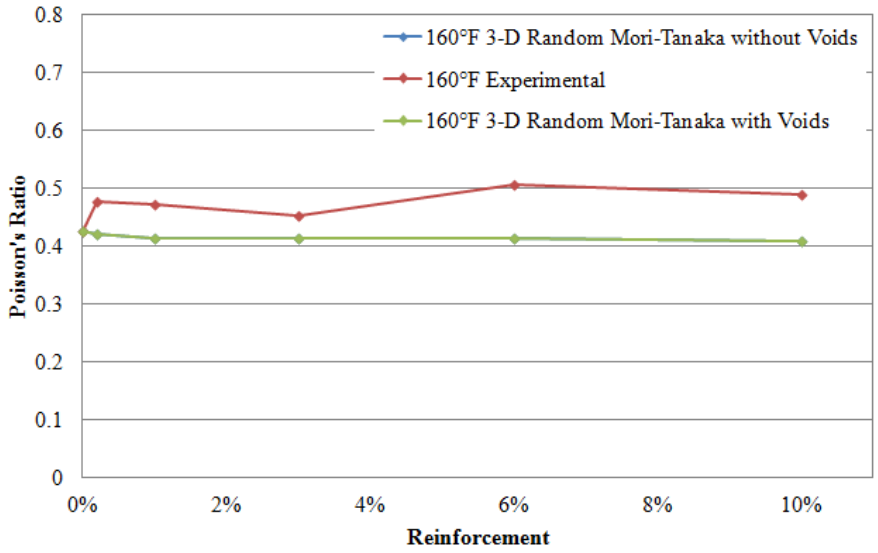


**Figure 4.44** Comparison of Young's modulus obtained from experiments and 3-D random Mori - Tanaka calculations with and without voids at 160°F

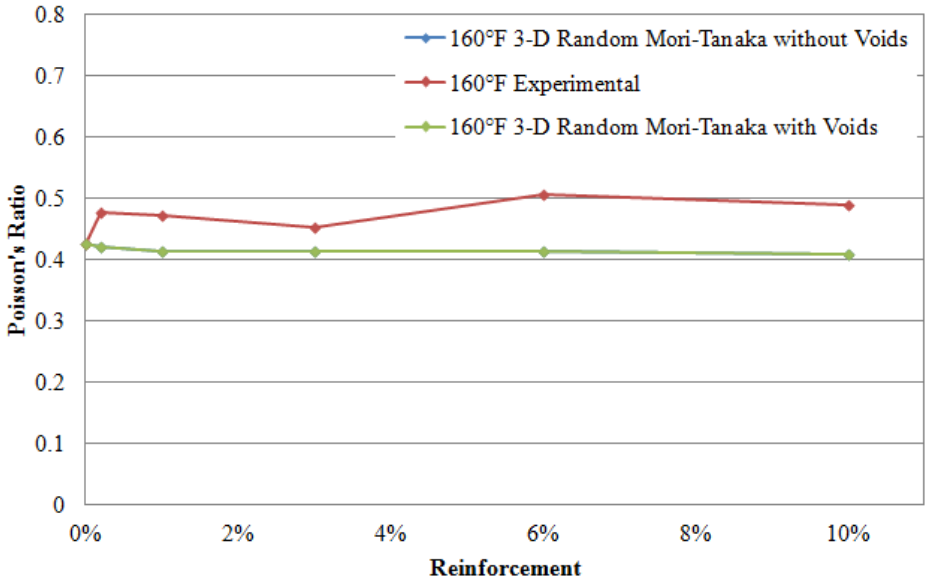


**Figure 4.45** Comparison of Poisson's ratio obtained from experiments and 3-D random Mori - Tanaka calculations with and without voids at 160°F

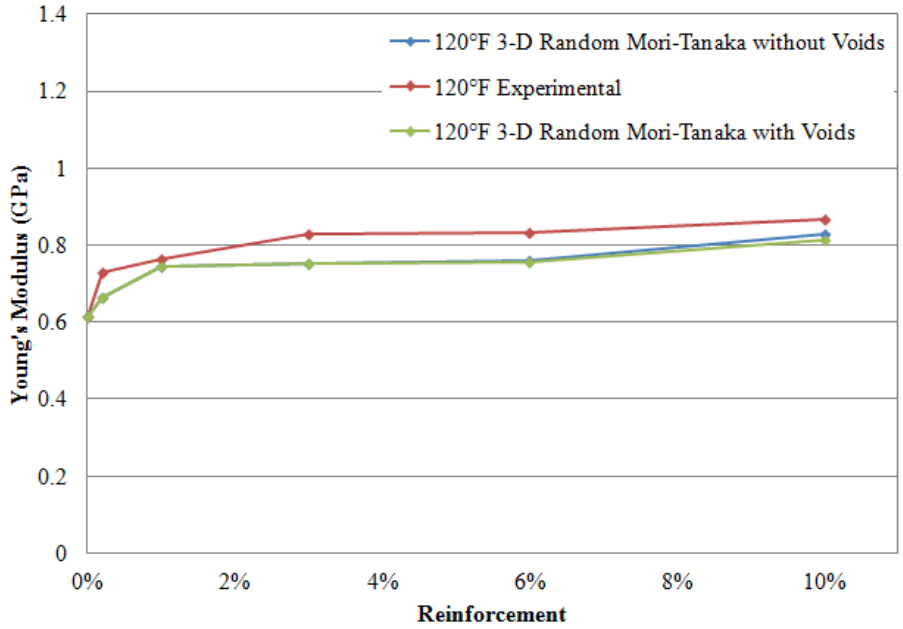


**Figure 4.46** Comparison of Young's modulus obtained from experiments and 3-D random Mori - Tanaka calculations with and without voids at 120°F

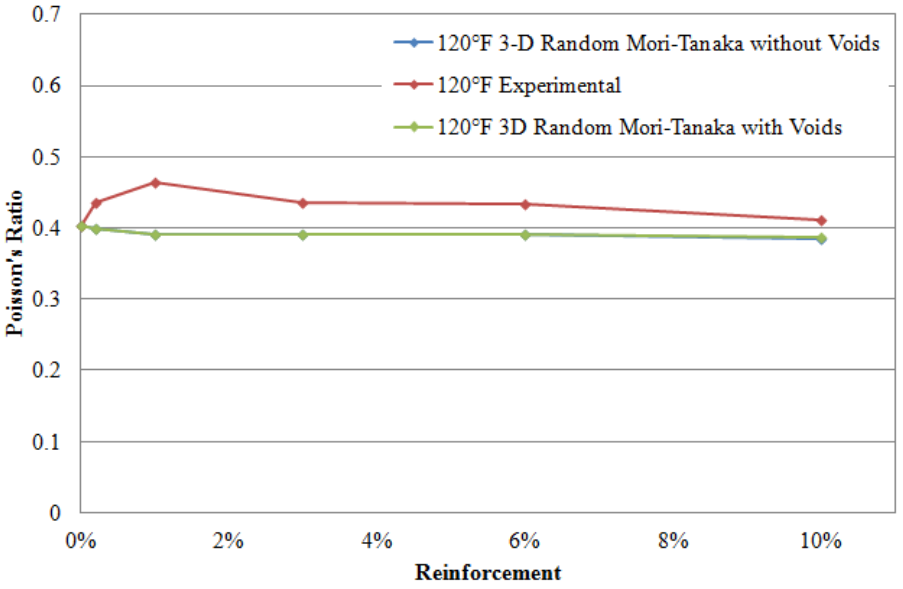


**Figure 4.47** Comparison of Poisson's ratio obtained from experiments and 3-D random Mori - Tanaka calculations with and without voids at 120°F

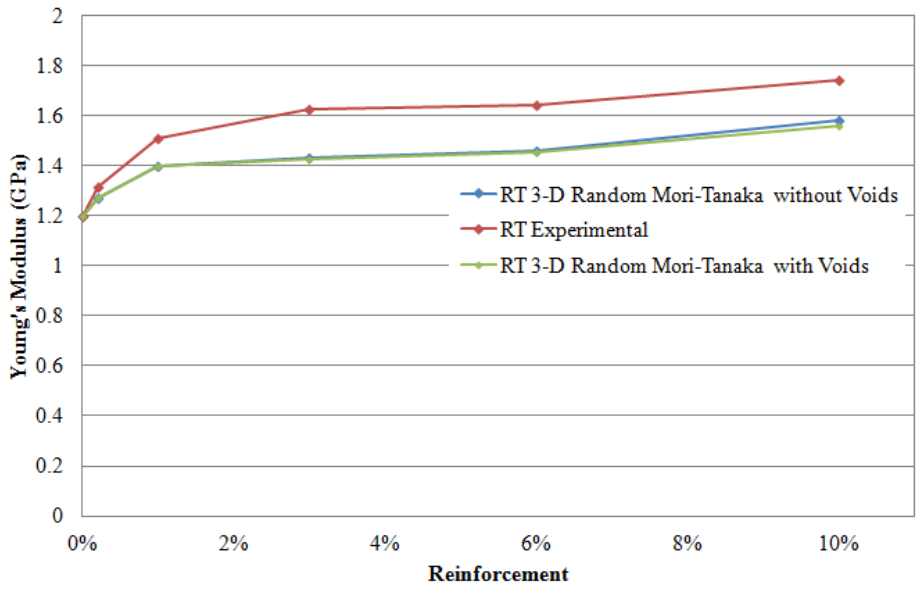


**Figure 4.48** Comparison of Young's modulus obtained from experiments and 3-D random Mori - Tanaka calculations with and without voids at RT

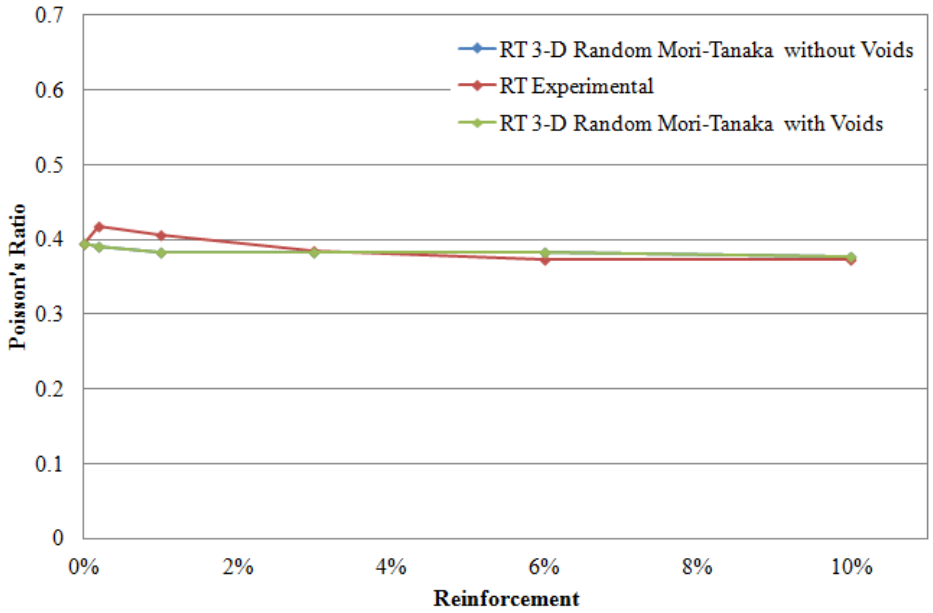


**Figure 4.49** Comparison of Poisson's ratio obtained from experiments and 3-D random Mori - Tanaka calculations with and without voids at RT

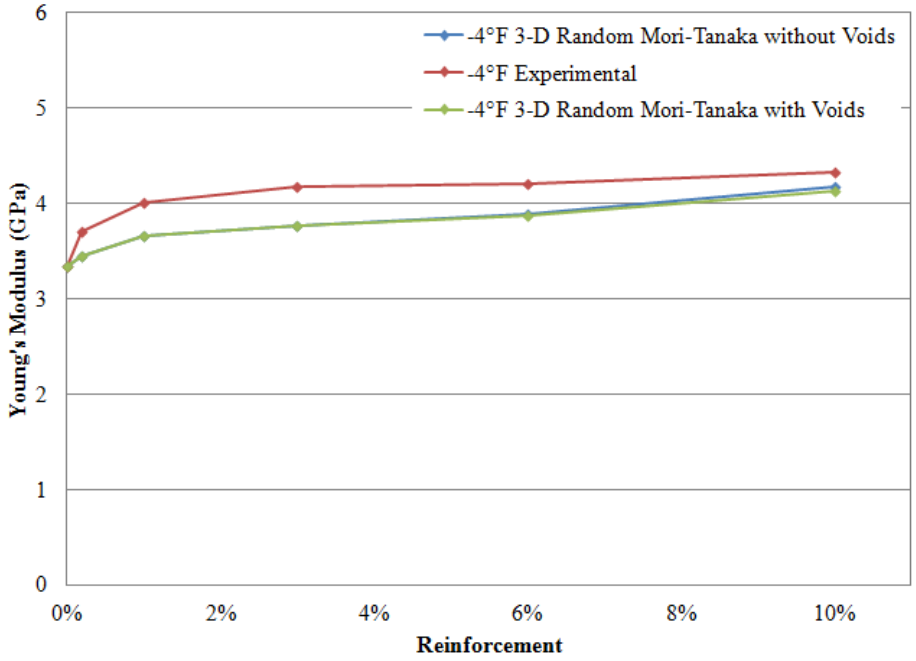


**Figure 4.50** Comparison of Young's modulus obtained from experiments and 3-D random Mori - Tanaka calculations with and without voids at -4°F

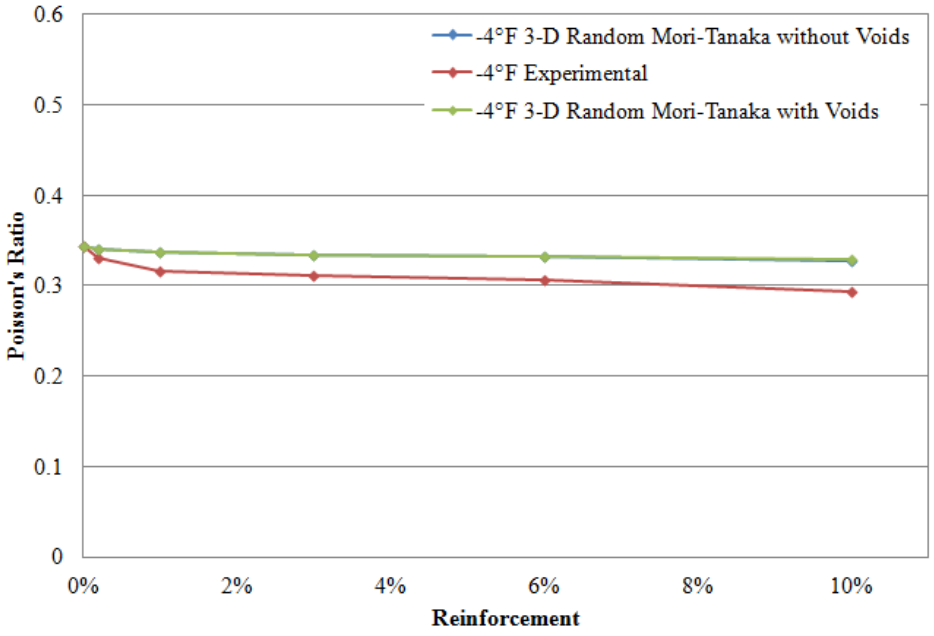


**Figure 4.51** Comparison of Poisson's ratio obtained from experiments and 3-D random Mori - Tanaka calculations with and without voids at -4°F

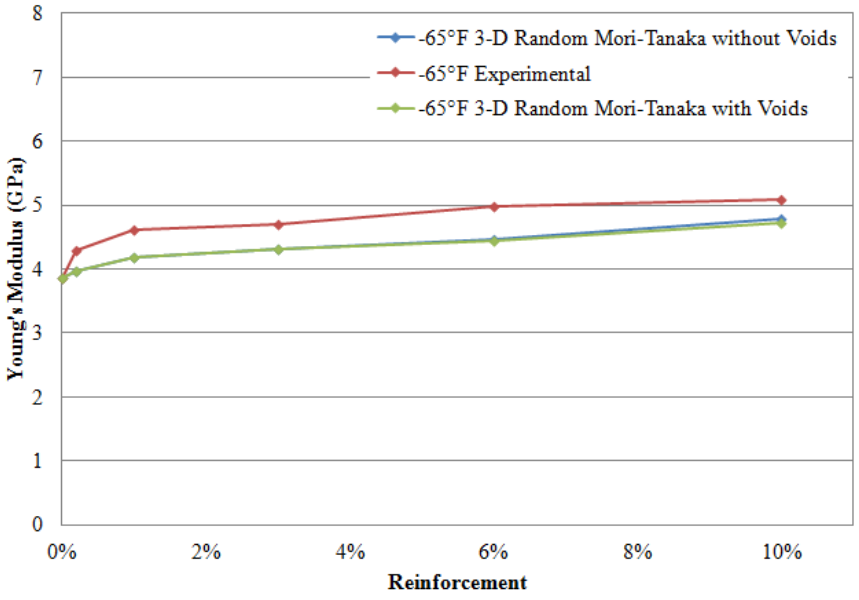


**Figure 4.52** Comparison of Young's modulus obtained from experiments and 3-D random Mori - Tanaka calculations with and without voids at -65°F

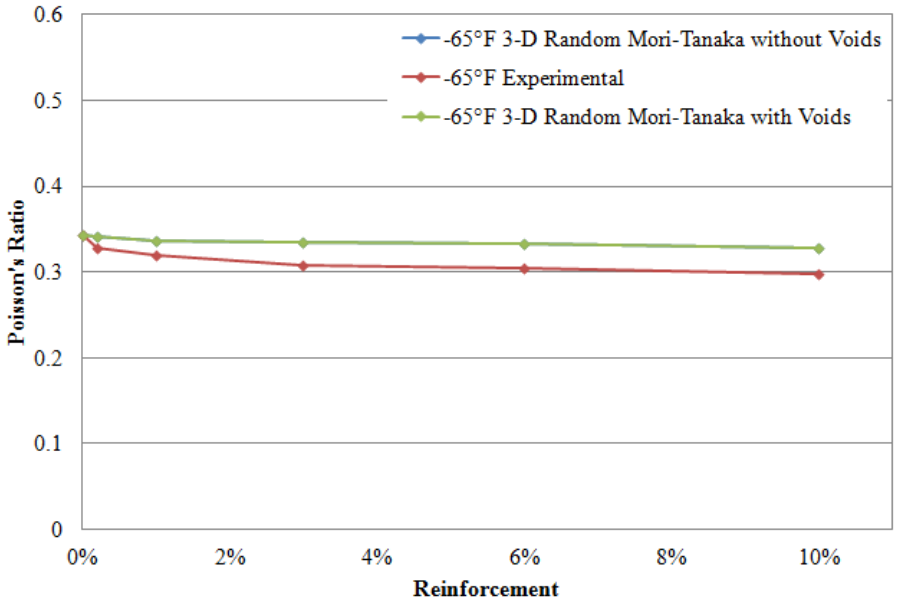


**Figure 4.53** Comparison of Poisson's ratio obtained from experiments and 3-D random Mori - Tanaka calculations with and without voids at -65°F

In general, the 3- D random Mori - Tanaka calculations give lower Young's modulus values than the experimental results and the inclusion of voids does not materially change the results.

### 4.1.4 Modification of Mori-Tanaka Model with the Inclusion of Temperature Effects

The Figures in sections 4.1.2 show that at the higher temperatures the Mori-Tanaka results do not match the experimental results well.

Since nanoclay reinforced PP specimens don't show a pronounced linear material behavior at high temperatures and Mori-Tanaka calculations depend on linear material properties, we decided to include the temperature effect into the Mori-Tanaka calculations for 120°F and 160° by redefining the Young's modulus.

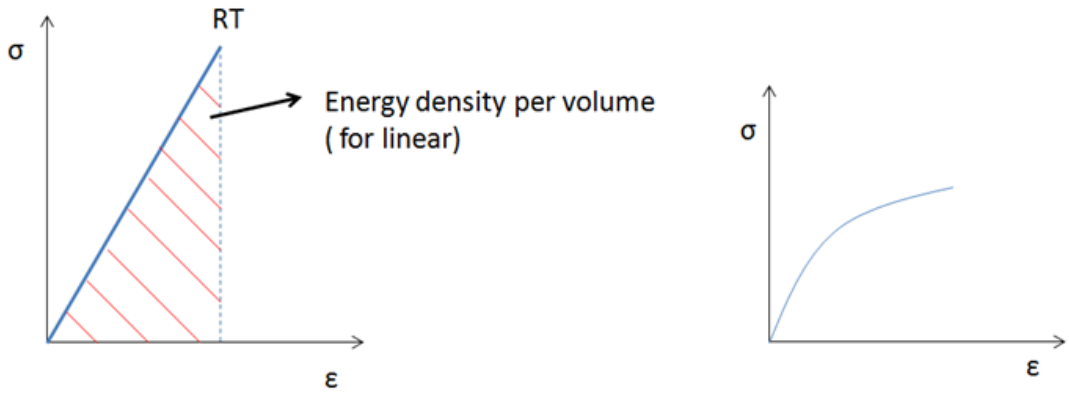


**Figure 4.54** Stress vs. strain curves for linear and non- linear materials

At room temperature we have a clear linear behavior for low strains (or stresses) and we can calculate the energy density per volume. But when we perform the tensile tests at higher temperatures the linear portion of the curve is less pronounced and the curve is more-or-less nonlinear (Figure 4.54). Even though we did not do unloading during the tensile tests, we believe that at higher temperatures the material shows viscoelastic behavior.

Due to viscoelastic behavior, at high temperatures there is energy loss during unloading as shown in Figure 4.55. Considering the nonlinear behavior of the material, at high temperatures

we believe that it is more appropriate to use the secant rather than the tangent in calculating the Young's modulus.

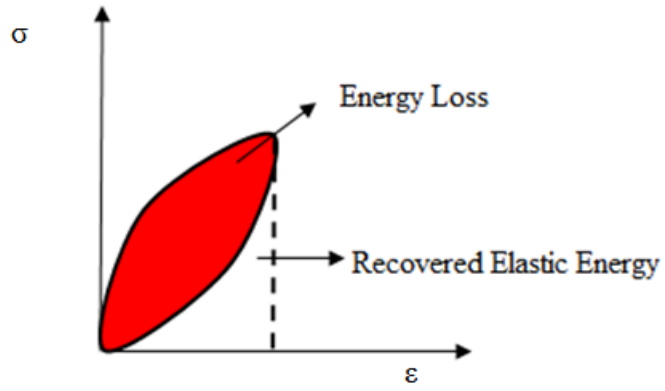


**Figure 4.55** Stress vs. strain curves for viscoelastic behavior and lost energy.

To calculate the Young's modulus at 120°F and 160°F we assume that the elastic energy density (recoverable energy) in calculating the Young's modulus at room temperature is the same at high temperatures.

Figure 4.56 shows schematically the secant line and the elastic energy density using the stress-strain curve at 120°F and 160°F.

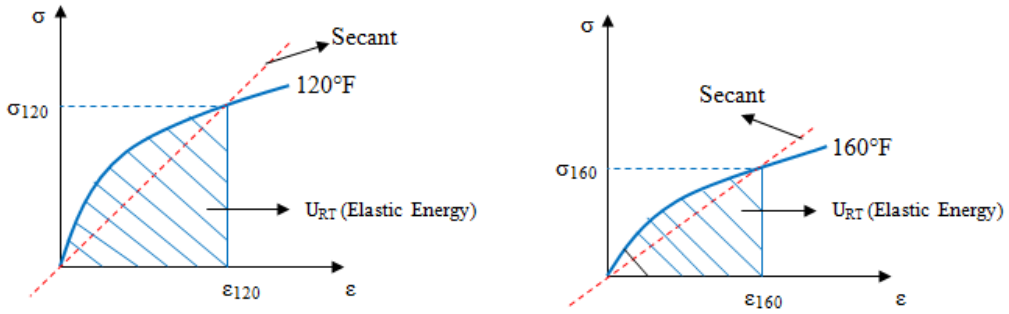


**Figure 4.56** Calculation of secant Young's modulus from nonlinear material curve at 120°F and 160°F

First we calculate the strain energy density from the linear portion of the stress-strain curve at room temperature and then use this elastic energy to determine the strain (or stress) to be used in the calculation of the secant Young's modulus at higher temperatures.

Using this procedure we recalculated the Young's Modulus of neat PP specimens at 120°F and 160°F based on the secant line as ( Figure 4.56): $E_{120} = \frac{\sigma_{120}}{\varepsilon_{120}}$; $E_{160} = \frac{\sigma_{160}}{\varepsilon_{160}}$ and we used these new values in the Mori-Tanaka calculations formulas given in Eqs. (1)-(6) and the composition assumed in Table 4.20 to calculate the elastic properties.

This temperature effect assumption was considered only for oriented particles in the Mori-Tanaka calculations.

In Figures 4.57, the Young's modulus values at 120ºF obtained experimentally and with Mori-Tanaka calculations using the tangent or secant definitions are plotted vs. nanoclay reinforcement percentage. Table 4.21 also shows the same results and the comparison of experimental Young's modulus with Mori-Tanaka calculations depending on the tangent or secant assumptions.

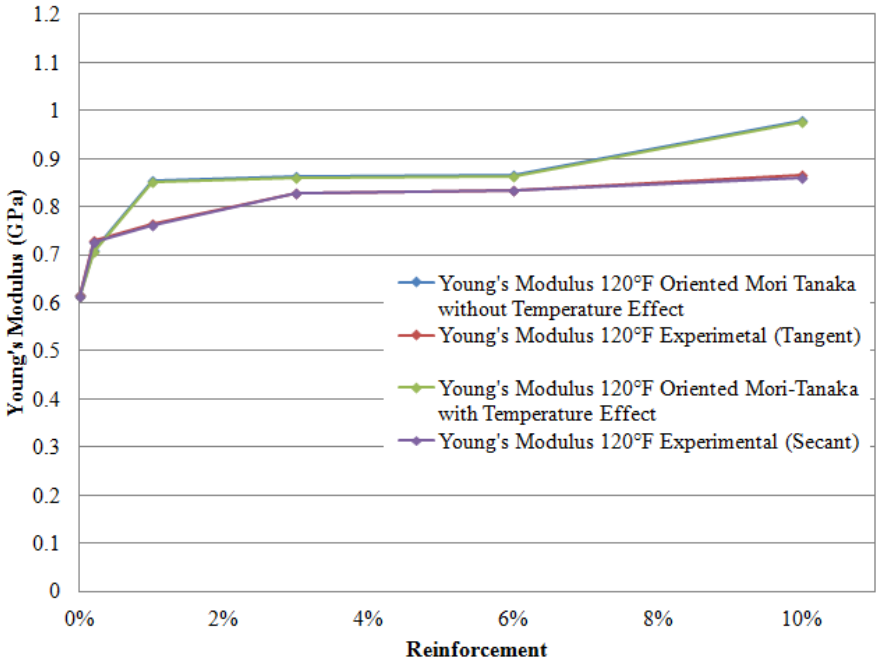


**Figure 4.57** Comparison of experimental and calculated Young's Modulus values at 120°F

**Table 4.21** Young's Modulus values based on tangent and secant calculations at 120°F

| 120°F | YM Exp. (GPa) (Tangent) | YM Mori- Tanaka Without Temperature Effect (GPa) | YM Exp (Secant) (GPa) | YM Mori-Tanaka With Temp. Effect (GPa) |
|---|---|---|---|---|
| 0% | 0.61595 | 0.61595 | 0.61389 | 0.61389 |
| 0.2% | 0.7285 | 0.7079 | 0.72561 | 0.7057 |
| 1% | 0.7646 | 0.85319 | 0.76208 | 0.85054 |
| 3% | 0.8283 | 0.86217 | 0.82759 | 0.85941 |
| 6% | 0.8332 | 0.8664 | 0.8328 | 0.8635 |
| 10% | 0.8664 | 0.9789 | 0.85936 | 0.9757 |

In Figure 4.58 the experimental and Mori-Tanaka results at 160ºF are compared using the tangent and secant calculations. The same values are also given in Table 4.22.

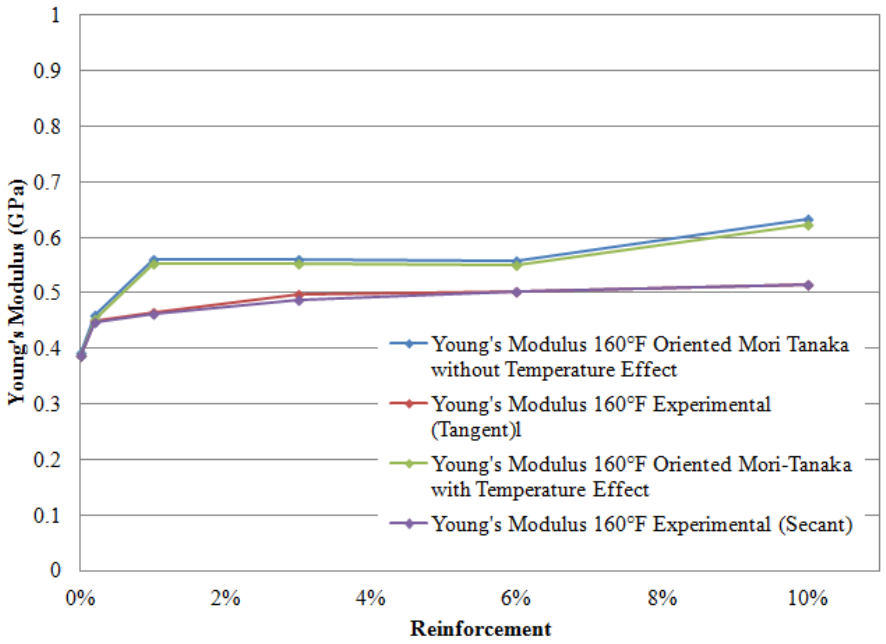


**Figure 4.58** Comparison of experimental and calculated Young's Modulus values for at 160°F

**Table 4.22** Young's Modulus values based on tangent and secant calculations at 160°F

| 160°F | YM Exp. (GPa) (Tangent) | YM Mori- Tanaka Without Temperature Effect(GPa) | YM Exp (Secant) (GPa) | YM Mori-Tanaka With Temp. Effect (GPa) |
|---|---|---|---|---|
| 0% | 0.39204 | 0.39204 | 0.38639 | 0.38639 |
| 0.2% | 0.4499 | 0.4586 | 0.44771 | 0.4522 |
| 1% | 0.4654 | 0.4654 | 0.46195 | 0.55355 |
| 3% | 0.4969 | 0.4969 | 0.48835 | 0.55199 |
| 6% | 0.5031 | 0.5583 | 0.50229 | 0.5504 |
| 10% | 0.5146 | 0.632 | 0.51415 | 0.623 |

The results in Figures 4.57 and Figure 4.58 show the effect of temperature on the Mori-Tanaka calculations. At 120°F, the temperature effect is not significant, because all the results are close to each other. But at 160°, we can clearly see the temperature effect. Thus at high temperatures since nanoclay reinforced PP specimens don't behave linearly, to obtain more reasonable Mori-Tanaka results one may have to consider the temperature effect by calculating the Young's Modulus values based on the secant assumption.

## 4.2 3-D FINITE ELEMENT MODELING FOR TENSILE TESTING

A 3-D finite element model of the nanocomposite was developed using ABAQUS software. The 3-D model is based on the concept of representative volume of the material.

The representative volume has dimensions of (40 unit) × (40 unit) × (40 unit) and includes the matrix and oriented disk shaped particles (parallel to the loading direction). The number of particles n is adjusted to result in a fixed $\frac{t}{D}$ aspect ratio (used in the Mori-Tanaka calculations) and the desired nanoclay reinforcement percentage which varies from 0.2% to 10%.

To demonstrate how the various particle parameters are calculated, consider the case for 0.2% nanoclay reinforcement. For 0.2% reinforcement, the volume fraction of nanoclay, using Eq.(28) or Table 4.1, is 0.095%.

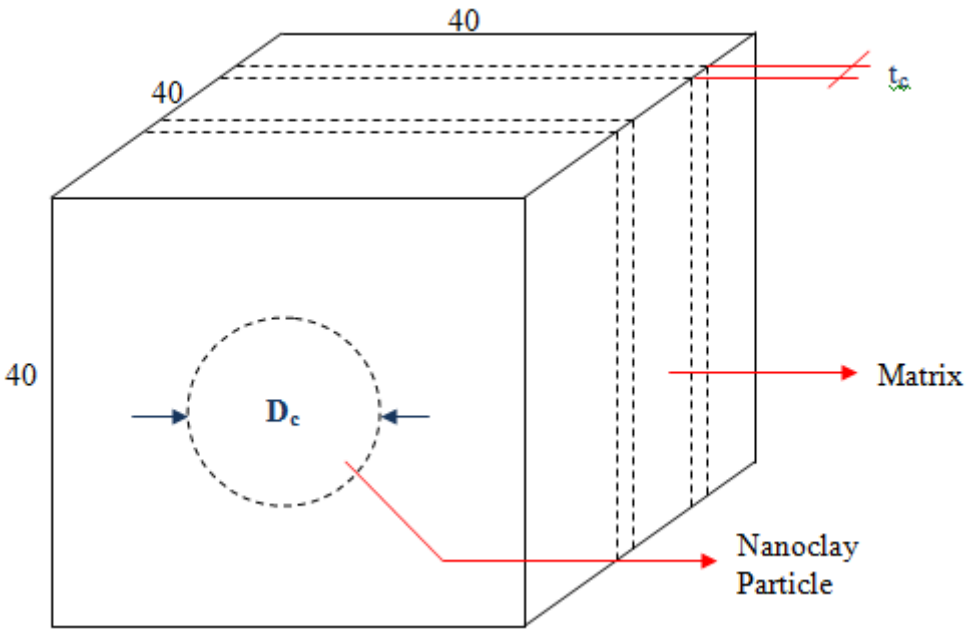


**Figure 4.59** Representative Volume Element

In the previous section for 0.2% the disk diameter and particle thickness were assumed as: D=200 nm and t=0.615 nm.

Thus, $\frac{t}{D} = \frac{1}{325.20}$ or D=325.20t.

To maintain the same aspect ratio, we write

$\frac{t_c}{D_c} = \frac{t}{D} = \frac{1}{325.20}$ or Dc=325.20$t_c$

Then, assuming n=2 and the total volume as V, from the volume fraction equation $t_c$ is found as:

$$\frac{n\frac{\pi D_c^{\,2}}{4}t_c}{V} = c \qquad (66)$$

or

$$\frac{2\pi\left(325.20\right)^2 t_c^{\,3}}{4\left(40\right)^3} = 0.00095 \rightarrow t_c = 0.0715 \text{ unit and } D_c = 23.25 \text{ unit.}$$

For 6% and 10%, $t_c$ and $D_c$ are calculated similarly. For 1% and 3%, since we have particles of different thickness the calculation, though in principle the same, is slightly different. To illustrate this, consider the case of 1% reinforcement.

As explained in section 4.2.2 and Table 4.20, for 1% we use a combination of particles with different thickness. The composition used was 40% of N=1 particles, 30% of N=2 particles and 30% of N=3 particles. The volume fraction c corresponding to 1% is (Table 4.1) 0.48%.

Again, to maintain the same aspect ratios used previously, we calculate the particle thicknesses as follows:

- For N=1 particles, D=200 nm, t=0.615 nm or D=325.20t. If we assume 2 layers with particles of this geometry, then with $D_c$=325.20$t_c$ we obtain:

$$\frac{2\pi\left(325.20\right)^2 t_c^{\,3}}{4\left(40\right)^3} = 0.4\left(0.0048\right) \rightarrow t_c = 0.0904\,\text{unit and } D_c = 29.41\,\text{unit.}$$

- For N=2 particles, D=200 nm, t=3.015 nm or D=66.33t. If we assume 2 layers with particles of this geometry, then with $D_c$=66.33$t_c$ we obtain:

$$\frac{2\pi\left(66.33\right)^2 t_c^{\,3}}{4\left(40\right)^3} = 0.3\left(0.0048\right) \rightarrow t_c = 0.2371\,\text{unit and } D_c = 15.73\,\text{unit.}$$

- For N=3 particles, D=200 nm, t=5.415 nm or D=36.93t. If we assume 1 layer with particles of this geometry, then with $D_c$=36.93$t_c$ we obtain:

$$\frac{\pi\left(36.93\right)^2 t_c^{\,3}}{4\left(40\right)^3} = 0.3\left(0.0048\right) \rightarrow t_c = 0.4414\ \text{unit and } D_c = 16.30\,\text{unit.}$$

The calculations for 3% are similar to those presented above. The calculated particle parameters for each reinforcement percentage are given in Table 4.23.

**Table 4.23** The particle parameters used in the finite element calculation for each reinforcement percentage

| **Reinforcement Percentage** | **n** | **$t_c$** | **$D_c$** |
|---|---|---|---|
| 0.2% | 2 | 0.0715 | 23.25 |
| 1% | 2 | 0.0904 | 29.41 |
| | 2 | 0.2371 | 15.73 |
| | 1 | 0.4414 | 16.30 |
| 3% | 2 | 0.3764 | 24.97 |
| | 2 | 0.5053 | 18.66 |
| | 1 | 0.8131 | 20.81 |
| 6% | 6 | 1.0125 | 19.82 |
| 10% | 10 | 1.1747 | 18.62 |

To explain the methodology used in the finite element model, consider the case for 0.2% reinforcement. Here, we have 2 layers with nanoclay particles, in the PP matrix. Figure 4.60 shows the symmetric finite element model constructed for this case. Then the appropriate boundary conditions were applied. The bottom surface was constrained in y-direction and one point in the middle of the bottom surface was fixed to prevent translational displacement. The boundary conditions and loading are shown in Figure 4.60. For loading, a unit displacement was applied at the top surface.

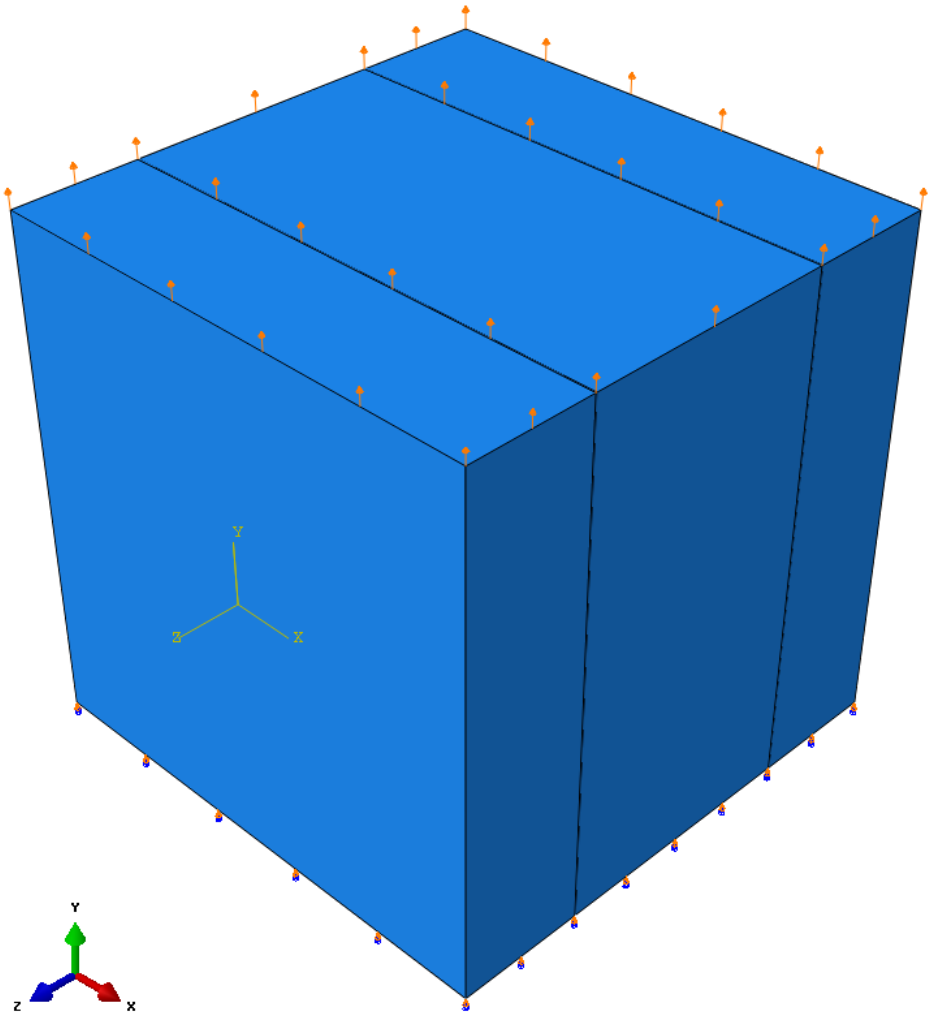


**Figure 4.60** The boundary conditions and displacement loading for the 0.2% specimens

The 3-D finite element mesh is shown in Figure 4.61.

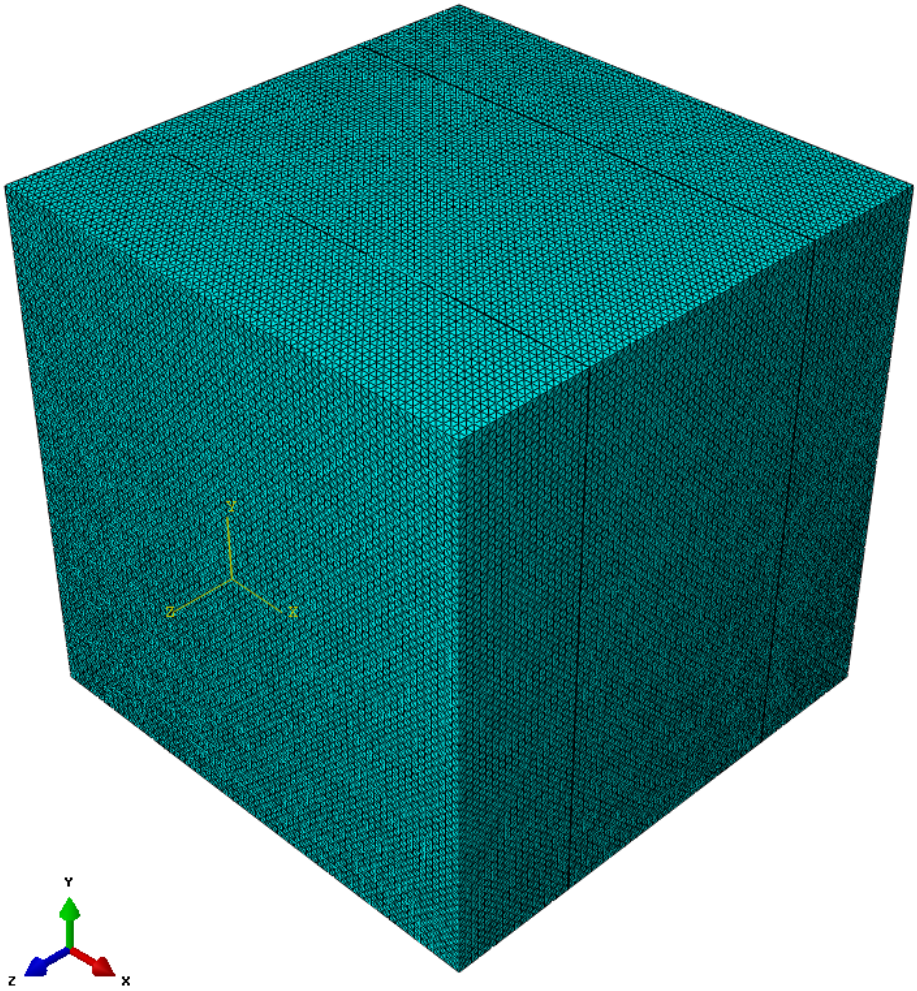


**Figure 4.61** The mesh structure of the finite element model

Some of the 3-D FE results obtained for the 0.2% nanoclay reinforced specimens are shown in Figures 4.62- 4.65.

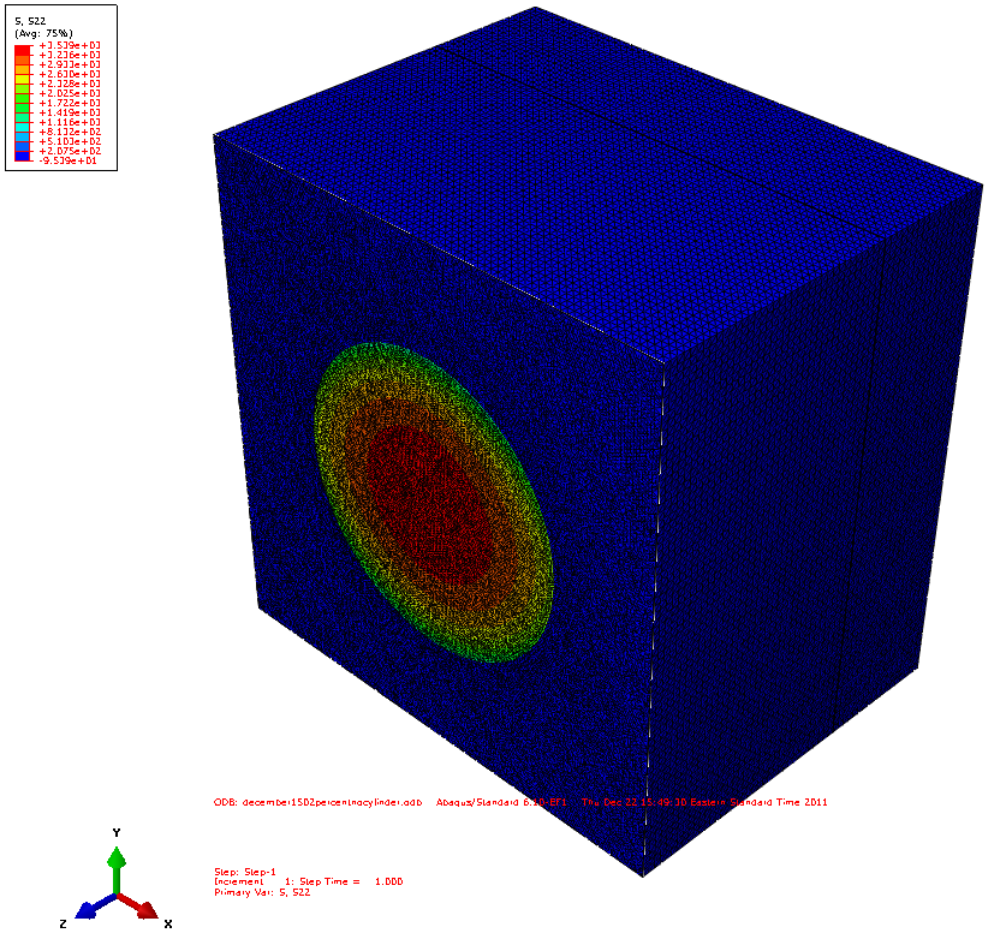


**Figure 4.62** Distribution of stresses in y- direction ($\sigma_{yy}$) at the particle plane

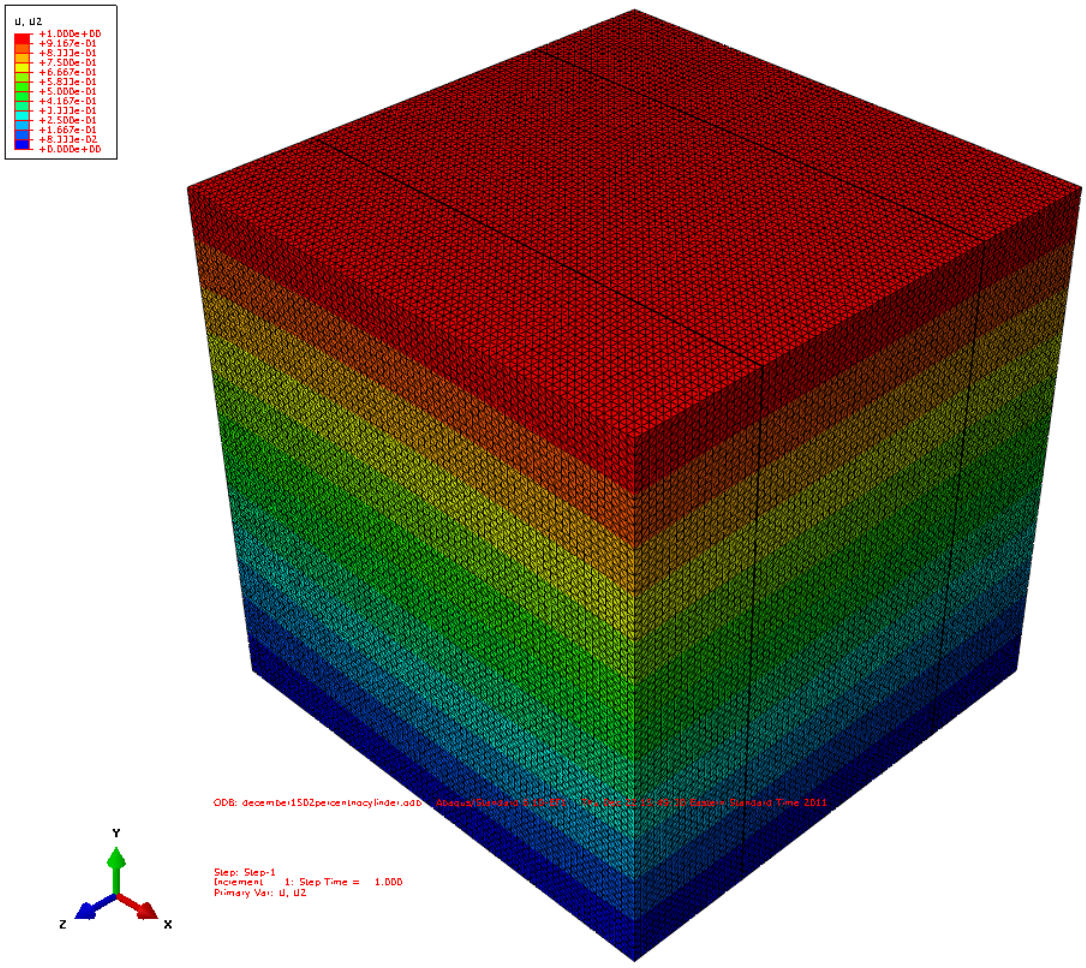


**Figure 4.63** Distribution of y-component of displacement ($U_{yy}$)

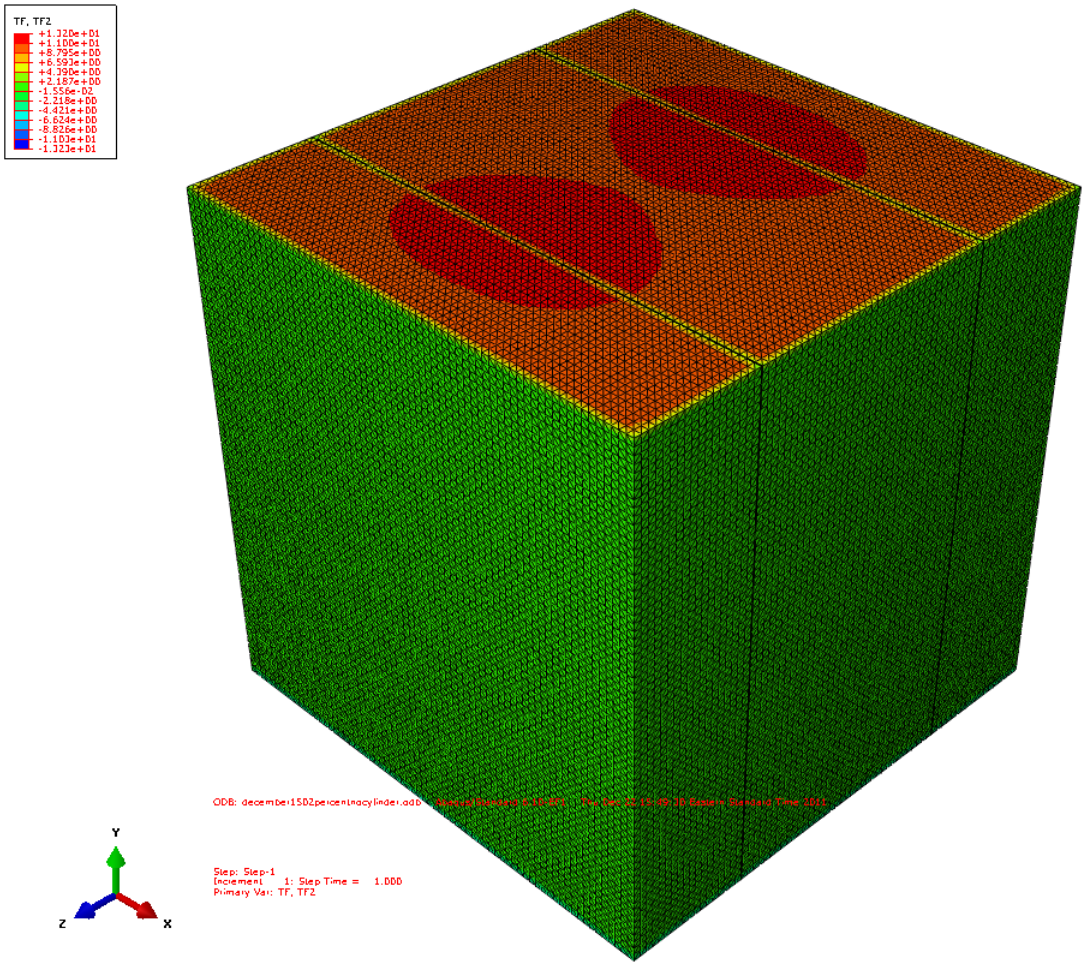


**Figure 4.64** Total force values in y-direction at the nodal points of the top surface ($TF_{yy}$)

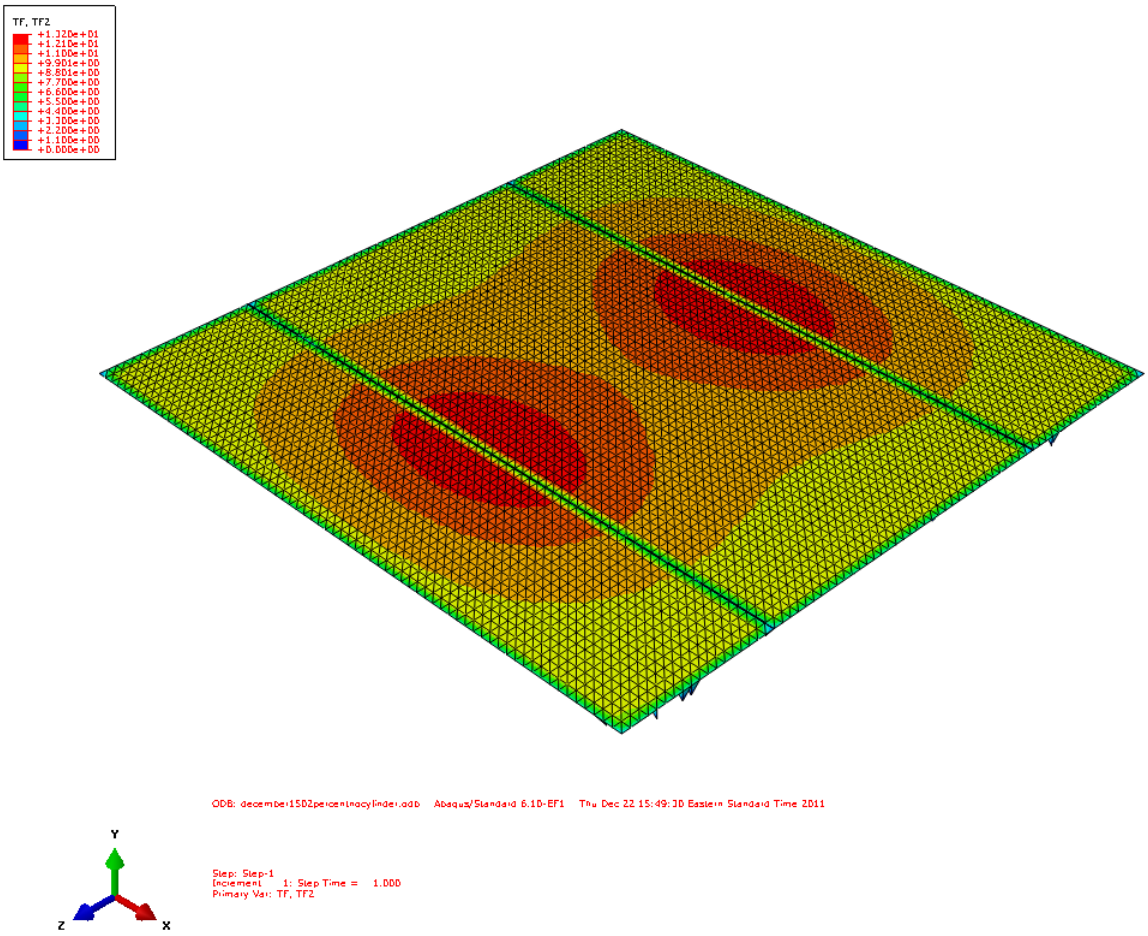


**Figure 4.65** Total force values ($TF_{yy}$) at elements of the top surface

To determine the Young's modulus of the nanocomposite we use the total force values shown in Figure 4.65.

Total force = 52536.5 N

$\sigma_y =$ 32.8353 MPa

$$\varepsilon_y = \frac{1}{40}$$

$$E = \frac{\sigma_y}{\varepsilon_y} = 1.313 \text{ GPa}$$

The Poisson's ratio is determined by using the ratio of the average strains $\varepsilon_x$ and $\varepsilon_y$ as:

$$\nu_{12} = -\frac{\varepsilon_x}{\varepsilon_y} = -\frac{(\Delta u)_{average} / 40}{1/40}$$

$\nu_{12} = 0.3845$

The Young's modulus and the Poisson's ratio were similarly calculated using the finite element technique for the remaining percentages, namely 1%, 3%, 6% and 10% at -65°F, -4°F and RT. The finite element results for Young's modulus and the Poisson's ratio are summarized in Tables 4.24 and 4.25 respectively and compared to those obtained from experiments and the Mori-Tanaka calculations for oriented particles.

**Table 4.24** Comparison of $E/E_m$ values obtained from experiments and the Mori-Tanaka calculations at various temperatures

| | $E/E_m$ | | | |
|---|---|---|---|---|
| **Reinforcement Percentage of PP 3371** | **Temperature** | **Experimental** | **Mori-Tanaka Calculation (Oriented)** | **FEM** |
| 0.2% | *-65ºF (-54ºC)* | 1.1083 | 1.0551 | 1.0489 |
| | *-4 ºF (-20ºC)* | 1.1095 | 1.0612 | 1.0539 |
| | *Room Temp.* | 1.0976 | 1.1148 | 1.0945 |
| 1% | *-65ºF (-54ºC)* | 1.1909 | 1.1559 | 1.1390 |
| | *-4 ºF (-20ºC)* | 1.1977 | 1.1722 | 1.1521 |
| | *Room Temp.* | 1.2569 | 1.3048 | 1.2544 |
| 3% | *-65ºF (-54ºC)* | 1.2146 | 1.2118 | 1.1757 |
| | *-4 ºF (-20ºC)* | 1.2487 | 1.2289 | 1.1877 |
| | *Room Temp.* | 1.3564 | 1.3458 | 1.2668 |
| 6% | *-65ºF (-54ºC)* | 1.2867 | 1.2498 | 1.2066 |
| | *-4 ºF (-20ºC)* | 1.2587 | 1.2638 | 1.2162 |
| | *Room Temp.* | 1.3718 | 1.3443 | 1.2751 |
| 10% | *-65ºF (-54ºC)* | 1.3174 | 1.4023 | 1.2452 |
| | *-4 ºF (-20ºC)* | 1.2948 | 1.4239 | 1.2533 |
| | *Room Temp.* | 1.4520 | 1.5455 | 1.3055 |

**Table 4.25** Comparison of $v_{12}/v_m$ values obtained from experiments and the Mori-Tanaka calculations at various temperatures $v_{12}/v_m$

| | $v_{12}/v_m$ | | | |
|---|---|---|---|---|
| **Reinforcement Percentage of PP 3371** | **Temperature** | **Experimental** | **Mori-Tanaka Calculation (Oriented)** | **FEM** |
| 0.2% | *-65ºF (-54ºC)* | 0.9574 | 1.0111 | 0.9798 |
| | *-4 ºF (-20ºC)* | 0.9618 | 1.0125 | 0.9869 |
| | *Room Temp.* | 1.0557 | 1.0317 | 0.9742 |
| 1% | *-65ºF (-54ºC)* | 0.9311 | 1.0281 | 0.9813 |
| | *-4 ºF (-20ºC)* | 0.9179 | 1.0312 | 0.9805 |
| | *Room Temp.* | 1.0276 | 1.0681 | 0.9764 |
| 3% | *-65ºF (-54ºC)* | 0.8970 | 1.0388 | 0.9725 |
| | *-4 ºF (-20ºC)* | 0.9057 | 1.0425 | 0.9724 |
| | *Room Temp.* | 0.9759 | 1.0813 | 0.9724 |
| 6% | *-65ºF (-54ºC)* | 0.8863 | 1.0462 | 0.9956 |
| | *-4 ºF (-20ºC)* | 0.8888 | 1.0497 | 0.9974 |
| | *Room Temp.* | 0.9429 | 1.0815 | 1.0106 |
| 10% | *-65ºF (-54ºC)* | 0.8699 | 1.0665 | 1.0382 |
| | *-4 ºF (-20ºC)* | 0.8516 | 1.0713 | 1.0418 |
| | *Room Temp.* | 0.9437 | 1.1140 | 1.0689 |

The results also are depicted in Figures 4.67-4.72.

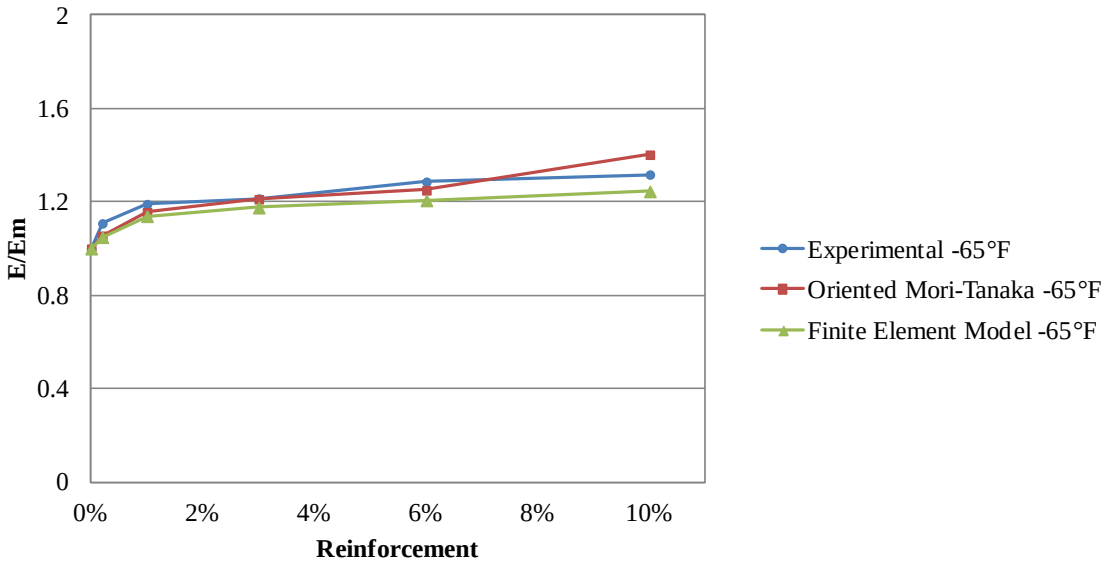


**Figure 4.66** Comparison of $E/E_m$ values obtained from the experimentally, Mori-Tanaka calculation and the finite element model at -65°F

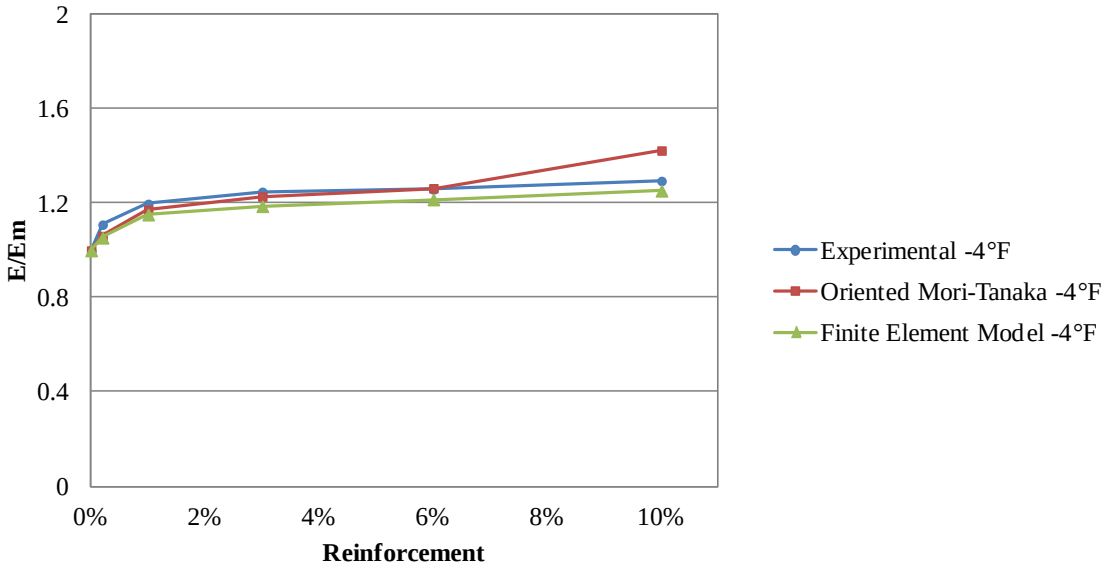


**Figure 4.67** Comparison of $E/E_m$ values obtained from the experimentally, Mori-Tanaka calculation and the finite element model at -4°F

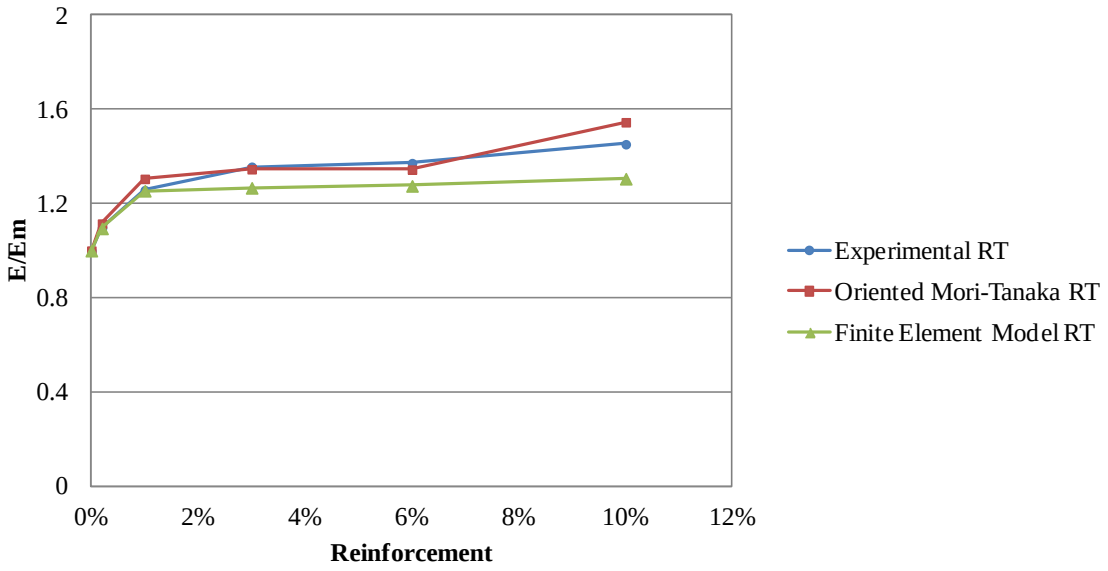


**Figure 4.68** Comparison of $E/E_m$ values obtained from the experimentally, Mori-Tanaka calculation and the finite element model at room temperature

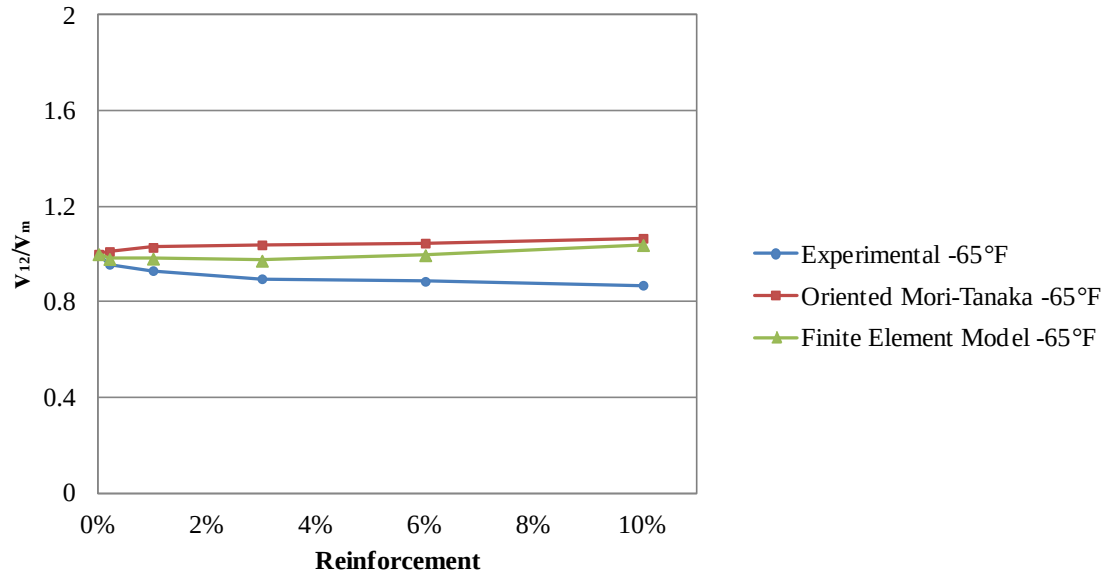


**Figure 4.69** Comparison of $\nu_{12}/\nu_m$ values obtained from the experimentally, Mori-Tanaka calculation and the finite element model at -65°F

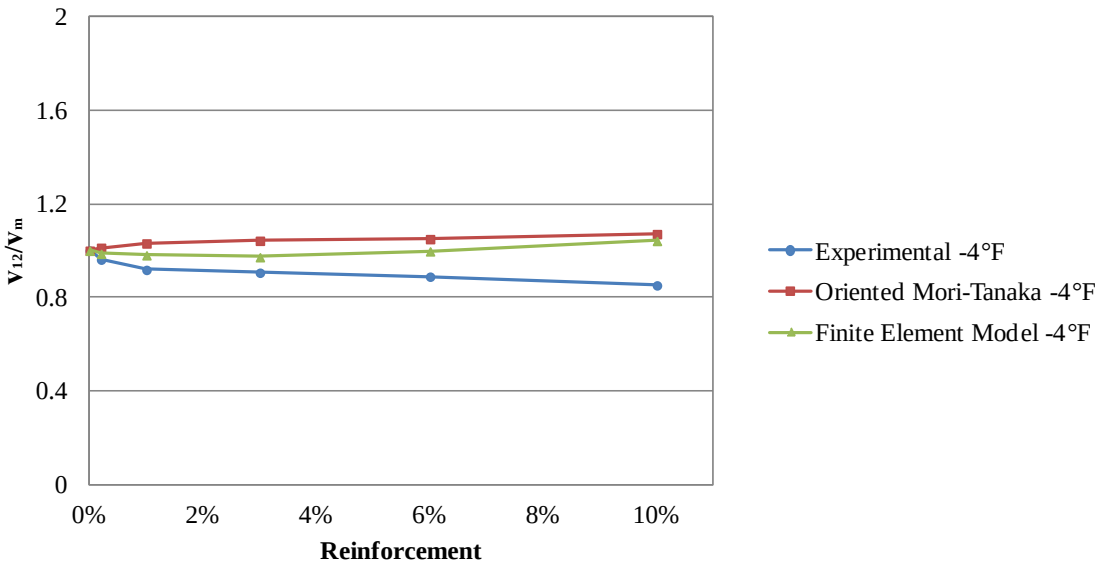


**Figure 4.70** Comparison of $v_{12}/v_m$ values obtained from the experimentally, Mori-Tanaka calculation and the finite element model at -4°F

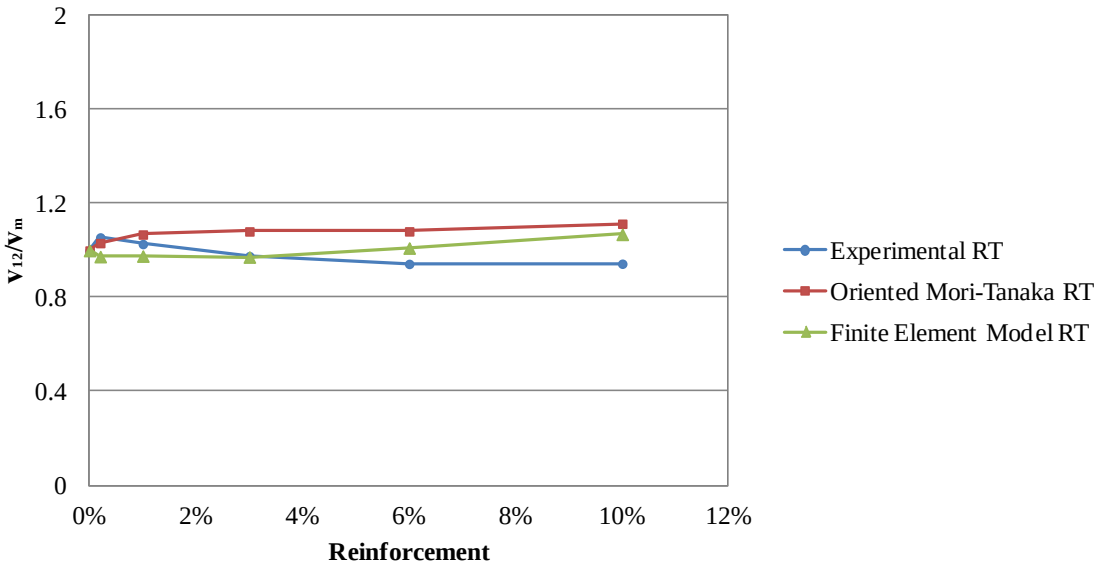


**Figure 4.71** Comparison of $v_{12}/v_m$ values obtained from the experimentally, Mori-Tanaka calculation and the finite element model at room temperature

The results given in Tables 4.24 and 4.25 and Figures 4.66-4.71 indicate that the finite element model may be a good predictive tool to determine the elastic properties of nanoclay reinforced polymers.

## 5. DISCUSSION AND CONCLUSIONS

An experimental and analytical study was conducted to study the mechanical properties of nanoclay reinforced polymer based composites. Also, a hierarchical multi-scale model to predict the properties of nanocomposites was constructed.

The experimental results were displayed as stress-strain curves at each reinforcement percentage and for various temperatures. Basic mechanical properties such as Young's modulus, Poisson's ratio and strength were calculated from the stress-strain curves and displayed graphically and tabular form. A careful analysis of the results indicates that both nanoclay reinforcement percentage and temperature have significant effect on the mechanical properties. For example an increase in nanoclay reinforcement improves both the stiffness and the strength of the material. The improvement in strength is especially more pronounced at lower percentages. Temperature has the reverse effect. At higher temperatures both the strength and stiffness of the material decrease, while at lower temperatures the material becomes stronger and stiffer. Also as at higher temperatures the material is highly ductile, but very brittle at lower temperatures. The plots of Young's modulus vs. temperature indicate that there is a drastic drop in the Young's modulus values as the temperature increases from -4°F to RT (~70°F). The reason for this drastic change is that PP has a glass transition temperature (GTT) of approximately 15°F and as the temperature is increased beyond the GTT, the material transitions from the glassy state resulting in the decrease observed in the value of the Young's modulus. Finally, it is also observed that the effect of temperature is more significant than that of nanoclay reinforcement.

The drop-weight test results were less revealing. It was observed that at RT as expected for 1% or higher reinforcement, the material became more brittle and most specimens were penetrated

upon impact. Temperature also had a significant effect on the impact behavior of the composite. At higher temperatures no specimen was penetrated even at 10% reinforcement. However, at lower temperatures all specimens were penetrated.

The epoxy based nanocomposite specimens had very different mechanical properties compared to PP based specimens. They had higher Young's modulus and very low failure strain which may be attributed to the brittle behavior of epoxy. It was also observed that the use of different PP resins resulted in significant change in the behavior of the nanocomposite.

Theoretical predictions using the Mori-Tanaka formulation and the finite element method (FEM) were obtained and compared with the experimental results. The predictions from the Mori-Tanaka calculations, in general, compared well with the experimental results, except at higher temperatures and higher reinforcement percentages. To improve the Mori-Tanaka calculations, the model was modified to include the effect of voids and temperature. The results obtained from the modified Mori-Tanaka calculations improved the match between the theoretical and experimental results.

For the finite element calculations, a representative volume element was constructed. Even though good match was obtained for low reinforcement percentages, the FE results were somewhat lower at higher percentages. This may be due to the approximate boundary conditions assumed in the FE calculations.

The following conclusions can be drawn:

a. The experimental results indicate that for nanoclay reinforced PP specimens as the percentage of reinforcement increases the Young's modulus and the ultimate stress of the nanocomposite also increase.

b. Temperature has a significant effect on the behavior of the nanocomposites. For PP based nanocomposites high temperature has a deleterious effect on the material properties. As the temperature increases, the Young's modulus and the ultimate tensile stress of the nanocomposites decrease. However, as the temperature decreases, the Young's modulus and ultimate tensile stress increase. At low temperatures the material becomes brittle and fails at relatively low strains.

c. The type of resin used has significant effect on the properties of the nanocomposite.

d. The results of drop weight impact tests indicate that the addition of nanoclay to PP made the specimens more brittle and most were penetrated at 1% or higher percentages at room temperature. At lower temperatures all specimens were penetrated. However, at higher temperatures no penetration was observed.

e. With a proper choice of geometric and material properties for the constituents, the Mori-Tanaka formulation may be a good tool in predicting the Young's modulus. The Mori-Tanaka results, especially those obtained for oriented particles, matched well with the experiments, except at high temperatures and high reinforcement percentages.

f. Inclusion of voids in the Mori-Tanaka formulation gave a somewhat better match with experimental data at higher reinforcement percentages.

g. The effect of temperature was included by using the secant instead of the tangent calculation for the Young's modulus. As a consequence, better match with experiments was obtained at higher temperatures.

h. The 3-D finite element model also provides a good estimate for the Young's modulus of the nanocomposite. As the results displayed in the figures show, the finite element results compare well with those obtained experimentally.

## 6. FUTURE WORK

The research outlined in this thesis opens new research venues on nanoclay reinforced polymers.The following future topics are suggested by the author:

a. Detailed electron microscopy study of the nanocomposite to determine the dispersion patterns of nanoclay in the matrix. This will enable the research to construct better predictive models.
b. Study of the effect of clay particles on fire retardation and toxicity.
c. Addition of nanoclay in fabric or fiber reinforced polymers to design better armor materials.
d. Develop a finite element model for randomly distributed particles.

## 7. REFERENCES


1. Kojima Y., Usuki A., Kawasumi M., Okada A., Fukushima Y., Kurauchi T., et al. *Mechanical properties of nylon 6-clay hybrid,* J. Mater Res., Volume 8, 1993, Pages 1185-1189.

2. Kojima Y, Usuki A, Kawasumi M, Okada A, Kurauchi T, Kamigaito O. Journal Polym Sci. Part A 1993; 31: 983.

3. Kojima Y, Usuki A, Kawasumi M, Okada A, Kurauchi T, Kamigaito O. J Polym Sci Part A 1993; 31: 1755

4. Liu L, Qi Z, Zhu X. J Appl Polym Sci 1999; 71: 1133.

5. Gilman W, Morgan A, Giannelis P, Wuthenow M, Manias E. Flame Retardancy 10th Annual BBC Conference Proceedings 1999; 1

6. Giannelis P. Appl Organomet Chem 1998; 12: 675.

7. Okada A, Kawasumi M, Usuki A, Kojima Y, Kurauchi T, Kamigaito O. In: Schaefer W, Mark E, editors. Polymer based molecular composites MRS Symposium Proceedings. Pittsburgh; 1990; vol. 171:45–50.

8. Giannelis P. Adv Mater 1996; 8: 29.

9. Giannelis EP, Krishnamoorti R, Manias E. Adv Polym Sci 1999; 138: 107.

10. LeBaron PC, Wang Z, Pinnavaia TJ. Appl Clay Sci 1999; 15: 11.

11. Vaia RA, Price G, Ruth PN, Nguyen HT, Lichtenhan J. Appl Clay Sci 1999; 15:67.

12. Biswas M, Sinha S. Adv Polym Sci 2001; 155: 167.

13. Gilman JW. Appl, Clay Sci. 1999; 15: 31.

14. Bins & Associates. Plastics Additives & Compounding 2002; 4(1): 30-33.

15. Lan T, Kaviratna PD, Pinnavaia TJ. Chem Mater 1994; 6: 573.

16. Gilman JW, Kashiwagi T, Lichtenhan JD. SAMPE J 1997; 33: 40.

17. Gilman JW. Appl Clay Sci 1999; 15: 31.

18. Dabrowski F, Bras L, Bourbigot S, Gilman JW, Kashiwagi T. Proceedings of the Eurofillers. Lyon-Villeurbanne, France 1999; 6:9.

19. Bourbigot S, LeBras M, Dabrowski F, Gilman JW, Kashiwagi T. Fire Mater 2000; 24:201.

20. Gilman JW, Jackson CL, Morgan AB, Harris R, Manias E, Giannelis EP, Wuthenow M, Hilton D, Phillips H. Chem Mater 2000; 12: 1866.

21. Kojima Y., Usuki A., Kawasumi M., Okada A., Fukushima Y., Kurauchi T., et al. *Sorption of water in nylon 6-clay hybrid*, J. Appl. Polym. Sci., Volume 49, 1993, Pages 1259-1264.

22. Nguyen Q. T., *Process for Improving Exfoliation and Dispersion of Nanoclay Particles into Polymer Matrices Using Supercritical Carbon Dioxide.* PhD. Dissertation , Blacksburg, VA, 2007.

23. Masenelli-Varlot K., Reynaud E., Vigier G., and Varlet J., Mechanical properties of clay-reinforced polyamide. *J. Polymer. Sci*., Part B: Polymer. Phys., 40 (2002), pp. 272.

24. Okada A., Fukoshima Y., Inagaki S., Usuki A., Sugiyama S., Kurashi T., Kamigaito O., U.S. 4,739,007 (1998).

25. Kato M., Usuki A. and Okada A., Synthesis of polypropylene oligomer - clay intercalation compounds. *J Appl Polym Sci* 66 (1997), pp. 1781.

26. Kawasumi M., Hasegawa N., Kato M., Usuki A. and Okada A., Preparation and Mechanical Properties of Polypropylene-Clay Hybrids. *Macromolecules* 30 (1997), pp. 6333.

27. Hasegawa N., Kawasumi M., Kato M., Usuki A. and Okada A., Preparation and mechanical properties of polypropylene-clay hybrids using a maleic anhydride-modified polypropylene oligomer *J Appl Polym Sci* 67 (1998), p. 87.

28. Liu X. and Wu Q., PP/clay nanocomposites prepared by grafting-melt intercalation. *Polymer* 42 (2001), p. 10013.

29. Nam P.H., Maiti P., Okamoto M., Kotaka T., Hasegawa N. and Usuki A., A hierarchical structure and properties of intercalated polypropylene/clay nanocomposites. *Polymer* 42 (2001), p. 9633.

30. Kurokawa Y., Yasuda H. and Oya A., Preparation of nanocomposites of polypropylene and smectite. *J Mater Sci Lett* 15 (1996), pp. 1481–1487.

31. Furuichi N., Kurokawa Y., Fujita K., Oya A., Yasuda H. and Kiso M., Preparation and properties of polypropylene reinforced by smectite. *J Mater Sci* 31 (1996), pp. 4307–4310.

32. Tudor J., Willington L., O'Hare D. and Royan B., Intercalation of catalytically active metal complexes in phyllosilicates and their application as propene polymerization catalyst. *Chem Commun* (1996), pp. 2031–2032.

33. Kurokawa Y., Yasuda H., Kashiwagi M. and Oya A., Structure and properties of a montmorillonite/polypropylene nanocomposite. *J Mater Sci Lett* 16 (1997), pp. 1670–1672

34. Nyden R. and Gilman J.W., Molecular dynamics simulations of the thermal degradation of nano-confined polypropylene. *Comput Theor Polym Sci* 7 (1997), pp. 191–198.

35. Kato M., Usuki A. and Okada A., Synthesis of polypropylene oligomer–clay intercalation compounds. *J Appl Polym Sci* 66 (1997), pp. 1781–1785

36. Usuki A., Kato M., Okada A. and Kurauchi T., Synthesis of polypropylene–clay hybrid. *J Appl Polym Sci,* 63 (1997), pp. 137–138.

37. Kawasumi M., Hasegawa N., Kato M., Usuki A. and Okada A., Preparation and mechanical properties of polypropylene–clay hybrids. *Macromolecules* 30 (1997), pp. 6333–6338.

38. Hasegawa N., Kawasumi M., Kato M., Usuki A. and Okada A., Preparation and mechanical properties of polypropylene–clay hybrids using a maleic anhydride-modified polypropylene oligomer. *J Appl Polym Sci* 67 (1998), pp. 87–92.

39. Oya A., Polypropylene–clay nanocomposites. In: T.J. Pinnavaia and G.W. Beall, Editors, *Polymer–clay nanocomposites*, Wiley, London (2000), pp. 151–172.

40. Hasegawa N., Okamoto H., Kato M. and Usuki A., Preparation and mechanical properties of polypropylene–clay hybrids based on modified polypropylene and organophilic clay. *J Appl Polym Sci* 78 (2000), pp. 1918–1922.

41. Oya A., Kurokawa Y. and Yasuda H., Factors controlling mechanical properties of clay mineral/polypropylene nanocomposites. *J Mater Sci* 35 (2000), pp. 1045–1050.

42. Lee J.W., Lim Y.T. and Park O.O., Thermal characteristics of organoclay and their effects upon the formation of polypropylene/organoclay nanocomposites. *Polym Bull* 45 (2000), pp. 191–198.

43. Zhang Q., Fu Q., Jiang L. and Lei Y., Preparation and properties of polypropylene/montmorillonite layered nanocomposites. *Polym Int* 49 (2000), pp. 1561–1564.

44. Garces J.M., Moll D.J., Bicerano J., Fibiger R. and McLeod D.G., Polymeric nanocomposites for automotive applications. *Adv Mater* 12 (2000), pp. 1835–1839

45. Hasegawa N., Okamoto H., Kawasumi M., Kato M., Tsukigase A. and Usuki A., Polyolefin–clay hybrids based on modified polyolefins and organoclay. *Macromol Mater Engng* 280/281 (2000), pp. 76–79.

46. Hambir S., Bulakh N., Kodgire P., Kalgaonkar R. and Jog J.P., PP/clay nanocomposites: a study of crystallization and dynamic mechanical behavior. *J Polym Sci, Part B: Polym Phys* 39 (2001), pp. 446–450.

47. Zanetti M., Camino G., Reichert P. and Mulhaupt R., Thermal behaviour of poly(propylene) layered silicate nanocomposites. *Macromol Rapid Commun* 22 (2001), pp. 176–180.

48. Galgali G., Ramesh C. and Lele A., A rheological study on the kinetics of hybrid formation in propylene nanocomposites. *Macromolecules* 34 (2001), pp. 852–858.

49. Solomon M.J., Almusallam A.S., Seefeldt K.F., Somwangthanaroj A. and Varadan

P., Rheology of polypropylene/clay hybrid materials. *Macromolecules* 34 (2001), pp. 1864–1872.

50. Gloaguen J.M. and Lefebvre J.M., Plastic deformation behavior of thermoplastic/clay nanocomposites. *Polymer* 42 (2001), pp. 5841–5847.

51. Garcia-Martinez J.M., Laguna O., Areso S. and Collar E.P., Polypropylene/mica composites modified by succinic anhydride-grafted atactic polypropylene: a thermal and mechanical study under dynamic conditions. *J Appl Polym Sci* 81 (2001), pp. 625–636.

52. Schmidt D., Shah D. and Giannelis E.P., New advances in polymer/layered silicate nanocomposites. *Curr Opin Solid State Mater Sci*, 6 (2002), pp. 205–212.

53. Reichert P., Hoffman B., Bock T., Thomann R., Mulhaupt R. and Friedrich C., Morphological stability of polypropylene nanocomposites. *Macromol Rapid Commun* 22 (2001), pp. 519–523.

54. Nam P.H., Maiti P., Okamoto M., Kotaka T., Hasegawa N. and Usuki A., A hierarchical structure and properties of intercalated polypropylene/clay nanocomposites. *Polymer* 42 (2001), pp. 9633–9640.

55. Liu X. and Wu Q., PP/clay nanocomposites prepared by grafting-melt intercalation. *Polymer* 42 (2001), pp. 10013–10019.

56. Nam P.H., Maiti P., Okamaoto M., Kotaka T., Foam processing and cellular structure of polypropylene/clay nanocomposites. Proceeding Nanocomposites, June 25–27, 2001, Chicago, Illinois, USA: ECM Publication; 2001.

57. Manias E., A direct-blending approach for polypropylene/clay nanocomposites enhances properties. *Mater Res Soc Bull* 26 (2001), pp. 862–863.

58. Okamoto M., Nam P.H., Maiti P., Kotaka T., Hasegawa N. and Usuki A., A house-of-cards structure in polypropylene/clay nanocomposites under elongational flow. *Nano Lett* 1 (2001), pp. 295–298.

59. Okamoto M., Nam P.H., Maiti M., Kotaka T., Nakayama T., Takada M., Ohshima M., Usuki A., Hasegawa N. and Okamoto H., Biaxial flow-induced alignment of silicate layers in polypropylene/clay nanocomposite foam. *Nano Lett* 1 (2001), pp. 503–505

60. Hambir S., Bulakh N., Kodgire P., Kalgaonkar R. and Jog J.P., PP/clay nanocomposites: a study of crystallization and dynamic mechanical behavior. *J Polym Sci, Part B: Polym Phys* 39 (2001), pp. 446–450.

61. Sun T. and Garces J.M., High-performance polypropylene–clay nanocomposites by in-situ polymerization with metallocene/clay catalysts. *Adv Mater* 14 (2002), pp. 128–130.

62. Maiti P., Nam P.H., Okamoto M., Kotaka T., Hasegawa N. and Usuki A., Influence of crystallization on intercalation, morphology, and mechanical properties of propylene/clay nanocomposites. *Macromolecules* 35 (2002), pp. 2042–2049.

63. Maiti P., Nam P.H., Okamoto M., Kotaka T., Hasegawa N. and Usuki A., The effect of crystallization on the structure and morphology of polypropylene/clay nanocomposites. *Polym Engng Sci* 42 (2002), pp. 1864–1871.

64. Nam P.H., Maiti P., Okamoto M., Kotaka T., Nakayama T., Takada M., Ohshima M., Usuki A., Hasegawa N. and Okamoto H., Foam processing and cellular structure of polypropylene/clay nanocomposites. *Polym Engng Sci* 42 (2002), pp. 1907–1918

65. Hambir S., Bulakh N. and Jog J.P., Propylene/clay nanocomposites: effect of

compatibilizer on the thermal, crystallization and dynamic mechanical behavior. *Polym Engng Sci* 42 (2002), pp. 1800–1807.

66. Kaempfer D., Thomann R. and Mulhaupt R., Melt compounding of syndiotactic polypropylene nanocomposites containing organophilic layered silicates and in situ formed core/shell nanoparticles. *Polymer* 43 (2002), pp. 2909–2916.

67. Lele A., Mackley M., Galgali G. and Ramesh C., In situ rheo-X-ray investigation of flow-induced orientation in layered silicate-syndiotactic polypropylene nanocomposite melt. *J Rheol* 46 (2002), pp. 1091–1110.

68. Zhang Q., Wang Y. and Fu Q., Shear-induced change of exfoliation and orientation in polypropylene/montmorillonite nanocomposites. *J Polym Sci, Part B: Polym Phys* 41 (2003), pp. 1–10.

69. Somwangthanaroj A., Lee E.C. and Solomon M.J., Early stage quiescent and flow-induced crystallization of intercalated polypropylene nanocomposites by time-resolved light scattering. *Macromolecules* 36 (2003), pp. 2333–2342

70. Morgan A.B. and Harris J.D., Effects of organoclay soxhlet extraction on mechanical properties, flammability properties and organoclay dispersion of polypropylene nanocomposites. *Polymer* 44 (2003), pp. 2113–2320.

71. Jeon H.G., Jung H.T., Lee S.W. and Hudson S.D., Morphology of polymer silicate nanocomposites. High density polyethylene and a nitrile. *Polym Bull* 41 (1998), pp. 107–113.

72. Heinemann J., Reichert P., Thomson R. and Mulhaupt R., Polyolefin nanocomposites formed by melt compounding and transition metal catalyzed ethane homo- and copolymerization in the presence of layered silicates. *Macromol Rapid Commun* 20 (1999), pp. 423–430.

73. Privalko V.P., Calleja F.J.B., Sukhorukov D.I., Privalko E.G., Walter R. and Friedrich K., Composition-dependent properties of polyethylene/Kaolin composites. Part II. Thermoelastic behavior of blow-molded samples. *J Mater Sci* 34 (1999), pp. 497–508.

74. Bergman J.S., Chen H., Giannelis E.P., Thomas M.G. and Coates G.W., Synthesis and characterization of polyolefin-silicate nanocomposites: a catalyst intercalation and in situ polymerization approach. *J Chem Soc Chem Commun* 21 (1999), pp. 2179–2180.

75. Rong J., Jing J., Li H. and Sheng M., A polyethylene nanocomposite prepared via in-situ polymerization. *Macromol Rapid Commun* 22 (2001), pp. 329–334.

76. Wang K.H., Choi M.H., Koo C.M., Choi Y.S. and Chung I.J., Synthesis and characterization of maleated polyethylene/clay nanocomposites. *Polymer* 42 (2001), pp. 9819–9826.

77. Alexandre M., Dubois P., Sun T., Graces J.M. and Jerome R., Polyethylene-layered silicate nanocomposites prepared by the polymerization-filling technique: synthesis and mechanical properties. *Polymer* 43 (2002), pp. 2123–2132.

78. Gopakumar T.G., Lee J.A., Kontopoulou M. and Parent J.S., Influence of clay exfoliation on the physical properties of montmorillonite/polyethylene composites. *Polymer* 43 (2002), pp. 5483–5491.

79. Jin Y.H., Park H.J., Im S.S., Kwak S.Y. and Kwak S., Polyethylene/clay nanocomposite by in situ exfoliation of montmorillonite during Ziegler–Natta polymerization of ethylene. *Macromol Rapid Commun* 23 (2002), pp. 135–140.

80. Bafna A., Beaucage G., Mirabella F. and Mehta S., 3D hierarchical orientation in polymer–clay nanocomposite films. *Polymer* 44 (2003), pp. 1103–1115.

81. Vaia R. A, Isii H., and Giannelis E. P., Synthesis and properties of two-dimensional nanostructures by direct intercalation of polymer melts in layered silicates. *Chem Mater* 5 (1993), pp 1694.

82. Vaia R. A., Jandt K. D., Edward J. K., and Giannelis E. P., Kinetics of Polymer Melt Intercalation. *Macromolecules* 28 (1995), pp. 8080.

83. Weiner M. W., Chen H., Giannelis E. P., and Sogah D. Y., *J. Am. Chem. Soc*. 122 (1999), pp. 1615.

84. Moet A. and Akelah A., Polymer-clay nanocomposites: polystyrene grafted onto montmorillonite interlayers. *Mater Lett*. 18 (1993), pp. 97.

85. Hasegawa N., Okamoto H., Kawasumi M., and Usuki A., Preparation and mechanical properties of polystyrene-clay hybrids. *J. Appl. Polym. Sci*., 74 (1999), pp. 3359.

86. Alexandre M. and Dubois P., Polymer-layered silicate nanocomposites: preparation, properties and uses of a new class of materials. *Mater. Sci, and Eng*., 28 (2000), pp. 1-63.

87. Lincoln D. M., Vaia R. A., Wang Z. G., and Hsiao B. S., Secondary structure and elevated temperature crystallite morphology of nylon-6/layered silicate nanocomposites. *Polymer* 42 (2001), pp. 1621-31.

88. Sall K., European Plastics News, March 14, 2002.

89. Messersmith P. B. and Giannelis E. P., Synthesis and barrier properties of poly(-caprolactone)-layered silicate nanocomposites. *J. Polym. Sci. Part A: Polym. Chem*., 33 (1995), pp. 1047.

90. Hackett E., Manias E. and Giannelis E.P., Computer simulation studies of PEO/layered silicate nanocomposites. *Chem Mater* 12 (2000), pp. 2161–2167.

91. Kuppa V. and Manias E., Computer simulation of PEO/layered-silicate nanocomposites: 2. Lithium dynamics in PEO/$Li^{+}$ montmorillonite intercalates. *Chem Mater* 14 (2002), pp. 2171–2175.

92. Aranda P. and Ruiz-Hitzky E., Poly(ethylene oxide)-silicate intercalation materials. *Chem Mater* 4 (1992), pp. 1395–1403.

93. Lan T., Kaviratna P. D., and Pinnavaia T. J., On the Nature of Polyimide-Clay Hybrid Composites. *Chem. Mater*., 6 (1994), pp 573.

94. Messersmith P. B. and Giannelis E. P., Synthesis and barrier properties of poly(-caprolactone)-layered silicate nanocomposites. J. Polym. Sci. Part A: Polym. Chem. Ed., 33 (1995), pp. 1407.

95. Yano K., Usuki A., Okada A., Kurauchi T. and Kamigaito O., Synthesis and properties of polyimide–clay hybrid. *Polym Prepr (Jpn)* 32 1 (1991), pp. 65–67.

96. Lan T., Kaviratna P.D. and Pinnavaia T.J., On the nature of polyimide–clay hybrid composites. *Chem Mater* 6 (1994), pp. 573–575.

97. Yano K., Usuki A. and Okada A.. Synthesis and properties of polyimide–clay hybrid films. *J Polym Sci, Part A: Polym Chem* 35 (1997), pp. 2289–2294.

98. Zhu Z.K., Yang Y., Yin J., Wang X.Y., Ke Y.C. and Qi Z.N.. Preparation and properties of organosoluble montmorillonite/polyimide hybrid materials. *J Appl Polym Sci* 73 (1999), p. 2063.

99. Yang Y., Zhu Z.K., Yin J., Wang X.Y. and Qi Z.E., Preparation and properties of hybrids of organo-soluble polyimide and montmorillonite with various chemical

surface modification methods. *Polymer* 40 (1999), pp. 4407–4414.

100. Tyan H.L., Wei K.H. and Hsieh T.E., Mechanical properties of clay–polyimide (BTDA-ODA) nanocomposites via ODA-modified organoclay. *J Polym Sci, Part B: Polym Phys* 38 (2000), p. 2873.

101. Yano K., Usuki A. and Okada A., Polyimide/montmorillonite hybrid. *Polym Prepr (201 ACS)* 32 (1991), pp. 65–66.

102. Gu A. and Chang F.C., A novel preparation of polyimide/clay hybrid films with low coefficient of thermal expansion. *J Appl Polym Sci* 79 (2001), pp. 289–294.

103. Gu A., Kuo S.W. and Chang F.C., Syntheses and properties of PI/clay hybrids. *J Appl Polym Sci* 79 (2001), pp. 1902–1910.

104. Hsiao S.H., Liou G.S. and Chang L.M., Synthesis and properties of organosoluble polyimide/clay hybrids. *J Appl Polym Sci* 80 (2001), pp. 2067–2072.

105. Tyan H.L., Leu C.M. and Wei K.H., Effect of reactivity of organics-modified montmorillonite on the thermal and mechanical properties of montmorillonite/polyimide nanocomposites. *Chem Mater* 13 (2001), pp. 222–226.

106. Huang J.C., Zhu Z.K., Ma X.D., Qian X.F. and Yin J., Preparation and properties of montmorillonite/organo-soluble polyimide hybrid materials prepared by a one-step approach. *J Mater Sci* 36 (2001), p. 871.

107. Agag T., Koga T. and Takeichi T., Studies on thermal and mechanical properties of polyimide–clay nanocomposites. *Polymer* 42 (2001), pp. 3399–3408.

108. Morgan J.W., Gilman J.W. and Jackson C.L., Characterization of the dispersion of clay in a polyetherimide nanocomposite. *Macromolecules* 34 (2001), pp. 2735–2738.

109. Leu C.M., Wu Z.W. and Wei K.H., Synthesis and properties of covalently bonded layered silicates/polyimide (BTDA-ODA) nanocomposites. *Chem Mater* 14 (2002), pp. 3016–3021.

110. Magaraphan R., Lilayuthalert W., Sirivat A. and Schwank J.W., Preparation, structure, properties and thermal behavior of rigid-rod polyimide/montmorillonite nanocomposites. *Compos Sci Technol* 61 (2001), pp. 1253–1264.

111. Delozier D.M., Orwoll R.A., Cahoon J.F., Ladislaw J.S., Smith J.G., and Connell J.W., Polyimide nanocomposites prepared from high-temperature reduced charge organoclays. *Polymer* 44 (2003), pp. 2231–2241.

112. Liang Z.M., Yin J. and Xu H.J., Polyimide/montmorillonite nanocomposites based on thermally stable, rigid-rod aromatic amine modifiers. *Polymer* 44 (2003), pp. 1391–1399.

113. Huang X., Lewis S., Brittain W.J. and Vaia R.A., Synthesis of polycarbonate-layered silicate nanocomposites via cyclic oligomers. *Macromolecules* 33 (2000), pp. 2000–2004.

114. Mitsunaga M., Ito Y., Sinha Ray S., Okamoto M. and Hironaka K., Polycarbonate/clay nanocomposites: nanostructure control and foam processing. *Macromol Mater Engng* 288 (2003), pp. 543–548.

115. Usuki A., Mizutani T., Fukushima Y., Fujimoto M., Fukumori K., Kojima Y., Sato N., Kurauchi T., and Kamigaito O., U.S. Patent 4,889,885 (1989).

116. Wang M. S. and Pinnavaia T. J., Clay-Polymer Nanocomposites Formed from Acidic Derivatives of Montmorillonite and an Epoxy Resin. *Chem Mater*. 6 (1994); pp 468.

117. Lan T. and Pinnavaia T. J., Clay-Reinforced Epoxy Nanocomposites. *Chem. Mater*. 6 (1994); pp 2216.

118. Lan T., Kaviratna P. J., and Pinnavaia T. J., Mechanism of Clay Tactoid Exfoliation in Epoxy-Clay Nanocomposites. *Chem. Mater*., 7 (1995), pp.2214

119. Kelly P.,Akelah A., Qutubuddin S., and Moet A., Synthesis and characterization of "epoxyphilic" montmorillonites. *J. Mater Sci*., 29 (1994), pp. 2274

120. Hu Y., Song L., Xu J. Y., Yang L., Chen Z. Y., Fan W.C., *Synthesis of polyurethone/clay intercalated nanocomposites*, Colloid Poly, Sci., Volume 279, 2001, Pages 819-822.

121. Song L., Hu Y., Li B.G., Chen Z. Y., Fan W.C., *A study on the synthesis and properties of polyurethane/clay nanocomposites*, Int. J. Polym Anal. Ch., Volume 8, 2003, Pages 317-326.

122. Zerda A.S., Lesser A.J., *Intercalated clay nanocomposites: morphology, mechanics, and fracture behavior*, J. Polym. Sci., Part B, Volume 39, 2001, Pages 1137-1146.

123. Lan T., Pinnavaia T. J., *Clay-reinforced epoxy nanocomposites*, Chem. Mater., Volume 6, 1994, Pages 2216-2219.

124. Yasmin A., Abot J.L., Daniel I.M., *Processing of clay/epoxy nanocomposites with a three-roll mill machine*, Mat. Res. Soc. Symp. Proc., Volume 740, 2003, Pages 75-80.

125. Yasmin A., Abot J.L., Daniel I.M., *Processing of clay/epoxy nanocomposites by shear mixing*. Scripta Mat., Volume 49, 2003, Pages 81-86.

126. Yasmin A., Abot J.L., Daniel, I.M., *Characterization of structure and mechanical behavior of clay/epoxy nanocomposites*. San Diego: ICCM -14; 2003.

127. Luo J-J, Daniel I.M.., *Characterization and modeling of mechanical behavior of polymer/clay nancomposites*, Comp. Sci. Tech., Volume 63, 2003, Pages 1607-1616

128. Wei C.,L., Zhang M. Q., Rong M. Z., Friedrich K., *Tensile performance improvement of low nanocomposites filled-polypropylene composites*, Comp. Sci. Tech., Volume 62, 2002, Pages 1327-1340.

129. Hussain F., Okamoto M., Gorga R.E., *Review article: Polymer-matrix nanocomposites, processing, manufacturing, and application: an overview*, Journal of Composite Materials, Volume 40, 2006, Pages 1511-1575.

130. Alexandre M., and Dubois P., *Polymer-layered silicate nanocomposites: Preparation, properties and uses of a new class of materials*, Mat. Sci. Eng. Rep., Volume 28, 2000,Pages 1-63.

131. Giannelis E.P., *Polymer layered silicates nanocomposites*, Advanced Materials, Volume 8, 1996, Pages 29-35.

132. Yalcin B. and Cakmak M., *Polymer* (2004), p. 1-16

133. Nam P.H., Maiti P., Okamoto M., Kotaka T., Hazegovva N., and Usuki A., *A hierarchical structure and properties of intercalated polypropylene/clay nanocomposite*, Polymer, Volume 42, 2001, Pages 9633-9640.

134. Huang J.C., Zhu Z-K, Yin J., Qian X. F., Sun Y.Y., Polymer, Volume 42, 2001, Page 873.

135. Cho J.W., Pail D.R., Polymer, Volume 42, 2001, Page 1083.

136. Hesegavva N., Okamoto H., Kato M., Tsukigaze A., Usuki A., Macro. Mater. Engineering, Volume 76, 2000, Pages 280-281.

137. Wu C.L., Zhang M.Q., Rong M.Z., Friedrich K., *Tensile performance improvement of low nanoparticles filled-polypropylene composites*, Composites Science and Technology, Volume 62, 2002,Pages 1327-1340.

138. Sharma S.K., Nayak S.K., *Surface modified clay/polypropylene (PP) nanocomposites: Effect on physics-mechanical, thermal and morphological properties*, Polymer Degradation and Stability, Volume 94, 2009, Pages 132-138.

139. Rohlmann C.O., Horst M.F., Quinzani L.M., Failla M.D., *Comparative analysis of nanocomposites based on polypropylene and different montmorillonites,* European Polymer Journal, Volume 44, 2008, Pages 2749-2760.

140. Wang Q., Song C., Lin W., *Study of the exfoliation process of epoxy-clay nanocomposites by different curing agents*, Journal of Applied Polymer Science, Volume 90,2003, Pages 511-517.

141. Jiankun L., Yucai K., Zongrang Q., Xiao-Su Y., *Study on intercalation and exfoliation behavior of organoclay in epoxy resin*, Journal of Polymer Science: Part B: Polymer Physics, Volume 39, 2001, Pages 115-120.

142. Xu W., Bao S., He P., *Intercalation and exfoliation behavior of epoxy resin/curing agent/ montmorillonite nanocomposites*, Journal of Applied Polymer Science,Volume 84, 2002, Pages 842-849.

143. Kornmann X., Lindberg H., Berglund L.A., *Synthesis of epoxy-clay nanocomposites influence of the nature of the clay on structure*, Polymer, Volume 42, 2001, Pages 1303-1310.

144. Sarathi R., Sahu R.K., Rajeshkumar P., *Understanding the thermal, mechanical and electrical properties of epoxy nanocomposites*, Materials Science and Engineering A., 2007, Pages 567-578.

145. Saber-Samandari S., Khatibi A.A., Basic D., *An experimental study on clay/epoxy nanocomposites produced in a centrifuge*, Composites: Part B Volume 38, 2007,Page 102-107.

146. Yasmin A., Luo J.J., Abot J.L., Daniel I.M., *Mechanical and thermal behavior of clay/epoxy nanocomposites*, Composites Science and Technology, Volume 66, 2006, Pages 2415-2422.

147. Chapleau N, Mohanraj J, Ajji A, Ward IM. Polymer, Volumw 46, 2005, Page 1956.

148. Yuan Q, Jiang W, Zhang HX, Yin JH, An LJ, Li RKY. J Polym Sci, Part B: Polym Phys, Volume 38, 2001, Pages 1855.

149. Liang JZ, Li RKY. Polymer, Volume 40, 1999, Pages 3191

150. Yuan Q, Jiang W, An LJ, Li RKY. Polym Adv Technol, Volume 15, 2004, Pages 409.

151. Liang JZ, Li RKY. Polym Compos, Volume 19, 1998, Pages 698.

152. Zuiderduin WCJ, Westzaan C, Huetink J, Gaymans RJ. Polymer, Volume 44, 2003, Pages 261.

153. Hadal RS, Misra RDK. Master Sci Eng A, Volume 374, 2004, Pages 374.

154. Hadal RS, Misra RDK. Master Sci Eng A, Volume 380, 2004, Pages 326.

155. Trotigon JP, Verdu J, de Vallios A. In: Sedlaucek B, editor. *Polymer composites: proceedings of prague IUPAC microsymposium on macromolecules*, July 8-11. New York: De Grugter; 1985. Pages 191.

156. Dasari A, Sarang S, Misra RDK. Mater Sci Eng A, Volume 368, 2004, Pages 191

157. Dasari A, Rohrmann J, Misra RDK. Mater Sci Eng A, Volume 364, 2004, Pages 357.

158. Dasari A, Misra RDK. Acta Materialia, Volume 52, 2004, Pages 1683.

159. Chan CM, Wu J, Li JX, Cheung YK. Polymer, Volume 43, 2002, Pages 2981.

160. Thio YS, Argon AS, Cohen RE, Weinberg M. Polymer, Volume 43, 2002, Pages 3661.

161. Haworth B, Raymond CL, Sutherland I. Polym Eng Sci, Volume 41, 2001, Pages 1345.

162. Albano C, Gonzalez J, Ichazo M, Rosales C, de Navarro CU, Parra C. Compos Struct, Volume 49, 2000, Pages 48.

163. Wang Y, Wang JJ. Polym Eng Sci, Volume 39, 1999, Page 190.

164. Gonzalez J, Albano C, Ichazo M, Diaz B. Eur Polym J, Volume 38, 2002, Page 2465.

165. Price GJ, Ansari DM. Polym Int, Volume 53, 2004, Page 430.

166. Vollenberg PHT, Heikens D. J Mater Sci, Volume 25, 1990, Page 3089.

167. Misra RDK, Nerlikar P, Bertrand K, Murphy D. Mater Sci Eng A, Volume 384, 2004, Page 284.

168. Tanniru M, Misra RDK, Bertrand K, Murphy D. Mater Sci Eng A, Volume 404, 2005, Page 208.

169. Tanniru M, Misra RDK. Mater Sci Eng A, Volume 405, 2005, Page 178.

170. Nathani H, Dasari A, Misra RDK. Acta Materialia, Volume 52, 2004, Page 3217.

171. Dolgovskij, M.K.; Fasulo, P.D.; Lortie, F.; Macosko, C.W.; Ottaviani R.A.; Rodgers, W.R. ANTEC 2003, 2255.

172. H.R Dennis, D.L Hunter, D Chang, S. Kim, J.L White, J.W Cho, D.R Paul, Effect of melt processing conditions on the extent of exfoliation in organoclay-based nanocomposites. *Polymer* 42 (2001), pp. 9513.

173. Nguyen Q.,T. and Baird D., G., *Process for Improving the Exfoliation and Dispersion of Nanoclay Particles into Polymer Matrices Using Supercritical Carbon Dioxide,* PhD thesis. Department of Chemical Engineering Virginia Polytehcni Institute and State Univerity.

174. Galgali G., Agarwal S., Lele A., *Effect of clay orientation on the tensile modulus of polypropylene nanoclay composites*, Polymer, Volume 45, 2004, Pages 6059-6069.

175. Bureau M.N., Ton-That M., Perrin-Sarazin F., *Essential work of fracture and failure mechanism of polypropylene-clay nanocomposites*, Engineering Fracture Mechanics, Volume 73, 2006, Pages 2360-2374.

176. Drozdov A.D., Lejre A.H., Christiasen J., *Viscoelasticity, viscoplasticity, and creep failure of polypropylene/clay nanocomposites*, Composites Science and Technology, Volume 69, 2009, Pages 2596-2603.

177. Dong Y., Bhattacharyya D., *Effect of clay type, clay/compatibilizer content and matrix viscosity on the mechanical properties of polypropylene/organoclay nanocomposites*, Composites: Part A, Volume 39, 2008, Pages 1177-1191.

178. Santos K.S., Liberman S.A., Oviedo M.A.S., Mauler R.S., *Optimization of the mechanical properties of polypropylene-based nanocomposites via the addition of a combination of organoclays*, Composites: Part A, Volume 40, 2009, Pages 1199-1209.

179. Zhao Q., and Hoa S.V., Toughening mechanism of epoxy resins with micro/nano particles, Journal of Composites Materials, Vol 41, 2007, No:2.

180. Fornes T.D., Paul D.R., Polymer, Volume 44, 2003, Pages 4993-5013.

181. Sheng, N., Boyce, M.C., Parks, D. M., Rutledge, G.C., Abes, J. I.,Cohen, R.E., *Multiscale Micromechanical Modeling of Polymer/Clay Nanocomposites and The Effective Clay Particle*, Polymer 45, 2004, pp. 487-506.

182. Yakobson B.I., Brabec C.J., Bernholc J., Phys Rev. Lett., Volume 76, 1996, Page 2511.

183. Yuan Q., Misra M.D.K., *Impact fracture behavior of clay-reinforced polypropylene nanocomposites*, Polymer, Volume 47, 2006, Pages 4421-4437.

184. Lin J., Chang L.C., Nian M.H., Ho H.L., *Mechanical behavior of various nanoparticle filled composites at low-velocity impact*, Composites Structures Volume 74, 2006, Pages 30-36.

185. Iqbal K., Khan S., Munir A., Kim J., *Impact damage resistance of CFRP with nanoclay filled epoxy matrix*, Composites Science and Technology, Volume 69, 2009, Pages 1949-1957.

186. Ye Y., Chen H., Wu J., Ye L., *High impact strength epoxy nanocomposites with natural nanotubes*, Polymer, Volume 48, 2007, Pages 6426-6433.

187. Chen B., Liu J., Chen H.B., Wu J.S., Chem. Mater., Volume 16, 2004, Pages 4864.

188. Wang K., Wang L., Wu J.S., Chen L., He C.B., Langmuir, Volume 21, 2005, Page 3613.

189. Blumstein A., *Polymerization of absorbed monolayers: II. Thermal degradation of the inserted polymers*, J. Polym. Sci., Volume A3, 1965, Pages 2665-2673.

190. Guo Z., Du B., Fang Z., *Effect of organo-clay and sodium dodecyl sulfonate intercalated layered double hydroxide on thermal and flame behavior of intumescent flame retarded polypropylene*, Polymer Degradation and Stability, Volume 94, 200), Pages 1979-1985.

191. Kashiwagi T., Harris Jr R.H., Zhang X., Bribe R.M., Cipriano B.H., Raghavan S.R., Awad W.H., Shields J.R., *Flame retardant mechanism of polyamide 6-clay nanocomposites*, Polymer, Volume 45, 2004, Pages 881-891.

192. Qin H., Zhang S., Zhauo C., Feng M., Yang M., Shu Z., Yang S., *Thermal stability and flammability of polypropylene/montmorillonite composites*, Polymer

Degradation and Stability, Volume 85, 2004, Pages 807-813.

193. Modesti M., Lorenzetti A., Bon D., Besco S., *Thermal behavior of competibilized polypropylene nanocomposites*: Effect of processing conditions.

194. Gilman J.W., *Flammability and thermal stability studies of polymer layered-silicate (clay) nanocomposites*, Appl. Clay Sci., Volume 15, 1999, Pages 31-49.

195. Gilman J. W., Kashiwagi T., Lomakin S., Giannelis E.P., Manias E., Lichtenhan J.D., Jones P., *Nanocomposites: Radiative gasification and vinyl polymer flammability in*: Proceeding of the 6th Europen meeting on fire retardancy of polymeric materials (FRPM'97) University of Lile, France 24-26 September 1997, Pages 203-221.

196. Tandon, G. P., and Weng, G. J., *The Effect of Aspect Ratio of Inclusions on the Elastic Properties of Unidirectionally Aligned Composites*, Polymer Composites, October 1984, Vol. 5, No. 4

197. Tandom, G. P., Weng, G. J., *Average Stress in the Matrix and Effective Moduli of Randomly Oriented Composites*, Composite Science and Technology, 27, 1986, pp. 111-132.